Republic of Iraq
Ministry of Higher Education
and Scientific Research
University of Babylon
College of Engineering
Mechanical Engineering Department

INVESTIGATION OF THE FORCED CONVECTION OF A TWO-PHASE FLOW IN A DUCT BANKS WITH A VORTEX GENERATORS

A Dissertation

Submitted to the College of Engineering/ University of Babylon in Partial Fulfillment of the Requirements for award of Degree of Doctorate of Philosophy in Engineering /Mechanical Engineering/ Power

By

Adnan Qahtan Ibrahim Issa

Supervised by

Prof. Dr. Riyadh Sabah Alturaihi

2023 A.M **1443 A.H**

جمهورية العراق
وزارة التعليم العالي والبحث العلمي
جامعة بابل / كلية الهندسة
قسم الهندسة الميكانيكية

تقصي الحمل الحراري القسري للجريان ثنائي الطور في مجمع أنابيب مع مولدات دوامية

أطروحة مقدمة الى قسم الهندسة الميكانيكية في جامعة بابل كجزء من متطلبات نيل درجة الدكتوراه في فلسفة علوم الهندسة / الهندسة الميكانيكية / القدرة

أعدت من قبل

عدنان قحطان ابراهيم عيسى

بأشراف

أ.د. رياض صباح الطريحي

1443 A.H

2023 A.M

بسم الله الرحمن الرحيم

(قَالُوا سُبْحَانَكَ لا
عِلْمَ لَنَا
إِلَّا مَا عَلَّمْتَنَا
إِنَّكَ أَنْتَ
الْعَلِيمُ الْحَكِيمُ)

صدق الله العلي العظيم

سورة البقرة
الأية 32

الخلاصة

يهدف العمل الحالي إلى تحسين معامل الحمل الحراري من خلال استخدام أشكال مختلفة للمولدات الدوامية في مجمع أنابيب لجريان أحادي وثنائي الطور. يتم حساب معدل انتقال الحرارة وانخفاض الضغط في القناة المستطيلة الأفقية.

تم تقييم الحمل الحراري للجريان عبر مجمع الانابيب مع الجنيحات داخل المبادل الحراري في جزئين عدديًا تحت مدى رينولدز للماء (3639-4813). يتعامل العمل العددي الحالي مع المحاكاة باستخدام الكود التجاري ANSYS FLUENT (19). الجزء الأول درس تأثير الجريان ثنائي الطور (الماء والهواء) على أداء نوعين من المولدات الدوامية (المثلثة والمستطيلة درس الجزء الثاني فعالية أربعة أشكال من الجنيحات (المثلثة ، المستطيلة ، المتعرجة ، والمتموجة) ، و مجمع انابيب دائرية أوبيضوية ، وتكوينات (CFU) أو (CFD). يتم تغير زاية الميل للجنيحات (15, 20, 25) درجة في الجريان ثنائي الطور.

درس هذا العمل بشكل تجريبي تأثير شكلين من المولدات الدوامية (المثلثة والمستطيلة) ومعدلات الجريان مختلفة للخليط (ماء-هواء) على معامل انتقال الحرارة.

في التدفق أحادي الطور (الماء) عندما زاد (Re) من (3646) إلى (4252) و (4813) ، زاد (Nu) بنسبة (8.3٪) و (17٪) عدديًا وبنسبة (8٪) و (17.13٪) تجريبياً. انخفض (f) بنسبة (12.5٪) و (9.6٪) عددياً وبنسبة (2.1٪) و (3.7٪) تجريبياً في حالة عدم استخدام مولدات دوامية. عند (Re = 3646) زاد (Nu) بنسبة (52.8٪) عددياً وبنسبة (53٪) تجريبياً ,عند (Re=4254) زاد بنسبة (45.16٪) عددياً وبنسبة (45.67٪) تجريبياً وأخيراً عند (Re=4813) زادت بنسبة (46.4٪) عددياً وبنسبة (45.68٪) تجريبياً في حالة استخدام الجنيحات المثلثة. كما أنه عند (Re = 3646) زاد (Nu) بنسبة (63.46٪) عددياً وبنسبة (62٪) تجريبياً , و عند (Re=4254) زاد بنسبة (60.16٪) عددياً وبنسبة (60.78٪) تجريبياً, وأخيراً عند (Re=4813) زادت بنسبة (59.1٪) عددياً وبنسبة (58.56٪) تجريبياً مع أستخدام الجنيحات المستطيلة مقارنة في حالة عدم استخدام مولدات دوامية. أفضل معامل أداء كان (2.4) عددياً و (2.8) تجريبياً مع الجنيحات المثلثة ، و (1.6) عددياً و (1.5) تجريبياً مع الجنيحات المستطيلة.

في الجريان ثنائي الطور (ماء - هواء) زاد (Nu) بنسبة (80٪) عددياً وبنسبة (81٪) تجريبياً مع استخدام الجنيحات المثلثة. كما زاد عدد (Nu) بنسبة (76.4٪) عدديا وبنسبة (71.7٪) تجريبيا مع استخدام الجنيحات المستطيلة. وانخفض (f) بنسبة (19.65٪) عددياً وبنسبة (19.6٪)

تجريبياً مع استخدام الجنيحات المثلثة , وانخفض (*f*) بنسبة (13.5٪) عددياً وبنسبة (5٪) تجريبياً مع استخدام الجنيحات المستطيلة مقارنة في حالة عدم استخدام مولدات دوامية. أفضل معامل أداء كان (2.24) عددياً و (2.25) تجريبياً مع استخدام الجنيحات المثلثة ، (2) عددياً و (1.81) تجريبياً مع مع استخدام الجنيحات المستطيلة.

تم الحصول على الأداء الحراري-الهيدروليكي الأفضل مع استخدام الجنيحات المثلثة عند زاوية ميل (15 درجة) مع مجمع انابيب بيضوية في الجريان ثنائي الطور ذو ترتيب (CFD) وبمعدل معتدل للجريان المضطرب.

Abstract

Present work aimed to improve the heat transfer coefficient by utilizing various types of vortex generators in the tube banks with single and two-phase flow. The rate of heat transfer and the pressure drop is calculated in the horizontal rectangular duct.

Thermal convection for flow across tube banks with winglets through the heat exchanger was evaluated in two portions numerically under the Reynolds number of water range (3639-4813). Present numerical work deals with the simulation using the commercial code ANSYS FLUENT (19). The first part studied the effect of two-phase flow (water and air) on the performance of two shapes of vortex generators (Delta and Rectangular) winglets. The second part studied the effectiveness of four shapes of winglets (Delta, Rectangular, Zikzak, and Sinusoidal wavy), circular or oval tube banks, and (CFU) or (CFD) configurations. It varied the angle of attack (15°, 20°, and 25°) in the two-phase flow.

This work investigated experimentally the effect of two shapes of vortex generators (Delta and Rectangular) and various flow rates of the mixture (water-air) on the heat transfer coefficient.

In a single-phase flow (water) when the Reynolds number increased from (3646) to (4252) and (4813), the (*Nu*) increased by (8.3%) and (17%) numerically and by (8%) and (17.13%) experimentally. The (*f*) decreased by (12.5%) and (9.6%) numerically and by (2.1%) and (3.7%) experimentally, without (VGs). At (Re = 3646) the (*Nu*) increased by (52.8%) numerically and by (53%) experimentally, at (Re = 4254) increased by (45.16%) numerically and by (45.67%) experimentally, and finally at (Re = 4813) increased by (46.4%) numerically and by (45.68%) experimentally with delta winglets. Also, At (Re = 3646) the (*Nu*) increased by (63.46%) numerically and by (62%) experimentally, at (Re =

4254) increased by (60.16%) numerically and by (60.78%) experimentally, and finally at (Re = 4813) increased by (59.1%) numerically and by (58.56%) experimentally with rectangular winglets compared to without (VGs). The best performance parameter was found to be (2.4) numerically and (2.8) experimentally with delta winglets, (1.6) numerically and (1.5) experimentally with rectangular winglets.

In a two-phase flow (water-air) the (*Nu*) increased by (80%) numerically and by (81%) experimentally with delta winglets. Also, the (*Nu*) increased by (76.4%) numerically and by (71.7%) experimentally with rectangular winglets. The (*f*) decreased by (19.65%) numerically and by (19.6%) experimentally with delta winglets and the (*f*) decreased by (13.5%) numerically and by (5%) experimentally with rectangular winglets compared to without (VGs). The best performance parameter was found to be (2.24) numerically and (2.25) experimentally with delta winglets, (2) numerically and (1.81) experimentally with rectangular winglets.

The best thermo-hydraulic performance is obtained by delta winglets at (15°) an angle of attack for the oval tube banks in the two-phase flow with (CFD) configuration and moderate turbulent flow rate.

Dedication

This Dissertation is dedicated to:

To the candles that are lightening my way

To the most merciful hearts, who inspirited my thinking

To the persons who deserve to be perfect my father and my mother

To the spring of my life and the candle of my path my wife and my daughters

To All People Who Assisted Me with All Gratitude and Love

ACKNOWLEDGEMENTS

Praise first to Allah for the guidance that has enabled me to complete my research.

I would like to express my deepest thanks and sincere gratitude to my supervisor, ***Prof. Dr. Riyadh Sabah Alturaihi****, for his supervision, support, understanding, and encouragement.*

I wish to express my thanks to head of mechanical department, Asst. Prof. Dr. Samer Mohammad Abd - Alhalim, and to my friends and all the staff members of mechanical engineering department.

I would like to thank everyone, who helped me in this study.

Adnan Qahtan Ibrahim Issa

23 / 2 / 2023

TABLE OF CONTENTS

NOMENCLATURES

Latin Symbols		
Symbol	**Description**	**Unit**
A	Cross-sectional area of duct	m^2
A_{min}	Minimum flow cross-section area	m^2
A_t	Total surface area of tube banks	m^2
c_p	Specific heat at constant pressure	J/kg. K
D	Diameter of tube	m
D_X, D_Y	Distance	m
D_h	Hydraulic Diameter of the duct	m
f	Friction factor	---
$\vec{F}$	Body force	N
h	Heat transfer coefficient	$W/m^2.{}^oC$
h_w	Height	m
h_k	The sensible enthalpy for phase *k*	J/kg
I	Current input from heaters	Ampere
j	Colburn factor.	---
k	Thermal conductivity	$W/m.{}^oC$
k_{eff}	The effective conductivity	$W/m.{}^oC$
k_t	The turbulent thermal conductivity	$W/m.{}^oC$
L	Length of tube	m
N	Number of tubes	
Nu	Nusselt number	---
P	Perimeter of duct	m
$q_{heaters}$	Heaters power	W
q_{conv}	Heat convection	W
Pr	Prandial number	---
Q	Flow rate	L/min
Q_t	Calculated flow rate	L/min

Re	Reynolds number	---
S_T	Transverse distance	m
S_L	Longitudinal distance	m
St	Stanton number	---
T_{inlet}	Inlet temperature	^oC
T_{outlet}	Outlet temperature	^oC
$\overline{T}_b$	Bulk temperature	^oC
T_f	Film temperature	^oC
T_{ts}	Tube surface temperature	^oC
t	Time	s
u_a	Superficial velocity of air	m/s
u	Fluid velocity	m/s
u_w	Superficial velocity of water	m/s
V	Voltage output from heaters	Volt
V_a	The volume of air	m^3
V_T	The total volume of the mixture	m^3
V_w	Volume of collected water	L
$\overrightarrow{v}_m$	The mass-averaged velocity	m/s
$\vec{v}_{dr,k}$	The drift velocity for the secondary phase k	m/s
x	Mass flow rate fraction of Air	
X,Y,Z	Cartesian coordinates	---

Greek Symbols

Symbol	Description	Unit
α	Attack angle	degree
$\propto_k$	The volume fraction of two-phase	-----
μ	Dynamic viscosity	kg/m.s
μ_m	The viscosity of the mixture	kg/m.s
n	The number of phases	----
ρ	Fluid density	kg/m^3

ρ_m	Density of two-phase	kg/m^3
ν	kinematic viscosity	m^2/s
φ_a	The air volume fraction	----
ΔP	Pressure drop	Pa
θ	Span angle	degree
ΔT_S	Temperature difference	^oC

ABBREVIATIONS	
Abbreviation	**Description**
CFU	Common Flow Upward
CFD	Common Flow Downward
CDWVGs	Curved Delta Winglet Vortex Generator
CWVGs	Curved Winglet Vortex Generator
CTW	Curved Trapezoidal winglets
DVGs	Delta Vortex Generators
HE	Heat Exchanger
LVGs	Longitudinal vortex generators
RWP	Rectangular Winglets Pair
RWVGs	Rectangular Winglets Vortex Generators
RW	Rectangular Winglet
SST	Shear Stress Transport model
SWWVGs	Sinusoidal Wavy Winglets Vortex Generators
2D	Two dimensions
3D	Three dimensions
VGs	Vortex Generators

VGW	Vortex Generator Winglets
ZWVGs	Zikzak Winglets Vortex Generators

Subscript	
Symbol	**Description**
b	Bulk
eff	Effective
f	Film
h	Hydraulic
ts	Tube surface
t	Total

CERTIFICATION

I certify that this Dissertation, entitled, **(Investigation of the Forced Convection of a Two-Phase Flow in a Duct Banks with a Vortex Generators)** and submitted prepared by the student **(Adnan Qahtan Ibrahim Issa)** was prepared under my supervision at the Department of Mechanical Engineering/ College of Engineering/ University of Babylon, as a part of the requirements for Degree of Doctorate of Philosophy in Engineering /Mechanical Engineering/ Power.

Prof. Dr. Riyadh Sabah Al-Turaihi

Supervisor

Date:

I certify that this Dissertation mentioned above has been completed in Mechanical Engineering in the College of Engineering/ University of Babylon.

Head of Department

Asst. Prof. Dr. Samer Abdulhaleem

Date:

Examining Committee Certificate

We certify that we have read this dissertation, entitled "Investigation of the Forced Convection of a Two-Phase Flow in a Duct Banks with a Vortex Generators" and as an examining committee, examined the student "Adnan Qahtan Ibrahim Issa", in its content and that in our opinion it meets the standard of a dissertation for the degree of Doctorate of Philosophy in Engineering /Mechanical Engineering/ Power.

Prof. Dr. Qasim Saleh Mahdi
Chairman
Date:

Prof. Dr. Ahmed Kadhim Hussein
Member
Date:

Prof. Dr. Alaa Abbas Mahdi
Member
Date:

Prof. Dr. Saba Y. Ahmed
Member
Date:

Prof. Dr. Hameed K. Hamzah
Member
Date:

Prof. Dr. Riyadh Sabah Al-Turaihi
Supervisor
Date:

Approval of Head of Department
Asst. Prof. Dr. Samer Abdulhaleem
Date:

Approval of the Dean of College
Prof. Dr. Hatem Hadi Obeid
Date:

CHAPTER ONE
Introduction

1.1 Background

In numerous industrial processes, fluid passes through ducts consisting of banks of tubes. Banks of tube heat exchangers are utilized in a diversity of technical applications, including heating, ventilation, air conditioning, and refrigeration systems, vehicles, petroleum, electronic cooling, and chemical industries. The fluid has a tendency to flow more quickly along the smooth duct wall, hence lowering the flow through the tube's banks, [1]. In any situation, the capacity to forecast the nature of the emerging flow pattern during the transition from one construction to another is essential for the development of new kinds of heat exchangers. This will enable the performance parameters of the devices to be determined and aid in the prevention of any issues. As heat convection coefficient of fluids, conventional fluids such as air, water, and ethylene glycol are typically employed. Although numerous techniques are employed to improve heat convection coefficient, the limited heat convection coefficient performance of conventional fluids impedes performance enhancement. Enhancing the heat transfer coefficient is one of the main tools for conserving energy in a variety of processes, [2].

1.2 Concept of Vortex Generators (VGs)

Vortex generation is used to enhance heat convection coefficient, which holds promise on the fluid side. As seen in Figure (1-1), vortex generators (VGs) such as wings and winglets can produce vortices into the fluid flow, resulting in an increase in the heat convection coefficient. On a heat transfer surface, vortex generators may be pierced, mounted, or imprinted. Vortices

are created when fluid flows around vortex generators because of the friction and separation on the vortex generator's edge, [3].

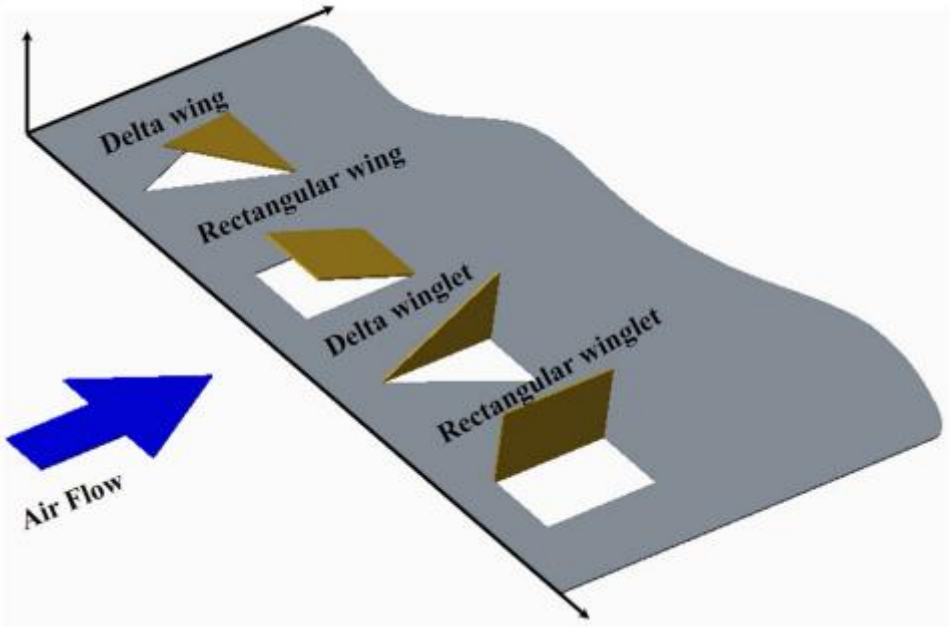

Figure (1-1) Schematic diagrams of four common (LVGs), [4]

Researchers have long focused on enhancing the performance of heat exchangers through design modifications due to their immense technological significance. It is commonly known that the insertion of vortex generator winglets (VGW) of various kinds, shapes, and configurations (rectangular, trapezoidal, delta, and curved trapezoidal) improves heat transfer coefficient, [5], as shown in Figure (1-2).

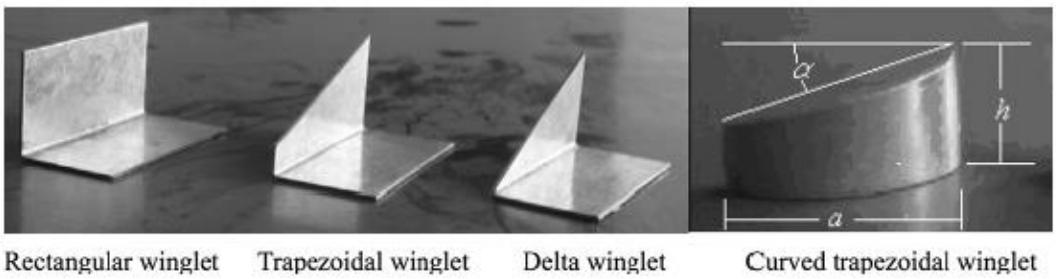

Figure (1-2) Various kinds of winglets, [3]

1.3 Types of Banks of Tube Heat Exchangers and Applications

Various industrial operations, such as the creation of steam in a boiler or the cooling of air conditioning coils, involve heat exchange to or from cross-flowing banks of tube heat exchangers. This can be classified according to the geometric arrangement of the tube rows of a bank, [6], as shown in Figure (1-3):

1) Inline tube rows of a bank

2) Staggered tube rows of a bank

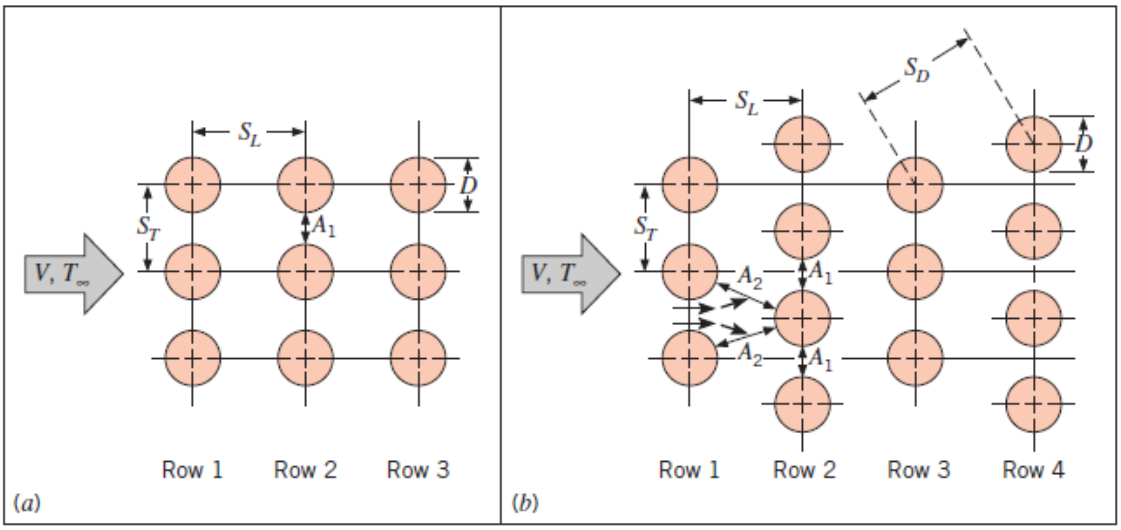

Figure (1-3) Tube configurations (a) Inline (b) Staggered, [6]

Applications of heat exchangers include heating, ventilation, air conditioning, automobiles, petroleum, electronic cooling, food processing, Aerospace, cooling of nuclear systems, and chemical industries. In the direction of the fluid velocity (V), the tube rows of a bank might be inline or staggered. The configuration is defined by the diameter of tube (D), the transverse distance (S_T), and the longitudinal distance (S_L) between tube centers. The tube of a bank can be either a circular tube, as shown in Figure (1-4) or an oval tube, as shown in Figure (1-5).

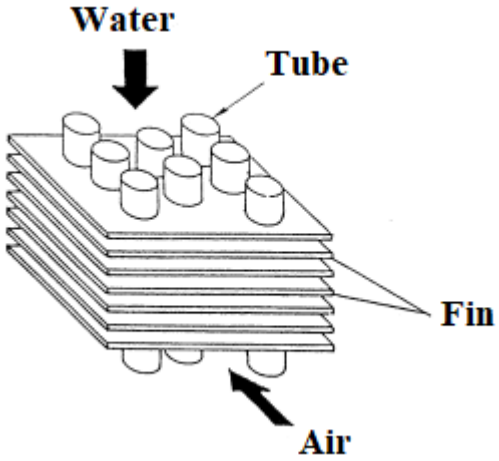

Figure (1-4) Banks of the circular tube heat exchanger staggered arrangements, [7]

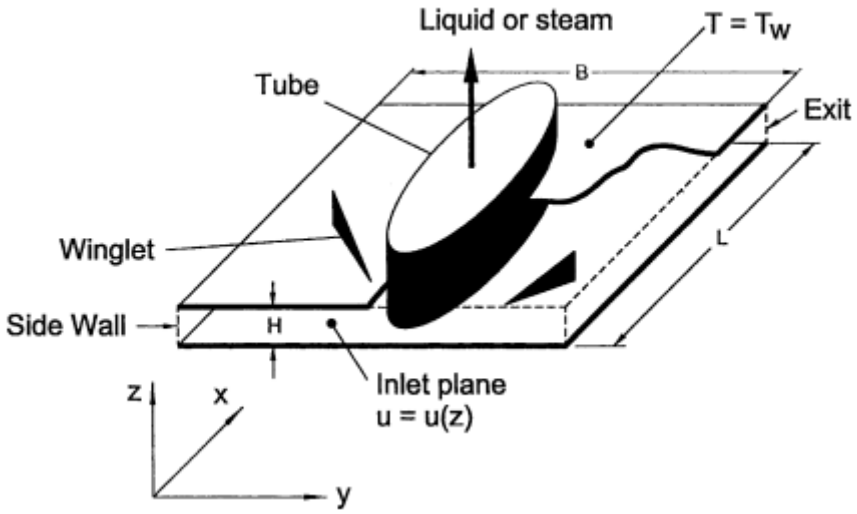

Figure (1-5) Heat exchanger with oval tube and vortex generators, [7]

1.4 Two-Phase Flow

Two-phase flow is used to reduce pressure drop in the duct at high flow velocities at Reynolds numbers of water range (3646-4805). Putting winglets inside the duct increases the heat transfer rate since the pressure drop must be minimized to prevent incurring additional costs. Heat transfer coefficient and

temperature distribution were investigated in the duct using various values for the flow rate of water and air with different shapes and positions of the vortex generators. The two-phase flow differs substantially from the single-phase flow. In addition to being characterized as laminar or turbulent, the structure of the flow must also be specified. In addition, it is essential to understand the characteristics typical of two-phase flow, such as phase slip velocity, local changeable flow rate, phase density, and volume fraction. Flow structure within the heat exchanger influences both the efficiency of heat transfer and the magnitude of flow resistance. It also impacts the heat convection coefficient of working fluid flow around tube banks, [8].

Since the nature of matter in a new state are clearly distinguishable, and two-phase flows should be categorized based on the states present in the flow field. Each class must be handled separately from the others, and the two-phase flows can be categorized as follows, [9]:

1) Gas-Liquid flow as the flow in side channel pump [10].
2) Solid-Liquid flow as the pipeline transportation of coke in petroleum [11].
3) Solid-Gas flow this type of flow is fundamental to many industrial processes such as pneumatic transport, particulate pollution control, combustion of pulverized coal, drying of food products, sand blasting, plasma-arc coating and fluidized bed mixing, [12].
4) Flow of plasma and liquid that involves the mixing of gas and electrically conducting of liquid.
5) Flow of plasma and solid that involves the mixing of gas and electrically charged of solid particles.

6) Flow of plasma and gas which also involves the interaction of various gases.

The practical applications of plasmas with liquid, solid, and gas as mixture are used in the field of power production, [13].

1.5 Flow Regimes in Horizontal Flow

Only horizontal single-phase and two-phase flow across tube banks in a heat exchanger are investigated in the present work. Gravity causes the asymmetric distribution of phases in horizontal co-current flow, which results in more complex flow patterns. The predicted horizontal flow regimes are depicted in Figure (1-6) and are described as follows, [14]:

1) **Bubbly flow:** This is a similar regime to vertical flow, except the bubbles have a tendency to move in the upper portion of the channel.

2) **Plug flow:** This is comparable to slug flow in a vertical scenario, with the exception that the layer of liquid buffering the bubble of gas from the wall of channel is frequently thicker at the bottom than at the top. Additionally, the bubble's nose is asymmetrical, as shown in Figure (1-6).

3) **Stratified flow:** In this situation, liquid and gas phases have been completely separated, with gas at the top and liquid flowing at the bottom of the channel.

4) **Wavy flow:** As in a stratified flow, the gas velocity increases, enormous surface waves begin to form on the liquid layer.

5) **Slug flow:** As the velocity of gas continues to increase in the zone of wavy flow, the waves suddenly reach the top of the channel. These are

propagated at a high velocity and wet the whole surface of the channel, leaving a film of liquid between the waves or slugs.

6) **Annular flow:** As the gas velocity continues to increase, a gas core punctures the slugs and the flow becomes annular, with a thicker layer of liquid at the bottom of the channel than at the top.

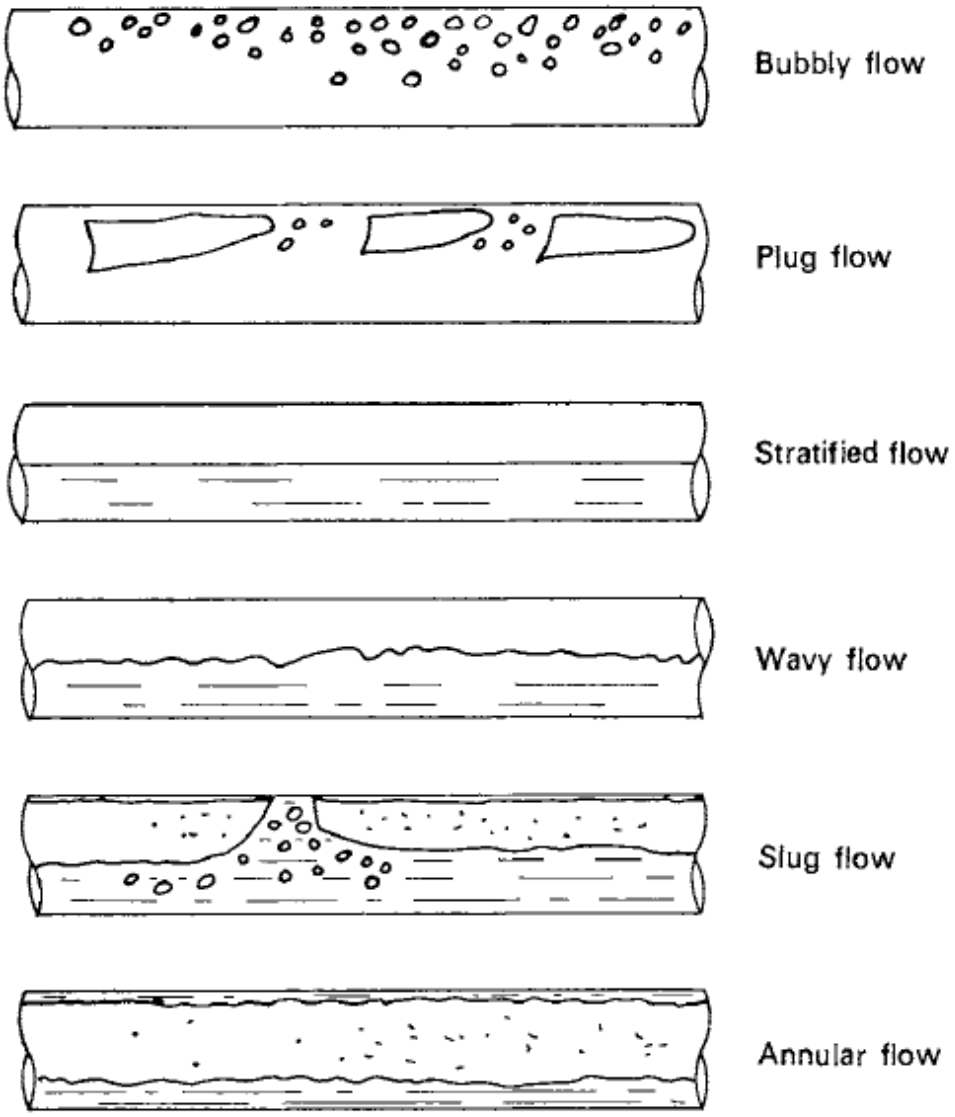

Figure (1-6) Flow regimes in horizontal flow, [14]

1.6 Objectives of Present Work

The present work aims to study the effect of using vortex generators with tube banks in line configuration in the heat exchanger for two-phase flow (water and air) to improve heat transfer rate and are described as follows:

1. Investigate the effects of using single-phase and two-phase flow over the tube banks of a heat exchanger.
2. Investigate numerically the thermo-hydraulic performance of heat exchangers with four types of winglets (Delta, Rectangular, Zikzak, and Sinusoidal wavy), with circular and oval tube banks, and common flow upward (CFU) or common flow downward (CFD) configurations.
3. Evaluate experimentally the influence of two types of winglets (Delta and Rectangular) with oval tube banks and common flow downward (CFD) configuration on the thermo-hydraulic performance of a heat exchanger.
4. Investigate numerically and experimentally the impact of various attack angles (15^o, 20^o, and 25^o) for winglets on the thermo-hydraulic performance of heat exchangers.

1.7 Motivations of Present Work

The purposes of the performance enhancements in heat transfer coefficient is to increase the overall heat convection and minimize the size and expense of the heat exchanger and are described as follows:

1. Vortex generation winglets are used to enhance heat transfer coefficient.
2. Two-phase flow is used to reduce pressure losses in the duct at high flow velocities. Putting winglets inside the duct increases the heat transfer rate since the pressure drop must be minimized to prevent incurring additional costs.

1.8 Plan of the Present Work

1. Numerical work focuses on Computational Fluid Dynamics (ANSYS FLUENT 19) used to predict water and airflow as two-phase flow and temperature fields in the heat exchanger. The Navier-Stokes equations for Continuity, Momentum, and Energy equations are solved numerically to accomplish present work.

2. Experimental requires numerous procedures, including the design and manufacture of the test section (rectangular duct) and the fabrication of the experimental rig including of all the required apparatuses and instruments. The working fluid is monitored of density, viscosity, temperature at the inlet and outlet of the duct, surface temperature of tube banks, and pressure at the inlet and outlet of the duct. In addition, the heat transfer coefficient and the Nusselt number must be measured.

CHAPTER TWO
LITERATURE REVIEW

2.1 Introduction

Enhancement of forced convection occurs when the heat transfer coefficient is increased, and the pressure penalty is reduced in the fluid flow across banks of tubes in (HEs) using a longitudinal vortex generators (LVGs) arrangement. Different shapes of vortex generators for flow through banks of the tubes heat exchanger are used. This review contains numerical and experimental studies interested in the heat transfer rate of banks of tubes with used (LVGs) studied under laminar and turbulent flow conditions. This chapter also includes the thermo-hydraulic performance parameters of (VGs) with tube banks for fluid flow in the duct are studied experimentally and numerically. Vortices motions induced by (VGs) build up the best fluid mixture, increasing the heat transfer rate.

2.2 Theoretical Studies

Biswas, et al. (1994), [15], studied numerically the flow structure and heat transfer improvement in a channel with an included circular tube and a winglet-type vortex generator. A modified version of Marker and Cell method has been employed to solve the equations. The geometrical configuration illustrated a component of a air-water cross-flow fin-tube heat exchanger. In the absence of a winglet-type vortex generator, relatively little heat transfer occured in the low-velocity fluid recirculation zone downstream of the circular tube. The flow field for ($500 \leq Re \leq 1000$) was found to be periodic, hence the heat transfer results are time avcragcd values. However, when a winglet-type longitudinal vortex generator was present in the wake zone behind the cylinder, heat transfer in this region was increased by as much as (240%). The results demonstrated a significant increase in overall

channel heat transfer. This improvement showed great promised for significantly reducing the size of heat exchangers.

Tiwari, et al. (2003), [7], showed numerically the impact of a single-row duct of banks of tubes of circular and elliptic shape with a pair of (VGs) was increased by 81% in the heat transfer rate can be obtained by comparing it with the channel work without (VGs). A three-dimensional study of laminar flow and heat transfer in a channel with built-in oval tube and delta winglets was carried out through the solution of the complete Navier–Stokes and energy equations using a body-fitted grid and a finite-volume method. Furthermore, when adding one pair of wings, vortex generators increased the heat transfer rate by (147%) compared to the planar duct. However, it also had reached that at (Re = 1000), for four pairs of (VGs) with interior wings pairs in the (CFU) and exterior wings pairs in the common flow downward stream with elliptical tubes. That result in a (100%) greater rate of heat transfer augmentation compared with the flow in the duct, which no use (VGs) pairs.

Hiravennavar, et al. (2007), [16], studied the impact of Delta winglets (VGs) on thermo-hydraulic performance numerically by solving the unsteady, three-dimensional, incompressible Navier–Strokes equations and energy equation using a modified Marker and Cell method. Air was used as working fluid. A delta winglet pair type vortex generator was placed in a hydrodynamically developed and thermally developing laminar channel flow and the computations are carried out at (Re = 790, 1000, 1580, 2000). It found that flow in a duct with single winglets and paired winglets augmented thermo-hydraulic performance by (33%) and (67%) compared to the duct without winglets.

Chu, et al. (2009), [17], studied (3-D) numerical for thermo-hydraulic performance in banks of oval-tube (HE) using VGs. The Navier–Stokes and energy equations and the boundary conditions equations are solved by using a

computational fluid dynamics code (FLUENT). For (Re) number instituted on the hydraulic diameter in the range (500–2500), it was forming that the intermediate Nusselt number for three rows of banks of the oval-tube (HE) with using augmented by (13.6–32.9)%; however, pressure drop also increased by (29.2–40.6)%. Three geometrical characteristics position of (VGs) (CFU) and (CFD), a row of banks of oval-tube number of the row was (n = 2, 3, 4 and 5) and angles of attack ($\alpha = 15^o$, 30^o, 45^o and 60^o) were also researched for characteristics optimisation. The (LVGs) with the position of (CFD), minimum tube row number and angles of attack ($\alpha = 30^o$) gave the better performance of (HE) by augmented in heat transfer rate.

Chu, et al. (2009), [18], reported numerically thermo-hydraulic performance in the fin-tube (HE) featuring a pair of rectangular winglets (RWP). The Navier–Stokes and energy equations with the boundary condition equations are solved by using a computational fluid dynamics code (FLUENT). For Reynolds numbers range (500-880), without (RWP) design was compared to three upgraded arrangements with (RWP): the aligned (1RWP) situation, the aligned (3RWP) situation, and the aligned (7RWP) situation. The air-side heat transfer coefficient enhanced by (28.1–43.9)%, (71.3–87.6)%, and (98.9–131)% for the three improved arrangements, with a pressure loss penalty rised of (11.3–25.1)%, (54.4–72.0)%, and (88.8–121.4)%, respectively. Among the three upgraded arrangements, the aligned-(1RWP) situation achieves the best overall performance, followed by the aligned-(3RWP) situation and the aligned-(7RWP) situation.

Ramadan, (2012), [19], investigated numerically for two-dimensional fluid flow across a staggered three-row oval-tube bank with rectangular (LVGs) left in each tube. The characteristics of average Nu number and skin friction coefficient are studied numerically by the aid of the computational fluid dynamics commercial code of FLUENT (6.3). The Reynolds numbers range (250 –1500), (x)-axis locations 3 and 2, and attack angles of (30^o and 45^o)on

(RVGs) were investigated. The emphasis of this investigation was the impact of the various VG shapes on the thermo-hydraulic performance of three rows of oval tube banks. The results demonstrated an increase in heat transfer and the coefficient of skin friction with increased (Re) number and decreased relative distance between (LVG) sites. Observations indicated the overall Nu_{av} number of three oval tubes improved by (10–20.4)% and by (10.4–27.4)% with angles of attack (30^o and 45^o), respectively, with an increased in the friction factor of three oval tubes approaching (53%) and (72%), respectively, compared to the situation without (VGs).

He, et al. (2013), [20], studied numerically the heat transfer improvement and pressure loss penalty for fin-and-tube heat exchangers with rectangular winglet pairs (RWPs) in a relatively low Reynolds number flow. In order to improved heat transfer, the (RWPs) was positioned in a certain orientation. undary condition equations are solved by using a computational fluid dynamics code (FLUENT). For the Reynolds number range (575-880), the overall performance of the (7-RWPs) case was inferior to the other cases. The results indicate that the heat transfer enhancement caused by (RWPs) outweighs the form drag introduced by the RWPs themselves at a relatively high Reynolds number. For (Re > 815), the single-RWPs case increased the (*j/f)* ratio by (1.7 - 2.7)% and the (3-RWPs) case improved the (*j/f)* ratio by (0.7 - 2.0)%.

Gholami, et al. (2014), [21], researched a numerical solution with the wavy rectangular winglet of continuity, momentum, and energy equations resolving by using FLUENT ANSYS (14). The effect of the Reynolds range (400-800) with longitudinal wavy rectangular winglets at a (30°) angle was investigated. The outcomes offered that the rectangular wavy obstacle turbulence can enhance the heat transfer rate of banks of tube (HEs) with a reasonable pressure drop and a better impact on the thermo-hydraulic

performance. This raised was more critical for the case of the wavy obstacle turbulence in (CFU) arrangement.

Albdoor, (2014), [22], investigated numerically the impact of (VGs) across banks of tube (HE) with various forms on thermo-hydraulic performance. A computational fluid dynamics code (FLUENT) was used to solve steady (2-D) Navier- Stokes and energy equations. (k-ε) model used to remedy the turbulent effects. Three different-shaped VGs were installed behind tubes with Reynolds numbers range (7000-11000). The effects of three winglet shapes (airfoil, rectangle, and triangle) with varied attack angles (30° and 45°) on average Nusselt number (Nu), friction factor, and pressure loss are examined. Using winglet pairs affects heat transfer, friction factor, and pressure loss, and heat transfer enhancement depended on the shape and angle of attack of the winglet. The triangle was the optimal shape for maximizing heat transfer, and an angle of attack (45°) was optimal for maximizing heat transfer.

Jedsadaratanachai and Boonloi, (2015), [23], evaluated numerically the heat transfer improvement, and flow arrangements of the fin-oval tube (HE) with (DVGs). (DVGs) similar to (V-ribs) were put on surfaces of the fin with the Vtip facing upstream, referred to as (CFU). The convective terms in the governing equations for momentum and energy were discretized with Powerlaw scheme and QUICK scheme, respectively. The SIMPLE algorithm has been applied on the coupling among pressure and velocity .The impacts angles of attack ($\alpha = 15^o$, 30^o, 45^o, and 60^o) and the pitch between the V tip and the center of the oval tube in the transverse distance (a = 3.77, 4.77, and 5.77 mm) on thermo-hydraulic performance are examined for (Re) numbers range (500-2500), based on the hydraulic diameter of the test duct. By (VG) flow and swirl flow across the test duct, it was discovered that (DVGs) can aid to improved thermo-hydraulic performance. In addition, increased in heat transfer and friction factor range from (1.15) to (1.55) and (1.5) to (3.4) times

the basic scenario, respectively. At (Re = 2500), (a = 5.77 mm), and (α= 15^{o}), the highest heat transfer coefficient enhancement approached (1.12).

Lu and Zhou, (2016), [24], analyzed numerically the thermal and flow properties of plane and curved longitudinal vortex generators (LVGs). The mathematical model of the air channel fitted with LVGs was solved using FLUENT (6.2) program. The Laminar model and RNG k-ε model are applied for laminar flow and turbulent flow, respectively. In a channel flow with (Re) range (700-2650) embedded with a pair of the flat and curved delta, trapezoidal, and rectangular winglet (LVGs), numerical simulations in three dimensions were performed. According to the results, the curved trapezoidal winglet pair (CTWP) gavethe optimum thermo-hydraulic performance. It was found that the (Nu_m/Nu_{m0}) of plane (VGs) was a little higher than that of corresponding curved ones for all (Re) and the deviation of (Nu_m/Nu_{m0}) between (TWP) and (CTWP) was as high as (3.5%) at (Re = 3000). (RWP) has the highest (Nu_m/Nu_{m0}) ranging between (1.21) and (1.42) followed by (TWP) and (DWP) successively.

Wanling, et al. (2017), [25], studied numerically the impact of three various shapes of (LVGs) such as rectangular, trapezoid and Delta winglets on thermo-hydraulic performance numerically and the swirling flow rate of banks of the tube (HE). The coupling of velocity and pressure was handled by the SIMPLE algorithm, within this algorithm, the momentum equations and pressure correction equation were solved sequentially and iterated to convergence. For studied (Re) range (200-1800), compared with the plain fn case, Nu increases about 3.1–14.4%, 1.7–6.3% and 2.1–8.8% for the cases with delta winglet (VGs), rectangular winglet (VGs) and trapezoid winglet (VGs), respectively. The outcomes offered that the overall average (*Nu*) augmentation corresponds to pressure drop due to its Reynolds number growth. Under the corresponding pumping power restrictions, this study

found that the optimum configuration of the (LVGs) was the Delta winglet for the research cases.

Naik and Tiwari, (2018), [26], investigate numerically the impact of winglet placement on the heat transfer properties of fin tube (HEs) with aligned tube configuration. The mathematical model was solved using commercial software ANSYS ICEM (17.2). Their work investigated RWVGs pair with a flow-down arrangement. Initially, the effects of various probable sites of (RWVGs), angles of attack range (15^o - 60^o), and (Re) number range (2000-4000) were examined. (*j/f*) was greater for upstream-placed (RWPs) because to lower pressure drop than for (RWVGs) mounted in other places. The value of (*j/f*) was greatest for the (RWVGs) positioned at (X = -2.0, Y = -1.25), and a (37.6%) improvement in heat transfer was observed in comparison to the configuration without (RWVGs).

Modi and Rathod (2019) [4] evaluated numerically the thermo-hydric performance of the fin-tube (HE) with elliptical curved and sinusoidal wavy kind, Rectangular winglet vortex generators (RWVG). The numerical analysis of the governing equations was carried out using commercial code ANSYS (16.2). Reynolds number range (400-1000) were examined. From the numerical results, it was observed that for Reynolds number (400), inlet and outlet temperature difference (ΔT) was found to be (44.6%) higher for flat and (47.4%) and (46%) higher for wavy – (CFU) and (CFD), and 46.3% and 36.6% higher for curved-up and down (RWVGs), respectively as compared to non-winglet baseline case. In addition, (CFU) wavy (RWVG) had the greatest improvement in heat transfer compared to all other (RWVG) arrangements evaluated. However, the Wavy (CFU) design had the lowest (*j/f*), while the curved (CFD) configuration had the highest (*j/f*) values. Curved (CFD) (RWVG) was shown to be more appropriate than other (RWVG) scenarios.

Haque and Rahman, (2020), [27], presented numerically a (3-dimension) for thermo-hydraulic performance in fluid flow across banks of circular and

elliptic pipes (HE) and used (LVGs). The heat transfer rate characteristics and hydraulic performances are measured numerically by using ANSYS FLUENT (15). It studied that under laminar flow conditions, (Re) was in the range (500-850), which found that the enhancement in heat transfer rate was better affected by the geometric shape of the tube. The heat transfer rate rised by (13 %) when the angle of attack changes from (15º) to (25º). However, pressure drop rises by (62 %) and (40 %) for the circular and elliptic pipes.

Gupta, et al. (2021), [28], investigated numerically the impact of extracting a rectangular winglet (RW) with a hole at the surface of the fin surface on heat transfer improvement and pressure drop in the fin-tube (HE). Their work had been conducted assuming Reynolds numbers in the range (1500-9000) and an angle of attack (45º). Numerical simulations were done using the shear stress transfer (SST) model of turbulence, which proved capable of generating separated flows. There was an increase in heat transfer of up to (34%) for the considered (Re) number range in the case of employed a punched rectangular winglet with the hole in a (CFU) arrangement in the upstream location, as compared to the situation of a without punched RW with the hole in the same arrangement and position. The results demonstrated that piercing an (RW) with a hole significantly enhanced the heat transfer coefficient and pressure drop of a winglet installed in a typical (CFU) arrangement at an upstream position.

Naik and Tiwari, (2021), [29], presented numerically a technique for performance evaluation of convective heat transfer augmentation devices including fin-tube heat exchangers. Three-dimensional numerical computations of highly complex flows in RWP mounted fintube heat exchanger were performed in ANSYS FLUENT (17.2). Turbulent flow conditions are solved by considering realizable (k–ε) two-equation eddy-viscosity turbulence closure. The method focused on quantifying irreversibility caused by rectangular winglet pairs (RWPs) in inline-arranged

fin-tube heat exchangers. Their analysis was enlarged for a few specific places by adjusting the angle of attack (15°-60°). Hence for airflow in a channel with Reynolds number range (2000-4000). The outcome for several (RWP) placements reveals that upstream (RWP) locations gave better performance.

Naik and Tiwari, (2021), [30], investigated numerically the airflow through heated fin-tube heat exchangers with winglet-type vortex generators was undertaken for both inline and staggered arrangements of circular tubes. Three-dimensional numerical computations are performed in ANSYS ICEM (17.2). The flow Reynolds number range (2000-4000). According to the absence of (RWPs), the inclusion of (RWPs) in an inline configuration increases heat transfer by a maximum of (39.6%), while the pressure loss increases by a significant (60.2%). In the event of a staggered arrangement, the presence of (RWPs) resulted in a maximum (29.4%) increased in heat transfer and a (22.1%) decreased in pressure. (RWPs) positioned upstream and distant from the tubes produce the highest (*j/f*) value due to a combination of increased heat transfer enhancement and decreased flow loss. For both inline and staggered situations, downstream (RWP) positions offer more overall heat transfer, but upstream (RWP) locations offered greater overall heat transfer from the bottom fin surfaces.

Wang, et al. (2021), [31], investigated numerically the effect of (VGs) on the heat transfer improvement and pressure loss of elliptical fin and tube (HEs) at angles of inclination ranged (15°-75°). As the working fluid in this investigation, transition regime airflow was chosen. To solve the non-closure of the fundamental turbulence equations, Reynolds numbers at the inlet range (1300-2100), and the shear stress transport (SST) model of turbulence was chosen. The ellipticity ratios of the analysis tubes range between (0.6) and (1.0). The efficiency coefficients for a (15°) (VG) angle of inclination for (0.6, 0.7, 0.8, and 0.9) ellipticity ratios are found to be greater than in the

comparable cases without (VGs). Therefore, from their study, it was concluded that the fin-and-elliptical tube heat exchanger with vortex generators at 15° inclination angles exhibit better performance.

Shi, et al. (2021), [32], investigated numerically the effect of the longitudinal placement of a curved delta winglet vortex generator (CDWVGs) on the thermo-hydraulic enhancement of the fin-tube (HE). The incompressible air in the flow channel is in steady-state without considering viscous dissipation. The Renormalization Group (k–ε) model can predict the flow and heat transfer accurately in the flow channel with (VGs) and was adopted for the turbulent flow. The range of Reynolds numbers range (600-5000) was studied. Compared to the plain fin and the original placement the friction coefficient increased by (12.2%–15.7%) and (4.8%–12.2%) at the best site, while the (Nu) enhanced by (15.2%–43.9%) and (5.4%–9.8%). The heat transfer coefficient of the ideal LVGs site rised by (8.1%), reached a maximum of (1.38). The (CDWVGs) had a lower pressure loss than its straight counterpart. The results are useful for developing and optimizing the finned tube (HE) with (CDWVGs) that were investigated.

Xie and Lee, (2022), [33], tested numerically the heat transfer and pressure drop of three (CRVGs) (VG 1, VG 2, and VG 3) in a fin and tube (HE). By employing VGs. Three-dimensional governing equations are discretized by the finite volume method and solved using the commercial software ANSYS FLUENT 19.2. Three tube row numbers (3, 4, 5) and six inlet velocities (1.0, 2.5, 3.75, 5.0, 6.25, and 7.5 m/s) with Reynolds numbers range (1369-10269). Significantly increased secondary flow and interaction between the temperature zones and flow, hence enhancing the heat transfer performance. By increasing the number of tube rows from three to five, the overall (Nu) number for all (VG) situations increased. For all (VG) designs, the arrangement with tube row number 3 was the most successful in terms of per-tube heat rejection augmentation. The results reveal that (VG 2) satisfies

the heat transfer and pressure drop and volume quality standards with the greatest equilibrium. The obtained thermal and volume goodness enhancement factors by (VG 2) reach as high as (1.42) and (1.24), respectively, manifesting its potential for the development of highperformance and compact heat exchangers

2.3 Experimental Studies

Feibig, et al. (1991), [34], investigated experimentally the heat transfer improvement and drag effect by delta and rectangular wings and winglets in laminar duct flow and found that the heat transfer improvement per unit vortex generator area was highest for delta wings closely followed by delta winglets; rectangular wings and winglets were less effective. The Reynolds number in this study lies range (1000-2000). The average heat transfer was increased by more than (50%) and the corresponding increase of drag coefficient was up to (45%)**.**

Garimella and Eibeck, (1991), [35], observed experimentally the heat transfer enhancement by a half delta wing was shown to grow with a rised Reynolds number in the laminar zone (up to 40%) but decreased to the order of 5% in the turbulent regime in air flow. The Reynolds number range (800-5500). Also, the enhancement was greater at the larger channel height. There was only a small increase in pressure drop due to the introduction of the vortex generators, when compared to staggering the elements, but the heat transfer enhancement was also lower and more localized with the vortex generators.

Tiggelbeck, et al. (1993), [36], investigated experimentally the flow structure, heat transfer, and drag by longitudinal vortices formed by double rows of delta winglets in transition channel flow to reduce the air-side heat transfer resistance of compact heat exchangers. The Reynolds number range (2000-8000). The investigations consist of flow visualization using laser light

sheets, liquid crystal thermography for local heat transfer, and drag measurements using a balance, as shown in Figure(2-1). The improvement of heat transfer was greater for aligned delta winglet double rows than for staggered rows. The angle of attack necessary for the production of longitudinal vortices was smaller behind the second row than it was behind the first. On walls, (40) times the size of the winglet, improvements in heat transfer of (80%) and increased in pressure drop of (160%) were observed. Higher Reynolds numbers result in a greater ratio of heat transfer improvement to increased drag.

Fiebig, et al. (1994), [37], carried out experimentally the impact of (VGs) on the heat transfer and pressure drop in the fin-tube (HEs) for Reynolds numbers range (600-3000). For the staggered tube configuration, it findings indicate that (HE) elements with round tubes and (VGs) enhanced heat transfer by about (10%), whereas flat tubes increase heat transfer by roughly (100%). In addition, it found that the pressure loss in a plane tube bank with a VG was approximately half that of a round tube bank with a (VG).

Gentry and Jacobi, (1997), [38], studied experimentally the increased of heat transfer rate by different (VGs) attached to a flat plate's leading edge. wing-chord length-optimal delta-wing designs were determined for Reynolds numbers of (600, 800, and 1000) with used a straightforward method for calculating this parameter from flow visualisation data. The median heat transfer across the plate's surface was increased by (50–60)% using delta-wing (VGs). The attack angle was measured between the plate and the lean of the delta. A delta-wing was equivalent to an isosceles triangle placed symmetrically to the flow. A delta-winglet, in contrast side, represents a right-angled triangle (or half delta) placed perpendicular to the plate, but at an incident, angle calculated parallel to the input flow. In this study, the attack angles were changed from (25^{o}) to (55^{o}), with the optimal improvement happening at (40^{o}).

Wang, et al. (2002), [39], illustrated the flow structure of an improved fin-and-tube heat exchanger with annular and delta winglet vortex generators. For the same winglet height, the delta winglet indicated more intense vertical motion and flow unsteadiness than the annular winglet; nevertheless, the pressure drop associated with the delta winglet was less than that of the annular winglet and Reynolds numbers range (500-2500). The frictional penalty of the proposed vortex generators was about (10–65)% higher than that of the plain fin geometry. The penalty of pressure drops of the proposed vortex generators to plain fin geometry was relatively insensitive to change of Reynolds number.

Torii, et al. (2002), [40], reported a technology that improved heat transfer and reduce pressure loss in a fin-tube heat exchanger with circular tubes in a relatively low Reynolds number flow by employing delta winglet-type vortex generators. For the objective of enhancing heat transfer, the winglets are arranged in a hitherto unexplored orientation. This design was known as the "common flow up" orientation. The proposed arrangement significantly delayed separation, minimized form drag, and eliminated the zone of poor heat transmission near the tubes' wake. In the case of staggered tube banks, the heat transfer was increased by (30%) to (10%), while the pressure loss was decreased by (55%) to (34%) for Reynolds numbers range (350-2100) (based on two times channel height). In the case of in-line tube banks, while the pressure loss was decreased by (55%) to (34%). In the case of in-line tube banks, heat transfer was increased by (20%) to (10%) while the pressure loss was decreased 15% to 8%.

Kim and Yang, (2002), [41], investigated experimentally the flow and heat transfer characteristics of a pair of delta winglet (VGs) were performed at a (Re = 31 400). In order to control the strength of longitudinal vortices, angle of attack of the vortex generators was varied from ($\pm 20^{o}$ to $\pm 45^{o}$), and the spacing between the vortex generators was (4 cm) apart. For the common-

flow-down cases, two maximum values in the local heat transfer distributions exist for the three angles of attack. With the common-flow-up cases, only one maximum value exists. Based on the findings, the common-flow-down arrangement of (VGs) better heat transfer characteristics than the common-flow-up cases.

Pesteei, et al. (2005), [42], studied experimentally exiting the heat transfer coefficient and pressure drop on the fin-tube (HE) with (WVGs) utilizing a single (2-inch) diameter heater and five different placements of (WVGs). The measurements were performed at a (Re = 2250). Utilizing (WVGs) significantly increased heat transfer. In comparison to a standard fin tube (HE), the average (Nu) enhanced by around (46%), while the local heat transfer coefficient enhanced by multiple orders of magnitude. The optimal placement of the winglets occurred when (X = 0.5D) and (Y = 0.5D). The rised in pressure loss under the current circumstance was around (18%).

Kwak, et al. (2005), [43], compared experimentally the performance of winglet vortex generators with common-flow-up and common-flow-down designs. For the three-row tube bundle in a staggered arrangement with winglet pairs, the heat transfer enhancement was (5–15)% more and the pressure loss penalty was (2–10)% greater compared to fin-tube bundles without winglets. Heat transfer enhancement and pressure-loss reduction with winglet-type vortex generators for fin-tube heat exchangers, winglet pairs built only in the first transverse row of a three-row tube bundle in a staggered arrangement successfully increased heat transfer by (10–30)% and reduced pressure loss by (34–55)% for Reynolds numbers range (350-2100). In comparison to a single transverse row of winglet pairs, heat transfer and pressure loss were increased by (6–15)% and (61–117)%, respectively, in the staggered arrangement. For an in-line configuration with two rows of winglets, the respective increased were (7–9)% and (3–9)%.

Allison and Dally, (2007), [44], reported an experimental work on the impacts of (DWVGs) on the operation of the fin-tube (HE). The water flow Reynolds numbers based on the hydraulic diameter range (2500-7500). The winglets used to have a flow-up configuration and were placed immediately upstream of the tube. The winglet surface was found to have (87%) of the louvre fin surface's heat transfer capacity but only (53%) of the pressure loss. It was determined that the heat transfer of the two surfaces of the fin differ greatly. The delta winglet fin has a less leading edge and primarily relies on increased heat transfer via vortex production. Based on the findings, the louvre fin was preferable to the delta vortex fin. Although vortices are produced by the first row of vortexes, the vortices produced by the winglets in the second row are of the same magnitude. This means that only the first row of vortexes may be useful for generating vortices that can enhance heat transfer.

Joardar and Jacobi, (2008), [45], studied experimentally the performance of winglet arrays in a full-scale heat exchanger. Based on the findings, the winglets placed in common-flow-up orientation could improved wake management The effectiveness of a (3VG) alternate-tube inline array of vortex generators was compared to a single-row vortex generator design and the baseline configuration. The winglets are placed in a common-flow-up orientation for improved tube wake management. The overall heat transfer and pressure drop performance are assessed under dry-surface conditions over a Reynolds number range based on hydraulic diameter range (220-960). It was found that the air-side heat transfer coefficient increased from (16.5%) to (44%) for the single-row winglet arrangement with an increased in pressure drop of less than (12%). For the three-row vortex generator array, the enhancement in heat transfer coefficient increased with Reynolds number from (29.9%) to (68.8%) with a pressure drop penalty from (26%) at (Re = 960) to (87.5%) at (Re = 220).

Lawson and Thole, (2008), [46], investigated experimentally the heat transfer enhancement by delta winglets on the tube surface of louvred fin heat exchangers, which induced the formation of stream-wise vortices and enhanced heat transfer between air flow and the surface on which the Delta winglets are placed for Reynolds numbers of (216, 577, and 955). Based on the findings, the addition of delta winglets to louvred fins increased heat transfer along the tube wall by up to (47%), accompanied by a (19%) rised in pressure losses. Comparisons of measured heat transfer coefficients with and without piercings demonstrated that piercings decreased average heat transfer enhancements, but considerable increased still occur in comparison to the absence of winglets.

Zhou and Ye, (2012), [5], studied experimentally by comparing traditional Delta winglets and Curved Trapezoidal winglets (CTW) and longitudinal rectangular obstacle turbulence, Delta (VGs) and Trapezoidal (VGs). Reynolds numbers range (700-26800) covered the laminar, transitional and turbulent region. The experiment was conducted in an air channel which was heated by hot water with counter-flow design. It found that Delta (VGs) pairs produced the best execution in the Transitional flow region and Laminar; however, curved trapezoidal winglets produced a higher heat transfer rate in the turbulent flow region. An appropriate spacing between the leading edges of a pair of (CTWVG) should be considered for different flow regions. In addition, double rows of (CTWP) do not showed better thermohydraulic performance due to the larger pressure drop and the spacing between the two rows of (CTWP) should also be optimized.

Kattea, (2012), [47], carried out an experimental investigation of the impact of (VGs) (circular and square) on thermo-hydraulic performance at different positions (X = 0.5, 1.5, 2.5 cm) in front of a (HE) with Reynolds number in the range of ($62000 \leq Re \leq 125000$) and heat flux in the range of (3000-8000) W/m^2. Before the (HE), at a distance of [X_m=0.5 cm], the

circular form has been determined to be the most effective for improving heat transfer. The square was the optimal shape for improved heat transfer at a distance of [X_m=2.5 cm] before the (HE), which was the optimal site for improved heat transfer. Using circular (VGs) improved heat transfer across the (HE) by (56%, 50%, and 36%) at locations (X=0.5, 1.5, and 2.5cm), while square (VGs) improved heat transfer by (39%, 42%, and 51%) at the same locations.

Zhou and Feng, (2014), [48], investigated experimentally the thermo-hydraulic performance of flat and (CWVGs) with and without punched holes. In both laminar and turbulent flow zones, (VGs) with curved winglets (CRWP, CTWP, and CDWP) offer thermo-hydraulic performance improvement than VGs with flat winglets with Reynolds number in the range of ($650 \leq Re \leq 21000$). In all flow areas, (CDWP) had the best heat transfer coefficient, followed by CTWP ($\alpha = 20°$). The punched holes enhanced the heat transfer coefficient of (VGs) and reduced the resistance to flow in all conditions. The hole was punched at a lower location along the vertical axis, and the center line along the lateral axis provides superior heat transfer enhancement and heat transfer performance and pressure loss. The results demonstrated the advantages of employed (VGs) with perforated surfaces and curved winglets to improve heat transfer.

Zdanski, et al. (2015), [49], presented experimentally the influences of vortex generators type Delta obstacle turbulence on the thermo-hydraulic parameters in series banks of the tube with Reynolds number in the range of ($2500 \leq Re \leq 13500$). The effects of the following characteristics on the thermo-hydraulic enhancement are estimated as the main target of this study, the (X) dimension from the bank of tubes to the vortex generators. The actual outcomes showed that the (Nu) increased when utilized (LVGs), being a high increased of nearly (30%). Furthermore, the pressure loss across the pipe banks increased and reached nearly (40%).

Prasopsuk, (2016), [50], studied experimentally the impact of longitudinal rectangular winglets (RW) on the effectiveness of (HEs) with the Reynolds number in the range (4100-26000). The (RW) parametric study includes five winglet to tube height ratios or blockage ratios (b / D = 0.15, 0.2, 0.25 and 0.3) at a single winglet inclination angle (α= 45°) and a pitch ratio (P / D =2). It accomplished that longitudinal rectangular winglet kind (LVGs) produce increased thermo-hydraulic efficiency as contrasted to the case without used (LVGs) with an increase in pressure loss in the duct. The experimental results show that the heat transfer and friction loss for the (RW) insert increased with the increment of pitch ratio. The (*Nu*) for the inserted tube was approximately (3.7–4.3) times higher than that for the smooth tube, while the (*f*) was approximately (19.4–45) times greater. For the studied pitch ratio ranges, the highest thermal enhancement factor of (1.46) was obtained for (pitch ratio = 0.2) at lower Reynolds number.

Syaiful, et al. (2019), [51], investigated experimentally the heat transfer performance and pressure drop of perforations (CDWVGs) in a rectangular duct with the Reynolds number in the range (2000-11000). Their study found that using three pairs of (CDWVGs) with three holes increased the heat transfer rate by up to (78.9%) of the baseline. This value was (27.3%) greater than when utilized a three-hole (VG) for delta winglets. Nonetheless, this enhancement in heat transfer rate was accompanied by a rised in the flow's pressure losses. When compared to the baseline, pressure loss was improved by up to five times with the installation of three pairs of three-hole (CDWVGs). Hole in vortex generators can reduce pressure drop by (35%) for (DWPVGs) and (17%) for (CDWPVGs). Longitudinal vortices generated from (CDWPVGs) were greater than those generated by (DWPVGs) based on visualization results.

Syaiful, et al. (2021), [52], focused on the application of flat and concave (VGs) with and without holes to enhance heat transfer with the Reynolds number in the range (2000-11000). In their study, the number of pairs of (VGs) at the attack angle 20◦ from the main flow direction was altered from one to three pairs for different types of (VGs). The airflow velocity through the duct was changed at (0.2 m/s) intervals between (0.4 and 2.0 m/s). In terms of the total Reynolds number, the usage of concave delta winglets without holes produced the best thermo-hydraulic performance for various pairs of (VGs). At a (Re = 9000), the maximum heat transfer enhancement factor was shown to be (1.42).

2.4 Theoretical and Experimental Studies

Leu, et al. (2004), [53], evaluated thermo-hydraulic performance in plate-fin and tube (HEs) using (VGs) of inclined block shape positioned behind the tubes, as shown in Figure (2-2). For Reynolds numbers for airflow range (400-3000), the impacted of various span angles (30^o, 45^o, and 60^o) are explored in depth. The governing equations are solved numerically using a finite difference formulation. Results suggested that the proposed technique for enhanced heat transfer might generate longitudinal vortices and enhanced thermo-hydraulic performance in wake zones. The scenario which equals (45^o) maximizes heat transfer enhancement. At (Re = 500), the fin area can be reduced by (25%) if embedded (VGs) are utilized instead of conventional fins.

Yousif, (2006), [54], investigated an experimental and numerical on the flow and heat transfer from a heated cylinder by using (rectangular, triangular, trapezium and elliptic) type vortex generators simulation by using finite volumes method where Reynolds number range (7200-14400) with an angle of attack (20°, 26°and 32°). The average heat transfer enhanced (4-15)% by using winglets vortex generators.

Awaad and Al-Khishali, (2012), [55], investigated numerically and experimentally were carried out on the effect of two types of vortex generators (circle cross sectional vortex generators and square cross sectional vortex generators) on the flow field and heat transfer from a duct heater. The flow Reynolds number ranging from ($32000 \leq Re \leq 83000$) with a constant heat flux of (43.09426 KW/m^2). In the numerical investigation, FLUENT package (6.3) was used to solve steady, (3-D) , continuity , momentum and energy equations with standard (k-ε) model was used to remedy the turbulent effects. Circle cross sectional vortex generators (either small or big circle cross sectional vortex generators) and square cross sectional vortex generators shapes were also used in the numerical study. Theoretically program (FLUENT program) shows that the presence of vortex generators (VGs) would save (27%) of heaters power. The experimental results (temperature values, Nusselt number calculations, and effectiveness calculations) of the flow over heaters with (VGs) were compared with the flow over heaters without (VGs), heat transfer around heaters was enhanced by (2.76-4.11)% using big circle cross section vortex generators and it was enhanced by (2.186 -3.75)% using small circle cross section vortex generators while it was enhanced by(1.3 -1.94)% by using square cross section vortex generators, all of these values were for 3rows of (VGs) at (X_d=2cm).

Al-khishali and Ebaid, (2015), [56], studied experimentally and numerically thermo-hydraulic performance augmentation in a rectangular wooden duct with constant heat flux and two different (VGs) forms (circular and square). These (VGs) are identical in size and were positioned in two positions (X_d=1 cm and X_d=2 cm) in front of the heater set for Reynolds numbers range (32000-83000). FLUENT version (6.3) simulates the influence of (VGs) using the (k–ε) turbulent model. The heat flow remained constant and equal to (43.09426 kW/m^2) for all Reynolds number values. The numerical and experimental results indicate that the presence of (VGs)

improved heat transfer. In addition, the numerical results demonstrated a (27%) reduction in heater power with the (VGs). The circular shape enhanced heat transfer by (2.186%) to (3.75 %), whereas the square shape enhanced heat transfer by (1.3%) to (1.9%). Also, the pressure loss at the exit of the duct rised by (166.7%–400)% when (CVGs) were used and by (133.3%–300)% when (SVGs) were utilized.

Hosseini, et al. (2016), [57], evaluated experimentally and numerically the impact of plane plate obstructions and rectangular and triangular bars on the cooling of a hot bar. All simulations are conducted in the Ansis FLUENT 13. Standard (k–ε) model was applied to simulate the turbulent flow of the wind tunnel. In the case of staggered tube banks for Reynolds numbers of (21913, 78787, 143623, and 204354). The results showed that heat transfer improved from (10%) to (30%), while pressure fell from (55%) to (34%). In the case of aligned tube banks and the same Reynolds area, heat transfer increased from (10%) to (20%) while pressure reduced from (15%) to (8%). In addition, this investigation demonstrated the Nusselt augmentation when the Reynolds number rose. In addition, the Nusselt variation relates to the rectangular vortexes that are flat as opposed to other modes.

Abdelatief, et al. (2017), [58], evaluated numerically and experimentally, with the support of the commercial code FLUENT (6.3.26), the impacts of relative positions (X or Y), heights (h_w), and span angle (θ) of (WVGs) on heat transfer performance improvement and pressure drop for (CFD) and/or (CFU) wing-shaped tubes bundle (HEs) for air ($1.85\times10^3 \leq Re \leq 9.7\times10^3$).The results indicated that increased counterclockwise (CFD) or clockwise (CFU) increased the (Nu) number values. (WVGs) with (+5° +45°) exhibited a (34%) to (48%) increased in (Nu) compared to the baseline instance. The lowest values of tube downstream friction coefficient (*f*) were achieved at (+5°) (CFD) and (15°) (CFU) in the baseline condition. From (0°)

to (5°), the upstream tube's (Nu) increased, however from (5°) to (15°), there was no discernible change.

Li, et al. (2018), [59], studied experimentally for normal fin surface with (12) longitudinal obstacle turbulence of Delta winglet over each tube in banks (HEs). Experiences of 4 rows of banks of the tube heat exchanger with actual geometry shape accomplished to contrast the overall properties for a suggested fin with the circular tube and wavy fin with Reynolds number in the range of ($2000 \leq Re \leq 10000$) . Laminar model was used for velocity from (1.5 m/s) to (3.5 m/s), and (k-ω) turbulence model was used for higher velocities. Also, the circular tube heat exchangers have six rows of circular tubes with two wavy fins. It used twelve (LVGs) and ten (LVGs). The inlet velocity of the air side varies from (1.5 m/s) to (7.5m/s), and the water side flow rate was fixed at a certain value at each air inlet velocity. The testing result showed the thermo-hydraulic performance and pressure drop increased by (LVGs) for banks of the tube heat exchanger, which used a fin with the five rows of banks of the tube with a normal fin surface. It can replace the six rows of wavy surface fins for the two surface fins. Also, the (LVGs) increased the Nusselt number for two cases that used the fin surface and the wavy fin surface.

2.5 Summary

The current reviews focused on thermo-hydraulic performance for banks of the tubes heat exchanger with improvement by using different shapes and sizes (VGs) with varying angles of attack and their position. (VGs) are ideal for reducing pressure loss and increasing the heat transfer rate for fluid flow through banks of tube heat exchangers in all numerical and experimental research. The present work shows a review of vortex generator designs in recent decades for their technological importance in the field of heat transfer.

(VGs) play an essential role in the advancement of heat transfer applications. The following summarized essential resulting observations on this review:

1) More efficient thermo-hydraulic performance in a rectangular duct with vortex generators because of low thermal properties on both water and airflow and increased heat transfer rate for (HEs).
2) Vortices are generated by winglets such as Rectangular and Delta winglets. These vortices are induced when the fluid passes through obstacle turbulence. Augmentation in thermo-hydraulic performance was induced in fluid flow within the duct because of more turbulence.
3) An increase in airflow velocity and vortices generation, in that case, reduces pressure throughout the duct because of friction between air particles and duct walls with tube walls which is inversely proportional to the airflow velocity.
4) Researchers used various angles of attack for (VGs) in their studies, which found the moderate angle of attack was an optimum angle.
5) Literature studies focused on the impact of various design characteristics for augmentation in thermo-hydraulic performance in multi-row banks of tubes (HEs) with the use number of vortex Generators at the specified shape and position, with circular and oval tubes row. The oval tube row is used to increase air velocity. This

technique increases thermo-hydraulic performance according to a minimum increase in pressure loss.

Researchers that have been reviewed previously are summarized in the following Table (2-1), as shown below, where they were divided into the numerical, numerical and experimental and experimental research:

Table (2-1) Summary of literature review

Author	Nature of Search	Re range	(VGs) shape type	Objective	Results
Biswas et al. (1994) [15]	Numerical simulation by using modified MAC method	500-1000	DWL VGs	The flow structure and the heat transfer improvement in a channel with an included circular tube and a winglet-type vortex generator	When a winglet-type longitudinal vortex generator was present in the wake zone behind the cylinder, heat transfer in this region was increased by as much as 240%
Tiwari et al. (2003) [7]	Numerical simulation by using Finitevolume scheme	1000	DWL VGs	The impact of a single-row duct of banks of tubes of circular and elliptic shape with a pair of (VGs)	That result in a 100% greater rate of heat transfer augmentation compared with the flow in the duct, which no use (VGs) pairs
Hiravennavar et al. (2007) [16]	Numerical simulation by using modified MAC method	790, 1000, 1580, 2000	DWL VGs	The impact of Delta winglets (VGs) on thermo-hydraulic performance	It found that flow in a duct with single winglets and paired winglets augmented thermo-hydraulic performance by 33% and 67% compared to the duct without winglets
Chu et al. (2009) [17]	Numerical simulation by using FLUENT	500-2500	DWVGs, RWVGs, DWLVGs, RWLVGs	The effect of thermo-hydraulic performance in banks of oval-tube (HE) using VGs	Nusselt number for three rows of banks of the oval-tube (HE) with using augmented by 13.6–32.9%; however, pressure drop also increased by 29.2–40.6%
Chu et al. (2009) [18]	Numerical simulation by using FLUENT	500-880	RWP	The effect of thermo-hydraulic performance in the fin-tube (HE) featuring a pair of rectangular winglets (RWP)	Heat transfer coefficient enhanced by 28.1–43.9%, 71.3–87.6%, and 98.9–131%, with a pressure loss penalty rised of 11.3–25.1%, 54.4–72.0%, and 88.8–121.4%, respectively

Ramadan (2012) [19]	Numerical simulation by using FLUENT	250-1500	WLVGs	The effect of two-dimensional fluid flow across a staggered three-row oval-tube bank with rectangular (LVGs) left in each tube	Nu_{av} number of three oval tubes improved by 10–20.4% and by 10.4–27.4% with angles of attack 30^{o} and 45^{o}, respectively, with an increased in the friction factor of three oval tubes approaching 53% and 72%, respectively
He et al. (2013) [20]	Numerical simulation by using FLUENT	575 -880	RWPs	The heat transfer improvement and pressure loss penalty for fin-and-tube heat exchangers with rectangular winglet pairs (RWPs)	For (Re) > 815, the single-RWPs case increased the (*j/f)* ratio by 1.7 - 2.7% and the 3-RWPs case improved the (*j/f)* ratio by 0.7 - 2.0%
Gholami et al. (2014) [21]	Numerical simulation by using FLUENT	400-800	CRWLVGs	The effect of banks of tube (HEs) with with the wavy rectangular winglet	Enhance the heat transfer rate with a reasonable pressure drop. This raised was more critical for the case of the wavy obstacle turbulence in (CFU) arrangement.
Albdoor (2014) [22]	Numerical simulation by using FLUENT	7000-11000	DWLVGs, RWLVGs, CWLVGs	The impact of (VGs) across banks of tube (HE) with various forms on thermo-hydraulic performance	The DWLVGs was the optimal shape for maximizing heat transfer, and an angle of attack 45° was optimal for maximizing heat transfer.
Jedsadaratanachai and Boonloi (2015) [23]	Numerical simulation by using Powerlaw scheme and QUICK scheme	500-2500	DVGs	The effect of the heat transfer improvement, and flow arrangements of the fin-oval tube HE with (DVGs)	Increased in heat transfer and friction factor range from 1.15 to 1.55 and 1.5 to 3.4 times the basic scenario, respectively

Lu and Zhou (2016) [24]	Numerical simulation by using FLUENT	700-2650	TWP, DWP, CTWP, RWP	The effect of the thermal and flow properties of plane and curved longitudinal vortex generators (LVGs)	The deviation of (Nu_m/Nu_{m0}) between (TWP) and (CTWP) was as high as 3.5% at Re = 3000. (RWP) has the highest (Nu_m/Nu_{m0}) ranging between 1.21 and 1.42 followed by (TWP) and (DWP) successively
Wanling et al. (2017) [25]	Numerical simulation by using the SIMPLE algorithm	200–1800	TWP, DWP, RWP	The impact of three various shapes of (LVGs) on thermo-hydraulic performance for banks of the tube (HE)	compared with the plain fn case, Nu increases about 3.1–14.4%, 1.7–6.3% and 2.1–8.8% for the cases with delta winglet (VGs)
Naik and Tiwari (2018) [26]	Numerical simulation by using commercial software ANSYS ICEM 17.2	2000-4000	RWVGs	The impact of winglet placement on the heat transfer properties of fin tube (HEs) with aligned tube configuration	The value of (*j/f*) was greatest for the (RWVGs) positioned at (X = -2.0, Y = -1.25), and a 37.6% improvement in heat transfer was observed in comparison to the configuration without (RWVGs)
Modi and Rathod (2019) [4]	Numerical simulation by using FLUENT	400-1000	Elliptical curved and sinusoidal wavy kind rectangular winglet vortex generators	The effect of the thermo-hydric performance of the fin-tube (HE) with LVGs	the Wavy (CFU) design had the lowest (*j/f*), while the curved (CFD) configuration had the highest (*j/f*) values. Curved (CFD) (RWVG) was shown to be more appropriate than other (RWVG) scenarios
Haque and Rahman (2020) [27]	Numerical simulation by using FLUENT	500-850	RWPs	The effect of thermo-hydraulic performance in fluid flow across banks of circular and elliptic pipes (HE) and used (LVGs)	The heat transfer rate rised by 13 % when the angle of attack changes from 15º to 25º. However, pressure drop rises by 62 % and 40 % for the circular and elliptic pipes

Gupta et al. (2021) [28]	Numerical simulation by using FLUENT	1500-9000	(RW) with a hole	The impact of a rectangular winglet (RW) with a hole at the surface of the fin surface on heat transfer improvement and pressure drop in the fin-tube (HE)	Piercing an (RW) with a hole significantly enhanced the heat transfer coefficient and pressure drop of a winglet installed in a typical (CFU) arrangement at an upstream position
Naik and Tiwari (2021) [29]	Numerical simulation by using FLUENT	2000-4000	RWPs	Evaluation performance of heat transfer augmentation devices including fin-tube heat exchangers	The outcome for several (RWP) placements reveals that upstream (RWP) locations gave better performance
Naik and Tiwari (2021) [30]	Numerical simulation by using ANSYS ICEM 17.2	2000-4000	RWPs	The effect of the airflow through fin-tube (HE) with WVGs for both inline and staggered arrangements of circular tubes	Staggered arrangement, the presence of (RWPs) resulted in a maximum 29.4% increased in heat transfer and a 22.1% decreased in pressure
Wang et al. (2021) [31]	Numerical simulation by using FLUENT	1300-2100	RWPs	The effect of (VGs) on heat transfer and pressure loss for (HEs) at angles of inclination range (15° -75°)	It was concluded that the fin-and-elliptical tube heat exchanger with vortex generators at 15° inclination angles exhibit better performance
Shi et al. (2021) [32]	Numerical simulation by using FLUENT	600-5000	CDWVGs	The effect of the (CDWVGs) on the thermo-hydraulic of the fin-tube (HE)	The friction coefficient increased by 12.2%–15.7% and 4.8%–12.2%, while the (Nu) enhanced by 15.2%–43.9% and 5.4%–9.8%
Xie and Lee (2022) [33]	Numerical simulation by using FLUENT	1369-10269	CRVGs	The effect of the heat transfer and pressure drop of three (CRVGs) (VG 1, VG 2, and VG 3) in a fin and tube (HE)	The obtained thermal and volume goodness enhancement factors by (VG 2) reach as high as 1.42 and 1.24, respectively

Feibig et al. (1991) [34]	Experimental	1000-2000	Delta and rectangular wings and winglets	The effect of the heat transfer and drag effect by delta and rectangular wings and winglets in duct	The average heat transfer was increased by more than 50% and the corresponding increase of drag coefficient was up to 45%
Garimella and Eibeck (1991) [35]	Experimental	800-5500	Half delta wing	The effect of the heat transfer enhancement by a half delta wing	Small increase in pressure drop due to the introduction of the vortex generators, but the heat transfer enhancement was also lower and more localized with the vortex generators
Tiggelbeck et al. (1993) [36]	Experimental	2000-8000	DWP	The effect of the flow structure, heat transfer, and drag by double rows of delta winglets in channel flow	Improvements in heat transfer of 80% and increased in pressure drop of 160% were observed
Fiebig et al. (1994) [37]	Experimental	600-3000	RWPs	The impact of (VGs) on the heat transfer and pressure drop in the fin-tube (HEs)	Enhanced heat transfer by about 10%, whereas flat tubes increase heat transfer by roughly 100%
Gentry and Jacobi (1997) [38]	Experimental	600, 800, and 1000	Delta-wing	The increased of heat transfer rate by (VGs) attached to a flat plate's leading edge	The median heat transfer across the plate's surface was increased by 50–60% using delta-wing (VGs)
Wang et al. (2002) [39]	Experimental	500-2500	Annular and Delta winglet VGs	Improved fin-and-tube (HE) with annular and delta winglet vortex generators	The frictional penalty of the proposed vortex generators was about 10–65% higher than that of the plain fin geometry

Torii et al. (2002) [40]	Experimental	350-2100	DWVGs	Improved heat transfer and reduce pressure loss in a fin-tube heat exchanger with circular tubes with DWVGs	In the case of staggered tube banks, the heat transfer was increased by 30% to 10%, while the pressure loss was decreased by 55% to 34%. In the case of in-line tube banks, heat transfer was increased by 20% to 10% while the pressure loss was decreased 15% to 8%
Kim and Yang (2002) [41]	Experimental	31 400	DWVGs	The impact of a pair of delta winglet (VGs) on the flow and heat transfer characteristics	In the case of staggered tube the common-flow-down arrangement of (VGs) better heat transfer characteristics than the common-flow-up cases
Pesteei et al. (2005) [42]	Experimental	2250	RWVGs	Exiting the heat transfer coefficient and pressure drop on the fin-tube (HE) with (WVGs)	The average (Nu) enhanced by around 46%, while the local heat transfer coefficient enhanced by multiple orders of magnitude
Kwak et al. (2005) [43]	Experimental	350-2100	RWVGs	The performance of WVGs with common-flow-up and common-flow-down designs	The heat transfer enhancement was 5–15% more and the pressure loss penalty was 2–10% greater compared to fin-tube bundles without winglets
Allison and Dally (2007) [44].	Experimental	2500-7500	DWVGs	The impacts of DWVGs on the operation of the fin-tube HE	The VGs achieved 87% of the louvre fin surface's heat transfer performance but only 53% of the pressure loss

Joardar and Jacobi (2008) [45]	Experimental	220-960	RWVGs	The performance of winglet arrays in a full-scale heat exchanger	Heat transfer coefficient increased from (16.5%) to (44%) for the single-row winglet arrangement with an increased in pressure drop of less than (12%). For the three-row vortex generator array, the enhancement in heat transfer coefficient increased with Reynolds number from (29.9%) to (68.8%) with a pressure drop penalty from (26%) at (Re = 960) to (87.5%) at (Re = 220)
Lawson and Thole, (2008), [46]	Experimental	216, 577, and 955	DWVGs	The heat transfer enhancement by delta winglets on the tube surface of louvred fin heat exchangers	The addition of delta winglets to louvred fins increased heat transfer along the tube wall by up to (47%), accompanied by a (19%) rised in pressure losses
Zhou and Ye, (2012), [5]	Experimental	700-26800	DWVGs, CTWVGs, RWVGs	DWVGs, CTWVGs, RWVGs in an air channel which was heated by hot water with counter-flow design	Double rows of (CTWP) do not showed better thermohydraulic performance due to the larger pressure drop and the spacing between the two rows of (CTWP) should also be optimized

Kattea, (2012), [47]	Experimental	62000 - 125000	(VGs) (circular and square)	Impact of (VGs) (circular and square) on thermo-hydraulic performance at different positions	Circular (VGs) improved heat transfer across the (HE) by (56%, 50%, and 36%) at locations (X=0.5, 1.5, and 2.5cm), while square (VGs) improved heat transfer by (39%, 42%, and 51%) at the same locations
Zhou and Feng, (2014), [48]	Experimental	650 - 21000	CRWP, CTWP, and CDWP with and without punched holes	the thermo-hydraulic performance of flat and (VGs) with and without punched holes	The advantages of employed (VGs) with perforated surfaces and curved winglets to improve heat transfer
Zdanski , et al. (2015), [49]	Experimental	2500 - 13500	DWVGs	The influences of vortex generators type Delta VGs on the thermo-hydraulic parameters in series banks of the tube	The (Nu) increased when utilized (LVGs), being a high increased of nearly (30%). Furthermore, the pressure loss across the pipe banks increased and reached nearly (40%)
Prasopsuk, (2016), [50]	Experimental	4100-26000	RW	The impact of longitudinal rectangular winglets (RW) on the effectiveness of (HEs)	The (Nu) for the inserted tube was approximately (3.7–4.3) times higher than that for the smooth tube, while the (f) was (19.4–45) times greater
Syaiful, et al. (2019), [51]	Experimental	2000-11000	CDWVGs	The heat transfer performance and pressure drop of perforations (CDWVGs) in a rectangular duct	using three pairs of (CDWVGs) with three holes increased the heat transfer rate by up to (78.9%) of the baseline
Syaiful, et al. (2021), [52]	Experimental	2000-11000	Flat and concave (VGs) with and without holes	The application of flat and concave (VGs) with and without holes to enhance heat transfer	The usage of concave DWVGs without holes produced the best thermo-hydraulic performance for various pairs of (VGs)

Leu, et al. (2004), [53]	Numerical simulation by using finite difference formulation and Experimental	400-3000	(VGs) of inclined block shape	Evaluated thermo-hydraulic performance in plate-fin and tube (HEs) using (VGs) of inclined block shape positioned behind the tubes	The scenario which equals (45^o) maximizes heat transfer enhancement. At (Re = 500), the fin area can be reduced by (25%) if embedded (VGs) are utilized instead of conventional fins
Yousif, (2006), [54]	Numerical simulation by using finite volumes method and Experimental	7200-14400	rectangular, triangular, trapezium and elliptic, type vortex generators	Investigated on the flow and heat transfer from a heated cylinder by using (rectangular, triangular, trapezium and elliptic) type vortex generators	The average heat transfer enhanced (4-15)% by using winglets vortex generators
Awaad and Al-Khishali, (2012), [55]	Numerical simulation by using FLUENT and Experimental	32000-83000	Circle cross sectional VGs and square cross sectional VGs	The effect of two types of vortex generators (circle cross sectional vortex generators and square cross sectional vortex generators) on the flow field and heat transfer from a duct heater	Heat transfer around heaters was enhanced by (2.76-4.11)% using big circle cross section vortex generators and it was enhanced by (2.186 - 3.75)% using small circle cross section vortex generators
Al-khishali and Ebaid, (2015), [56]	Numerical simulation by using FLUENT and Experimental	32000-83000	Two different (VGs) forms (circular and square)	Thermo-hydraulic performance augmentation in a rectangular wooden duct with constant heat flux and two different (VGs) forms (circular and square)	(CVGs) enhanced heat transfer by (2.186%) to (3.75 %), whereas (SVGs) enhanced heat transfer by (1.3%) to (1.9%). Also, the pressure loss at the exit of the duct rised by (166.7%–400)% when (CVGs) were used and by (133.3%–300)% when (SVGs) were utilized

Hosseini, et al. (2016), [57]	Numerical simulation by using FLUENT and Experimental	21913, 78787, 143623, and 204354	Plane plate obstructions and rectangular and triangular bars	The impact of plane plate obstructions and rectangular and triangular bars on the cooling of a hot bar	heat transfer improved from (10%) to (30%), while pressure fell from (55%) to (34%)
Abdelatief, et al. (2017), [58]	Numerical simulation by using FLUENT and Experimental	1.85×10^3 - 9.7×10^3	Wing-shaped tubes bundle	The impacts of relative positions (X or Y), heights (h_w), and span angle (θ) of (WVGs) on heat transfer performance improvement and pressure drop for (CFD) and/or (CFU) wing-shaped tubes bundle (HEs)	Indicated that increased counterclockwise (CFD) or clockwise (CFU) increased the (Nu) number values. (WVGs) with (+5° +45°) exhibited a (34%) to (48%) increased in (Nu) compared to the baseline instance
Li, et al. (2018), [59]	Numerical simulation by using FLUENT and Experimental	2000 - 10000	DWVGs	The impacts of fin surface with (12) longitudinal obstacle turbulence of Delta winglet over each tube in banks (HEs)	DWVGs increased the Nusselt number for two cases that used the fin surface and the wavy fin surface
Present Work	Numerical simulation by using FLUENT and Experimental	3639-4813	DWVGs, RWVGs, ZWVGs, SWWVGs	Sigel-phase (water) and two-phase flow (water and air) over bank of the circular or oval tubes with various shapes and arrangement of vortex generators through rectangular duct	

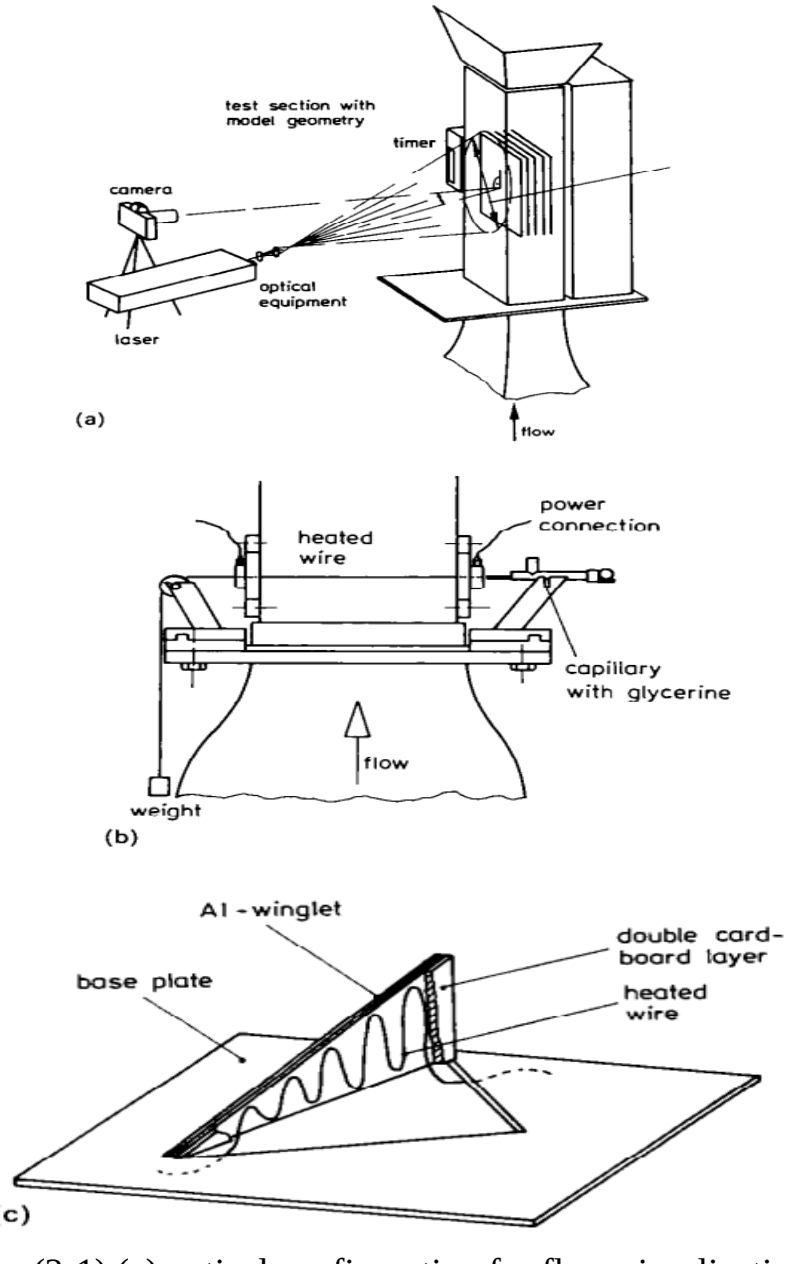

Figure (2-1) (a) optical configuration for flow visualization and smoke techniques (b) smoke wire (c) direct evaporation, [36]

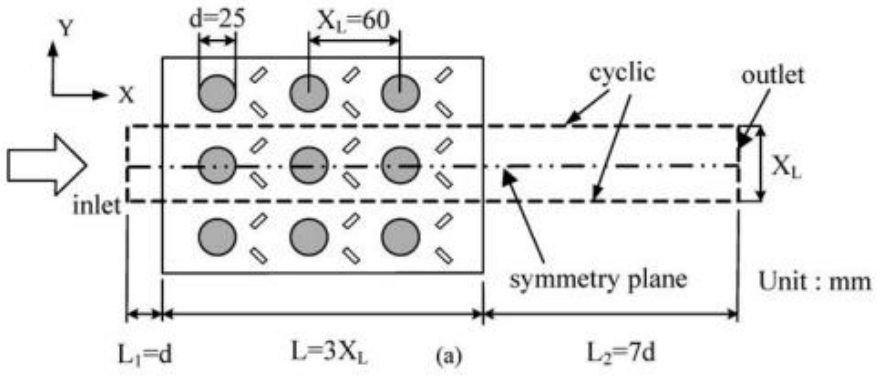

Figure (2-2) The computational domain, [53]

2.6 Novel Points of Present Work

From the above literature, it was concluded that most of the works focused on enhancing the thermo-hydraulic performance by using (VGs) in the tube banks (HEs) under turbulent conditions. Several previous experimental and theoretical studies on different shapes, different locations and varied angles of attack of vortex generators to reach optimum design to the requirement of smaller volume of the heat exchanger, low cost, quiet, and high efficiency in operation, the high-efficiency (HEs) is very necessary to achieve these objectives. The objective of this work are:

1) FLUENT PACKAGE 19 is used to numerically analyse three-dimensional flow to predict temperature difference, heat transfer coefficient, Nusselt number, pressure drop, and velocity distributions for single-phase and two-phase flow over tube banks in the rectangular duct with a vortex generators.
2) Temperature difference, heat transfer coefficient, Nusselt number, pressure drop, and velocity distributions are predicted experimentally for two shapes (Delta and Rectangular) winglets over the bank of oval tubes in a rectangular duct with different water-air flow rates, different locations, varying angles of attack, and common flow upward or common flow downward configurations of vortex generators in order to reach optimum design.

CHAPTER THREE

Mathematical Model and the Numerical Analysis

3.1 Introduction

FLUENT is computational fluid dynamics program for simulating fluid flow problems. It employs the finite volume technique to solve the fluid's governing equations. Workbench (19.0) enables the use of different physical simulations, such as incompressible or compressible, inviscid or viscous, and laminar or turbulent flow. The law of conservation of mass, momentum, and energy governs the fluid problem framework of FLUENT. This law is defined in terms of a discretized partial differential equation based on a finite volume, [60].

The present work deals with the simulation using the commercial code ANSYS FLUENT (19). ANSYS FLUENT predicts temperature distribution, pressure gradient and velocity for single and two-phase flow (water-air) through a bank of circular and oval tubes with and without (VGs). Heat convection coefficient and temperature gradient were investigated in the duct by changing the superficial velocities of water and air with multi shapes and arrangements of the vortex generators.

3.2 The Geometric Model

3.2.1 Modeling the Single and Two-Phase Flow

The characteristics of the problem and boundary condition for the single and two phase-flows can be shown in Figure (3-1). The rectangular duct inlet is represented as the fluid inlet's superficial velocities. Oval tubes wall are exposed to a constant heat flux, while the outlet pressure is represented at the outlet of the rectangular duct. The remaining portion of the duct walls is put to be adiabatic.

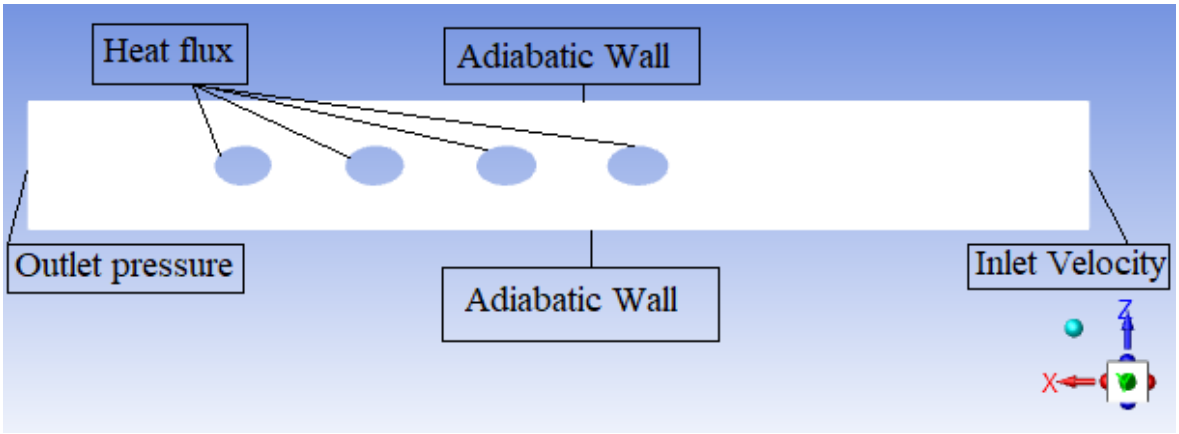

Figure (3-1) Problem Boundary Condition

3.2.2 The Geometry of the Testing Section and Design Considerations

In order to simulate the system, it has been modeled as a (3-D) model by using Solid Works (2018) combined with ANSYS Workbench (19.0). The model has been drawn as a rectangular shape and its dimensions are (12 cm × 2 cm × 100 cm). The geometry of the testing section is set to be fluid as shown in Figure (3-2). All dimensions were taken based on Ref. [27] with scale (1/2) to provide the necessary pressure for the flow and the flow rate of the mixture in the duct. Using the diameter of the tube (D) as the characteristic length scale, all dimensions of the duct are calculated as (L = 10D, W = 1.2D, and H = 0.2D), respectively.

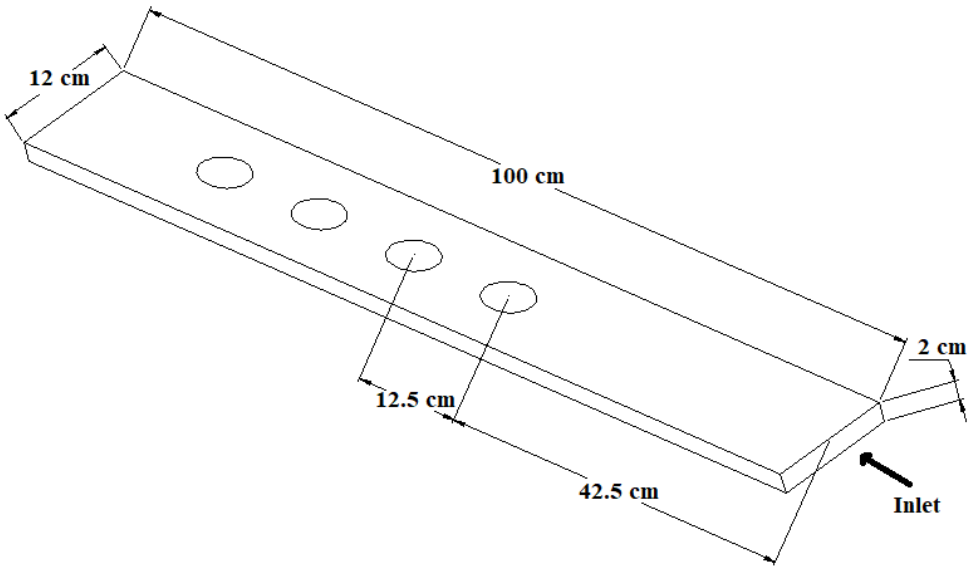

Figure (3-2) Computational domain for test section

3.2.3 Vortex Generators Model

Four models of (LVGs) are used in this simulation and its dimensions are (3 cm × 1cm × 0.1 cm). (LVGs) are placed in the duct to study the behavior of heat transfer and pressure drop. (LVGs) addition has complex effects on the flow pattern and heat convection coefficient, suggesting a numerical investigation. The purpose of evaluating the flow pattern is to determine the optimal (LVG) form and location in the duct. LVGs models are shown in Figure (3-3).

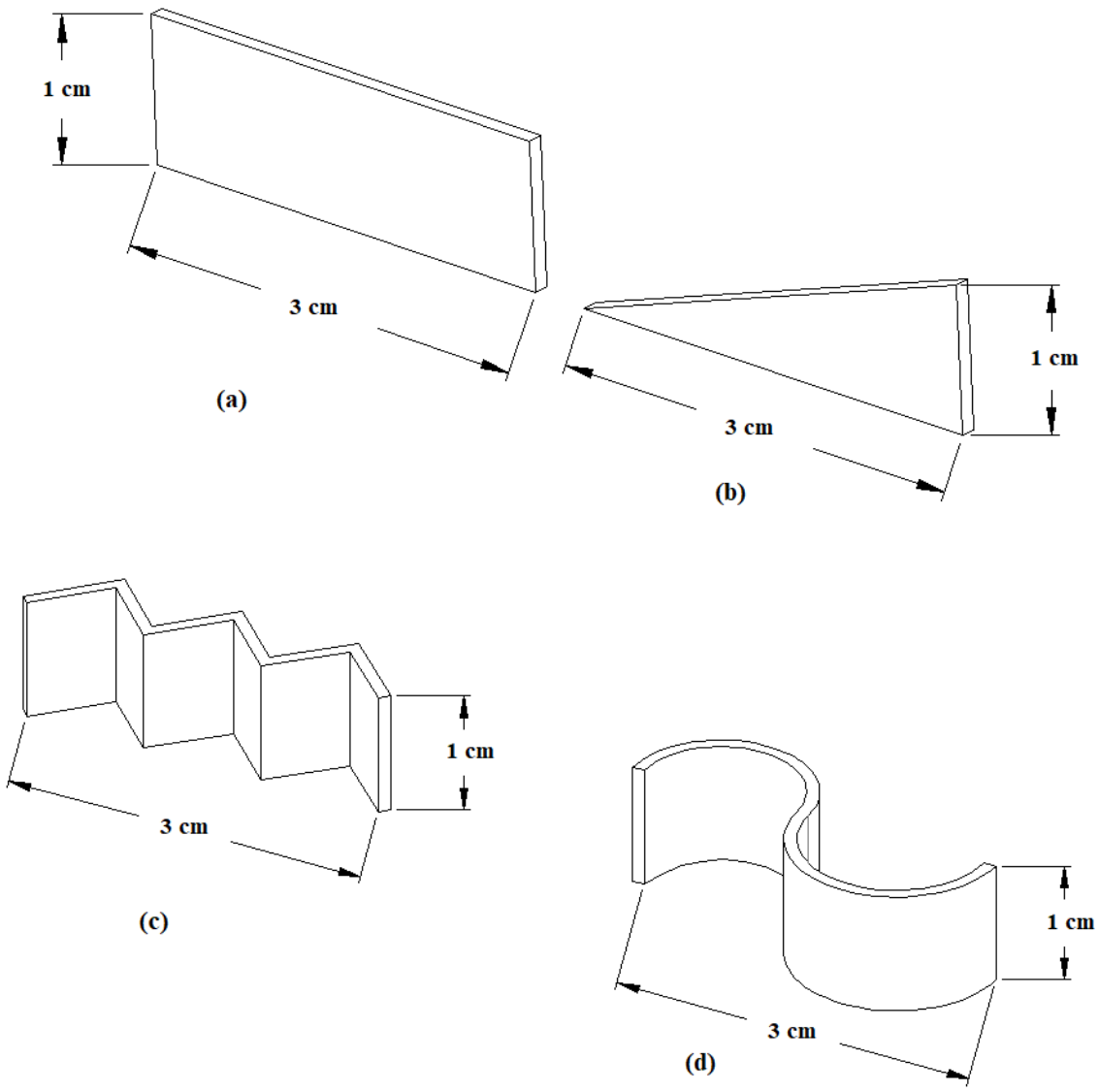

Figure (3-3) (LVGs) models (a) Rectangular (b) Delta (c) Zikzak (d) Sinusoidal wavy

3.2.4 Mesh Generation

Because there are so many mesh types to choose from, it's important to consider factors like flow field, geometry, and complexity when choosing which mesh to use. The required (CPU) time, solution accuracy, and convergence rate are all influenced by the size and kind of mesh, [61].

In this study, the meshing procedure is carried out in the ANSYS Workbench (19.0) application using quadrilateral structured grid elements. The meshing sizes for maximum and minimum meshing sizes are set to be equal (0.001 m) for oval and circular tubes as shown in Figures (3-4) and (3-5) respectively. Tables (3-1) and (3-2) also show how many elements and nodes each situation in this study contains for oval and circular tubes respectively.

Table (3-1) The number of elements and nodes for banks of oval tube

No.	Case	Nodes No.	Elements No.
(a)	Duct without VGs	204309	182760
(b)	Duct with Delta	124721	624332
(c)	Duct with Rectangular	124831	624663
(d)	Duct with Zikzak	124826	624657
(e)	Duct with Sinusoidal	134436	674249

Table (3-2) The number of elements and nodes for banks of circular tubes

No.	Case	Nodes No.	Elements No.
(a)	Duct without VGs	205443	184160
(b)	Duct with Delta	125186	624464
(c)	Duct with Rectangular	125217	624655
(d)	Duct with Zikzak	125359	624988
(e)	Duct with Sinusoidal	134144	670464

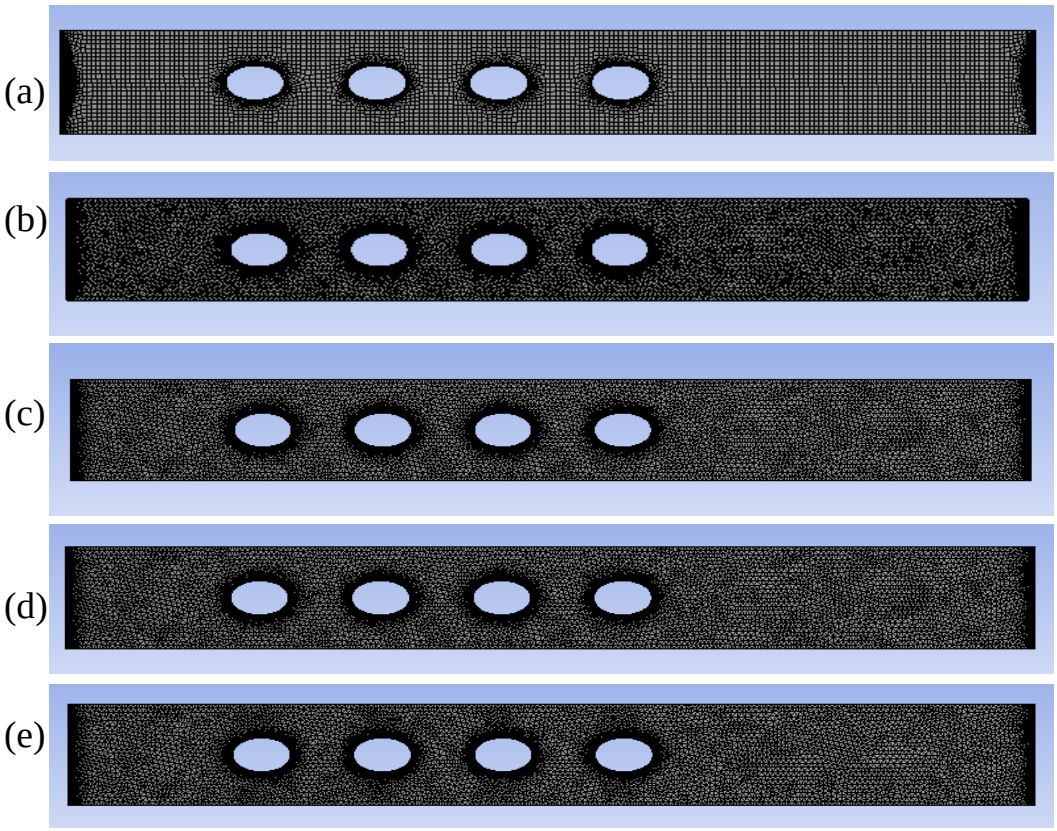

Figure (3-4) The mesh of oval tubes

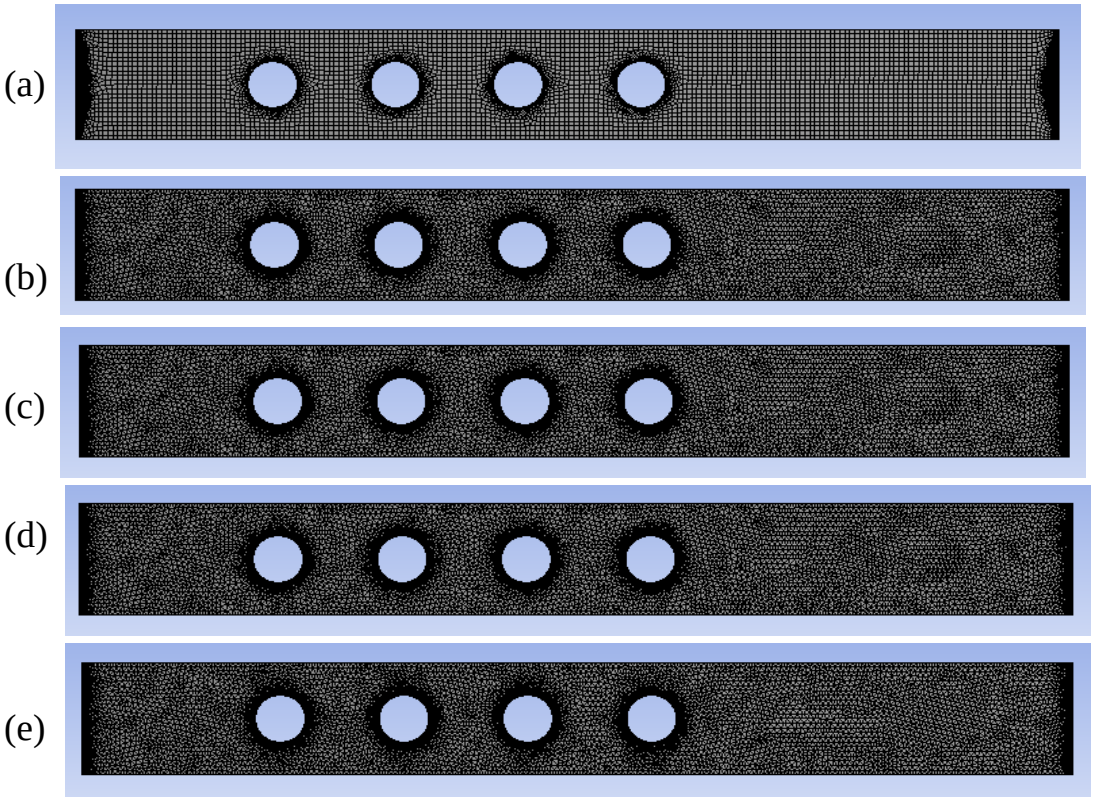

Figure (3-5) The mesh of circular tubes

3.2.5 Grid Independence

A grid-independent solution is required to enhance the precision of the computations. The present work on grid independence consists of three parts: convergence index, grid refinement, and General Richardson. Two various winglet positions relative to the center of each tube are used. For forward ($\Delta X= -1$, $\Delta Y= \pm 4$), downward ($\Delta X= 1$, $\Delta Y= \pm 4$) of each tube with ($\alpha=15^{o}$) and (Re= 3643.5).

A grid refinement was carried out to get a grid-independent solution. Table (3-3) indicates that the result for grid refinements is satisfactory. Case (2) components are employed for the solution domain in this problem. Utilizing additional elements are time-consuming and do not greatly improve the outcome.

Table (3-3) Grid Independence

Case	Elements No.	*Nu*	*Δp* (Pa)	Time rate of Iteration (It. /hr.)
1	485993	8.1	16.3	285.7
2	624332	10.2	18.1	222.2
3	985840	11.7	19.7	133.3
4	1317805	13.5	21	83.3

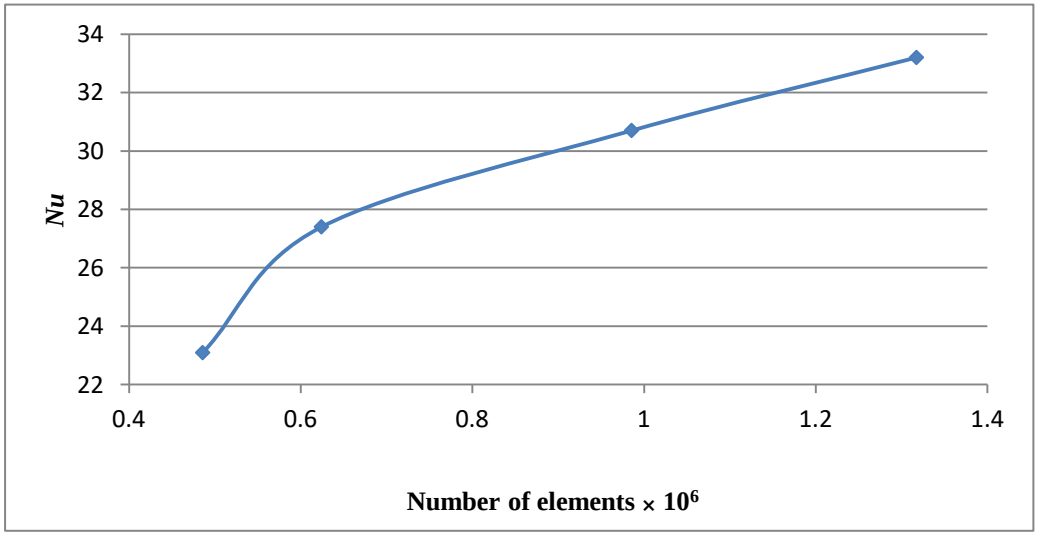

Figure (3-6) Grid independence

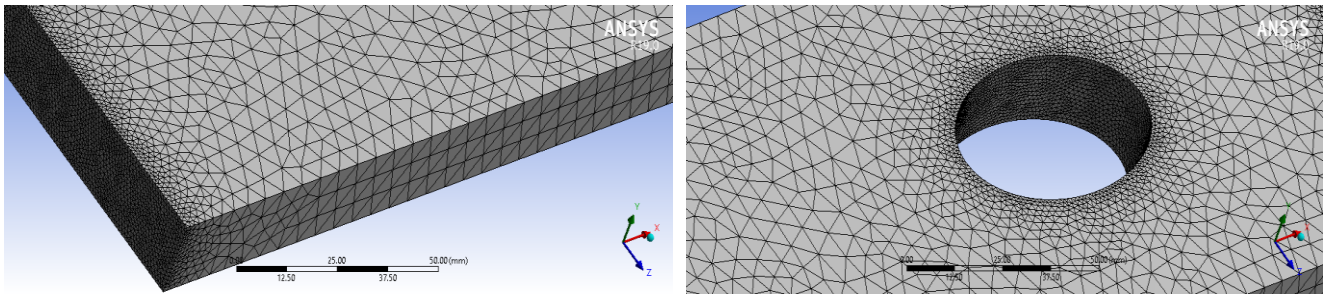

Case (1)

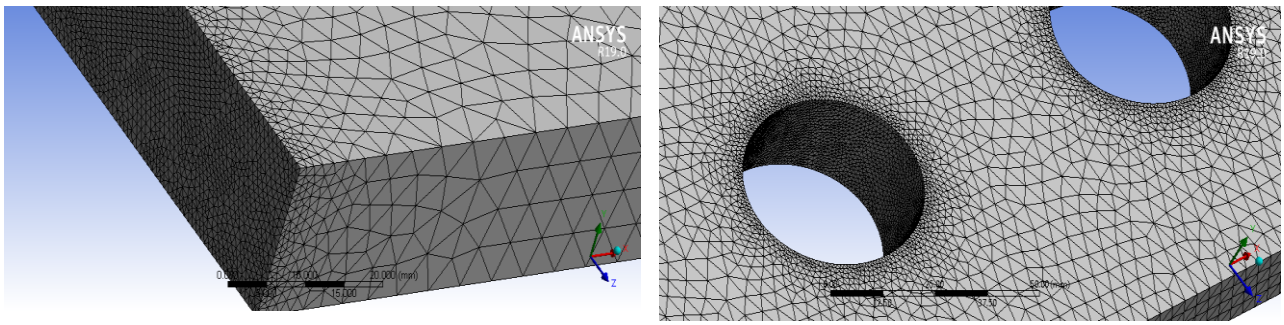

Case (2)

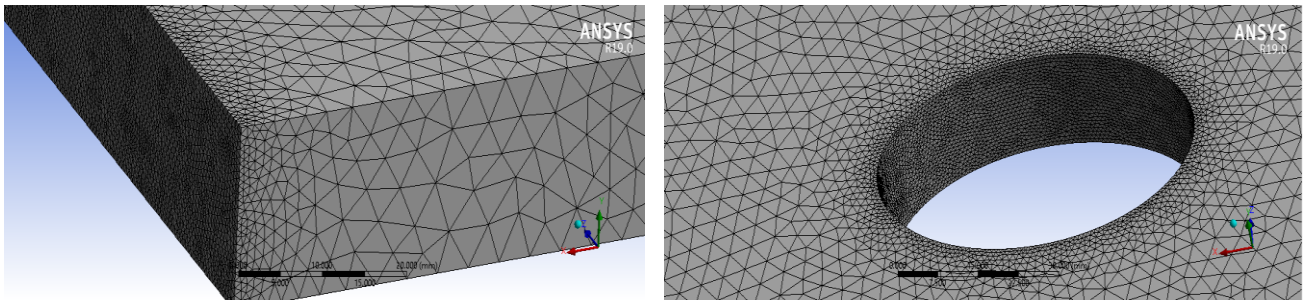

Case (3)

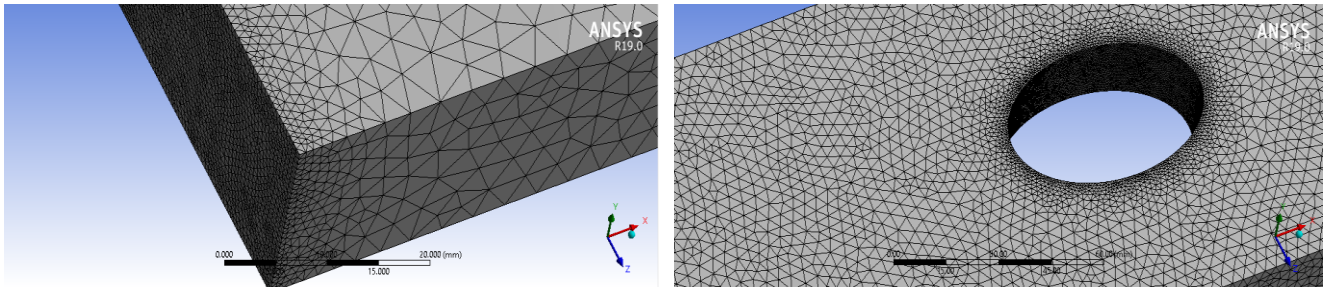

Case (4)

Figure (3-7) Mesh of duct

3.3 Problem Assumptions

In the present study, the air is used as a second phase with water to increase vortex generators' efficiency by reducing pressure loss in the duct. The following assumptions are used to simulate the model:

1) Unsteady state flow
2) Turbulent flow
3) The Zone has a three-dimensional space
4) The pressure is based on the solver
5) Newtonian flow
6) Incompressible flow
7) Constant properties of working fluid (density, viscosity, specific heat, and thermal conductivity)
8) Negligible viscous dissipation and body force

3.4 Governing Equations

The problem to be solved involves the flow pattern and thermal performance through a bank of oval and circular tubes with LVGs in a rectangular duct. The continuity, momentum, and energy equations for the two-phase, the volume fraction equations for the secondary phases, and the algebraic formulations for the relative velocities are all solved in the current work using the two-phase model. The (k-ω) standard model is used instated of the (k-ε) model because the (k-ε) model limited predictions for rotating and swirling flows and fully developed flows in non-circular channels, [62]. The governing equations are presented as shown below:

1. Continuity Equation

The volume fraction of the phase has been obtained using the continuity equation. For a given control volume, the volume fractions of the

primary (water) and secondary (air) phases can take on any value between zero to one, depending on how much space is occupied by each.

$$\frac{\partial}{\partial t}(\rho_m) + \nabla.(\rho_m \overrightarrow{v}_m) = 0 \quad (3\text{-}1)$$

$$\overrightarrow{v}_m = \frac{\sum_{k=1}^{n} \propto_k \rho_k \overrightarrow{v}_k}{\rho_m} \quad (3\text{-}2)$$

$$\rho_m = \sum_{k=1}^{n} \propto_k \rho_k \quad (3\text{-}3)$$

2. Momentum Equations

The common form of this equation is given by:

$$\frac{\partial}{\partial t}(\rho_m \vec{v}_m) + \nabla.(\rho_m \vec{v}_m \vec{v}_m) = -\nabla p + \nabla.[\mu_m (\nabla \vec{v}_m + \nabla \vec{v}_m^T)] + \rho_m \vec{g} + \vec{F} + \nabla.[\sum_{k=1}^{n} \alpha_k \rho_k \vec{v}_{dr,k} \vec{v}_{dr,k}] \quad (3\text{-}4)$$

$$\mu_m = \sum_{k=1}^{n} \alpha_k \mu_k \quad (3\text{-}5)$$

$$\vec{v}_{dr,k} = \vec{v}_k - \vec{v}_m \quad (3\text{-}6)$$

3. Energy Equations

The following expression represents the energy equation for the mixture:

$$\frac{\partial}{\partial t}\sum_{k=1}^{n}(\alpha_k \rho_k E_K) + \nabla.\sum_{k=1}^{n}(\alpha_k \vec{v}_k (\rho_k E_k + p)) = \nabla.(k_{\text{eff}} \nabla T) + S_E \quad (3\text{-}7)$$

$$k_{\text{eff}} = (\sum_{k=1}^{n}(k_k + k_t)) \quad (3\text{-}8)$$

The first term on the right-hand side of equation (3-7) reflects conduction-based energy transfer. The symbol S_E includes any other volumetric heat sources.

In Equation (3-7) $E_K = h_k - \frac{p}{\rho_k} + \frac{v_k^2}{2}$ for a compressible phase, and $E_k = h_k$ for an incompressible phase.

3.5 Turbulence Model

Models are utilized to have the capacity for characterizing and predicting the physics of the multiphase flow. Also, these models are suitable for different applications that have multiphase flow. Some of the demonstrating approaches are the Euler-Lagrange approach, the Volume of fluid approach, The Euler-Euler method and distributed phase modeling. The Euler-Lagrange method is computationally expensive and is suitable for dilute dispersed flows, which are flows with a small volume proportion of the dispersed phase, [63].

Also, the (k-ω) standard turbulence model will be used to simulate the flow-through test section. The single and two-phase flow is modeled by utilizing the mixture of the model with various parameters by relying on the testing variables and the results of the experiments to contrast and validate the results that will be obtained from the computational fluid dynamics, [64 and 65]. These parameters are passing in the course of a rectangular duct for single and two-phase flow over a bank of circular and oval tubes with and without (VGs), [66]. Three different turbulence models' results are compared in Table (3-4).

Table (3-4) Turbulence models' results

Model	***Nu***	***Δp*** **(Pa)**	**Time rate of Iteration (It. /hr.)**
(k-ε) standard	9.1	16	222.2
(k-ε) RNG	9.1	16.1	148.15
(k-ω) standard	10.2	18.1	222.2

The solution to the turbulent situation focuses on the viscosity of the turbulent viscosity solution. The viscosity of the turbulent is evaluated based

on the turbulence model, the kinetic energy (k), and the dissipation rate (ω). In this concept, (ω) represents the inverted time scale involved with turbulence. Two additional partial differential equations are solved using this model. A modified form of the (k) equation is employed in the (k-ω) model. The turbulent viscosity is then calculated as follows:

$$\mu_t = \rho \frac{k}{\omega} \tag{3-9}$$

for turbulent kinetic energy (k) and specific rate of dissipation (ω)

$$\frac{\partial(\rho u_j k)}{\partial x_j} = P_k - \beta^* \rho\omega k + \frac{\partial}{\partial x_j}\left[\left(\mu + \frac{\mu_t}{\rho_k}\right)\frac{\partial k}{\partial x_j}\right] \tag{3-10}$$

$$\frac{\partial(\rho u_j \omega)}{\partial x_j} = \alpha\frac{\omega}{k}P_k - \beta\rho\omega^2 + \frac{\partial}{\partial x_j}\left[\left(\mu + \frac{\mu_t}{\rho_\omega}\right)\frac{\partial \omega}{\partial x_j}\right] \tag{3-11}$$

And $P_k = \mu_t \left[\frac{\partial u_i}{\partial x_j} + \frac{\partial u_j}{\partial x_i}\right]\frac{\partial u_i}{\partial x_j}$

The eddy viscosity, (μ_t), is defined in terms of the turbulent kinetic energy (k) and the specific dissipation rate (ω):

$$\mu_t = \alpha^* \frac{\rho k}{\omega} \tag{3-12}$$

In the present work, the turbulent kinetic energy (k) is (5.539644×10^{-5}) m^2/s^2 and the specific dissipation rate (ω) is (5.513134) 1/s. In Wilcox's model, the constants are found as $\alpha^* = 1.0$, $\beta^* = 0.09$, $\alpha = 0.52$, $\beta = 0.072$ and $(\sigma_k) = (\sigma_\omega) = 2.0$.

3.6 The Boundary Conditions

The fluids used in this study include water, designated as the first phase, and air, designated as the second phase. The inlet of the duct represents the entry point of the air and water, and the superficial velocities of water and air are considered entry boundary conditions. The values of these velocities have been taken from the experimental data shown in Table (3-5) for water and air.

Table (3-5) Mixture superficial velocity

Q_w (L/min)	V_w (m/s)	Q_a (L/min)	V_a (m/s)
15	0.10417	8.33	0.057917
17.5	0.1215417	16.67	0.117
20	0.1375	25	0.17375

The boundary conditions of the mixture flow systems are presented in Table (3-6). The Model constant which is used in the numerical simulation of the FLUENT model is shown in Table (3-7).

Table (3-6) Boundary conditions, all dimensions in (cm)

Location			Zone	Boundary conditions	
x	y	z		Fluid	Energy
0	0-2	0-12	Inlet	Velocity	293 k
42.5, 55, 67.5, 80	0-2	3.5-8.5	Tube walls	No-slip	21883.8 W/m^2
0-100	0-2	0	Duct side walls	Symmetry	Adiabatic
----	----	----	Winglets	No-slip	Adiabatic
100	0-2	0-12	Outlet	Pressure	Adiabatic

Table (3-7) Model constants

Variable	Relaxation factors
	Two-Phase (Water-Air)
Dispersion Pr Number	0.75
Energy Pr Number	0.85
Wall Pr Number	0.85
Production Limiter Clip Factor	10

3.7 Fluids and Material Properties

The properties of the fluids and materials utilized in the model are detailed in Table (3-8).

Table (3-8) Properties of Fluids and Materials, [67]

Property	Water – Liquid	Aluminum – Solid	Air – Gas
Density (kg/m^3)	998.2	2719	1.225
Thermal conductivity (W/m.K)	0.6	202.4	0.0242
Viscosity (kg/m.s)	0.001003	---	1.7894×10^{-5}

3.8 Simulation steps

The simulation of a three-dimensional turbulent thermal transfer system in the bank heat exchangers by ANSYS FLUENT (19.0) is frequently required to evaluate the flow pattern and temperature region in the turbulent area in order to build the program by implementing the following steps:

1) Design the geometry of the model in the present work by:
    a) Define the geometry of the model and fluid characteristics with ANSYS Workbench (19.0).
    b) Mesh generation based on the difference in temperature to enhance the temperature distribution prediction
    c) The model is chosen
    d) The material used is defined
    e) The phases are set and the boundary condition determined
    f) Boundary conditions for mixture flow in the turbulent forced-convection problem are set with residual monitors for all parameters (10^{-6}). The solution would be obtained when the convergence reached for the residual at (10^{-6})
    g) The solution is initialized
2) Solve the governing equations through the k-ω turbulent model
3) Run the ANSYS FLUENT solver

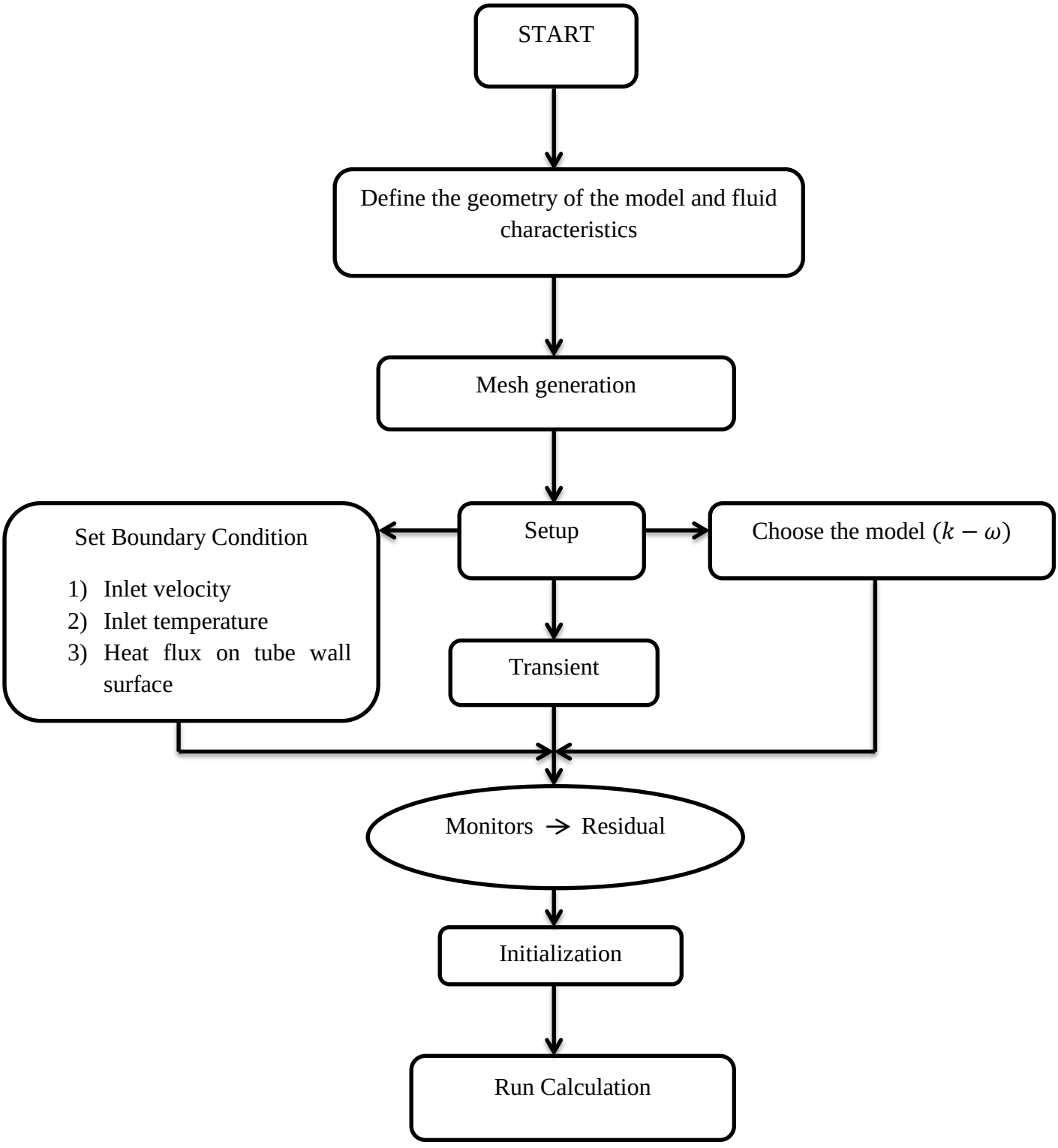

Figure (3-8) The flow chart for simulation by ANSYS FLUENT (19.0)

3.9 The Physics of Work

3.9.1 Superficial velocity

The superficial velocity of the two-phase flow (Water and Air) is determined and used to demonstrate the possibility of enhancing it on the pressure drop and heat transfer rate between the wall surface of oval tubes and a mixture flow. The superficial velocity can be calculated directly from the flow rate measured by the fluid flow meter using equation (3-13), [68], which yielded the values in Table (3-4).

$$Q = u \times A \tag{3-13}$$

3.9.2 Air Volume Fraction

The air volume fraction φ_a of air volume is defined as the volume of air (V_a) divided by the total volume of the mixture (Water and Air) (V_T), [69]:

$$\varphi_a = \frac{V_a}{V_T} \tag{3-14}$$

Air volume fraction from equation (3-14) yielded the values in Table (3-9).

Table (3-9) Air volume fraction

Q_w (L/min)	Q_w (m^3/s)	Q_a (L/min)	Q_a (m^3/s)	φ_a
15	0.00025	8.33	0.000139	0.357
15	0.00025	16.67	0.00028	0.528
15	0.00025	25	0.000417	0.625
17.5	0.0002917	8.33	0.000139	0.3227
17.5	0.0002917	16.67	0.00028	0.49
17.5	0.0002917	25	0.000417	0.588
20	0.00033	8.33	0.000139	0.296
20	0.00033	16.67	0.00028	0.459
20	0.00033	25	0.000417	0.558

3.9.3. Reynolds Number

Reynolds number in single phase flow can be found by equation:

$$Re = \frac{\rho \times u \times D_H}{\mu} \tag{3-15}$$

Reynolds number in two-phase flow for water phase can be found by equation, [70]:

$$Re_w = \frac{(1-x) \times \rho_w \times u_w \times D_H}{\mu_w} \tag{3-16}$$

Also, the Reynolds number in two-phase flow for the air phase can be found by the equation:

$$Re_a = \frac{x \times \rho_a \times u_a \times D_H}{\mu_a} \tag{3-17}$$

The air mass fraction and Reynolds number of water are listed in Table (3-10).

Table (3-10) Air mass fraction and Reynolds number of water

$\dot{m}_w$ (kg/s)	$\dot{m}_a$ (kg/s)	Air Mass Fraction	Re_w
0.25	0	0	3645.95
0.25	0.0001668	0.000666755	3643.5
0.25	0.000336	0.00134	3641
0.25	0.0005004	0.0019976	3638.67
0.2917	0	0	4254
0.2917	0.0001668	0.00057149	4251.57
0.2917	0.000336	0.00115	4249
0.2917	0.0005004	0.00171	4246.7
0.33	0	0	4812.5
0.33	0.0001668	0.000505199	4810
0.33	0.000336	0.001017	4807.6
0.33	0.0005004	0.001514	4805.2

3.9.4. Data Analysis

Simplified steps were used to analyze the heat transfer process for the water as single-phase flow and water and air as two-phase flow, [55]:

$$q_{heaters} = I \times V \quad (3\text{-}18)$$

$$q_{heaters} = q_{conv} = h \times A_t \times \Delta T_S \quad (3\text{-}19)$$

The local heat transfer coefficient can be obtained as:

$$h = \frac{q_{conv}}{A_t \times \Delta T_S} \quad (3\text{-}20)$$

$$Nu = \frac{h \times D_h}{k} \quad (3\text{-}21)$$

$$A_t = \pi \times N \times D \times L \quad (3\text{-}22)$$

$$\overline{T}_b = \frac{T_{inlet} + T_{outlet}}{2} \quad (3\text{-}23)$$

$$\Delta T_S = T_{ts} - \overline{T}_b \quad (3\text{-}24)$$

$$D_h = \frac{4 \times A}{P} \quad (3\text{-}25)$$

The average values of the other parameters can be calculated based on calculation of average tube surface temperature and average bulk mixture temperature as follows:

$$T_f = \frac{T_{ts} + \overline{T}_b}{2} \quad (3\text{-}26)$$

All the physical properties $\rho, \mu, v,$ and k were evaluated at (T_f).

3.9.5. Performance Parameter

The Colburn factor (*j*) and the friction factor (*f*) are derived from Equations (3-27) and (3-28) to calculate the performance parameter (*j/f*), [71].

$$j = St.Pr^{2/3} \quad (3\text{-}27)$$

$$f = \frac{\Delta P}{\frac{\rho v^2}{2} \frac{A_t}{A_{min}}} \quad (3\text{-}28)$$

$$St = \frac{Nu}{Re \times Pr} = \frac{h}{\rho \times c_p \times V} \quad (3\text{-}29)$$

$$Pr = \frac{\mu \times c_p}{k} \quad (3\text{-}30)$$

3.10 Convergence Criteria

Table (3-11) shows the residual error for continuity, velocities, energy equations, (k), (ω), and (φ_a) for four different types of vortex generators. The residual monitor are shown in Figures (3-9) and (3-10) for case of without (VGs) and case of with (VGs), respectively.

Table (3-11) Residual error

Equation	continuity	X-Velocity	Y-Velocity	Z-Velocity	Energy	K	ω	φ_a
R. error	10^{-6}	10^{-6}	10^{-6}	10^{-6}	10^{-6}	10^{-6}	10^{-6}	10^{-6}

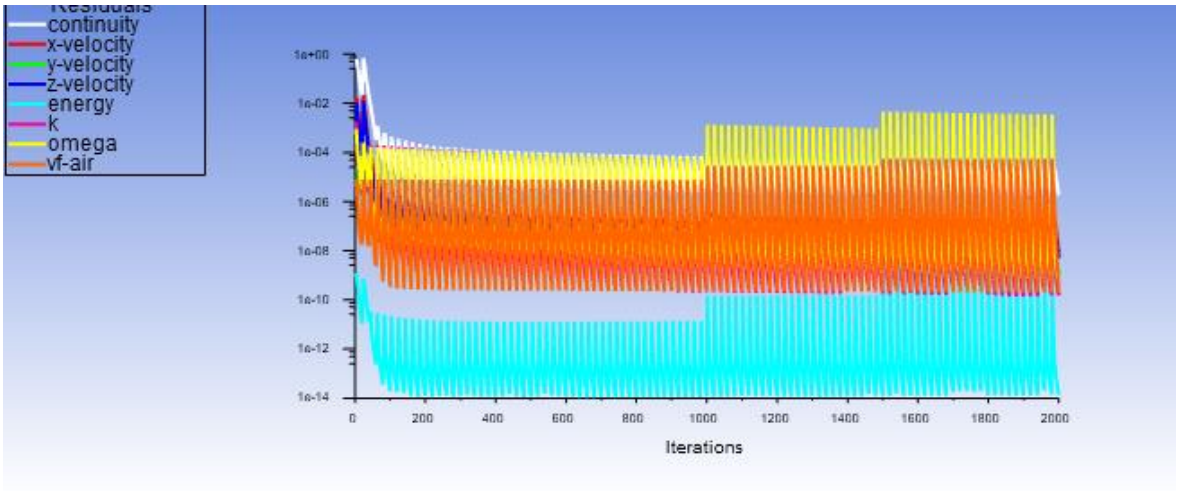

Figure (3-9) Residual plot from FLUENT program to converge for case of without (VGs)

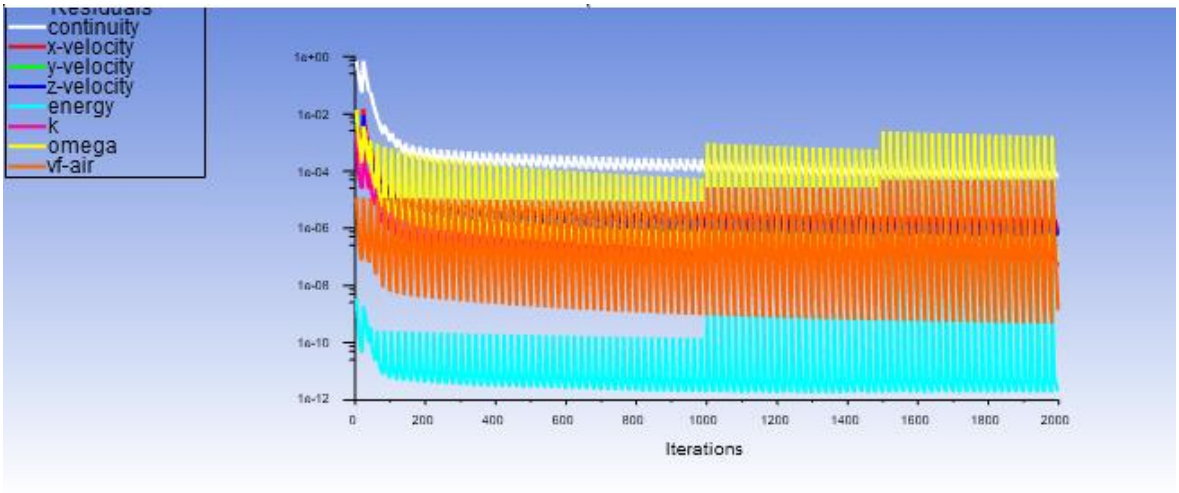

Figure (3-10) Residual plot from FLUENT program to converge for case of with (VGs)

3.11. Error Calculation for the Validation

Using the following equation, the absolute total error of the simulation results was compared to the experimental results, [72]:

$$E = \sum_{i=1}^{n} \frac{|X^i{}_{CFD} - X^i{}_{EXP}|}{X^i{}_{EXP}} * 100 \quad (3\text{-}31)$$

In the duct, (X) might be either (Nu) or (f). $|X^i{}_{CFD} - X^i{}_{Exp}|$ is the difference between the simulated values and the experimental measurement values for variable (X) and (n) number of measurements.

CHAPTER FOUR
EXPERIMENTAL WORK

4.1 Introduction

The experimental study in the present work includes fabricate and manufacture of an experimental rig. The test rig has been built in the mechanical engineering fluid laboratory at University of Babylon to study the effect of vortex generators (VGs) on heat transfer rate and the pressure drop in the duct. This chapter discusses in detail all of the experimental progress indicators. All experiments were performed at an ambient laboratory temperature and atmospheric pressure. The duct was fabricated to fully develop turbulent flow before reaching the oval tube banks, [73].

4.2 Experimental Apparatus

The experimental rig consists of a rectangular duct with four-row oval tubes with vortex generators for the heat exchanger. A pair of winglets is glued out on the duct surface symmetrically in (CFD) configuration for each oval tube. It also includes all the required instruments to study the heat flow augmentation with a corresponding pressure drop through the duct illustrated in Figure (4-1a).

Figure (4-1b) displays the experimental rig. The testing rig used in the present work consists of the following main parts and measuring instruments:

1-The test section consists of rectangular duct, heaters and vortex generators, as shown in Figure (4-1c).

2- Water tank

3- Water pump

4- Flowmeter of water

5- Flowmeter of air

6- Pressure regulator

7- Pressure gauge

8- Air tank

9- Air compressor

10- Power analyzer

11- Electrical voltage regulator

12- Manometer

13- Temperature recorder

14- Digital camera

The cycle of liquid flow consists of a water tank, pump, water flow meter, valve, gate valve, way valve and piping system. The cycle of airflow consists of a compressor, air tank, pressure gage, valve, pressure regulator, air flow meter, way valve, and piping system) with a mixing pipe (1/4 in copper tube).

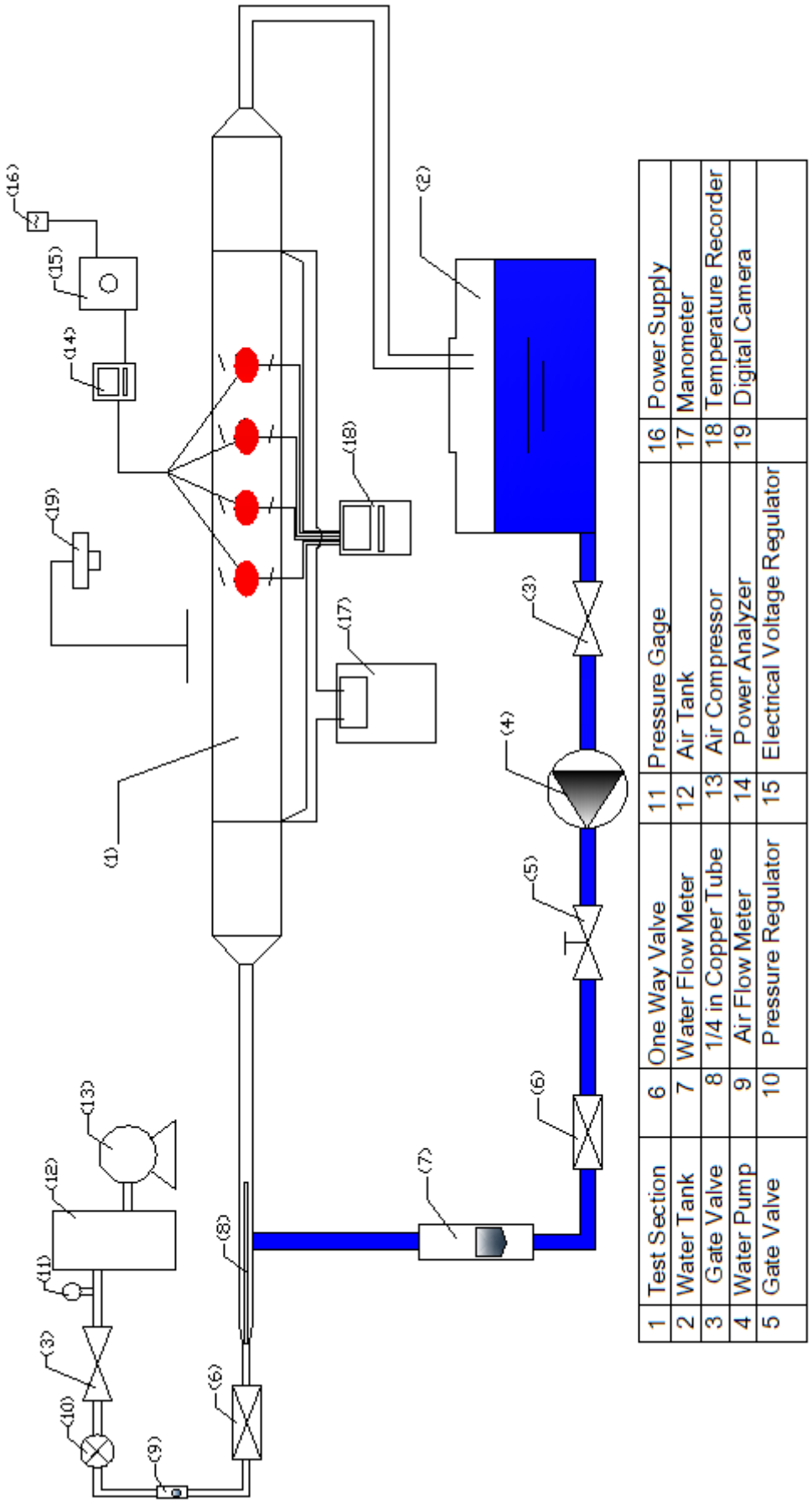

Figure (4-1a) Schematic diagram of test rig

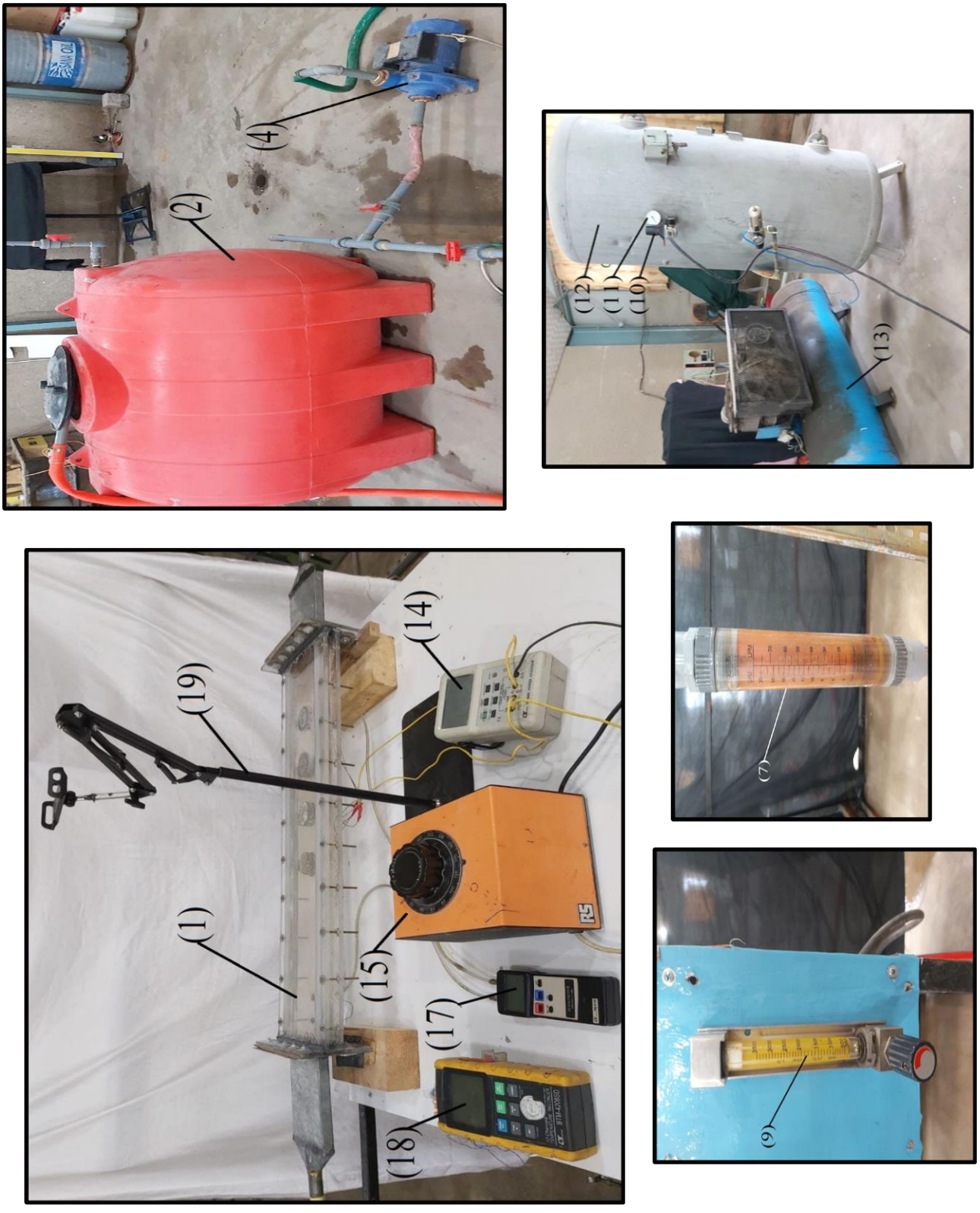

Figure (4-1b) Photograph of the experimental tested rig

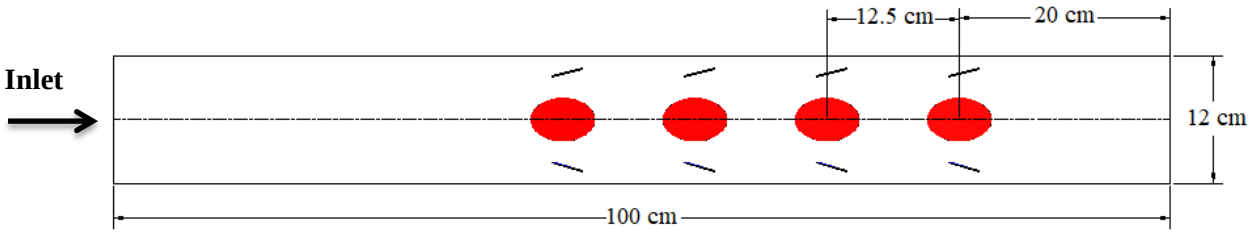

(a)

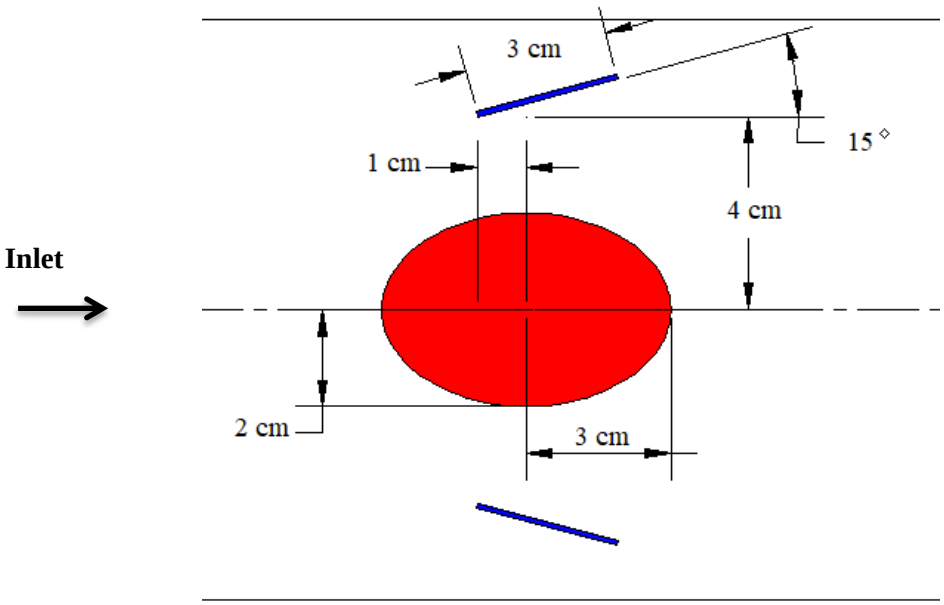

(b)

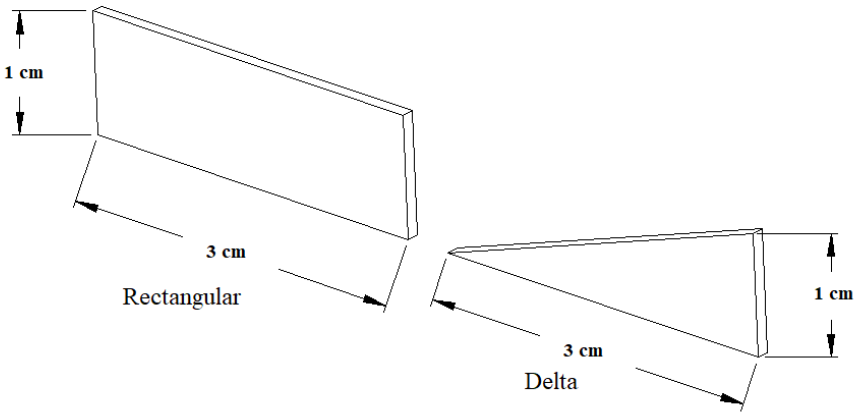

(c)

Figure (4-1c) Dimension of (a) top view of test section; (b) oval tube and position of vortex generators; (c) vortex generators

4.2.1 Test Section

The test section is made from a transparent cast acrylic sheet certified by (ISO 9001) in (2015) to observe and record two-phase (air-water) flow behavior. The test section is a rectangular duct with a dimension of (100 cm × 12 cm × 2 cm). Also, the duct involves four rows of oval tubes arranged in banks. Figure (4-2) illustrates the test section.

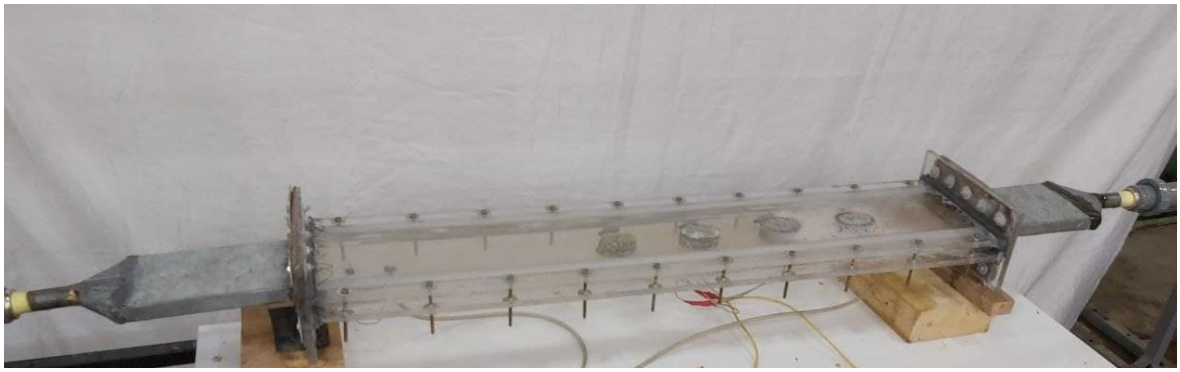

Figure (4-2) Test section

4.2.2 Vortex Generators (VGs)

Vortex Generators are manufactured from aluminum in two shapes (Delta and Rectangular) winglets. The manufacturing process of vortex generators was performed by specialized engineers in one of the engineering workshops in Babylon city using a digital milling machine Computer Numerical Control. Vortex generators are manually affixed to the interior surface of the rectangular duct. The dimensions of vortex generators are selected depending on the dimensions of the duct and based on previous reference. Figure (4-3) illustrates the shapes of vortex generators. The dimensions of the duct, the position and dimensions of the vortex generators, the oval tube, and the angle of attack (15^{o}) were set after simulations of many configurations of vortex generators, angle of attack, and tube type to reach the optimum dimensions for the test section, which provided the best performance.

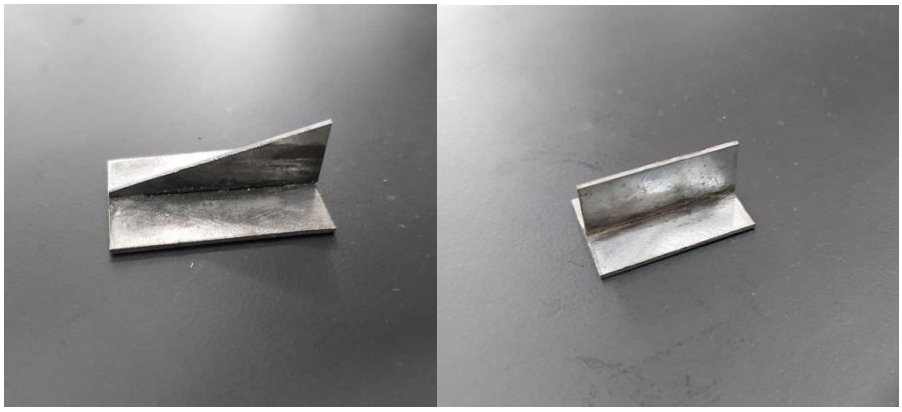

(a) (b)

Figure (4-3) Shapes of vortex generators (a) Delta winglet (b) Rectangular winglet

4.2.3 Water Tank

In the experimental test, water was stored in a circular cross-section tank with a capacity of (500L). The tank was made entirely of plastic.

4.2.4 Water Pump

Water was pumped into the channel via the water pump (Stream). It has a maximum head of (20 m), a minimum discharge rate of (480 L/min), and voltage (220 Volts); as illustrated in Figure (4-4).

Figure (4-4) Water pump

3.2.5 Flowmeter of Water

The flow rate of water in the duct was measured by using a float-type flowmeter. The flow meter range is (15-75 L/min), as illustrated in Figure (4-5).

Figure (4-5) Flowmeter of water

4.2.6 Air Compressor

An Air compressor was used to supply air, which converted the energy generated into potential energy stored in pressurized air. The operating pressure is (0.1 MPa), the voltage is (220 V), the horsepower is (hp), and the frequency is (50) Hz, as illustrated in Figure (4-6).

Figure (4-6) Air compressor

4.2.7 Flowmeter of Air

A flowmeter with a range of (350 to 3500 L/h) was used to specify the airflow rate that entered the channel. It is used to determine the volume flow rate of air passing through a device in a unit of time, as illustrated in Figure (3-7).

Figure (4-7) Flowmeter of air

4.2.8 Heaters

The heating system Figure (4-8) was designed using four heaters measuring (50) mm in length and (8) mm in diameter. The heaters work by converting electrical energy to heat; each one has a power rating of (100 W); consequently, the total power rating is (400 W) and operates at 220 volts. These heaters are installed in the center of the oval tubes.

Figure (4-8) Heaters

4.2.9 Thermocouples

The thermometer is a temperature-measuring instrument with twelve channels and a universal thermocouple as the thermal input. The thermometer used in this work is the (BTM-4208SD) thermometer, which was used to measure temperature at numerous locations throughout the duct, as illustrated in Figure (4-9).

Figure (4-9) Digital thermometer

4.2.10 Power Analyzer and Voltage Regulator

A power analyzer is a device used to supply electrical energy to heaters. It consists of control functions that have been expanded to complete loop control to take advantage of digital hardware and software algorithms. The function of a power supply is to transform a variable input voltage into a constant output value. The voltage regulator is used to control the voltage input to the power analyzer and set the required electrical power to the heaters, as shown in Figure (4-10).

Figure (4-10) Power analyzer and voltage regulator

4.3 The Experimental Work's Flow Phases

4.3.1 The Continuous Phase

The continuous phase experimented with water at ambient conditions. The water pump pumps water into the test section from the water tank and is regulated by a valve gate to maintain the desired water flow rate.

4.3.2 The Dispersed Phase

The dispersed phase is used to air at ambient conditions in the experimental work. A compressor pumps air into the test section, which is then regulated by a pressure regulator and mixed with water.

4.4 Instruments calibration

The water flow meter and thermometer were calibrated to increase the accuracy of the measuring devices.

4.4.1 Water flow meter calibration

The flow meter used to determine the water flow rate was calibrated using a scaled container filled with water flowing from the test pipe at a specified flow rate. The period required for the water to reach a specified point on the container was recorded.

This procedure was repeated four times, and the values were plotted alongside the flow meter readings. Water flowing through the flow meter over a specified period is collected in a measuring container, and the measured flow rate is calculated using the following equation:-

$$Q_t = V_w/t \quad (4\text{-}1)$$

The details of the calibration process can be seen in appendix [A].

4.4.2 Calibration of the Thermocouples

In order to get accurate readings, the temperature sensors (thermocouples) and thermocouples have been calibrated in the Metrological Department at Central Organization for Standardization and Quality Control. The details of the calibration process can be seen in appendix [A].

4.5 Experimental Procedures

The experiments were designed to evaluate and analyze the test section's heat transfer coefficient, temperature distributions, and the reduction in pressure. Furthermore, the influence of various types of vortex generators on single-phase and two-phase flow phenomena for water and air over the bank of oval tubes with varying flow rates ($3645.95 \leq Re \leq 4805.2$) and constant heat flux is explained. Comparing two vortex generators (Delta and Rectangular) winglets concludes that any vortex generator provides the best heat flow. Thus, tests were conducted using the superficial velocity of water and air, with a constant heat power of (110W). The experimental procedure was as follows:-

1- Within the duct, install the vortex generator (first model) in (CFD) arrangement with a 15^{o} angle of attack.

2- Switch on the water pump and set the initial flow rate to (15 L/min).

3- Connect the heater to an electrical power source and turn it on.

4- Allow 10-15 minutes for the heated oval tubes to reach a stable surface temperature.

5- Run the compressor and supply air at the initial value (8.33 L /min).

6- Record the temperature of the six sensors (four on the oval tubes' walls and two on the inlet and outlet duct). It was simultaneously recording a video with the camera to observe the nature of the fluid flow and measuring the pressure at the test section's inlet and outlet to determine the total reduction in pressure inside the duct.

7- Begin by changing the airflow rate (while keeping the water flow constant) and repeating the previous steps.

8- Continue until all varying air discharges have been completed.

9- Alternate the water flow rate and repeat all of the steps above. Continue until all water has been discharged, as illustrated in Table (4-1).

10- All preceding steps should be repeated four times to ensure the accuracy of the readings taken.

11- All preceding steps should be repeated for the remaining two vortex generator models.

Table (4-1) The values used in the experiments for the working conditions

Heat Power (W)	Q_w (L/min)	Q_a (L/min)
110	15	0
110	17.5	8.33
110	20	16.67
110	----	25

4.6 Uncertainty

The precise measurement of the experimental work is dependent on the precision and quality of the instruments, as well as the reading of results through the devices. Examine the dependability of the results and inferences generated from the data. For each test, the experiment is repeated four times under identical conditions.

Errors in devices and equipment can impact measurement uncertainty, which results in uncertainty propagation (σ_x). Consequently, the inaccuracy of experimental results for the complete experimental apparatus is ±5% when the square of uncertainty is assumed. It was considered a measurement of x that is subject to some device error, each of uncertainty σ_i see Appendix [B] for more detailed information, [74].

$$\sigma = \sqrt{\frac{\sum_1^n (x_i - \bar{x})^2}{n-1}} \tag{4.2}$$

Where i = 1, 2, ..., I.

CHAPTER FIVE
RESULTS AND DISCUSSION

5.1 Introduction

The experimental and numerical results of a single-phase and two-phase flow (water-air) over a tube banks in a rectangular duct with four different types of vortex generators (Delta, Rectangular, Zikzak, and Sinusoidal wavy) winglets are presented and discussed in this chapter. The effects of vortex generators and different flow rates of the mixture (water-air) on the heat transfer coefficient have been demonstrated through comparisons between experimental and numerical results. Heat transfer coefficient and temperature distribution were investigated in the duct by using various values for the flow rate of water and air with different shapes and positions of the vortex generators. As well as to compare the four different types of vortex generators and determine which vortex generators and discharges provide the maximum heat transfer with the lowest pressure drop in a turbulent flow.

5.2 Model Validation

The computational fluid dynamics model is validated by numerical simulations of flow through a fin-and-tube heat exchanger with an intake Reynolds number range (500-850). The numerical results are compared with the numerical results obtained by Chu, et al., [18], and then tested to determine the most suitable technique for the current analysis.

The maximum errors of heat transfer coefficient between the present model results and the numerical results of Chu, et al., [18] are (0.68 %, 1.58 %, and 1.36 %), corresponding to (500, 700, and 850) Reynolds numbers, respectively. The maximum pressure drop deviations between the present numerical results and Chu, et al., [18] are (0.25 %, 2 %, and 4.12 %);

corresponding to (500, 700, and 850) Reynolds numbers, respectively. The model validation results are shown in Figure (5-1).

Also, the computational fluid dynamics model validation by numerical simulations of flow through the heat exchanger with an intake of the Reynolds number range (600-2700) was compared to the experimental outcomes of Fiebig, et al., [75].

The maximum errors between the present model findings and the experimental outcomes of Fiebig, et al., [75] are (4.35%) for (*Nu*) and (5.825%) for (*f*). The model validation results are shown in Figure (5-2). From the above analyses, the high degree of agreement between these outcomes illustrates the model's reliability in precisely forecasting the flow structure and heat transfer properties.

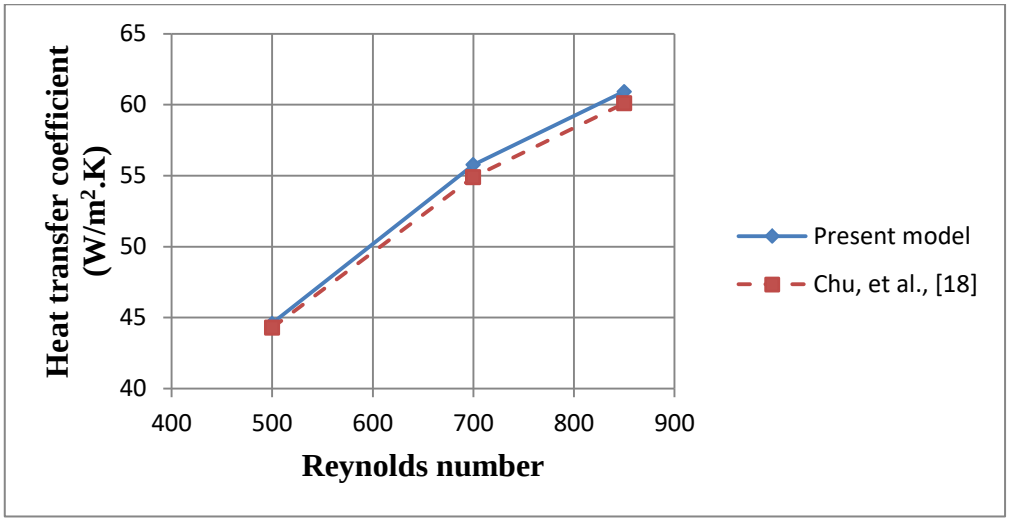

(a)

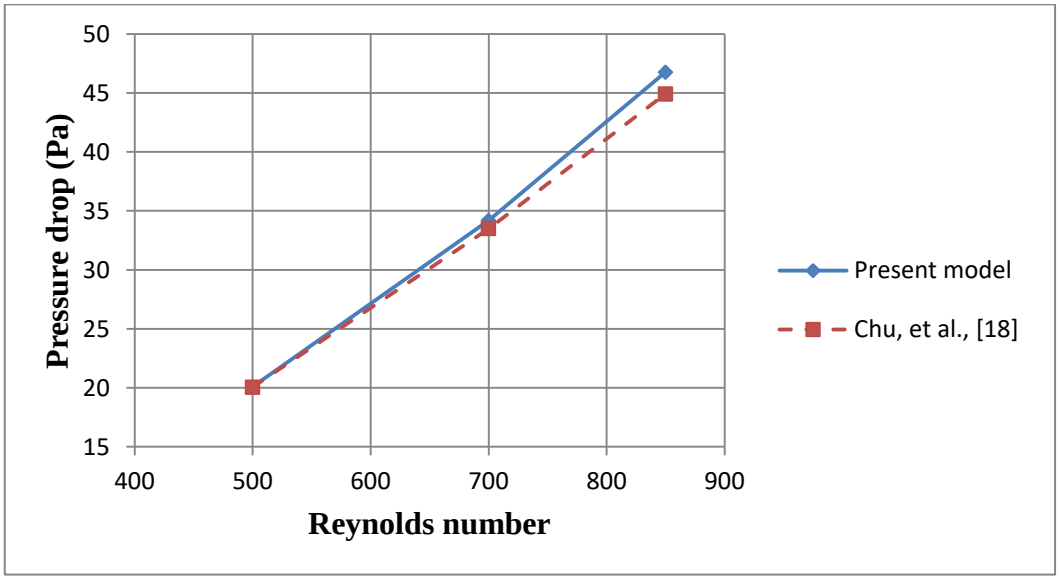

(b)

Figure (5-1) Validation of the present model with the germane work Chu, et al., [18] for (a) Heat transfer coefficient, and (b) Pressure drop

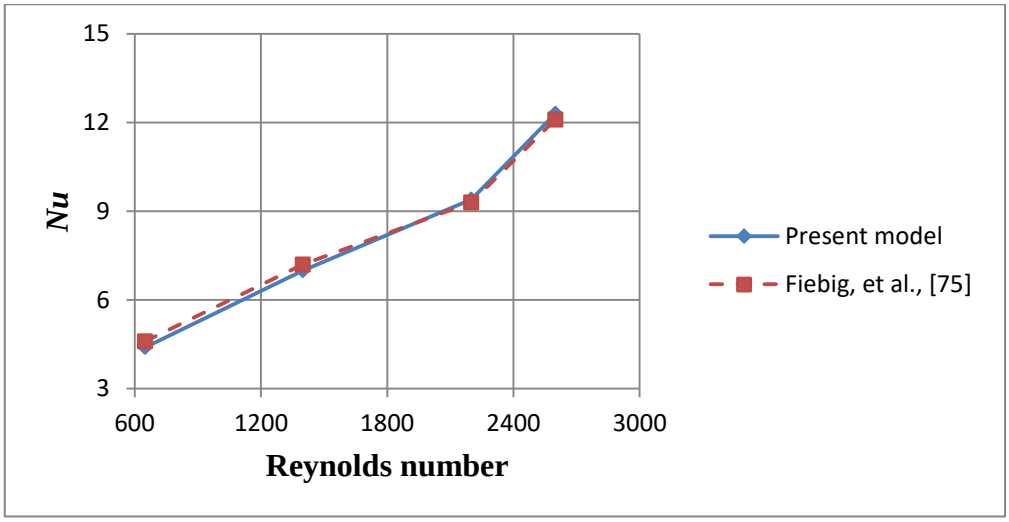

(a)

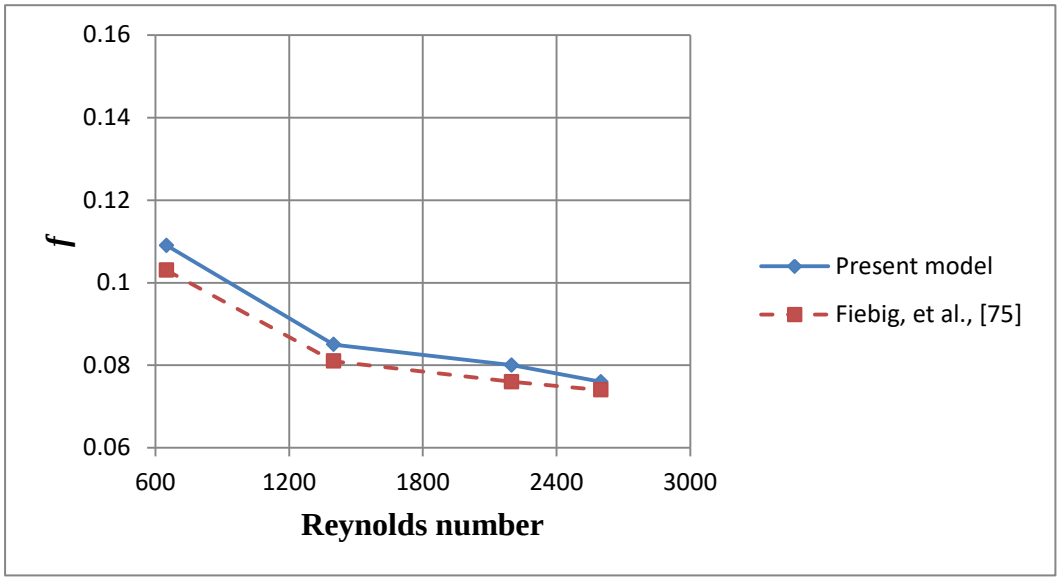

(b)

Figure (5-2) Validation of the present model with the germane work Fiebig, et al., [75] for (a) Nusselt number, and (b) Friction factor

5.3 The Numerical Results

Two-phase flow reduces pressure drop in the duct at high flow velocities, [76]. In the present study, the air is used as a second phase with water to increase vortex generators' efficiency by reducing pressure drop in the duct. The heat transfer rate is enhanced by adding vortex generators inside the duct, considering that the pressure drop must be minimized to reduce additional costs, [77]. Four shapes of vortex generators (Delta, Rectangular, Zikzak, and Sinusoidal wavy) winglets are investigated numerically. Workbench (19.0) is used to compute the results and analyzes for turbulent two-phase flow area. Other parameters are used in this investigation of the oval and circular tube banks, (CFU) and (CFD) configurations, and the (k-ω) standard turbulence model is used. In Table (5-1), the initial conditions of numerical work are presented:

Table (5-1) The initial conditions

Inlet Temperature (^oC)	Flow rate of water (Lpm)	Flow rate of air (Lpm)	Air volume fraction	Heat flux (W/m^2)	Angle of attack (Degree)
20	15	8.33	0.357	21883.8	15
----	----	----	----	----	20
----	----	----	----	----	25

5.3.1 Circular Tube Banks

5.3.1.1 Effect of configuration, angle of attack, and shape of vortex generators

Table (5-2) describes all situations in the duct when various vortex generators are used. Figure (5-3) shows the temperature gradient between water-air flow and surfaces of the circular tube at various points in the duct,

and Figure (5-4) illustrates the inlet and outlet pressure in the duct at an angle of attack (15^o).

Table (5-2) angle of attack (15^o)

Vortex type		**Rate of decreasing in ΔT (%)**	**ΔP**	
			Rate of increasing (%)	Rate of decreasing (%)
Delta	CFU	27.9	----	9.86
	CFD	28	---	8.46
Rectangular	CFU	30	---	0.2
	CFD	33	0.09	---
Zikzak	CFU	34	34.78	---
	CFD	33.13	36	---
Sinusoidal	CFU	34.3	90	---
	CFD	31.5	45.6	---

Figure (5-5) shows the performance parameter at various positions in the duct at an angle of attack (15^o). The performance of Delta winglets in the (CFU) configuration is higher than the other winglets.

Table (5-3) describes all situations in the duct when various types of vortex generators are used. Figure (5-6) shows the temperature gradient between water-air flow and surfaces of the circular tube at various points in the duct, and Figure (5-7) illustrates the inlet and outlet pressure in the duct at an angle of attack (20^o).

Figure (5-8) shows the performance parameter at various positions in the duct at an angle of attack (20^o). Delta winglets in the (CFU) arrangement perform better than the other vortex generators.

Table (5-3) angle of attack (20^o)

Vortex type		**Rate of decreasing in ΔT (%)**	**ΔP**	
			Rate of increasing (%)	Rate of decreasing (%)
Delta	CFU	30.6	---	7
	CFD	28	---	5.56
Rectangular	CFU	29.1	8	---
	CFD	30.88	7.7	---
Zikzak	CFU	29.8	44.1	---
	CFD	32.15	41.7	---
Sinusoidal	CFU	36.75	101.7	---
	CFD	32.83	50.14	---

Table (5-4) describes all situations that occur in the duct when various types of vortex generators are used. Figure (5-9) shows the temperature gradient between water-air flow and surfaces of the circular tube at various points in the duct and Figure (5-10) illustrates the inlet and outlet pressure in the duct at an angle of attack (25^o).

Figure (5-11) shows the performance parameter at various positions in the duct at an angle of attack (25^o). The performance of the delta winglets in the (CFD) arrangement is better compared to the other winglets.

Table (5-4) Angle of attack (25^{o})

Vortex type		**Rate of decreasing in ΔT (%)**	**ΔP**	
			Rate of increasing (%)	Rate of decreasing (%)
Delta	CFU	27.78	---	1.8
	CFD	28.5	---	0.8
Rectangular	CFU	30.66	21.16	---
	CFD	32.1	20.19	---
Zikzak	CFU	28.2	54.86	---
	CFD	29.67	49.93	---
Sinusoidal	CFU	36	119.5	---
	CFD	32.18	56.38	---

The overall performance of delta winglets with (CFD) and (CFU) configurations is better compared to other kinds of winglets. Due to the pressure difference and frictional flow effects, high longitudinal vortices are generated behind the delta winglet pairs. As the induced velocity of longitudinal vortices is considerably higher than that of the frontal velocity, vortices transport the fluid from the wake region of the circular tube banks to the main flow regions, promoting enhanced mixing of the bulk fluid.

The above observed that in all cases, any types of vortex generators were used in circular tube banks that promoted thermo-hydraulic performance in the (HE). There was usually a pressure drop which can illustrate as follows; for the case without used vortex generators, the resistance of the flow of air in the duct results only from the friction between air particles and duct walls with circular tube walls. The resistance of the airflow in the duct when vortex

generators were used not only results from the friction between air particles and duct walls with circular tube walls but also from extra resistance, which causes an increase in pressure drop through flow in the duct.

Figure (5-12) shows performance parameter for delta winglets in (CFU) and (CFD) configuration at ($\alpha = 15^o, 20^o, 25^o$). The overall performance of delta winglets with (CFD) and (CFU) configurations is better at an angle of attack of ($\alpha = 15^o$) compared to the other two angles of attack. This occurs because a low angle of attack can generate more turbulence, vortex intensity, and impinging flows than a high angle of attack. As seen, ($\alpha = 15^o$) performs the best temperature distribution, while the case of ($\alpha = 20^o, 25^o$) provide the opposite result. This angle ($\alpha = 15^o$) generates the greatest vortex intensity, which results in the most effective mixing of the fluid flow throughout the test duct.

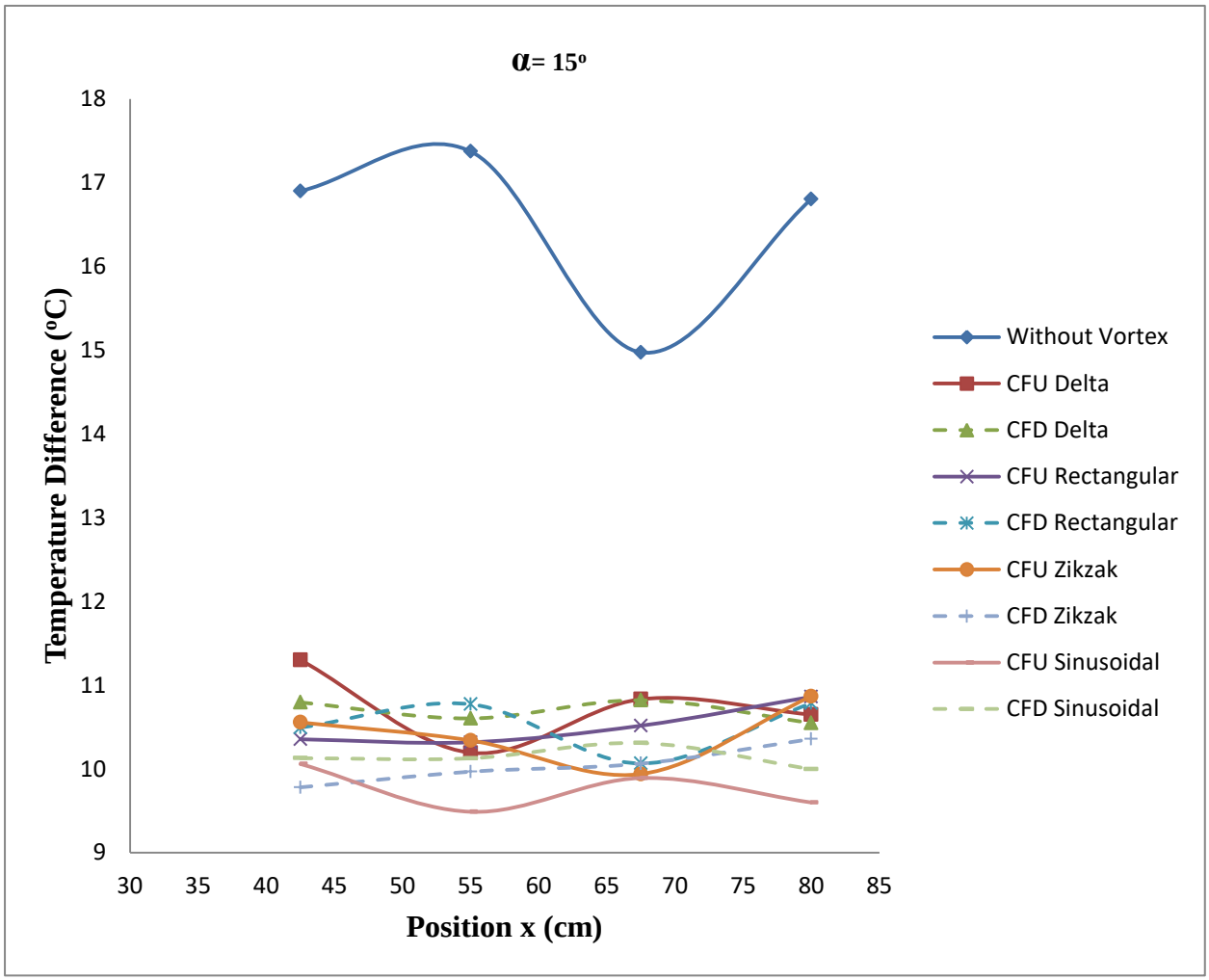

Figure (5-3) The temperature difference between two-phase flow (water and air) and circular tube surfaces at many positions in the duct (x = 42.5, 55, 67.5, and 80 cm)

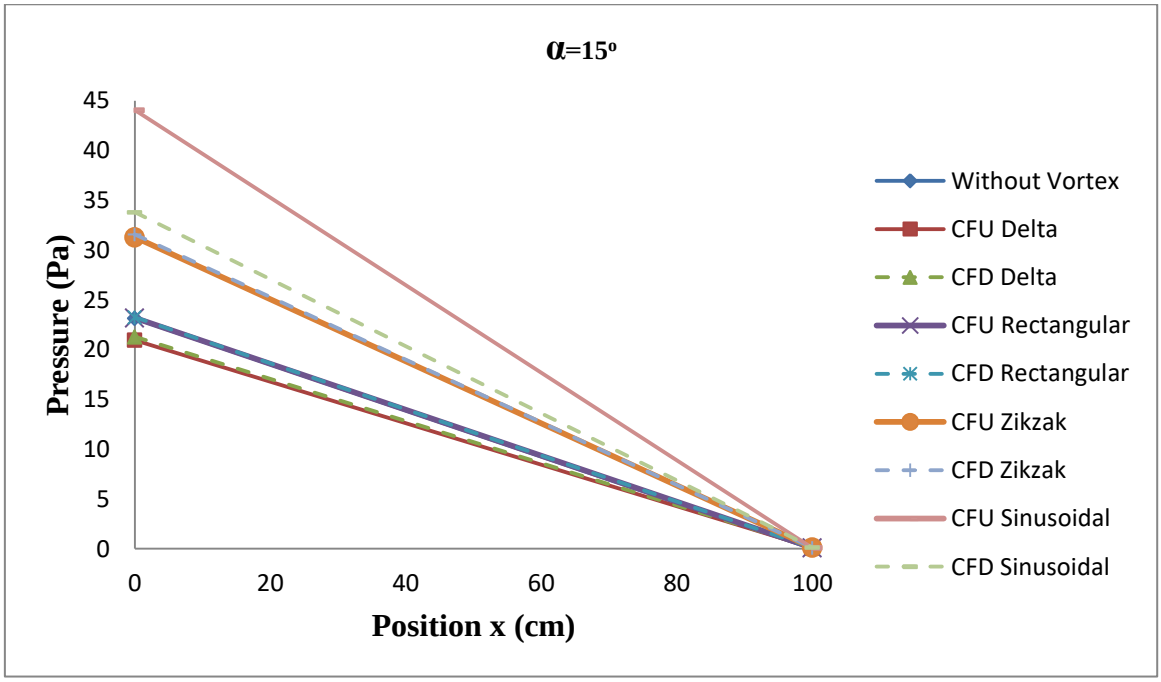

Figure (5-4) Inlet and outlet pressure in the duct

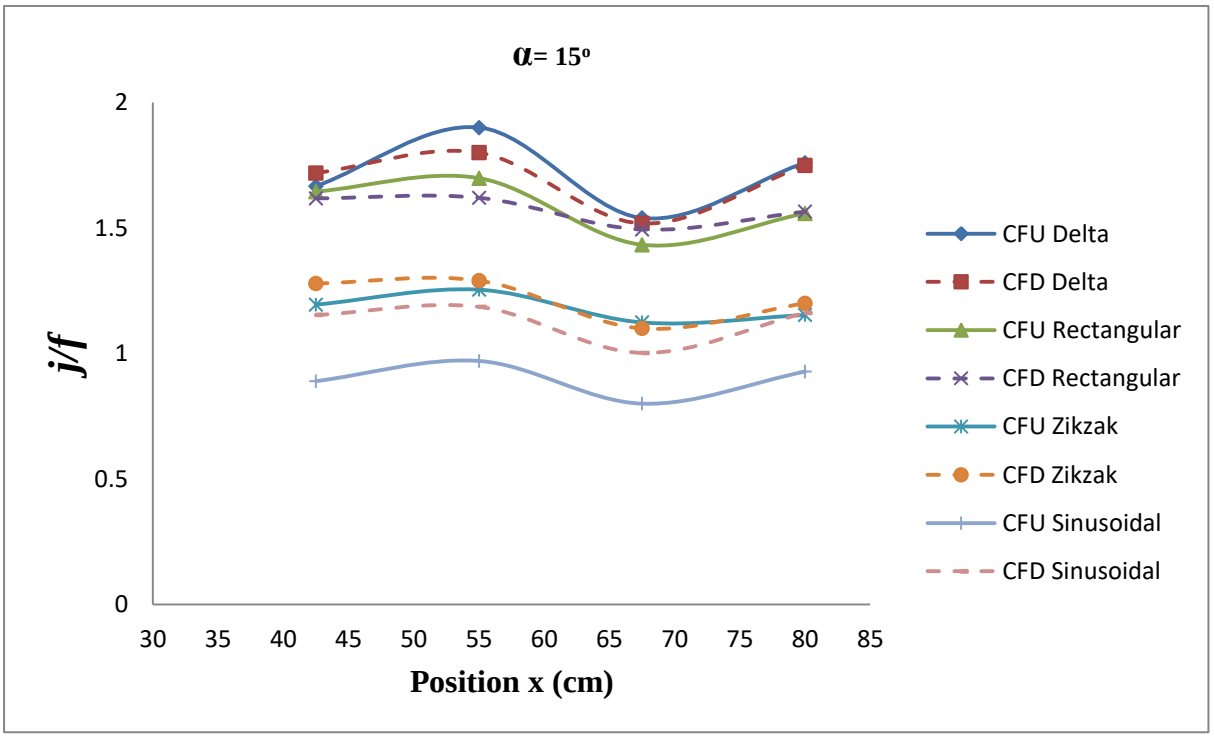

Figure (5-5) Performance parameter

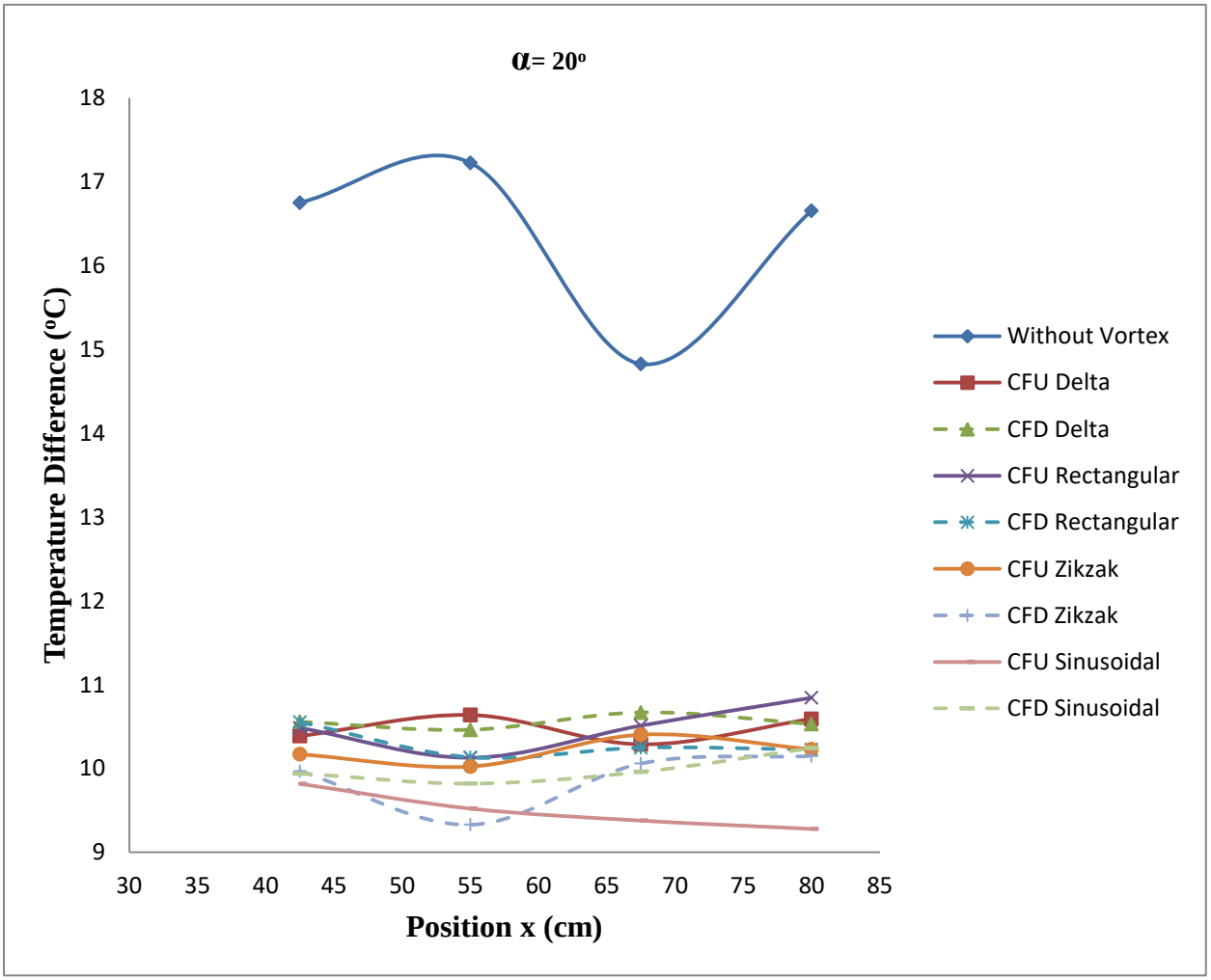

Figure (5-6) The temperature difference between two-phase flow (water and air) and circular tube surfaces at many positions in the duct (x = 42.5, 55, 67.5, and 80 cm)

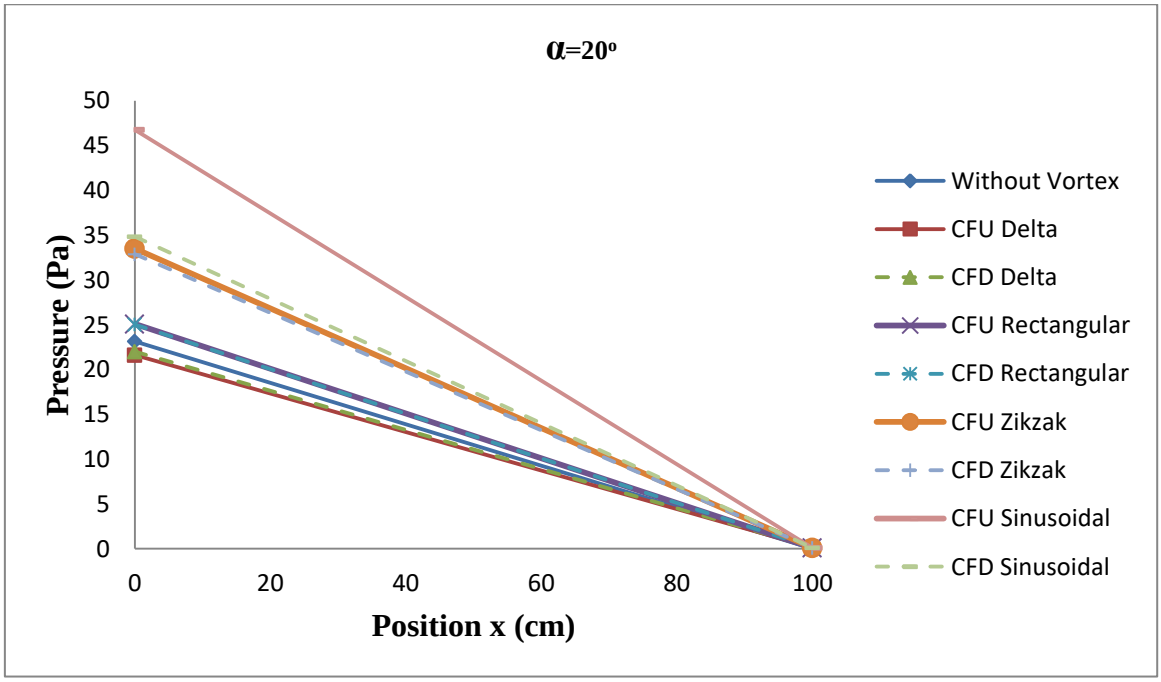

Figure (5-7) Inlet and outlet pressure in the duct

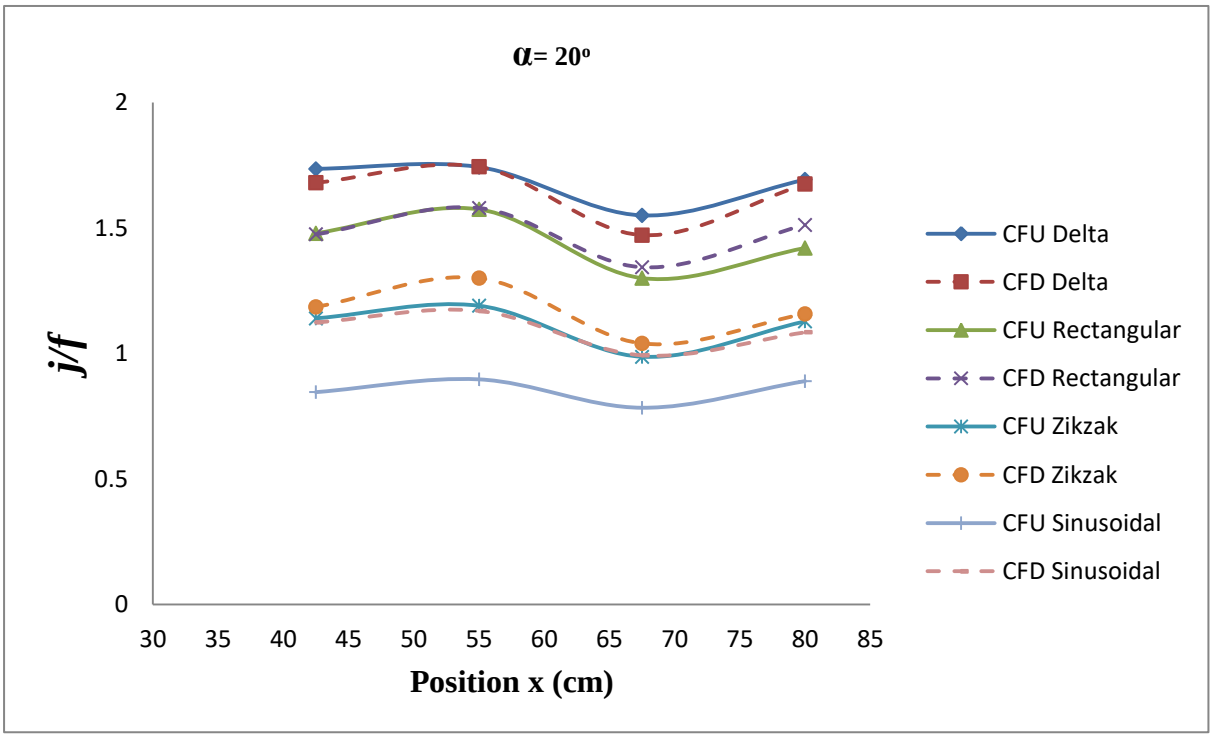

Figure (5-8) Performance parameter

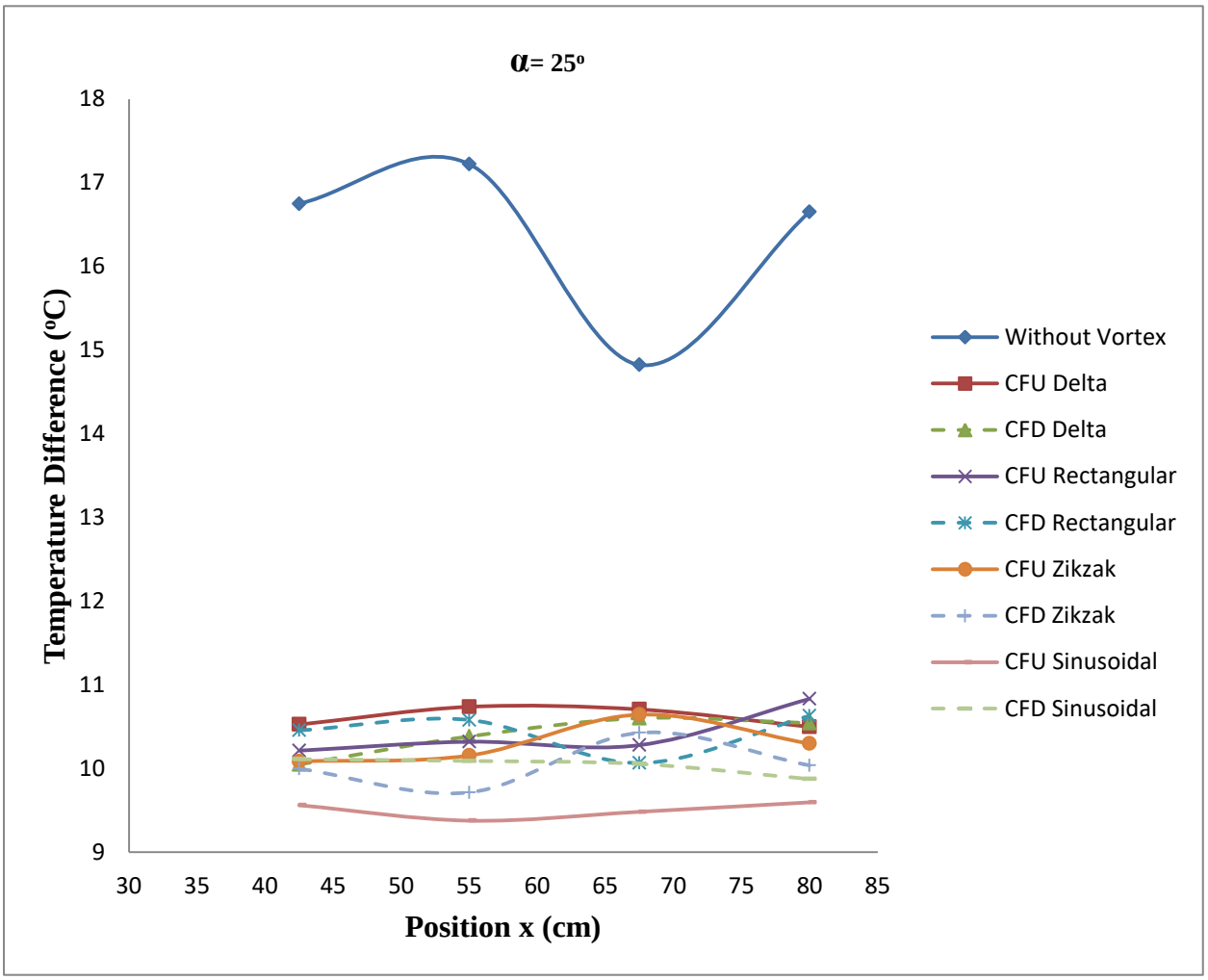

Figure (5-9) The temperature difference between two-phase flow (water and air) and circular tube surfaces at many positions in the duct (x = 42.5, 55, 67.5, and 80 cm)

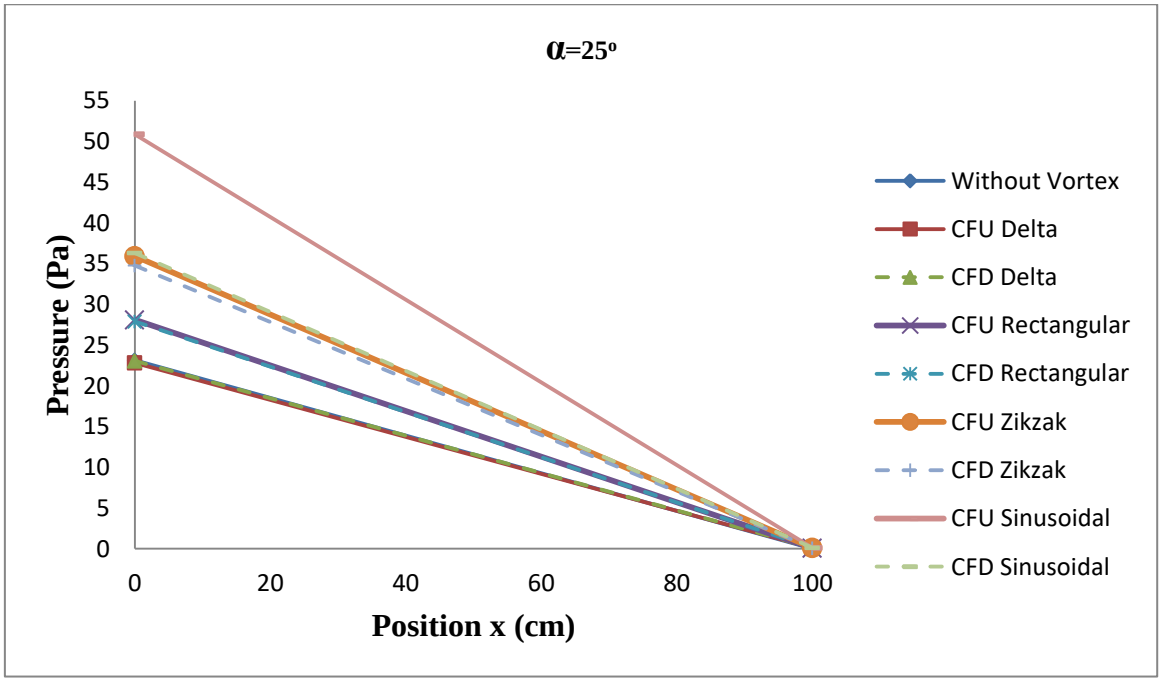

Figure (5-10) Inlet and outlet pressure in the duct

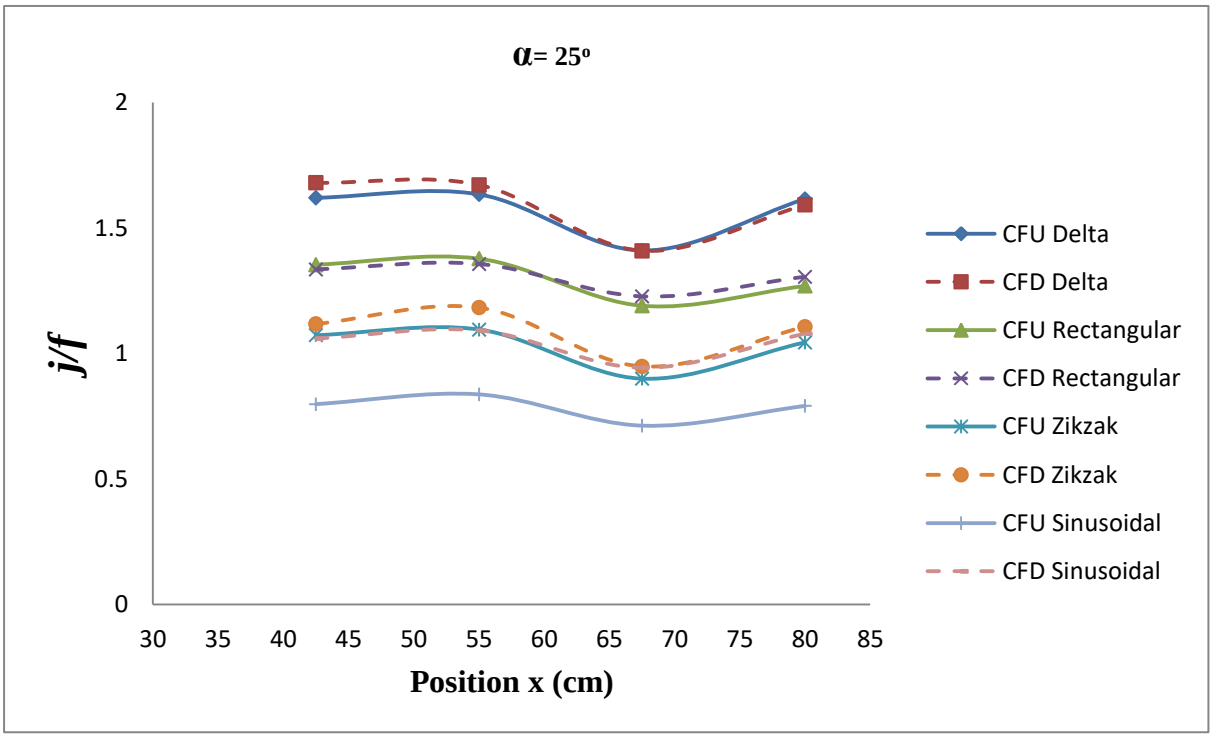

Figure (5-11) Performance parameter

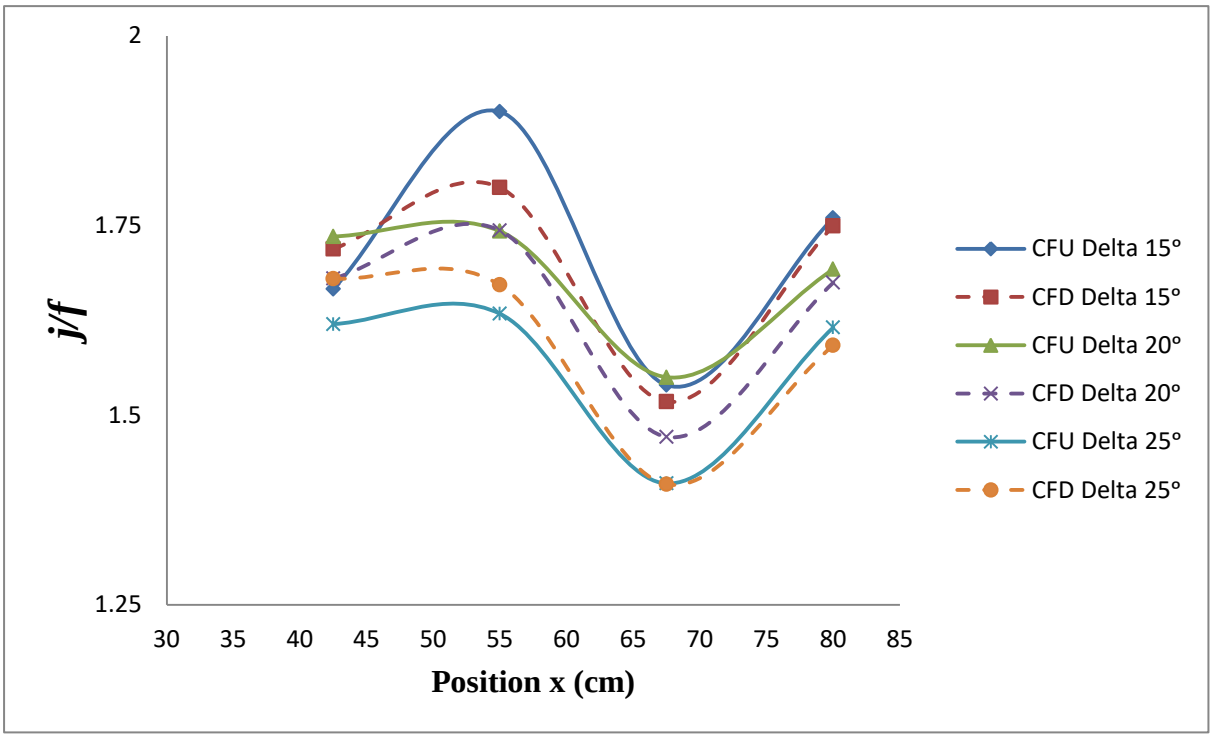

Figure (5-12) Performance parameter for delta winglets in (CFU) and (CFD) configuration at ($\alpha = 15^{o}, 20^{o}, 25^{o}$)

5.3.1.2 Velocity vector

Figures (5-13) to (5-15) illustrate that the velocity vector for two-phase flow across circular tube banks with and without (VGs) from Workbench (ANSYS - FLUEMT19.0) when the flow rate of air (8.33 Lpm) and the flow rate of water (15 Lpm).

Figure (5-13) shows the velocity vector for a two-phase flow without vortex generators.

Figure (5-14) shows the velocity vector for a two-phase flow with (VGs) in a (CFU) configuration. It can be observed that the flow velocity is increased, and the flow is directed toward the circular tube's surface by (VGs).

Figure (5-15) shows the velocity vector for two-phase flow with (VGs) in a (CFD) configuration. It can be observed that the flow velocity is increased, and the flow is directed toward the circular tube's surface by (VGs).

The (CFU) configuration shows velocity of longitudinal vortices is higher than the (CFD). As the induced velocity of longitudinal vortices is considerably higher than that of the frontal velocity, vortices transport the fluid from the wake region of the tubes to the main flow regions, promoting enhanced mixing of the bulk fluid.

The velocity distributions at the entrance region show uniformity. After the flow passes the first pair of the winglet vortex generators, the velocity of the flow increases at near the second row of the circular tubes regimes, but the velocity behind the winglet vortex generators is seen to decrease. These behaviors are found again between the second row of the winglet vortex generators and the third row of the circular tubes. The variations of the flow attack angles show a similar profile of the velocity distributions. The effect of the flow attack angles, at ($\alpha = 15^{o}$), provides the highest velocity values, while ($\alpha = 20^{o}, 25^{o}$) perform the lowest values at similar conditions. This is due to the fact that ($\alpha = 15^{o}$) provides the greatest vortex strength and turbulence level in compared to other cases. In addition, at ($\alpha = 15^{o}$) results in the increase in the vortex intensity and also provides the highest values of the velocity distributions over the circular tube banks heat exchanger.

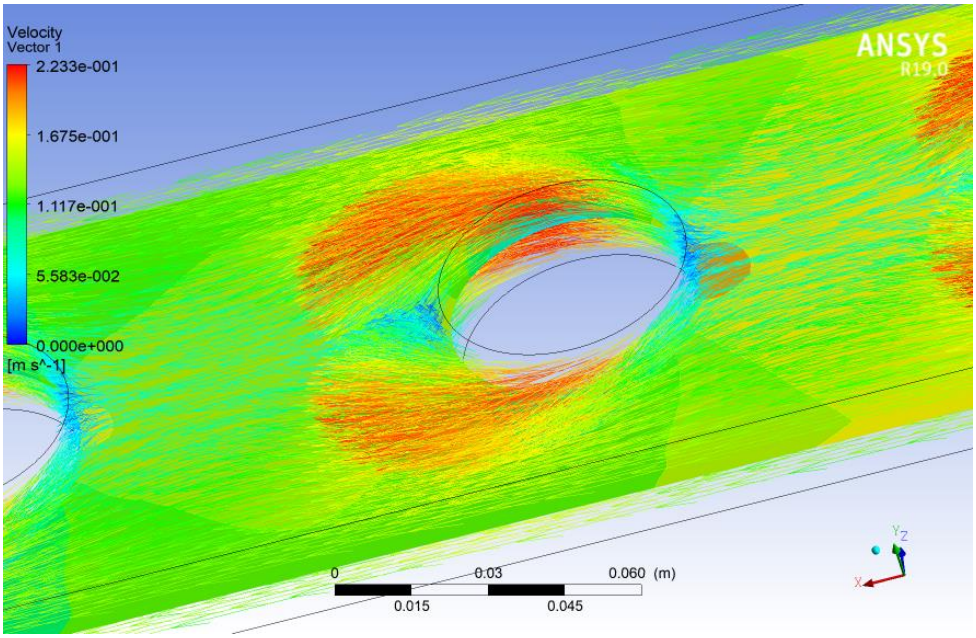

Figure (5-13) Velocity vector for two-phase flow across circular tube banks without vortex generators at (x = 55 cm)

α = 15°

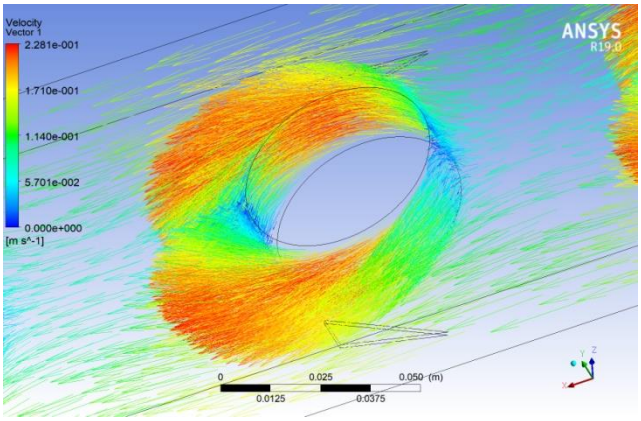

(a)

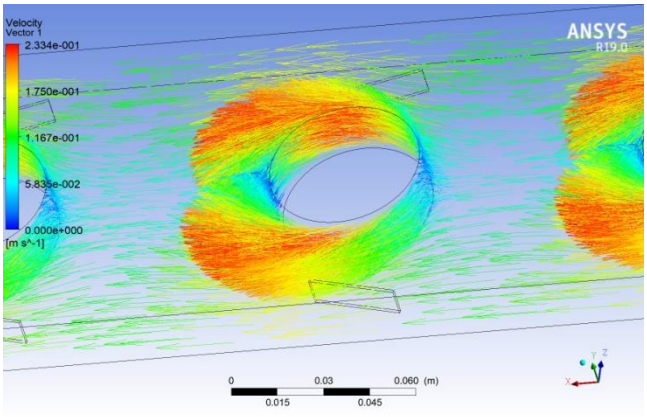

(b)

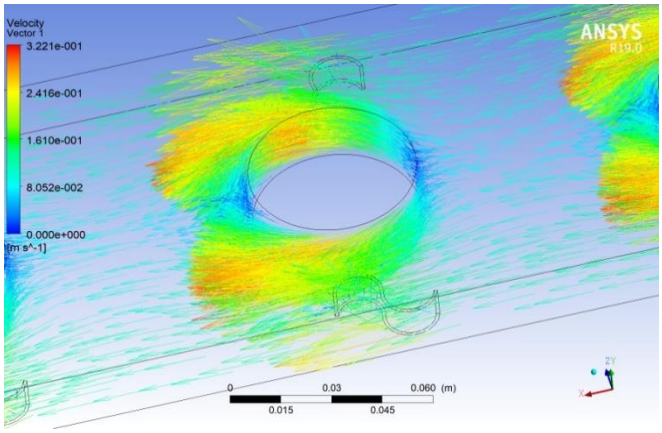

(c)

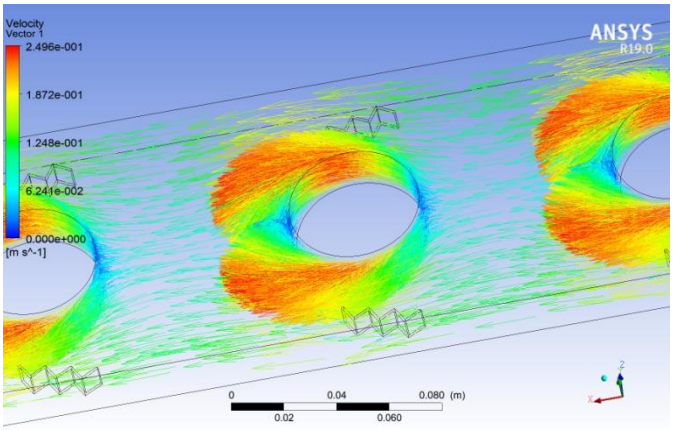

(d)

$\alpha = 20^{o}$

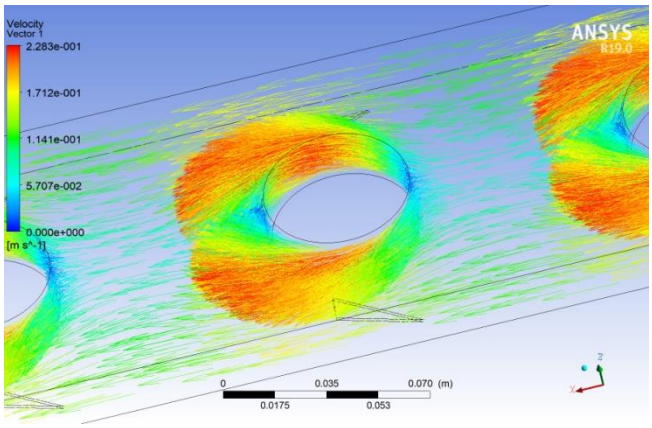

(a)

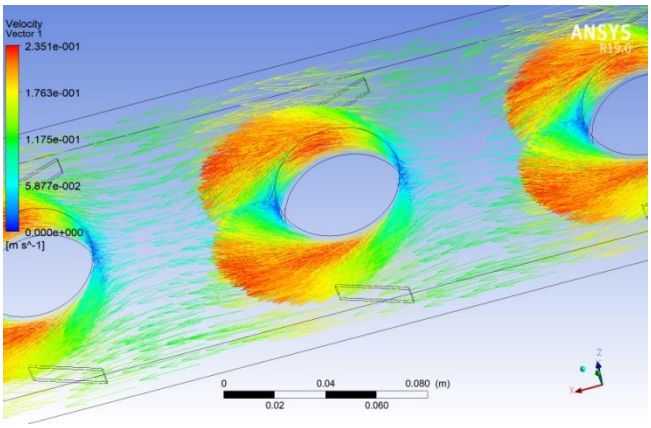

(b)

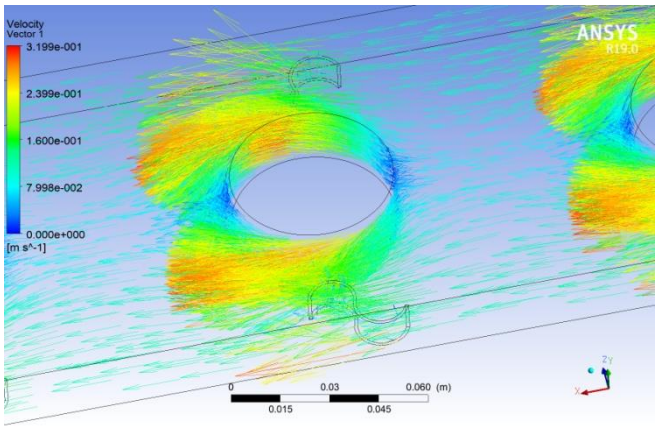

(b)

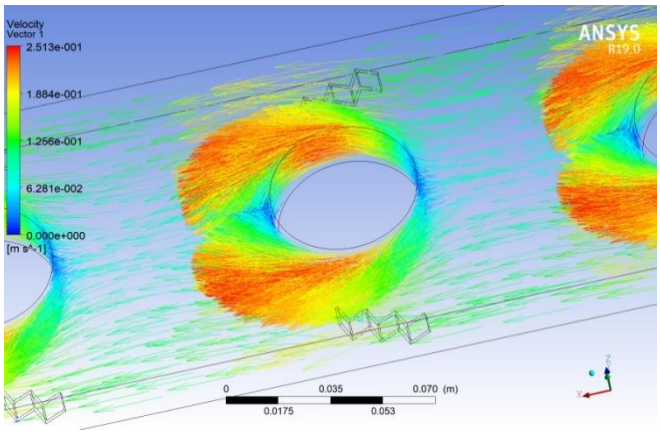

(d)

α = 25°

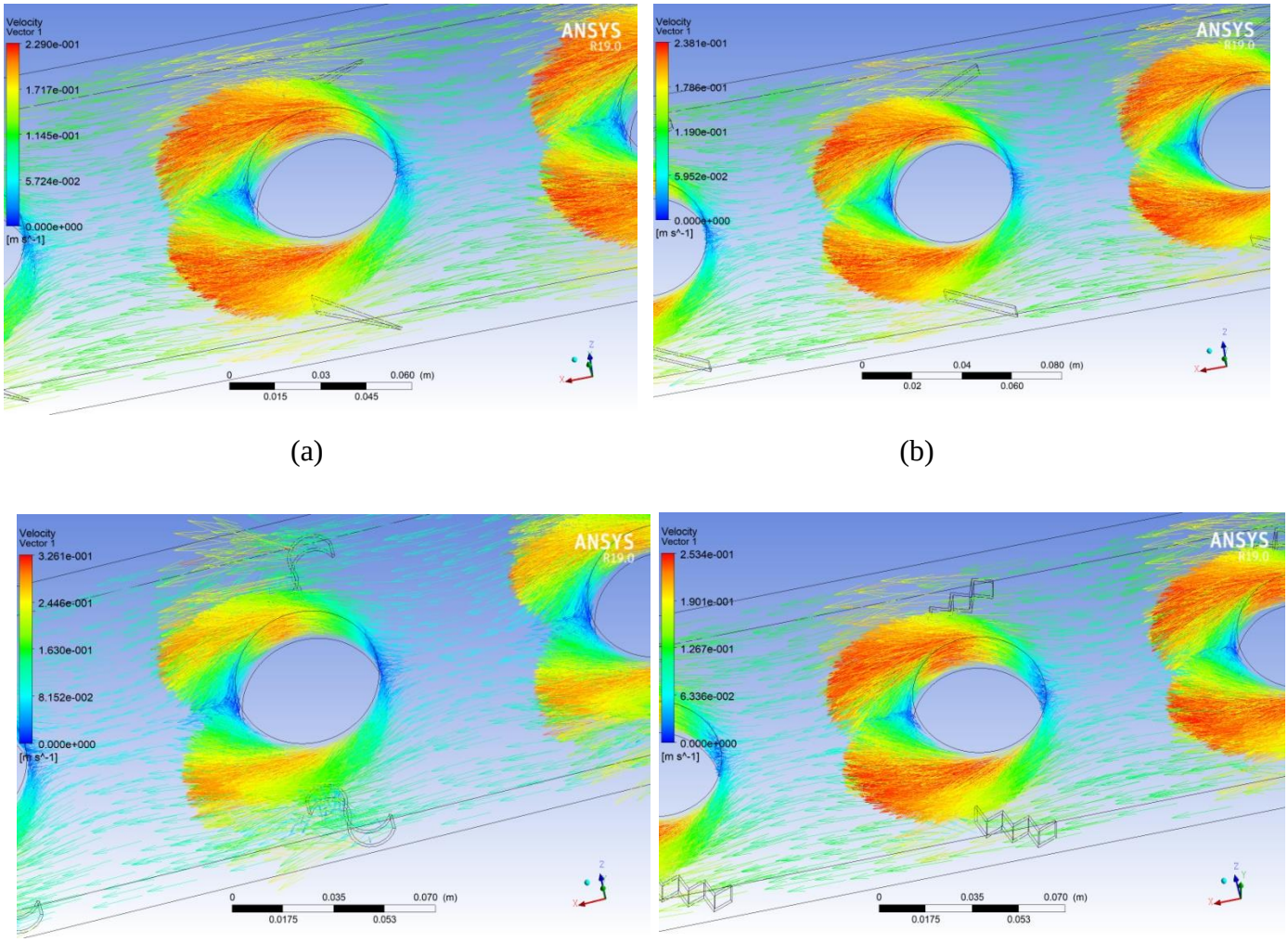

(a) (b)

(c) (d)

Figure (5-14) Velocity vector for two-phase flow across circular tube banks with (VGs) in (CFU) configuration at (x = 55 cm) (a) delta (b) rectangular (c) sinusoidal wavy (d) zikzak

$\alpha = 15^{o}$

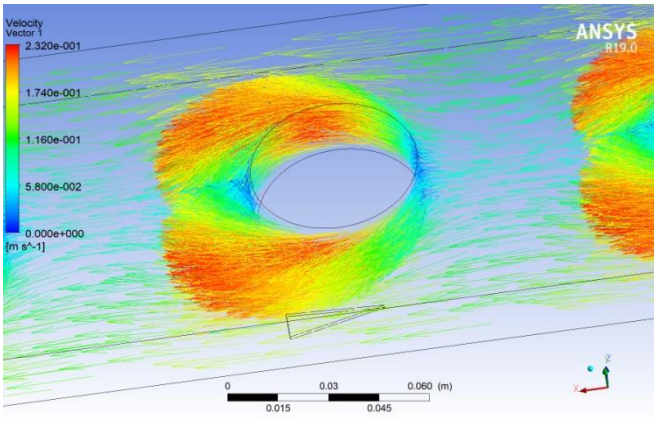

(a)

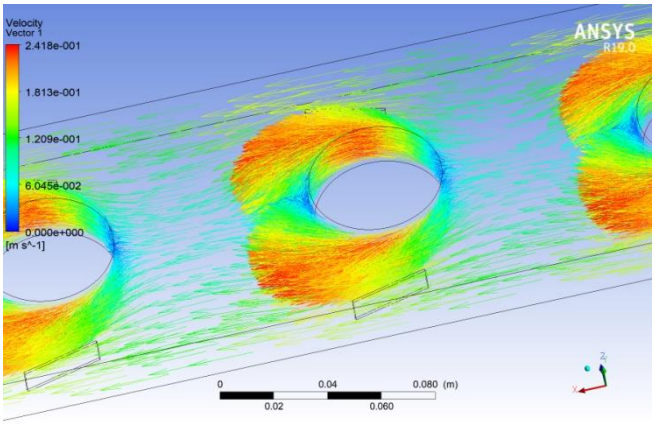

(b)

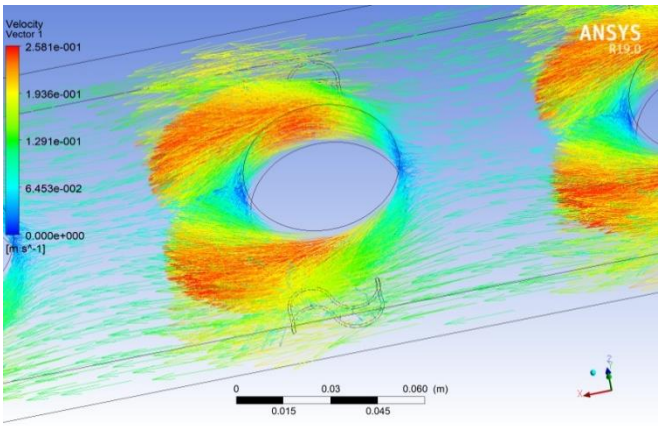

(b)

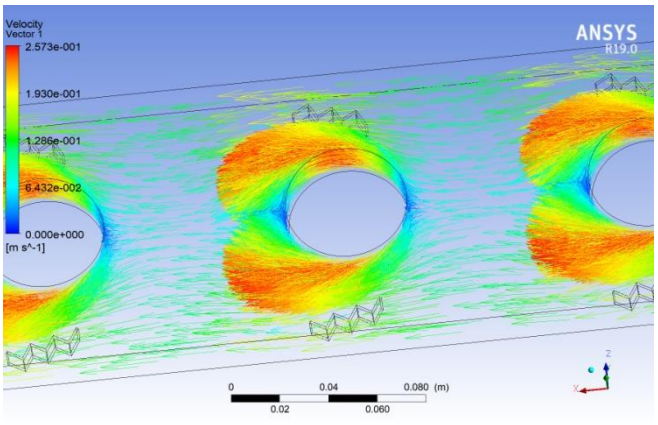

(d)

$\alpha = 20^{o}$

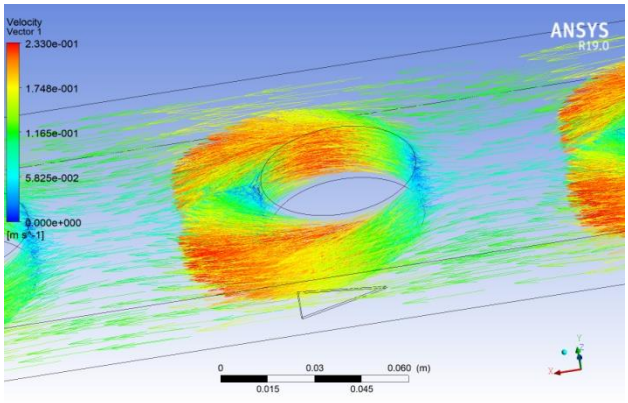

(a)

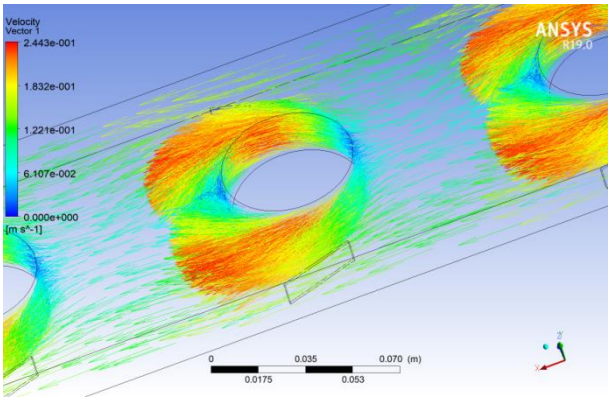

(b)

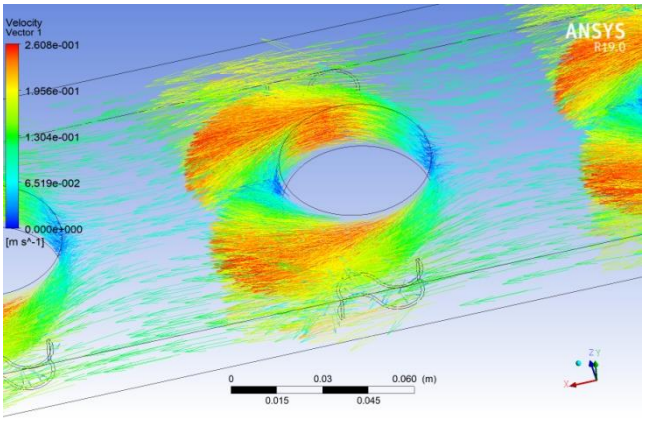

(c)

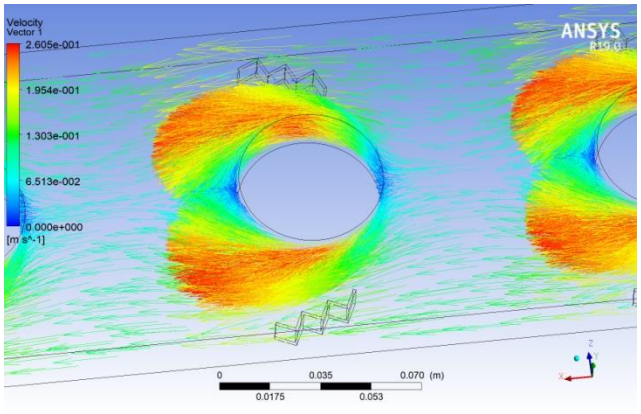

(d)

α = 25°

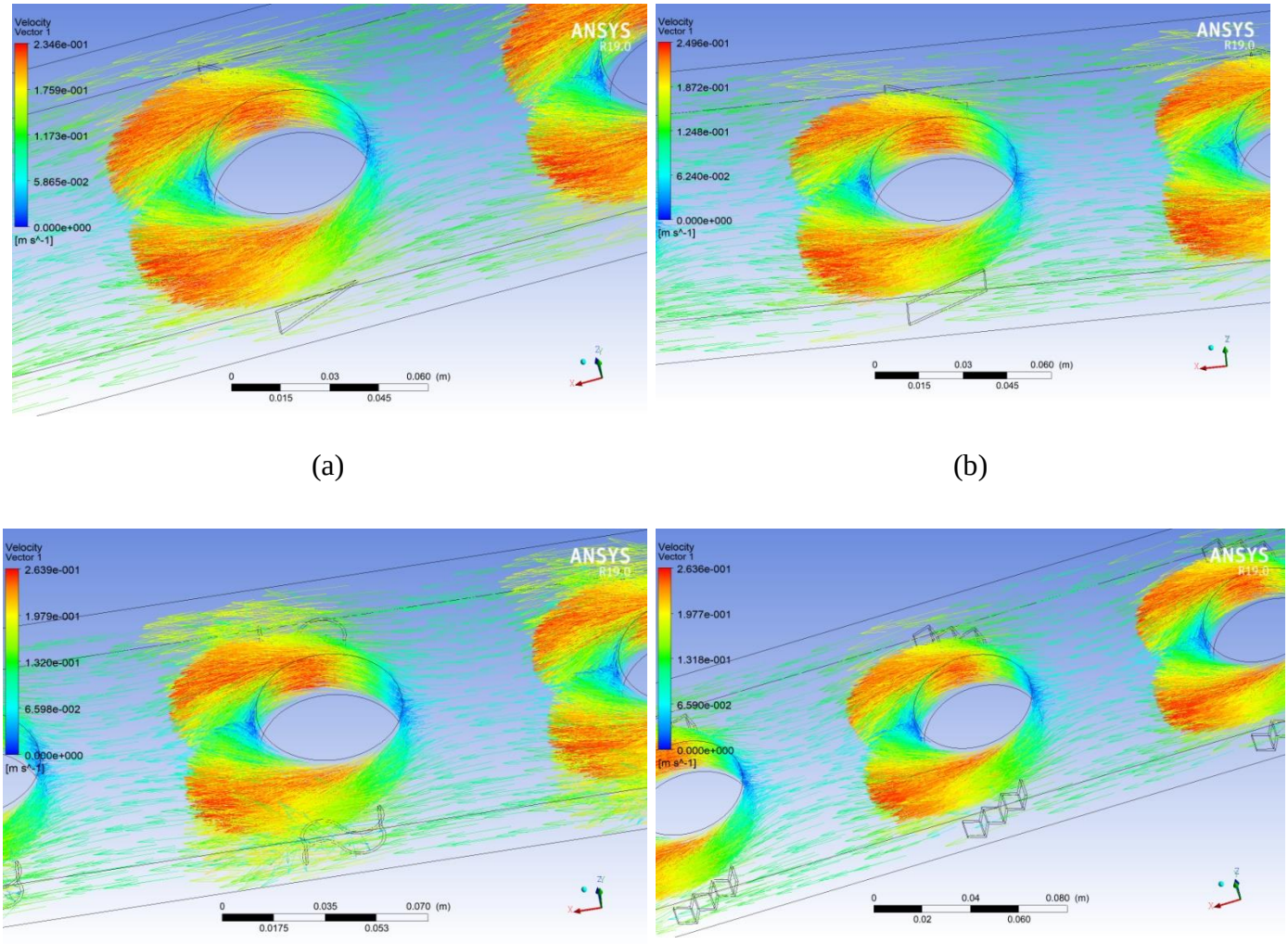

Figure (5-15) Velocity vector for two-phase flow across circular tube banks with (VGs) in (CFD) configuration at (x = 55 cm) (a) delta (b) rectangular (c) sinusoidal wavy (d) zikzak

5.3.2 Oval Tube Banks

5.3.2.1 Effect of configuration, angle of attack, and shape of vortex generators

Table (5-5) describes all situations in the duct when various types of vortex generators are used. Figure (5-16) shows the temperature gradient between water-air and surfaces of the oval tube at many points in the duct, and Figure (5-17) illustrates the inlet and outlet pressure in the duct at an angle of attack (15^o).

Table (5-5) Angle of attack (15^o)

Vortex type		**Rate of decreasing in ΔT (%)**	**ΔP**	
			Rate of increasing (%)	Rate of decreasing (%)
Delta	CFU	42.5	---	8
	CFD	42.2	---	7.13
Rectangular	CFU	42.88	---	3.8
	CFD	42.86	0.1	---
Zikzak	CFU	43.26	30.8	---
	CFD	43.24	32	---
Sinusoidal	CFU	42.83	65.34	---
	CFD	42.8	39.47	---

Figure (5-18) shows the performance parameter at many positions in the duct at an angle of attack (15^o). The delta winglets' performance is more excellent than the other winglets in the (CFU) and (CFD) arrangements.

Table (5-6) describes all situations in the Duct when various vortex generators are used. Figure (5-169) shows the temperature gradient between

water-air flow and surfaces of the oval tube at many points in the duct, and Figure (5-20) illustrates the inlet and outlet pressure in the duct at an angle of attack (20^o).

Figure (5-21) shows the performance parameter at many positions in the duct at an angle of attack (20^o). The performance of Delta winglets in the (CFU) and (CFD) configurations is more significant compared to the other winglets.

Table (5-6) Angle of attack (20^o)

Vortex type		**Rate of decreasing in ΔT (%)**	**ΔP**	
			Rate of increasing (%)	Rate of decreasing (%)
Delta	CFU	40	---	4.93
	CFD	41.28	---	4.1
Rectangular	CFU	43.17	6.6	---
	CFD	42.74	6.95	---
Zikzak	CFU	44.5	36.77	---
	CFD	42	35.38	---
Sinusoidal	CFU	44.6	76.58	---
	CFD	41.63	41.76	---

Table (5-7) describes all situations in the duct when various types of vortex generators are used. Figure (5-22) shows the temperature gradient between water-air flow and surfaces of the oval tube at many points in the duct, and Figure (5-23) illustrates the inlet and outlet pressure in the duct at an angle of attack (25^o).

Table (5-7) Angle of attack (25^o).

Vortex type		**Rate of decreasing in ΔT (%)**	**ΔP**	
			Rate of increasing (%)	Rate of decreasing (%)
Delta	CFU	36.54	---	1.6
	CFD	41.34	---	0.025
Rectangular	CFU	42	18.5	---
	CFD	43.57	17.4	---
Zikzak	CFU	41.84	44.4	---
	CFD	41.59	41.94	---
Sinusoidal	CFU	43	92.1	---
	CFD	44.2	49	---

Figure (5-24) shows the performance parameter at many positions in the duct at an angle of attack (25^o). The performance of Delta winglets in the (CFD) arrangement is higher than the other winglets.

The (CFD) configuration shows a better overall performance than the (CFU). Due to the pressure difference and frictional flow effects, longitudinal vortices are generated behind the winglet pairs. As the induced velocity of longitudinal vortices is considerably higher than that of the frontal velocity, vortices transport the fluid from the wake region of the oval tubes to the main flow regions, promoting enhanced mixing of the bulk fluid.

The above observed that in all cases, any types of vortex generators were used in oval tube banks that promoted thermo-hydraulic performance in the (HE). There was usually a pressure drop which can illustrate as follows; for the case without used vortex generators, the resistance of the flow of air in the

duct results only from the friction between air particles and duct walls with oval tube walls. The resistance of the airflow in the duct when vortex generators were used not only results from the friction between air particles and duct walls with oval tube walls but also from extra resistance, which causes an increase in pressure drop through flow in the duct.

Figure (5-25) shows performance parameter for delta winglets in (CFU) and (CFD) configuration at ($\alpha = 15^o, 20^o, 25^o$). The overall performance of delta winglets with (CFD) configuration is better at an angle of attack of ($\alpha = 15^o$) compared to the other two angles of attack. This occurs because a low angle of attack can generate more turbulence, vortex intensity, and impinging flows than a high angle of attack. As seen, ($\alpha = 15^o$) performs the best temperature distribution, while the case of ($\alpha = 20^o, 25^o$) provide the opposite result. This angle ($\alpha = 15^o$) generates the greatest vortex intensity, which results in the most effective mixing of the fluid flow throughout the test duct.

Figure (5-26) shows performance parameter for delta winglets with circular or oval tube banks in (CFU) and (CFD) configuration at ($\alpha = 15^o$). Circular tube with (VGs) in (CFU) and (CFD) configurations show a better heat transfer ability than oval tubes in (CFU) and (CFD) configuration in the first two rows of tubes, however, the opposite is observed in the last two rows of tubes because of more intensification of the mixing motion. Due to a manifested reduction in pressure drop penalty, the overall performance of the oval tube is better than the circular tubes for all cases. For a more meaningful insight into the relative performance, heat transfer per unit pressure drop is noted that oval tubes with delta (VGs) in a (CFD) configuration yield the optimum output if the pressure drop penalty is considered.

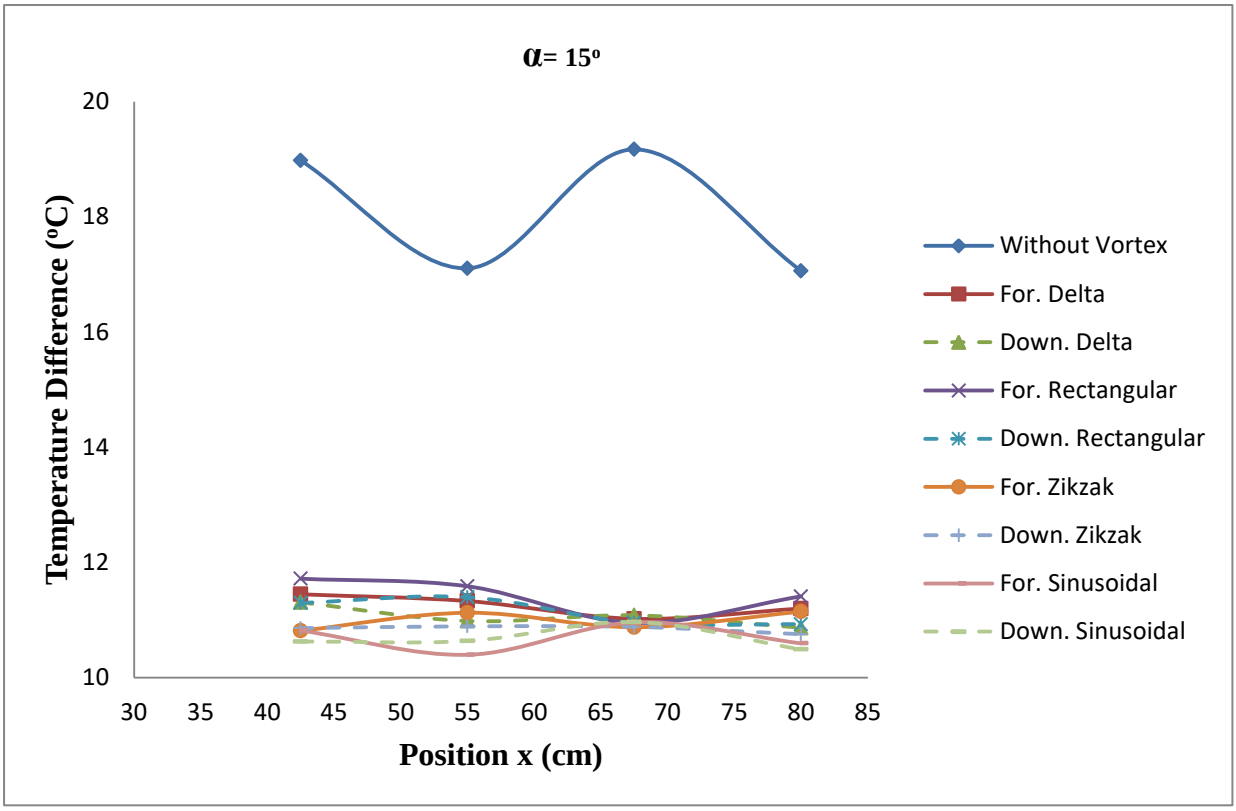

Figure (5-16) The temperature difference between two-phase flow (water and air) and oval tube surfaces at many positions in the duct (x = 42.5, 55, 67.5, and 80 cm)

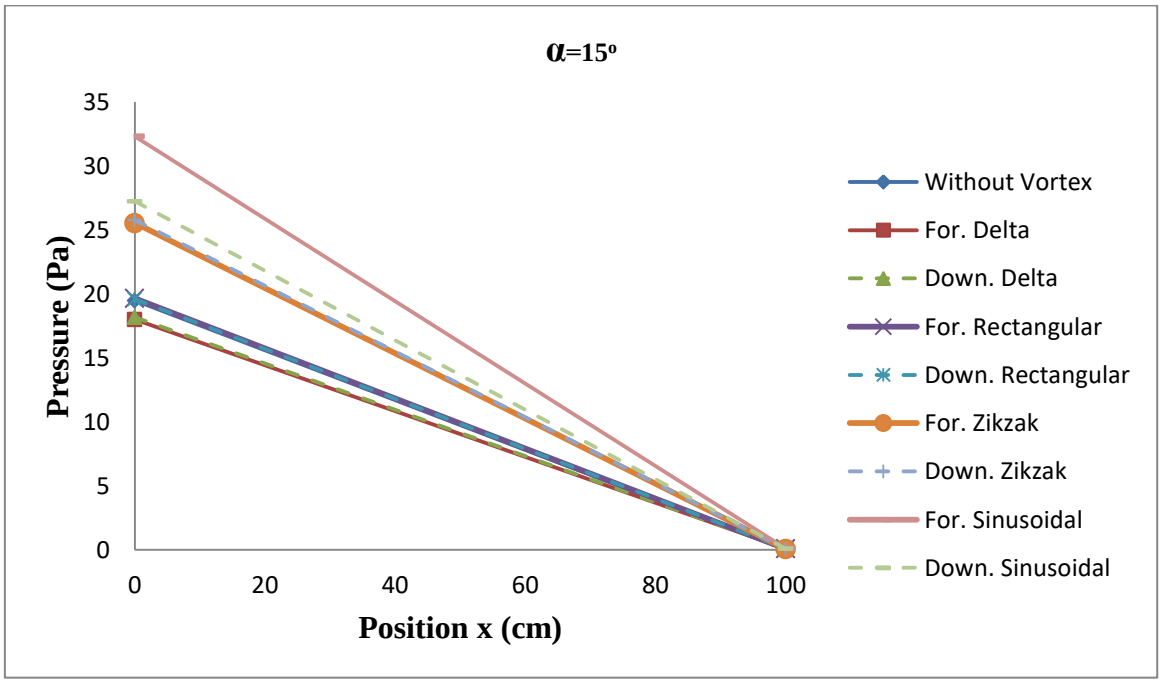

Figure (5-17) Inlet and outlet pressure in the duct

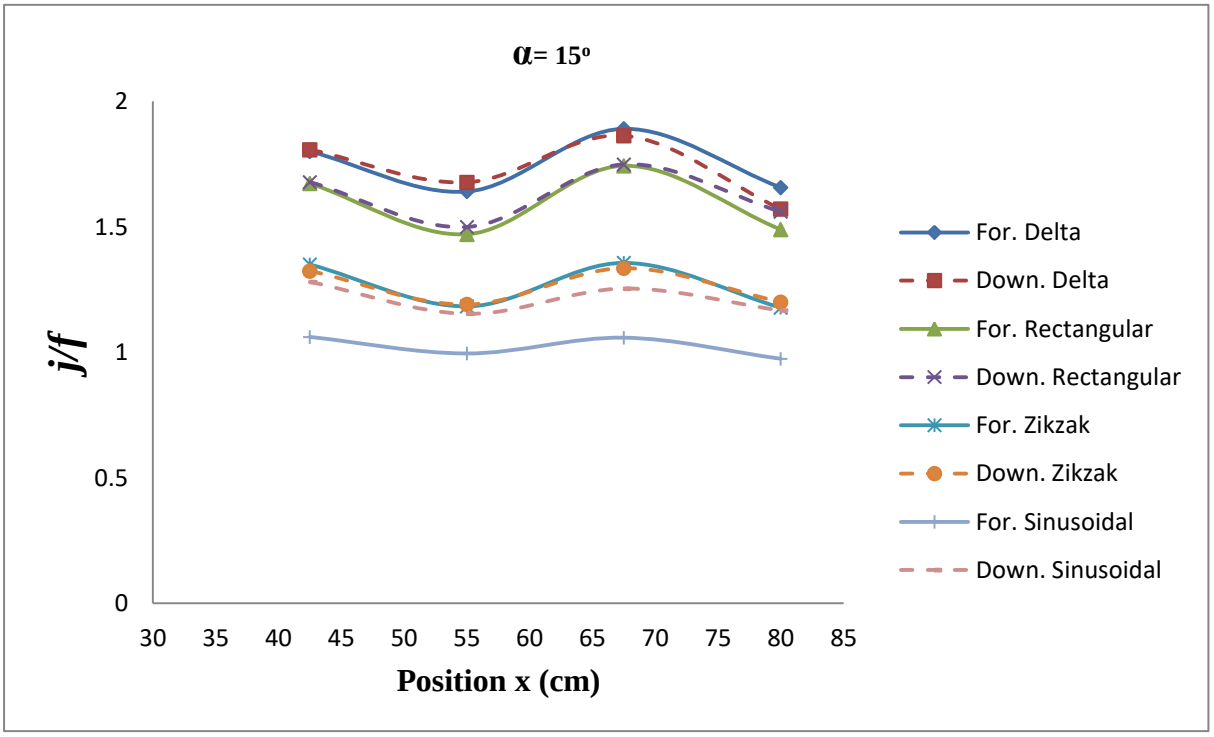

Figure (5-18) Performance parameter

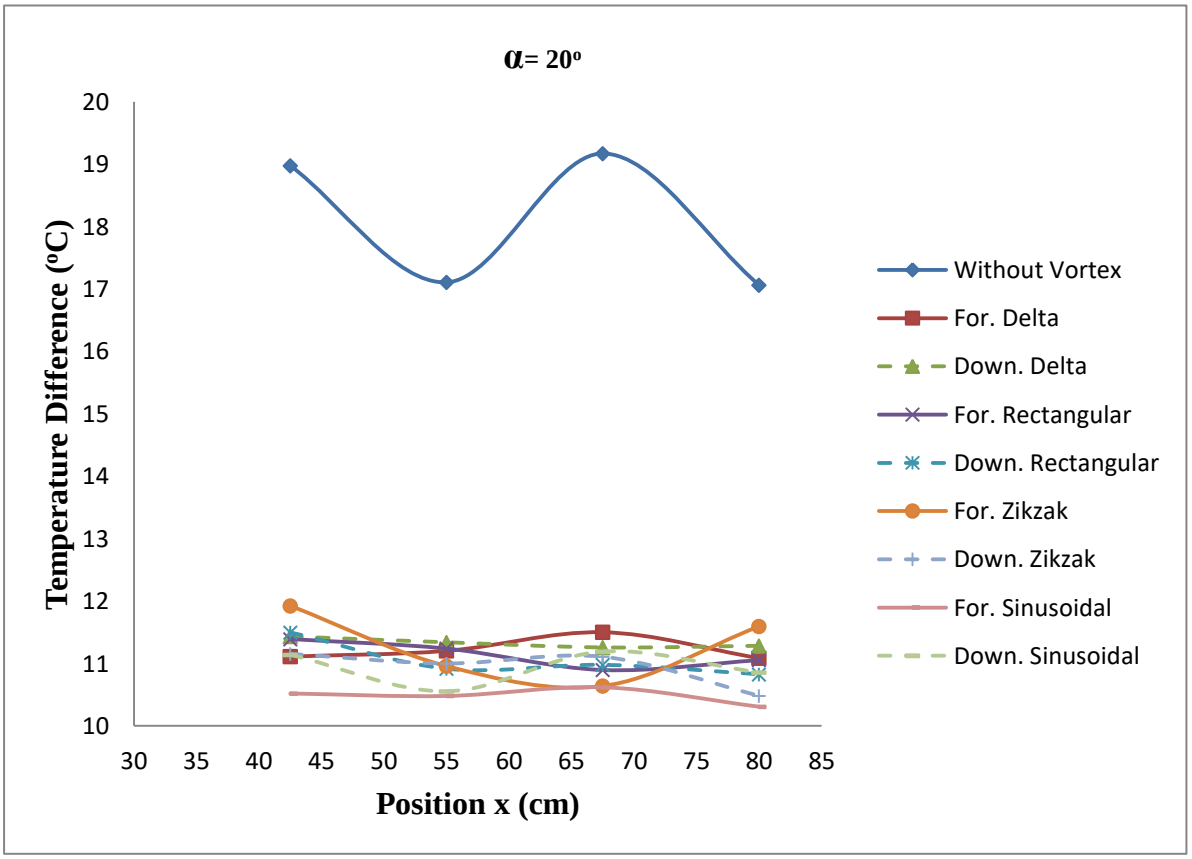

Figure (5-19) The temperature difference between two-phase flow (water and air) and oval tube surfaces at many positions in the duct (x = 42.5, 55, 67.5, and 80 cm)

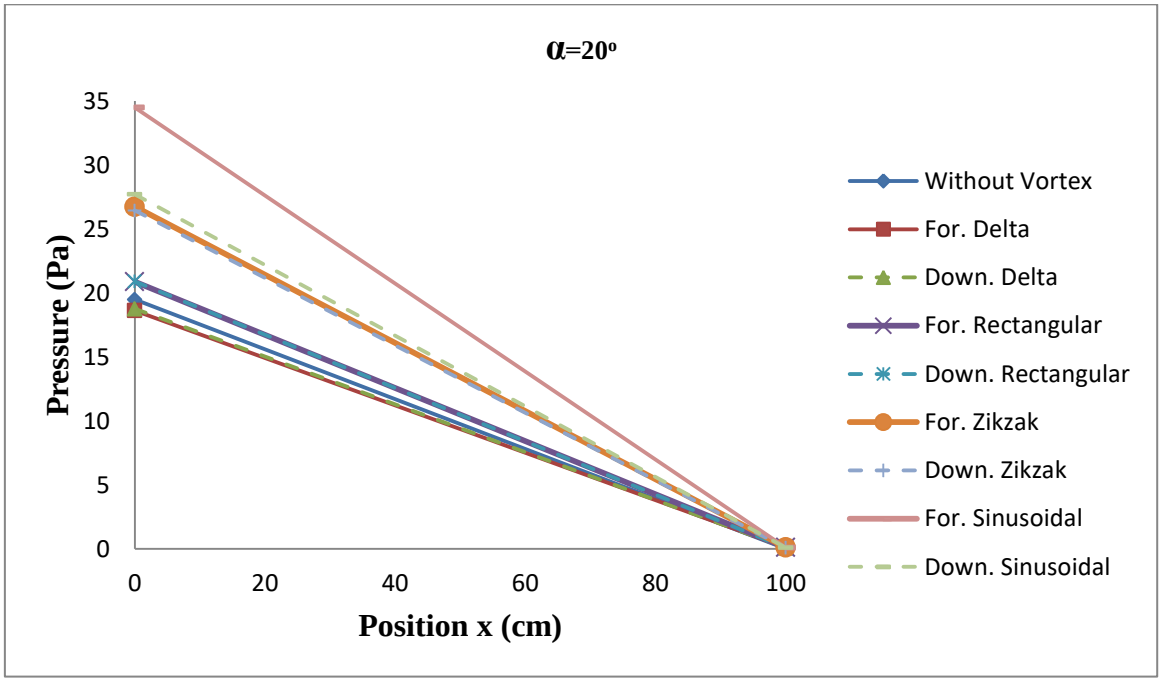

Figure (5-20) Inlet and outlet pressure in the duct

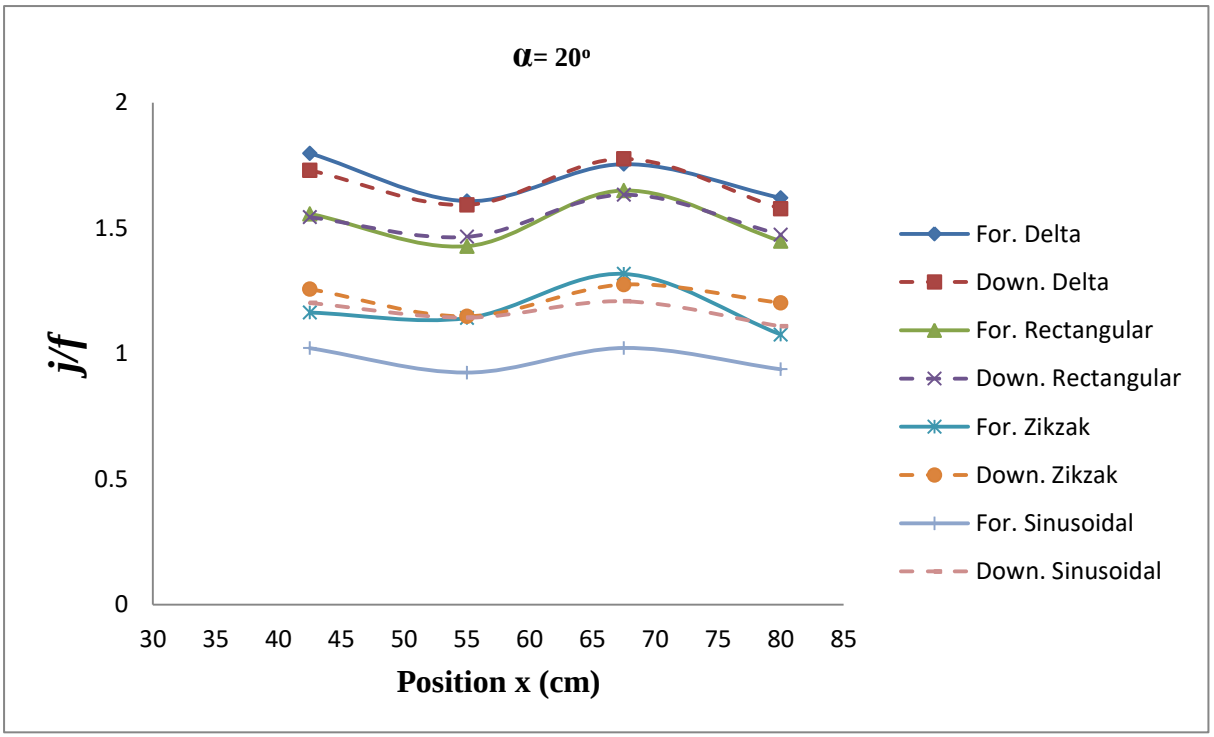

Figure (5-21) Performance parameter

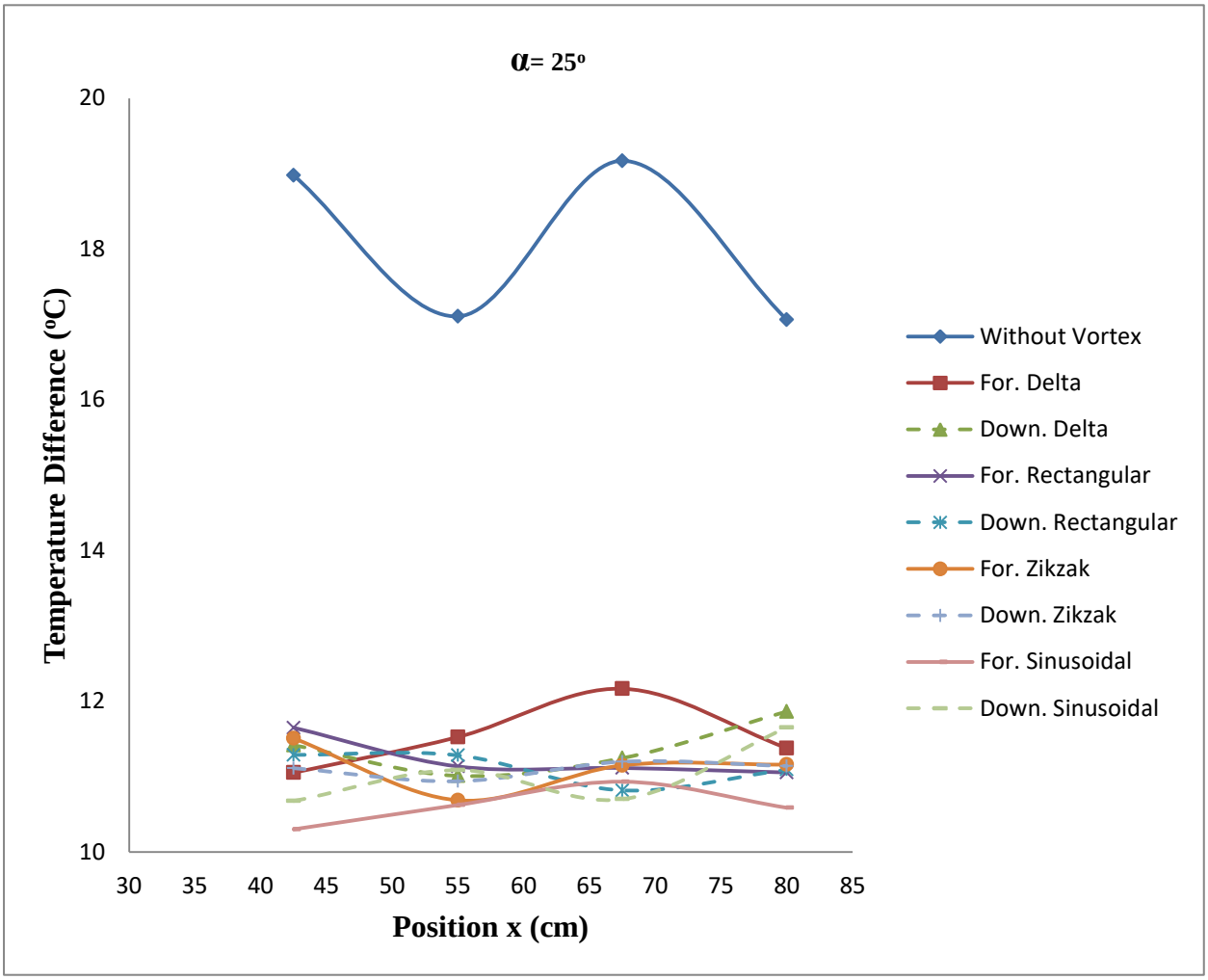

Figure (5-22) The temperature difference between two-phase flow (water and air) and oval tube surfaces at many positions in the duct (x = 42.5, 55, 67.5, and 80 cm)

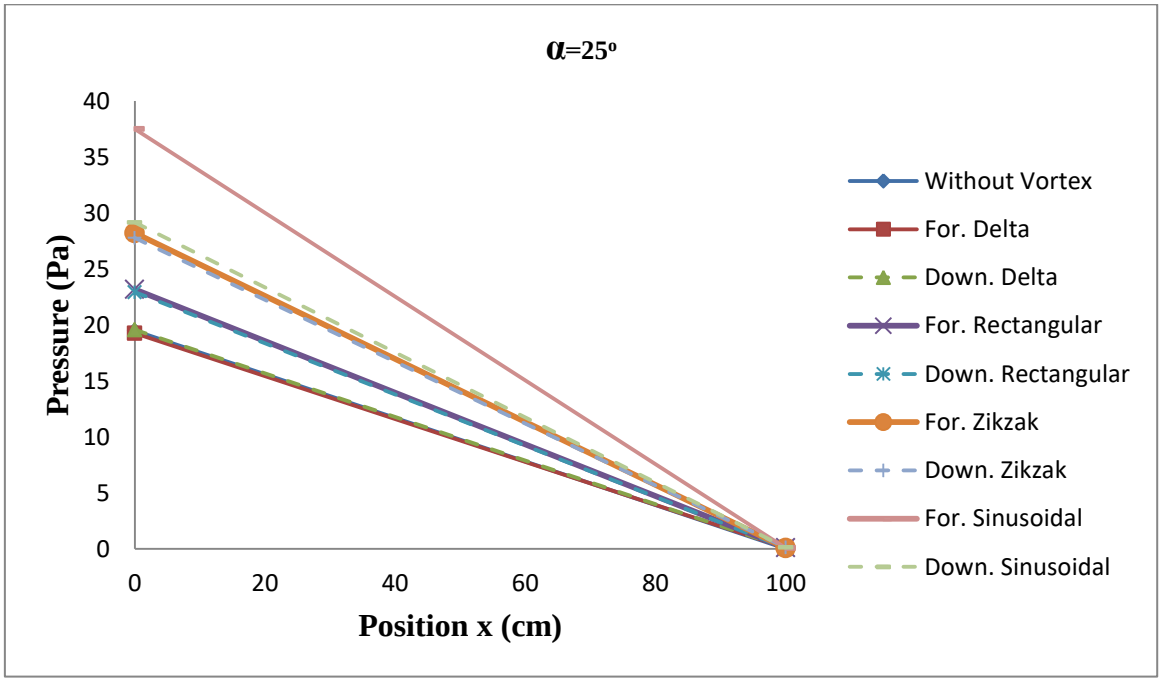

Figure (5-23) Inlet and outlet pressure in the duct

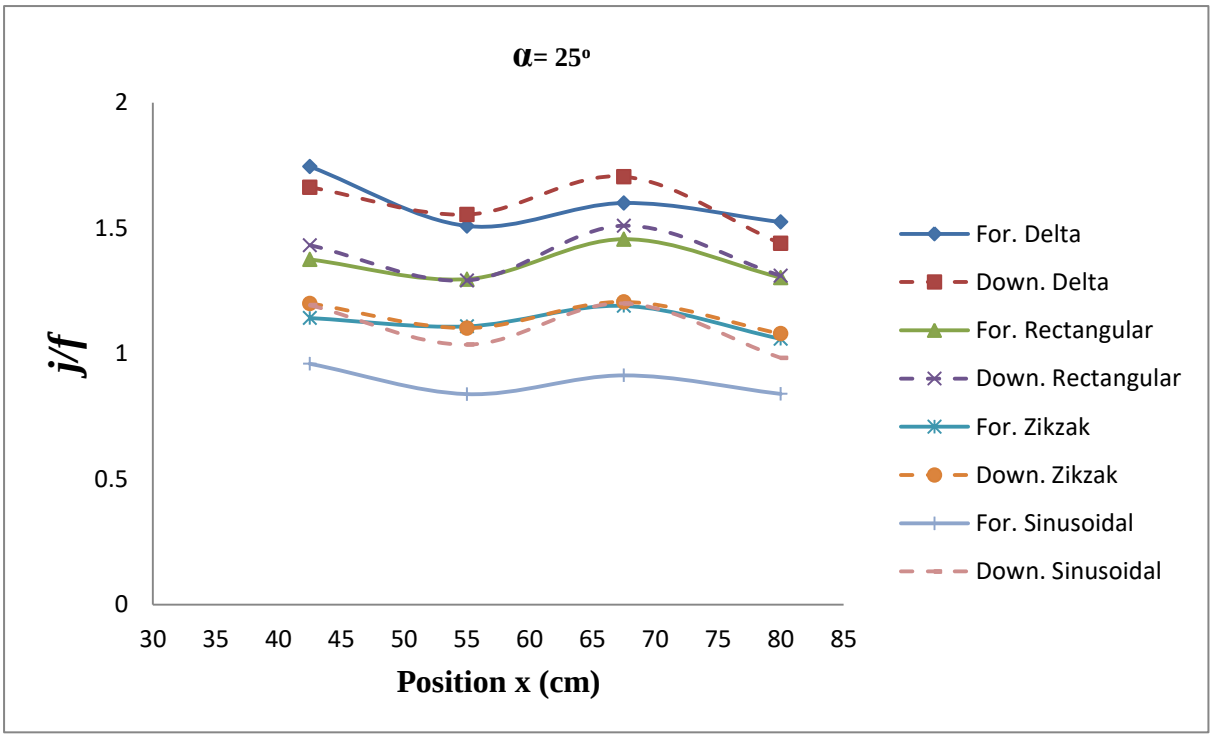

Figure (5-24) Performance parameter

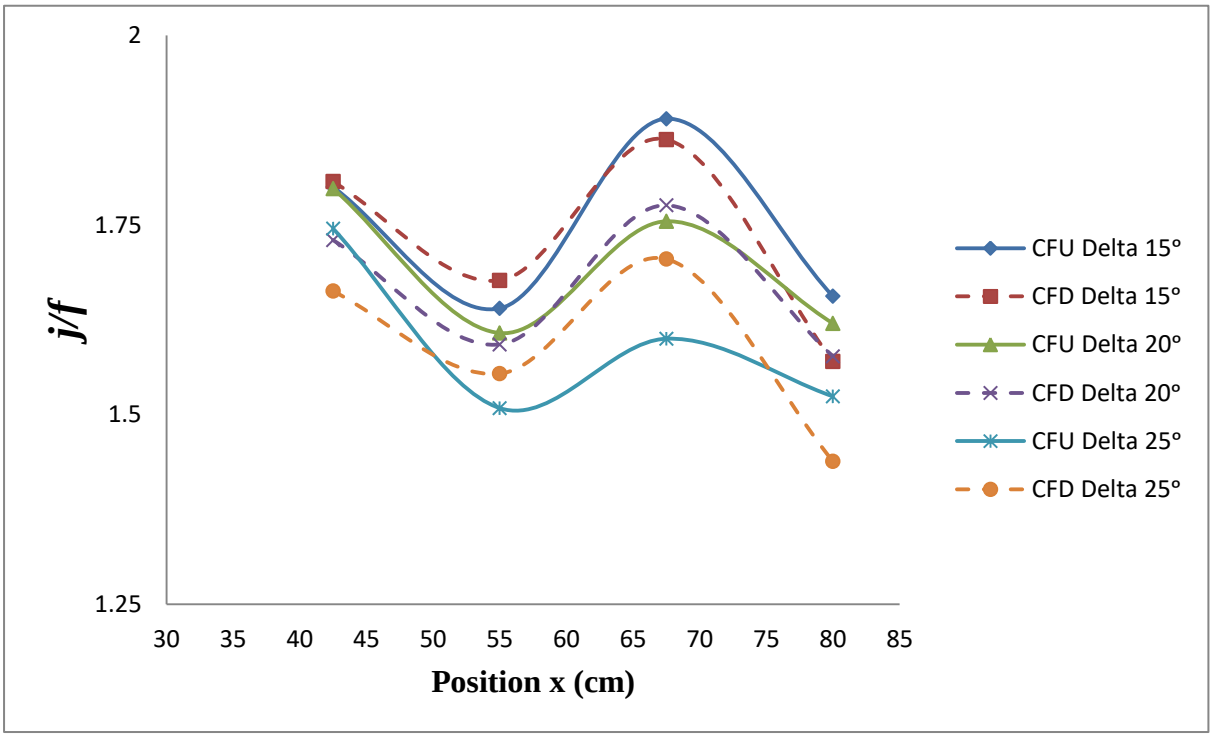

Figure (5-25) Performance parameter for delta winglets in (CFU) and (CFD) configuration at ($\alpha = 15^{o}, 20^{o}, 25^{o}$)

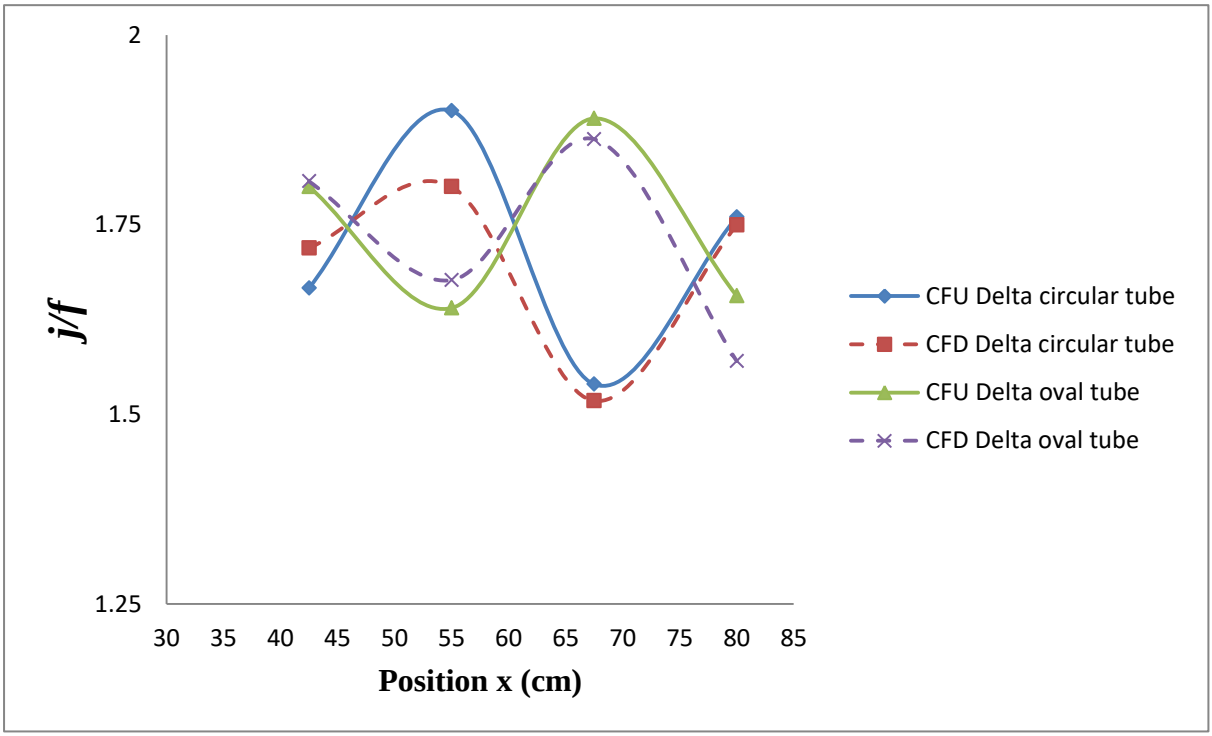

Figure (5-26) Performance parameter for delta winglets with circular or oval tube banks in (CFU) and (CFD) configuration at ($\alpha = 15^{o}$)

5.3.2.2 Velocity vector

Figures (5-27) to (5-29) illustrate that the velocity vector for two-phase flow across oval tube banks with and without (VGs) from Workbench (ANSYS – FLUENT 19.0) when the flow rate of air (8.33 Lpm) and the flow rate of water (15 Lpm).

Figure (5-27) shows the velocity vector for a two-phase flow without vortex generators.

Figure (5-28) shows the velocity vector for a two-phase flow with (VGs) in a (CFU) configuration. It can be observed that the flow velocity is increased, and the flow is directed toward the oval tube's surface by (VGs).

Figure (5-29) shows the velocity vector for a two-phase flow with (VGs) in a (CFD) configuration. It can be observed that the flow velocity is increased, and the flow is directed toward the oval tube's surface by (VGs).

The (CFU) configuration shows velocity of longitudinal vortices is higher than the (CFD). As the induced velocity of longitudinal vortices is considerably higher than that of the frontal velocity, vortices transport the fluid from the wake region of the tubes to the main flow regions, promoting enhanced mixing of the bulk fluid.

The velocity distributions at the entrance region show uniformity. After the flow passes the first pair of the winglet vortex generators, the velocity of the flow increases at near the second row of the oval tubes regimes, but the velocity behind the winglet vortex generators is seen to decrease. These behaviors are found again between the second row of the winglet vortex generators and the third row of the oval tubes. The variations of the flow attack angles show a similar profile of the velocity distributions. The effect of the flow attack angles, at ($\alpha = 15^o$), provides the highest velocity values, while ($\alpha = 20^o, 25^o$) perform the lowest values at similar conditions. This is due to the fact that ($\alpha = 15^o$) provides the greatest vortex strength and turbulence level in compared to other cases. In addition, at ($\alpha = 15^o$) results in the

increase in the vortex intensity and also provides the highest values of the velocity distributions over the oval tube banks heat exchanger.

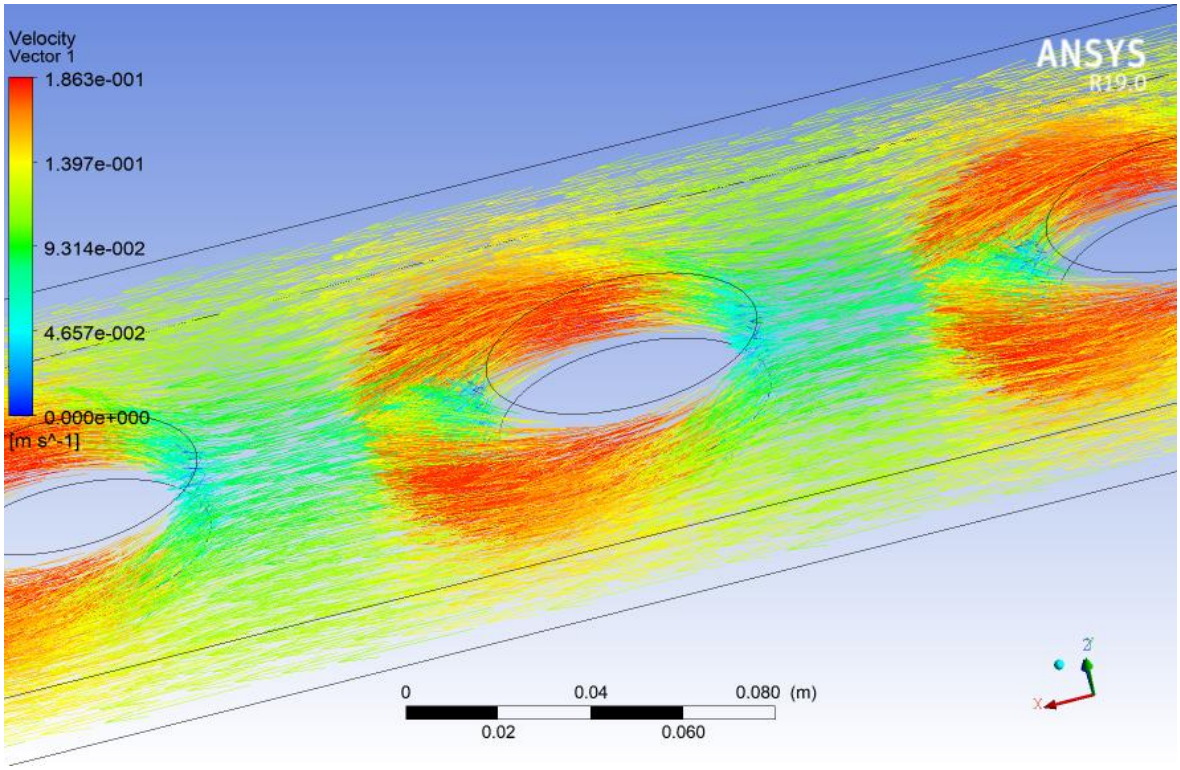

Figure (5-27) Velocity vector for two-phase flow across oval tube banks at (x = 55 cm) without vortex generators

$\alpha = 15^{o}$

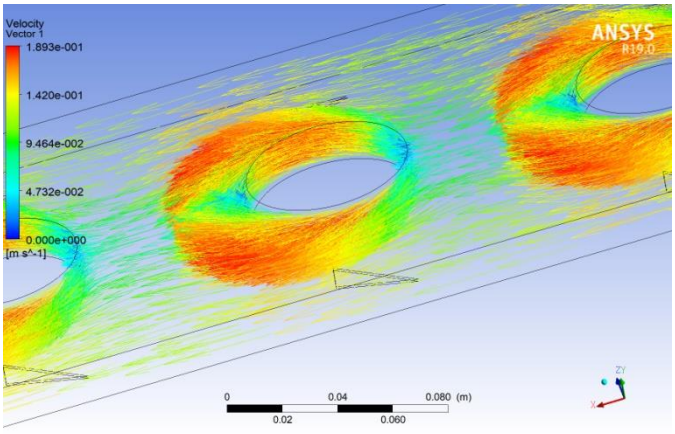

(a)

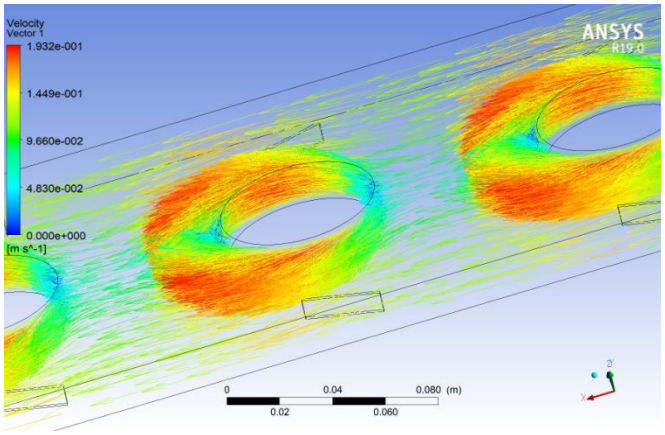

(b)

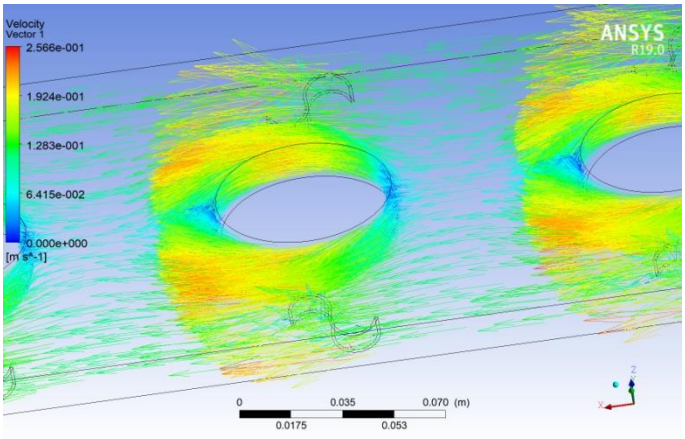

(c)

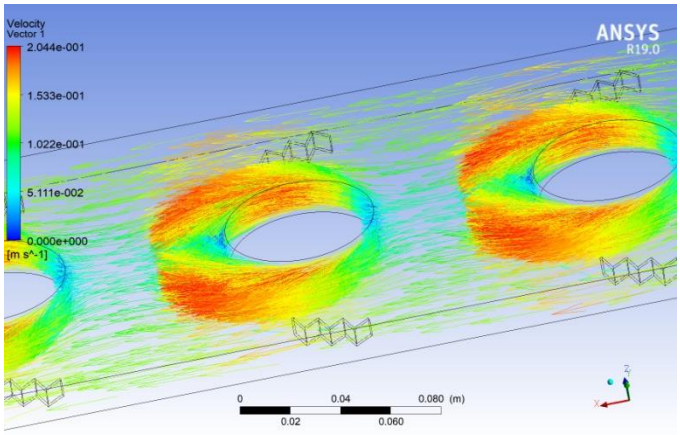

(d)

$\alpha = 20^{o}$

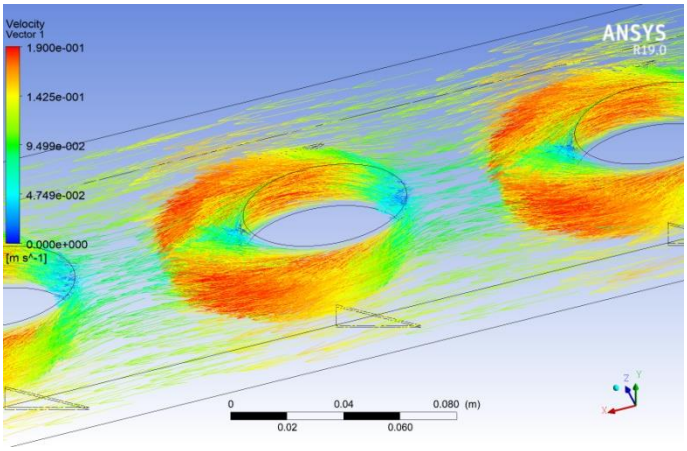

(a)

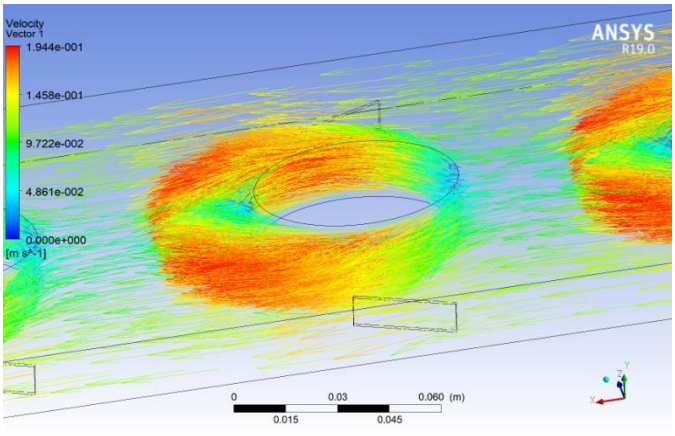

(b)

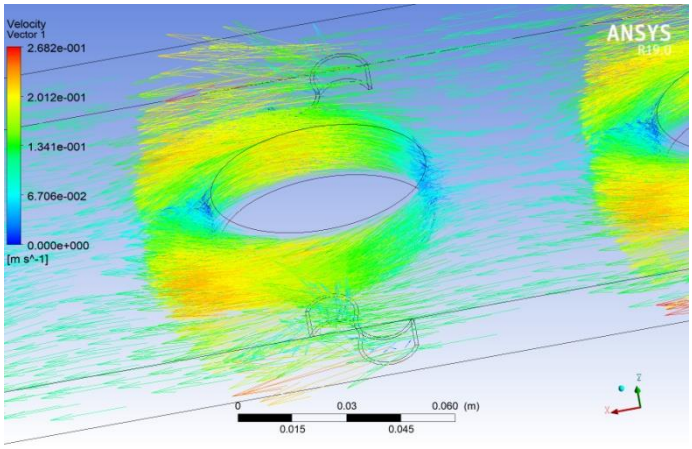

(c)

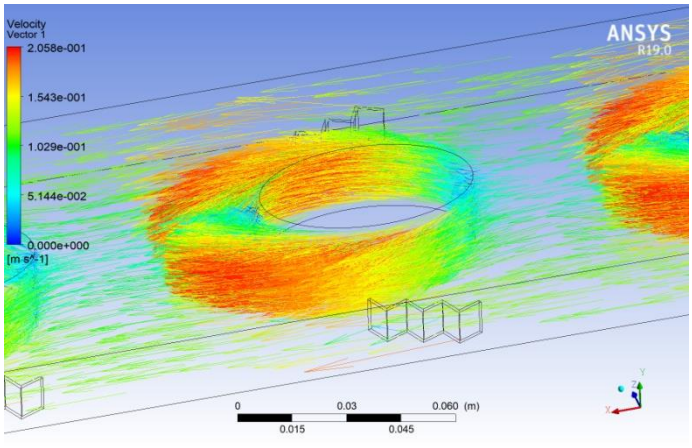

(d)

$\alpha = 25^0$

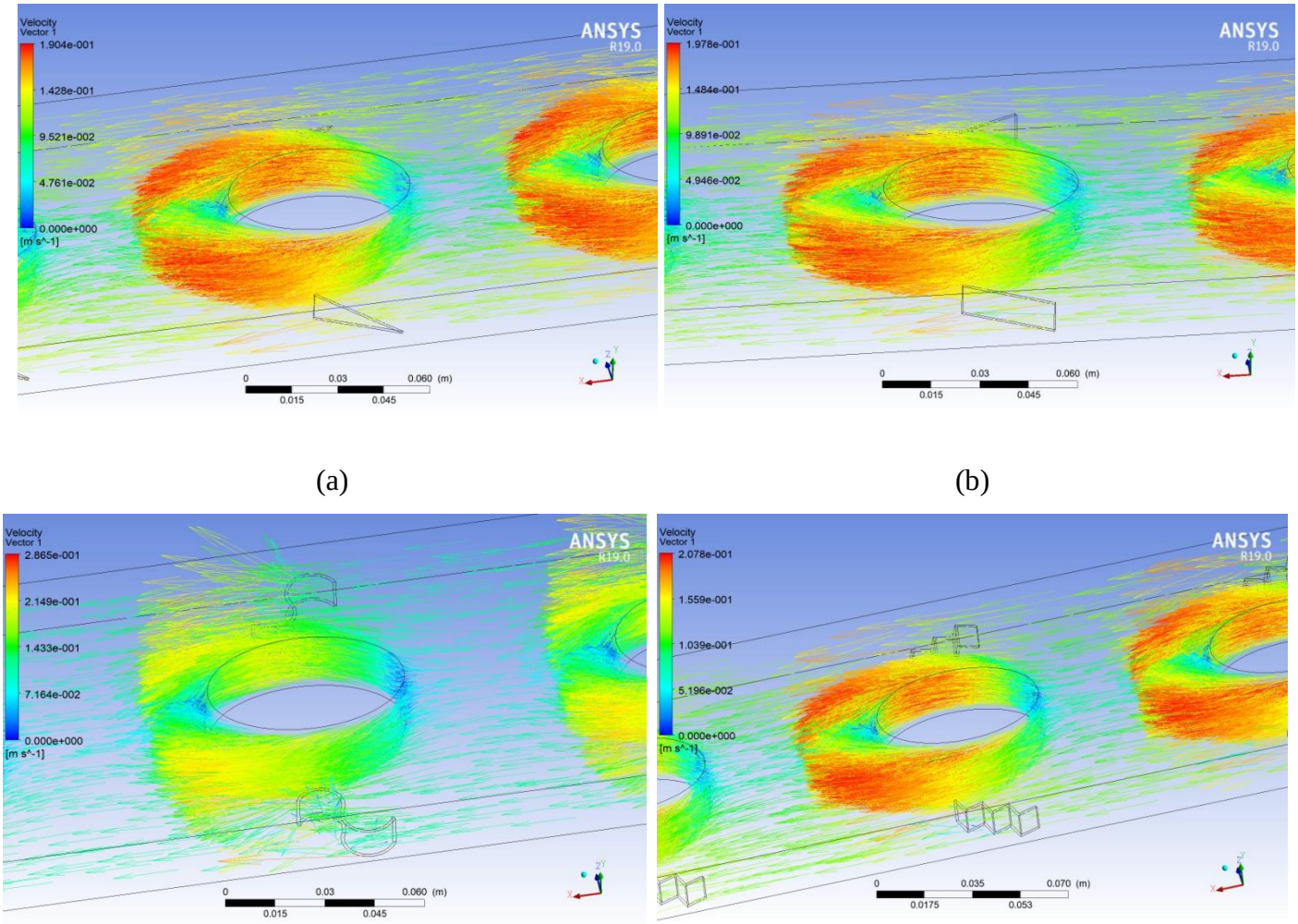

Figure (5-28) Velocity vector for two-phase flow across oval tube banks with (VGs) in (CFU) configuration at (x = 55 cm) (a) delta (b) rectangular (c) sinusoidal wavy (d) zikzak

α = 15°

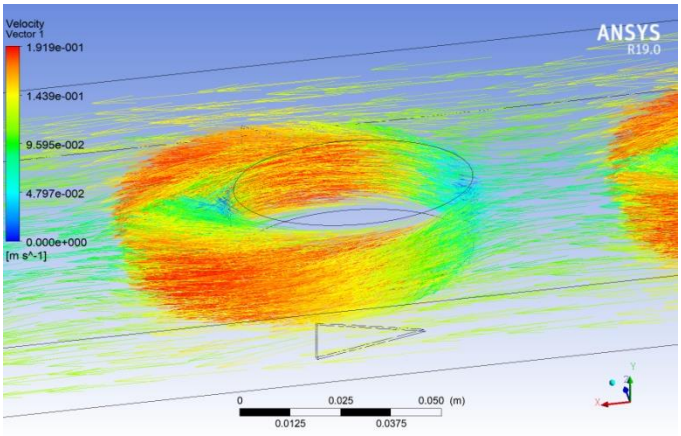
Velocity
Vector 1
1.919e-001
1.439e-001
9.595e-002
4.797e-002
0.000e+000
[m s^-1]
ANSYS
R19.0
0
0.025
0.050 (m)
0.0125
0.0375

(a)

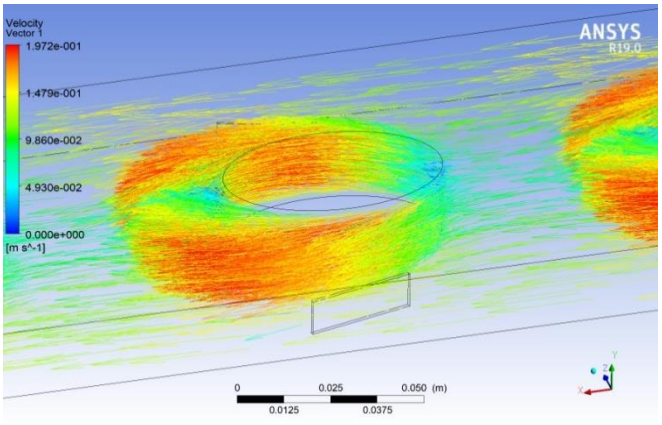
Velocity
Vector 1
1.972e-001
1.479e-001
9.860e-002
4.930e-002
0.000e+000
[m s^-1]
ANSYS
R19.0
0
0.025
0.050 (m)
0.0125
0.0375

(b)

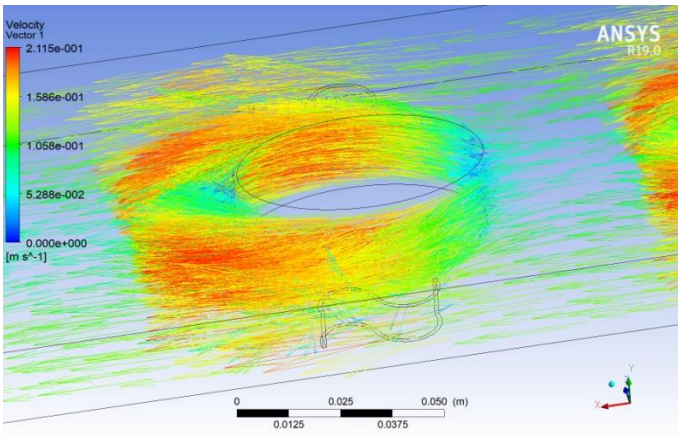
Velocity
Vector 1
2.115e-001
1.586e-001
1.058e-001
5.288e-002
0.000e+000
[m s^-1]
ANSYS
R19.0
0
0.025
0.050 (m)
0.0125
0.0375

(c)

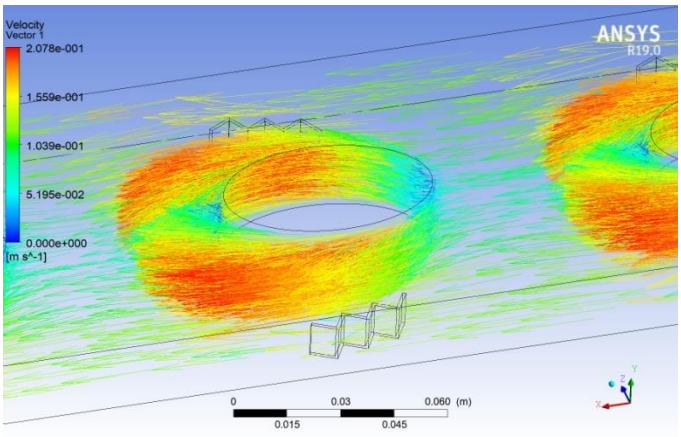
Velocity
Vector 1
2.078e-001
1.559e-001
1.039e-001
5.195e-002
0.000e+000
[m s^-1]
ANSYS
R19.0
0
0.03
0.060 (m)
0.015
0.045

(d)

$\alpha = 20^{o}$

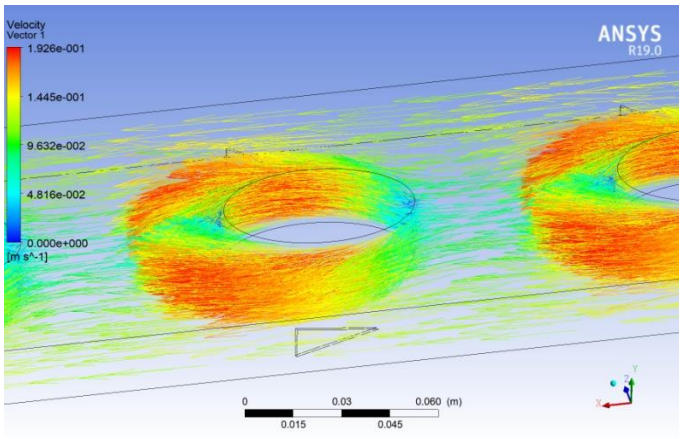

(a)

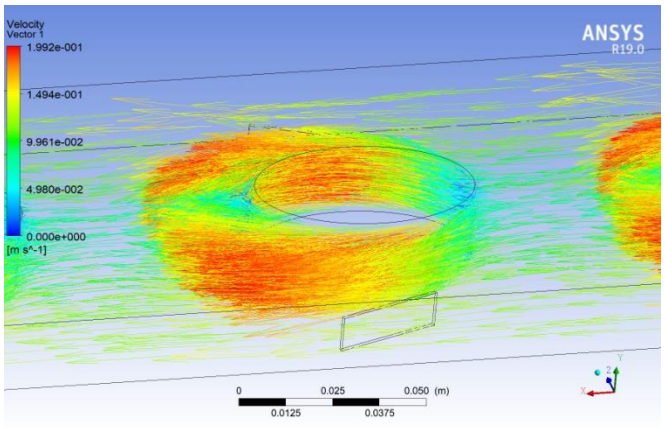

(b)

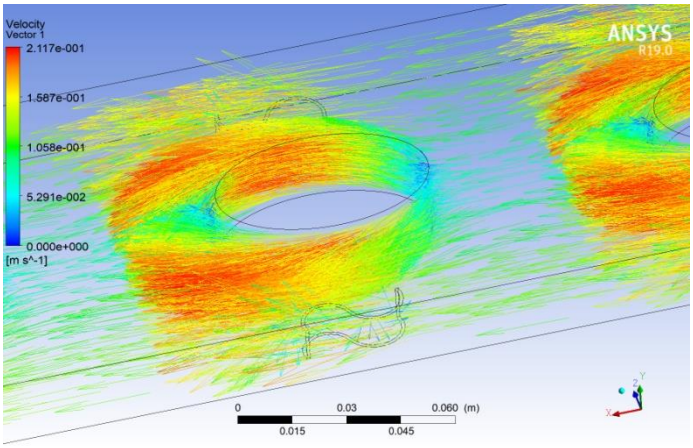

(c)

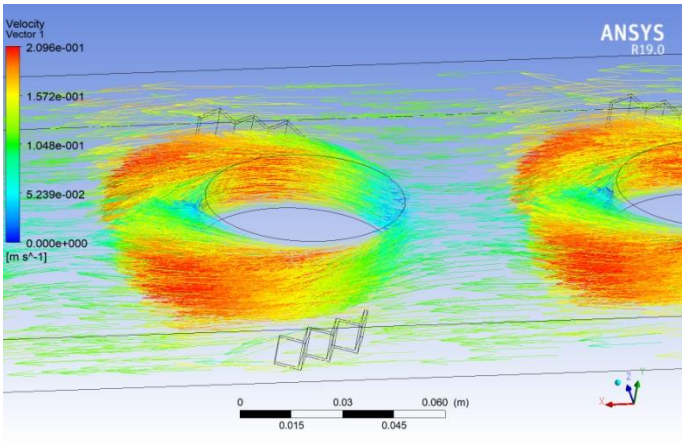

(d)

α = 25°

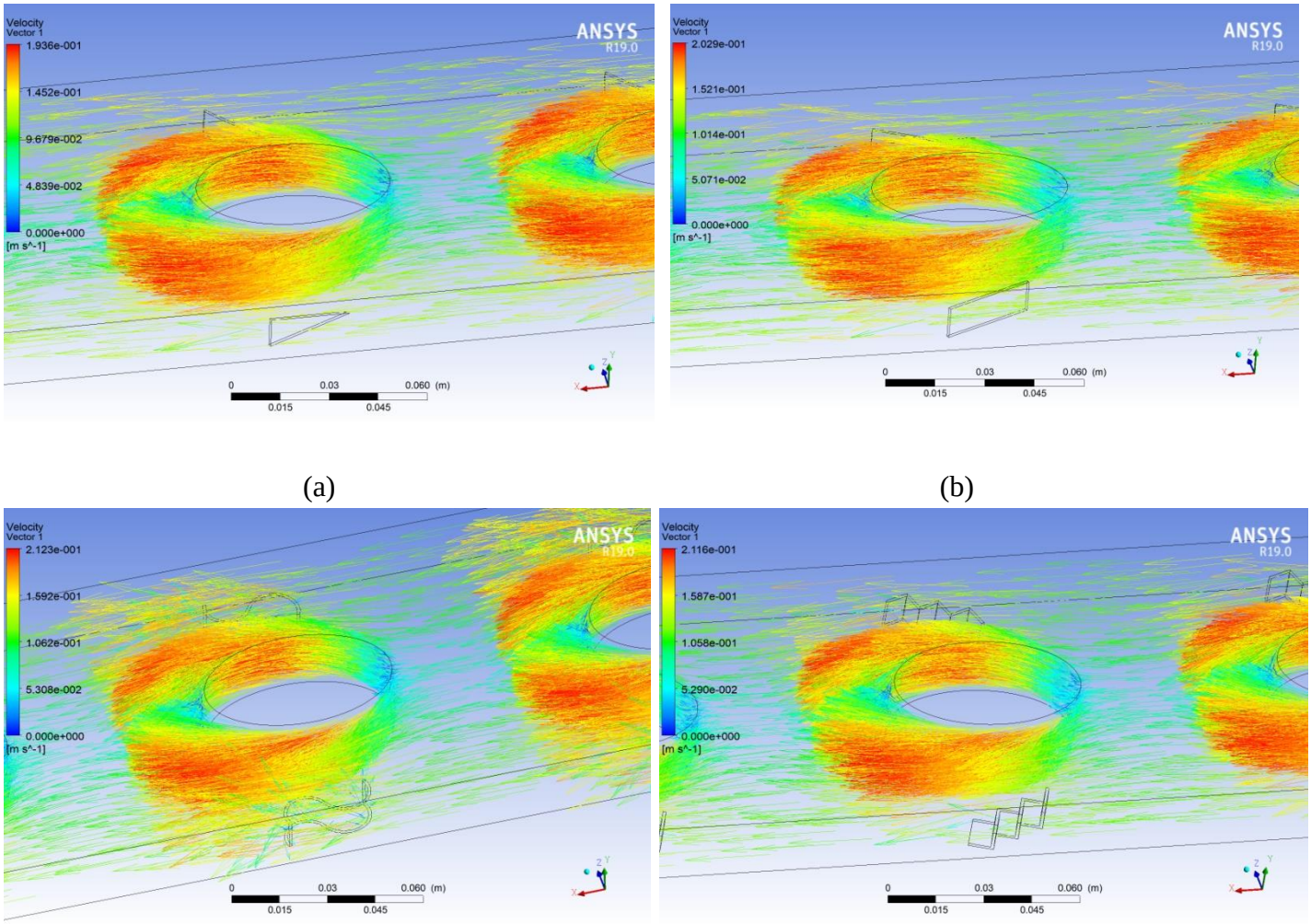

Figure (5-29) Velocity vector for two-phase flow across oval tube banks with (VGs) in (CFD) configuration at (x = 55 cm) (a) delta (b) rectangular (c) sinusoidal wavy (d) zikzak

5.4 Experimental Results

Various parameters have been investigated experimentally to determine their effect on the temperature distribution and heat transfer coefficient. These parameters are presented in Table (5-8):

Table (5-8) Experiment parameters

V_w (m/s)	V_a (m/s)	Heat power (W)
0.10417	0.057917	110
0.1215417	0.117	110
0.1375	0.17375	110

Two shapes of vortex generator are used (Delta and Rectangular), (CFD) with a (15^o) angle of attack. The temperature distributions for two different vortex generator models in two-phase flow over a bank of oval tubes under turbulent conditions have been compared. Every line represents a different type of vortex generator. Also, there is a comparison between various flow rates for two-phase flow and pressure drop through the duct.

After completing the laboratory experiments and analyzing the outcomes, the same boundary conditions accompanying them are examined for inclusion in ANSYS Workbench (19.0). Following the program, data were collected for analysis and comparison to laboratory results.

5.4.1 Single-phase flow

5.4.1.1 Effect of flow rate

Figure (5-30) shows the temperature difference between single-phase flow (water) and oval tube surfaces at many positions in the duct (x = 42.5, 55, 67.5, and 80 cm) without vortex generators for various water flow rates (15, 17.5, and 20 Lpm) experimentally with Reynolds number of (3645.95,

4254, and 4812.5). From this figure, when the water flow rate increased, the temperature difference decreased experimentally by (9.15%) and (6.33%), respectively, for reduced temperature difference at increased flow velocity. Therefore, the heat transfer coefficient increased. For without vortex generators, the subsequent peaks in front of the second and third tubes become lower and flatter because the low-speed separated flow in the wake of the preceding tube becomes the stagnation flow of the following tube. The increased velocity in front of the second tube due to the blockage of the first tube causes a stronger vortex and a higher heat transfer peak. The third peak is due to the vortex region heat transfer of the tube in the last row. The peak caused by the third tube row is lower than that of the second row because the third tube row lies in the wake of the first row. In this location, additional fluid is pumped to the hot tube surface side, substantially strengthening the mixing. Thus, heat transfer is significantly improved.

Figure (5-31) shows inlet and outlet pressure in the duct for single-phase flow (water) at many positions in the duct (x = 42.5, 55, 67.5, and 80 cm) without vortex generators for various water flow rates (15, 17.5, and 20 Lpm). The water flow rate increased the pressure drop in the duct by (33.3%) and (66.67%), respectively. The pressure drop is increased in the duct during the flow of water due to increase of form drag of the tube banks by its shape.

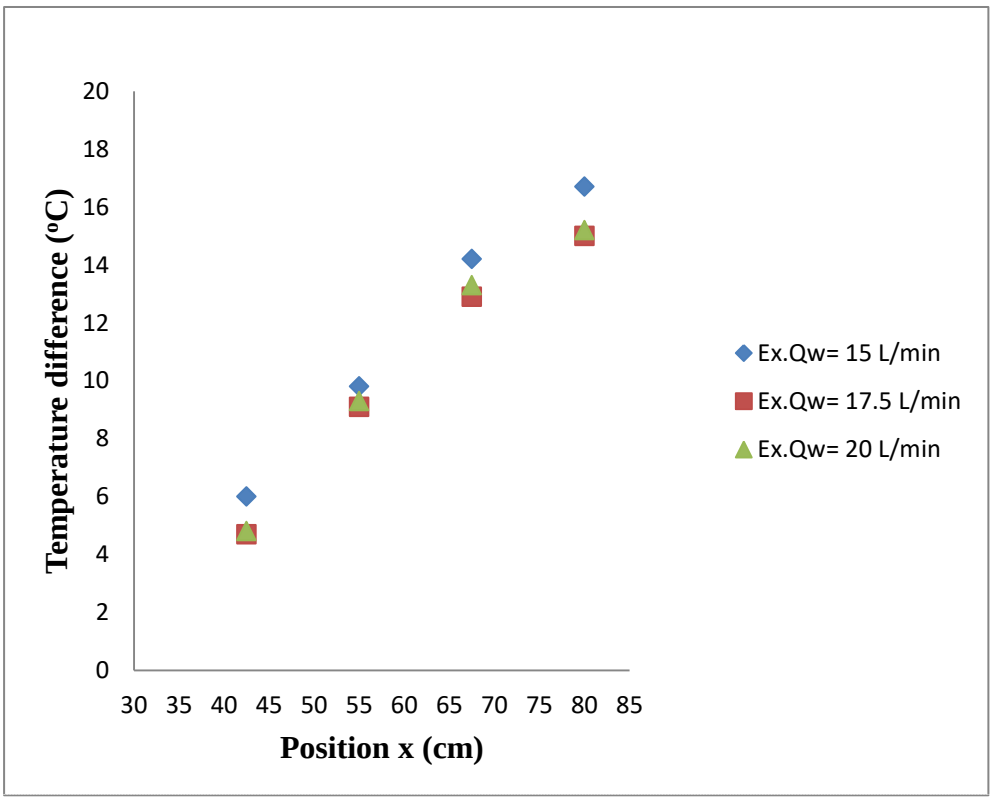

Figure (5-30) The temperature difference between single-phase flow (water) and oval tube surfaces at many positions in the duct (x = 42.5, 55, 67.5, and 80 cm) without vortex generators for various water flow rates (15, 17.5, and 20 L/min) experimentally

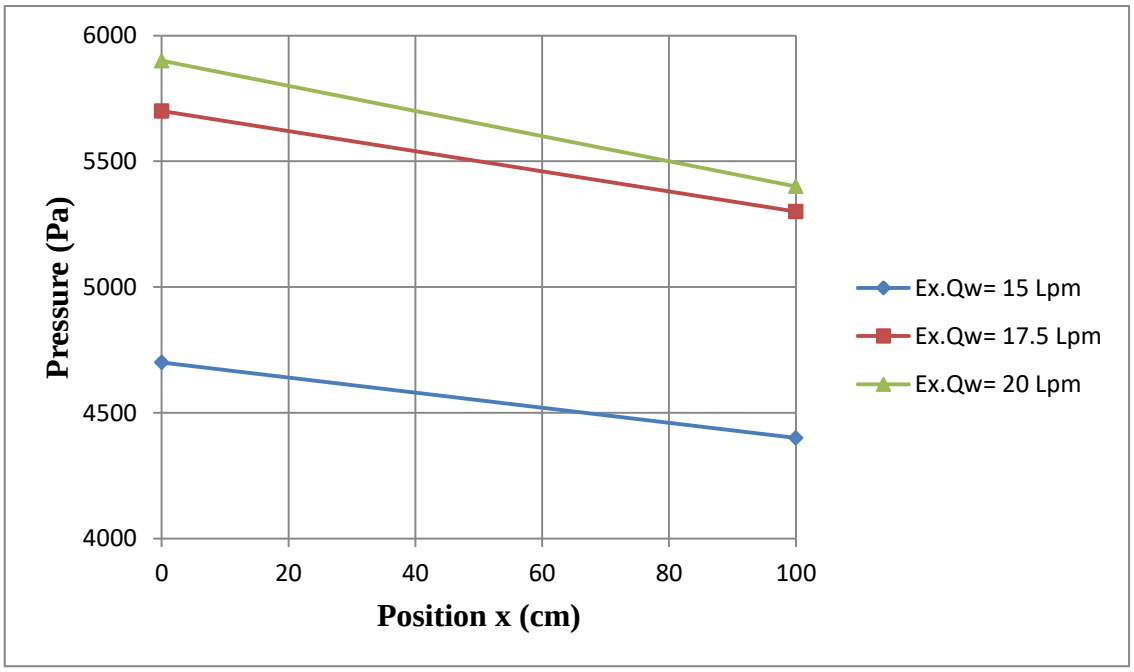

Figure (5-31) Inlet and outlet pressure in duct without vortex generators for single-phase flow

5.4.1.2 Effect of vortex generators

Adding vortex generators in the duct can increase the velocity of single-phase flow, creating vigorous turbulence intensity inside the duct that enhances the heat transfer coefficient. It can be noted that the temperature difference decrease as the flow velocity increase, and when directing the flow toward the oval tube's surface, it can be observed that the temperature difference is inversely proportional to the velocity of flow.

Figure (5-32) illustrates the temperature difference between single-phase flow (water) and oval tube surfaces at many positions in the duct (x = 42.5, 55, 67.5, and 80 cm) when delta winglets are used as vortex generators in the duct for various water flow rate (15, 17.5, and 20 Lpm) experimentally. From this figure, notice that when the water flow rate increased, the temperature difference compared to without vortex generators decreased by (26.76%, 27.75%, and 35.34%), respectively. Also, when the water flow rate increased in single-phase flow with the delta winglets as vortex generators, the heat transfer coefficient increased with the oval tube surfaces' temperature decreasing due to the working fluid becoming focused on it by the winglets.

Figure (5-33) shows inlet and outlet pressure in the duct for single-phase flow (water) at many positions in the duct (x = 42.5, 55, 67.5, and 80 cm) with the delta winglets as vortex generators for various water flow rate (15, 17.5, and 20 Lpm). When the water flow rate increased, the pressure drop in the duct compared without vortex generators decreased by (33.3%) and (25%) at water flow rate of (15 Lpm) and (17.5 Lpm), respectively and increased by (20%) at a water flow rate of (20 Lpm). When the delta winglets are used as vortex generators, the reduction in pressure increases compared to without vortex generators in the duct.

Figure (5-34) shows the temperature difference between single-phase flow (water) and oval tube surfaces at many positions in the duct (x = 42.5, 55, 67.5, and 80 cm) when the Rectangular winglets are used as vortex

generators in the duct for various water flow rate (15, 17.5, and 20 Lpm) experimentally. From this figure, notice that when the water flow rate increased, the temperature difference compared to without vortex generators decreased by (23.9%, 30.2%, and 33%), respectively. Also, when the water flow rate increased in single-phase flow with the rectangular winglets as vortex generators, the heat transfer coefficient increased with the oval tube surfaces' temperature decreasing due to the working fluid becoming focused on it by the winglets. For oval tube banks, the greater contact volume between mixing fluid results in a higher heat transfer coefficient, the bulk fluid is mixing increases at each subsequent tube, transferring heat more effectively and hence yielding an enhancement of the heat transfer performance. As a result, the heat transfer coefficient for oval tube banks is found to increase with the (VGs).

Figure (5-35) illustrates inlet and outlet pressure in the duct for single-phase flow (water) at many positions in the duct (x = 42.5, 55, 67.5, and 80 cm) with the Rectangular winglets as vortex generators for various water flow rate (15, 17.5, and 20 Lpm). When the water flow rate increased, the pressure drop in the duct compared without vortex generators increased by (33.3%, 50%, and 40%), respectively. When the Rectangular winglets are used as vortex generators, the reduction in pressure increases compared to without vortex generators in the duct. The narrow passages of the fluid flow might give rise to a jet impingement effect and hence increased pressure drop.

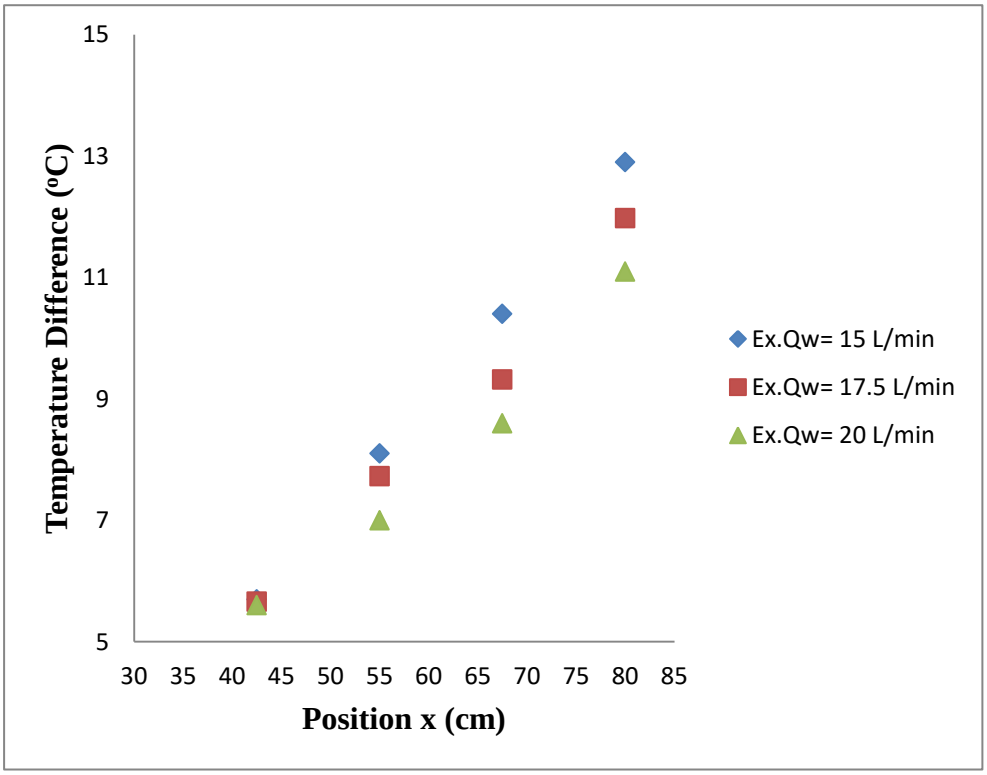

Figure (5-32) The temperature difference between single-phase flow (water) and oval tube surfaces at many positions in the duct (x = 42.5, 55, 67.5, and 80 cm) with delta winglets as vortex generators for various water flow rates (15, 17.5, and 20 L/min) experimentally

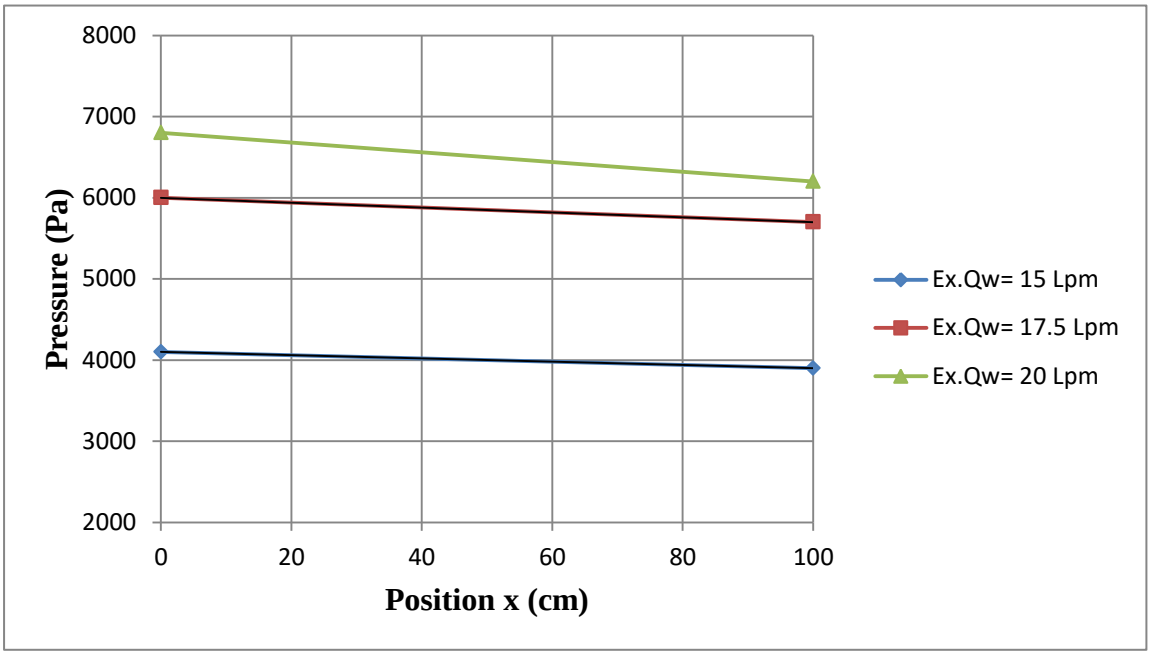

Figure (5-33) Inlet and outlet pressure in the duct with delta winglets as vortex generators

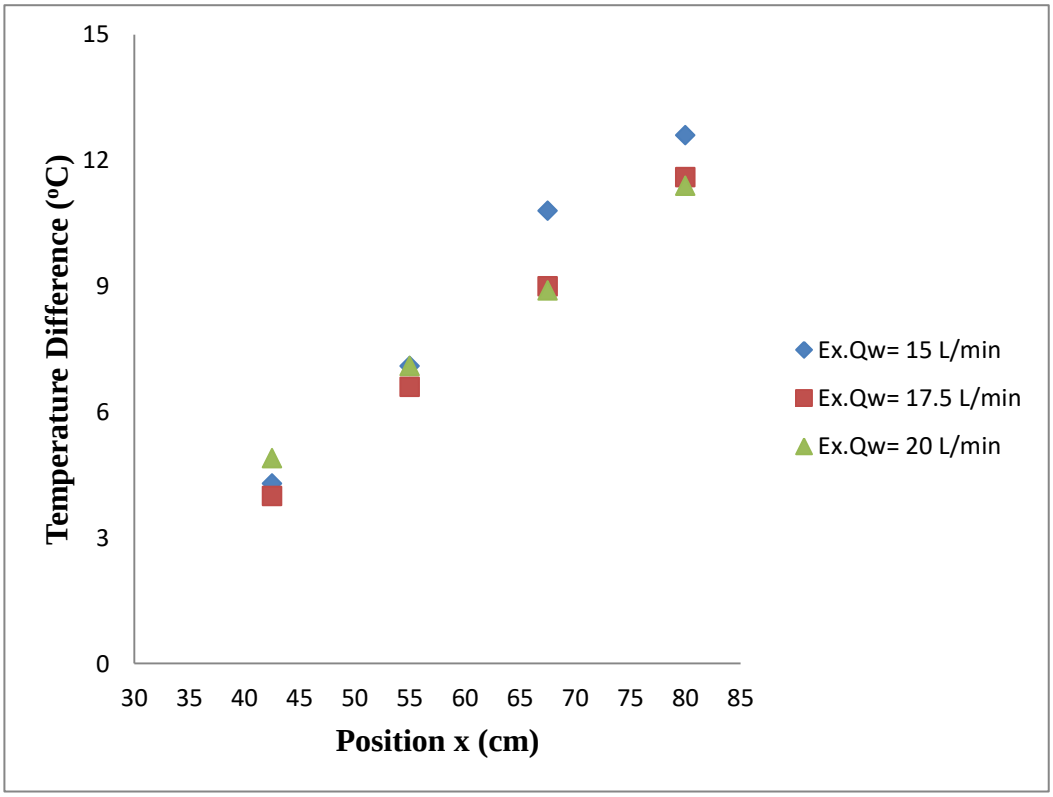

Figure (5-34) The temperature difference between single-phase flow (water) and oval tube surfaces at many positions in the duct (x = 42.5, 55, 67.5, and 80 cm) with rectangular winglets as vortex generators for various water flow rates (15, 17.5, and 20 L/min) experimentally

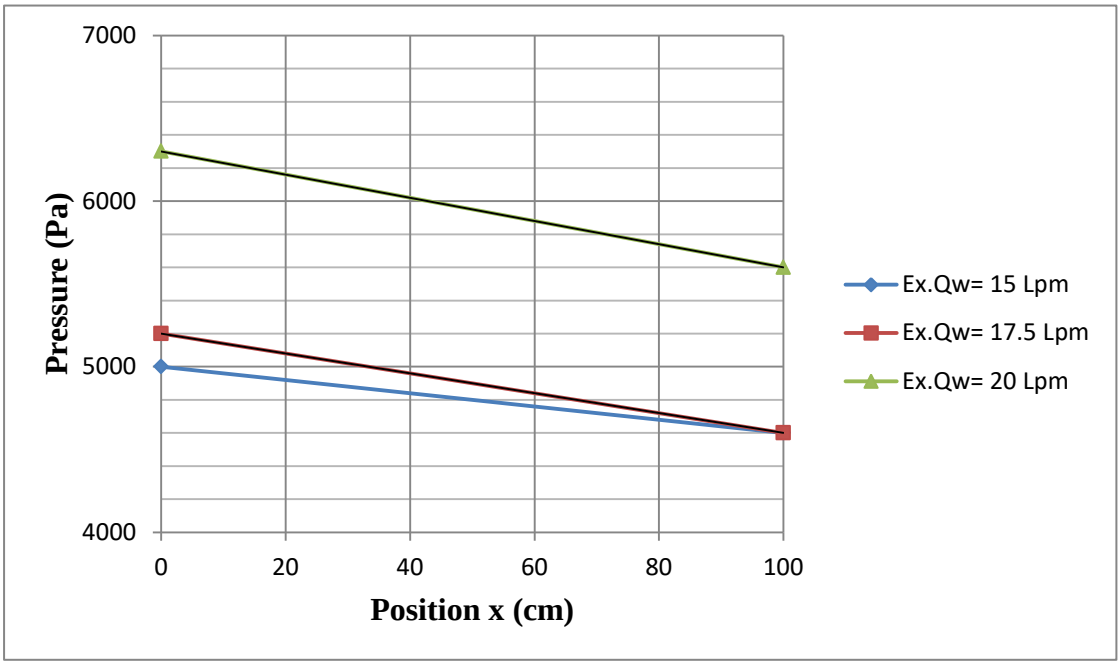

Figure (5-35) Inlet and outlet pressure in the duct with rectangular winglets as vortex generators

5.4.2 Two-phase flow

5.4.2.1 Effect of flow rate

Figures (5-36) to (5-38) show the temperature difference between two-phase flow (water and air) and oval tube surfaces at many positions in the duct (x = 42.5, 55, 67.5, and 80 cm) without vortex generators experimentally with Reynolds number range (3638 - 4810). At these points, the airflow rate increases (8.33, 16.67, and 25 Lpm) with a constant water flow rate and heat flux.

Figure (5-36) shows that the temperature difference between two-phase flow and oval tube surfaces increased by (59.8%, 71.8%, and 102%), respectively at a constant water flow rate (15 Lpm).

Figure (5-37) shows that the temperature difference between two-phase flow and oval tube surfaces increased by (25.6%, 70.5%, and 99%), respectively at a constant flow rate of water (17.5 Lpm).

Figure (5-38) shows that the temperature difference between two-phase flow and oval tube surfaces increased by (5.3%, 42%, and 63.2%), respectively at a constant flow rate of water (20 Lpm).

Additionally, when water and air flow rates in two-phase flow are increased without vortex generators, the heat transfer coefficient falls due to the temperature difference growing with less intensity. The increased velocity in front of the second tube due to the blockage of the first tube causes a stronger vortex and a higher heat transfer peak. The third peak is due to the vortex region heat transfer of the tube in the last row.

Figures (5-39) to (5-341) show inlet and outlet pressure in the duct without vortex generators for two-phase flow (water and air) at many positions in the duct (x = 42.5, 55, 67.5, and 80 cm) experimentally. At these points, the airflow rate increases (8.33, 16.67, and 25 Lpm) with a constant water flow rate and heat flux.

Figures (5-39) show that the pressure drop in the duct decreased by (66.67%, 66.67%, and 100%), respectively at a constant flow rate of water (15 Lpm).

Figure (5-40) shows that the pressure drop in duct in two-phase flow without using vortex generators decreased by (50%, 50%, and 50%), respectively at a constant flow rate of water (17.5 Lpm)

Figure (5-41) shows that the reduction in pressure in the duct in two-phase flow without using vortex generators decreased by (66.67%, 75%, and 100%), respectively at a constant flow rate of water (20 Lpm).

Furthermore, when the two-phase flow rate (water and air) is increased without vortex generators, the pressure drop is decreased. Because an increase in air flow rate corresponds to an increase in the percentage of air in a two-phase flow mixture, the pressure drop in the air flow is lower than the pressure drops in the water flow, resulting in a reduction in the overall pressure drop within the duct.

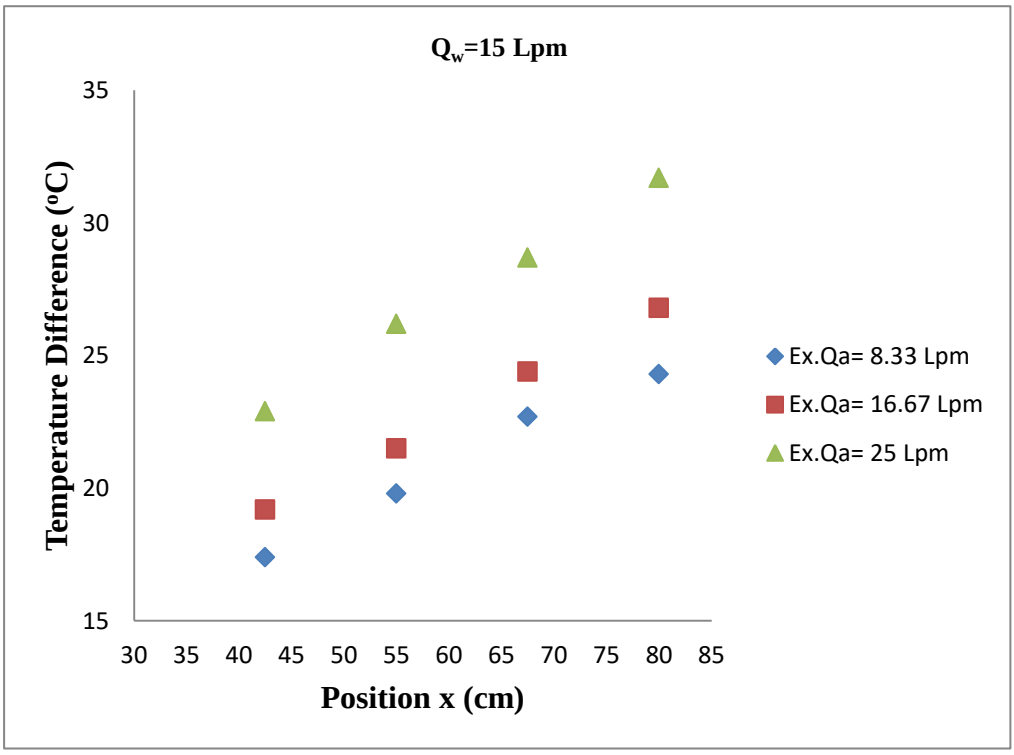

Figure (5-36) The temperature difference between two-phase flow (water and air) and oval tube surfaces at many positions in the duct (x = 42.5, 55, 67.5, and 80 cm) without vortex generators experimentally

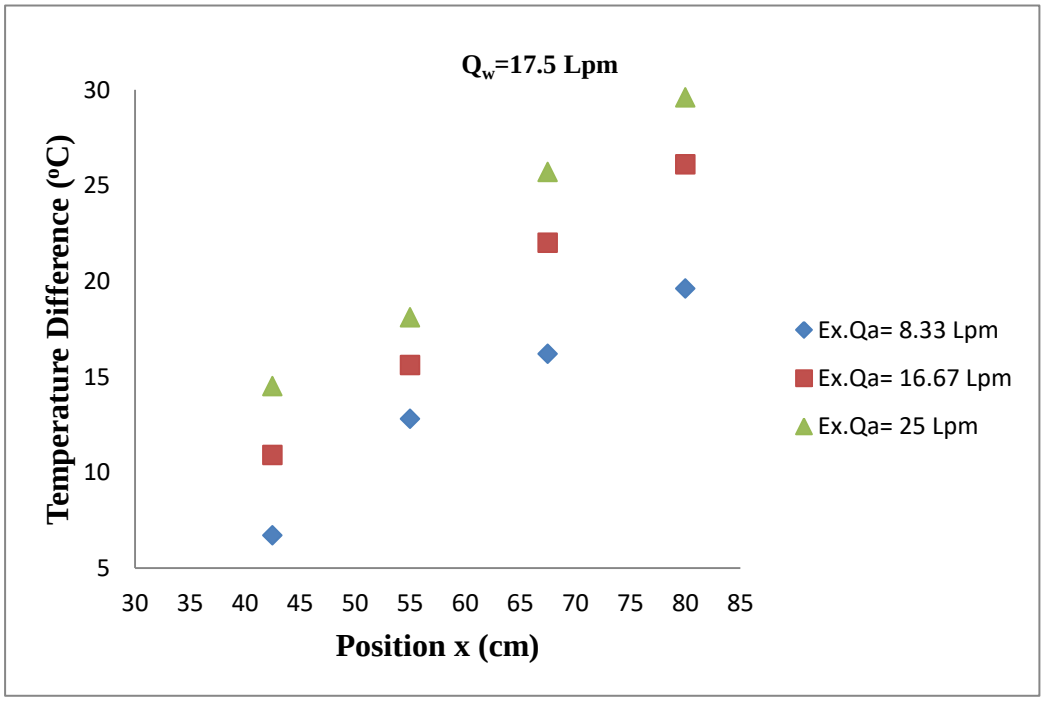

Figure (5-37) The temperature difference between two-phase flow (water and air) and oval tube surfaces at many positions in the duct (x = 42.5, 55, 67.5, and 80 cm) without vortex generators experimentally

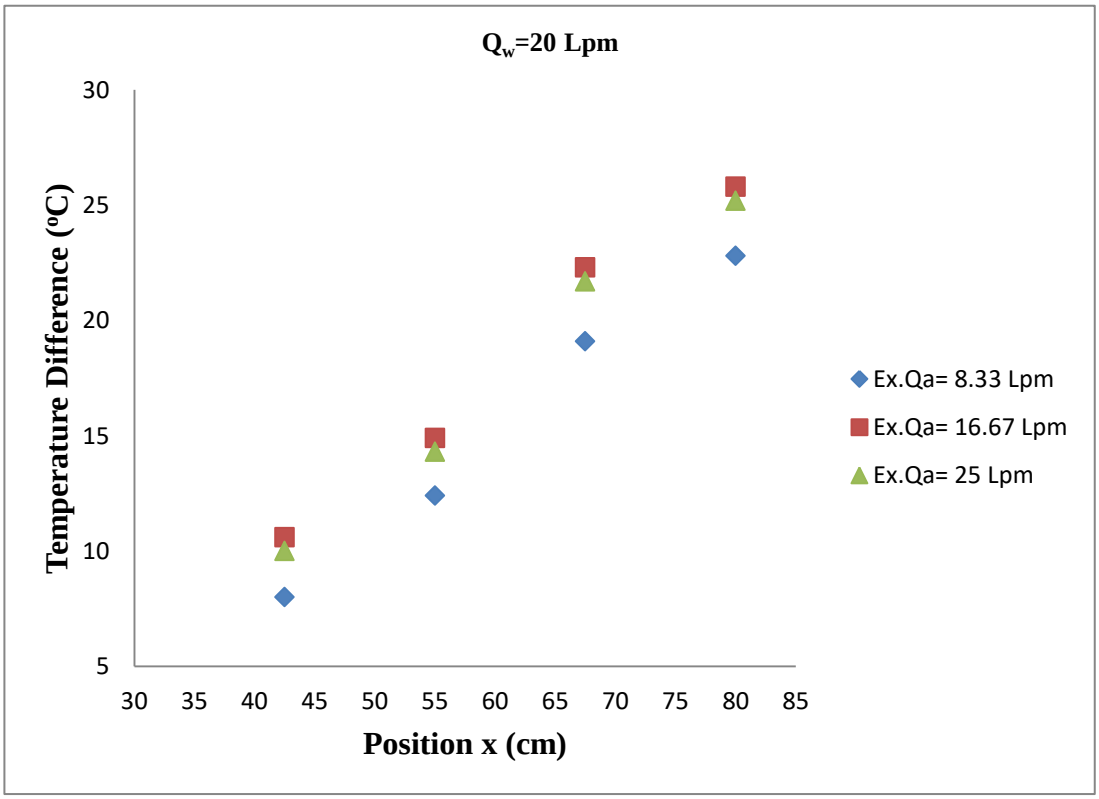

Figure (5-38) The temperature difference between two-phase flow (water and air) and oval tube surfaces at many positions in the duct (x = 42.5, 55, 67.5, and 80 cm) without vortex generators experimentally

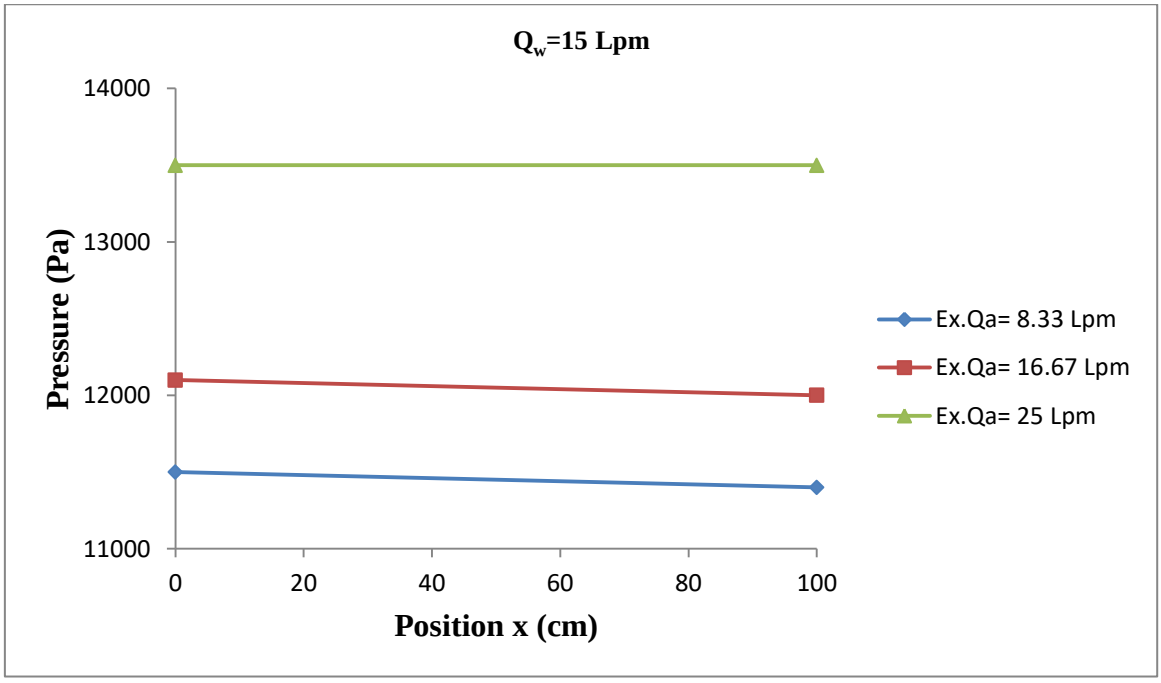

Figure (5-39) Inlet and outlet pressure in the duct without vortex generators

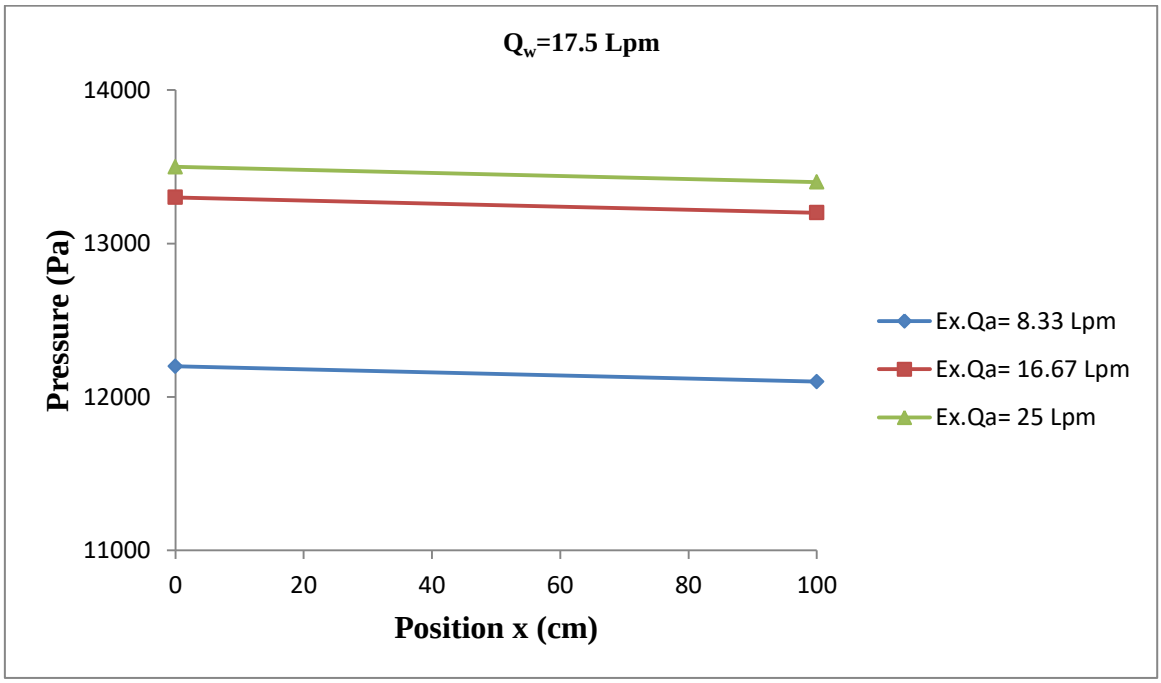

Figure (5-40) Inlet and outlet pressure in the duct without vortex generators

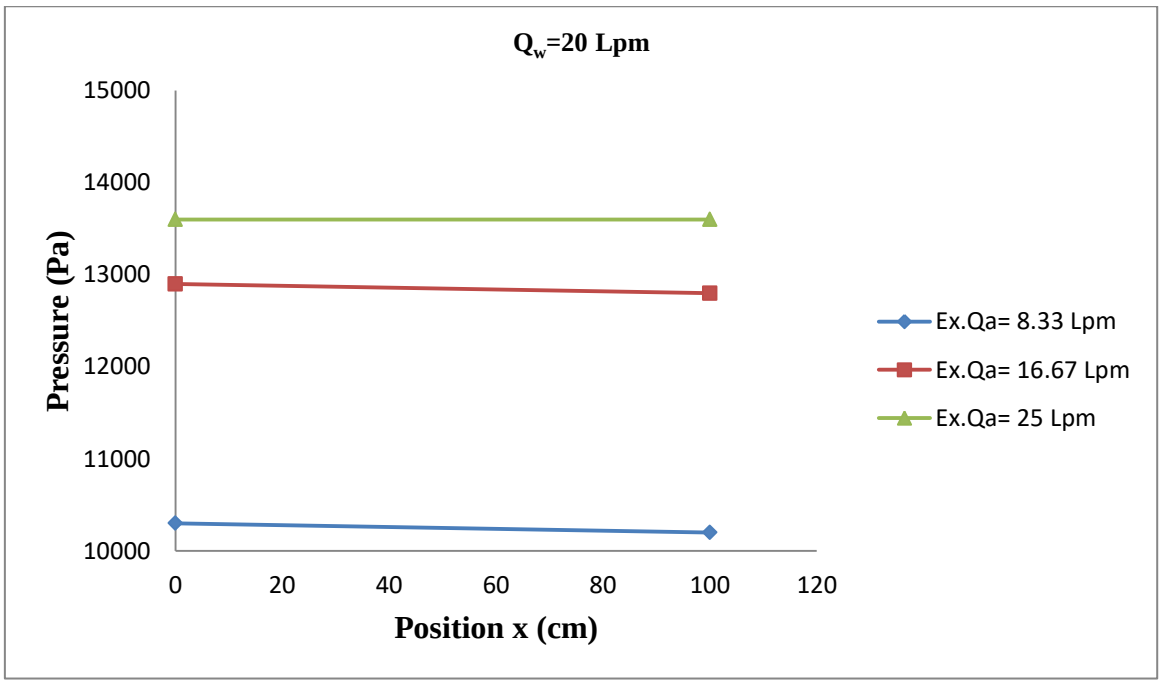

Figure (5-41) Inlet and outlet pressure in the duct without vortex generators

5.4.2.2 Effect of vortex generators

The velocity of two-phase flow (air and water) can be increased in the duct by adding vortex generators, which increases the turbulence within the duct and improves the heat transfer coefficient. When the flow is directed towards the surface of the oval tube, it can be observed that the temperature difference is inversely proportional to the flow velocity and that the temperature difference decreases as the flow velocity increases. The airflow rate increased from (8.33, 16.67, and 25 Lpm) at a constant water flow rate with a constant heat power of (110 W).

Figures (5-42) to (5-44) illustrate temperature differences when delta winglets are used as vortex generators in the duct for two-phase flow. Also, the experimental heat transfer coefficient increased, corresponding that the temperature difference decreased because the working fluid is focused on the tube surface by the winglets.

Figure (5-42) shows that when delta winglets are used as vortex generators in the duct the temperature difference between two-phase flow and oval tube surfaces decreased by (40.1%, 37.3%, and 34.15%), respectively at constant water flow rate (15 Lpm).

Figure (5-43) shows that when delta winglets are used as vortex generators in the duct the temperature difference between two-phase flow and oval tube surfaces decreased by (24.1%, 33.2%, and 33.85%), respectively at constant water flow rate (17.5 Lpm).

Figure (5-44) shows that when delta winglets are used as vortex generators in the duct the temperature difference between two-phase flow and oval tube surfaces decreased by (20%, 31.2%, and 29.5%), respectively at a constant water flow rate (20 Lpm).

Also, when water and air flow rates are increased in two-phase flow with the delta winglets as vortex generators, the heat transfer coefficient increase and the temperature difference decreases with less intensity.

Figure (5-45) shows the pressure loss for the two-phase flow and compared to the single-phase flow with delta winglets as vortex generators in the duct decreased by (50%, 50%, and 50%), respectively at a constant flow rate of water (15 Lpm).

Figure (5-46) shows the pressure loss for the two-phase flow and compared to the single-phase flow with delta winglets as vortex generators in the duct decreased by (50%, 50%, and 50%), respectively at a constant flow rate of water (17.5 Lpm).

Figure (5-47) shows that the pressure loss for the two-phase flow and compared to the single-phase flow with delta winglets as vortex generators in the duct decreased by (50%, 50%, and 50%), respectively at a constant discharge of water (20 Lpm).

The pressure drops are increased compared to the delta winglets in the duct that are not used. Additionally, with an increase in the flow rate of water and air in two-phase flow with delta winglets acting as vortex generators, the pressure drops in the duct are reduced.

Figures (5-48) to (5-50) illustrate temperature differences when Rectangular winglets are used as vortex generators in the duct for two-phase flow. Also, the experimental heat transfer coefficient increased, corresponding that the temperature difference decreased because the working fluid is focused on the tube surface by the winglets.

Figure (5-48) shows that when Rectangular winglets are used as vortex generators in the duct the temperature difference between two-phase flow and oval tube surfaces decreased by (36.56%, 36.5%, and 32%), respectively at a constant water flow rate (15 Lpm).

Figure (5-49) shows that when rectangular winglets are used as vortex generators in the duct the temperature difference between two-phase flow and oval tube surfaces decreased by (25.9 %, 35.45%, and 35.8%), respectively at a constant water flow rate (17.5 Lpm).

Figure (5-50) shows that when rectangular winglets are used as vortex generators in the duct the temperature difference between two-phase flow and oval tube surfaces decreased by (22.1%, 28%, and 23.5%), respectively at a constant water flow rate (20 Lpm).

Moreover, when water and air velocity flow is increased in two-phase flow with rectangular winglets acting as vortex generators, the heat transfer coefficient increases and the temperature difference decreases. The enhancement of heat transfer from the fin surfaces is achieved by placing winglets vortex generators on the surfaces in the neighborhood of the oval tube banks. Longitudinal vortices develop along the side edge of the winglets due to the pressure difference between the front surface (facing the flow) and the back surface. These vortices interact with an otherwise two-dimensional boundary layer and produce a three-dimensional swirling flow that mixes near oval tube surface. This enhances the mixing of fluid from the periphery and the core regions of the flow field. Thus the thermal boundary layer is disrupted and heat transfer is enhanced.

Figure (5-51) shows that the pressure drops for the two-phase flow and compared to the single-phase flow with rectangular winglets as vortex generators in the duct decreased by (25%, 50%, and 25%), respectively at a constant flow rate of water (15 Lpm).

Figure (5-52) shows that the pressure drops for the two-phase flow and compared to the single-phase flow with rectangular winglets as vortex generators in the duct decreased by (33.3%, 50%, and 66.67%), respectively at a constant flow rate of water (17.5 Lpm).

Figure (5-53) shows that the pressure drops for the two-phase flow and compared to the single-phase flow with rectangular winglets as vortex generators in the duct decreased by (42.9%, 71.4%, and 85.7%), respectively at a constant flow rate of water (20 Lpm).

When using rectangular winglets as vortex generators, the pressure drops are increased compared to not using rectangular winglets in the duct. Additionally, when the water and air flow rate increases in the two-phase flow with rectangular winglets acting as vortex generators, the pressure drops in the duct are reduced. The additional pressure losses are modest because the form drag for such winglets slender bodies is low.Because an increase in air flow rate corresponds to an increase in the percentage of air in a two-phase flow mixture, the pressure drop in the air flow is lower than the pressure drops in the water flow, resulting in a reduction in the overall pressure drop within the duct.

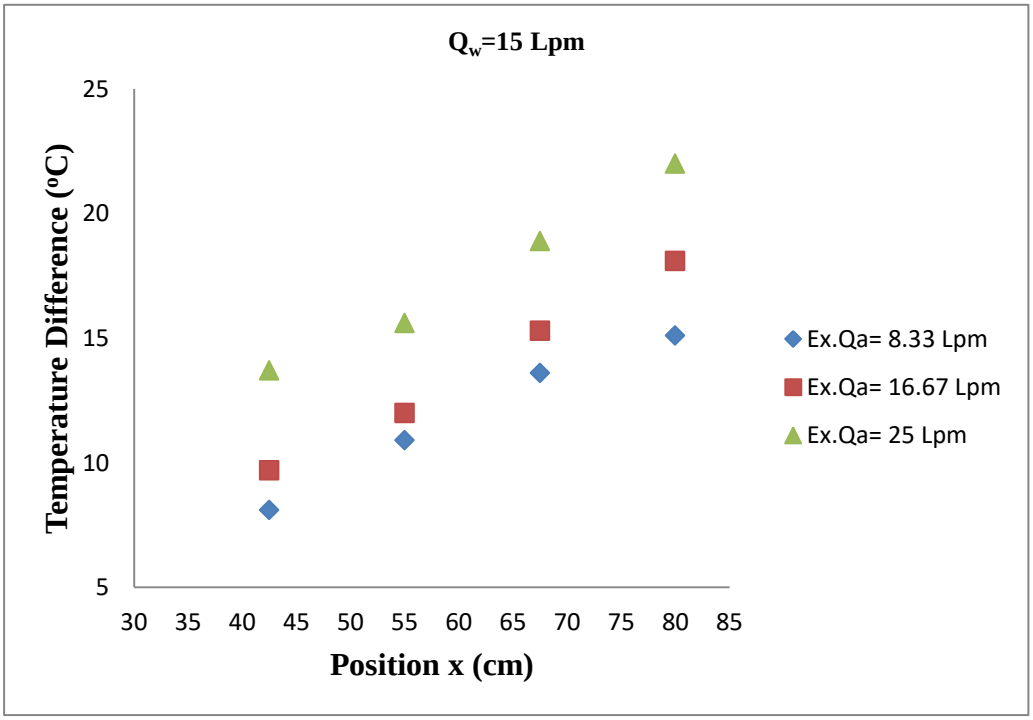

Figure (5-342) The temperature difference between two-phase flow (water and air) and oval tube surfaces at many positions in the duct (x = 42.5, 55, 67.5, and 80 cm) with delta winglets as vortex generators experimentally

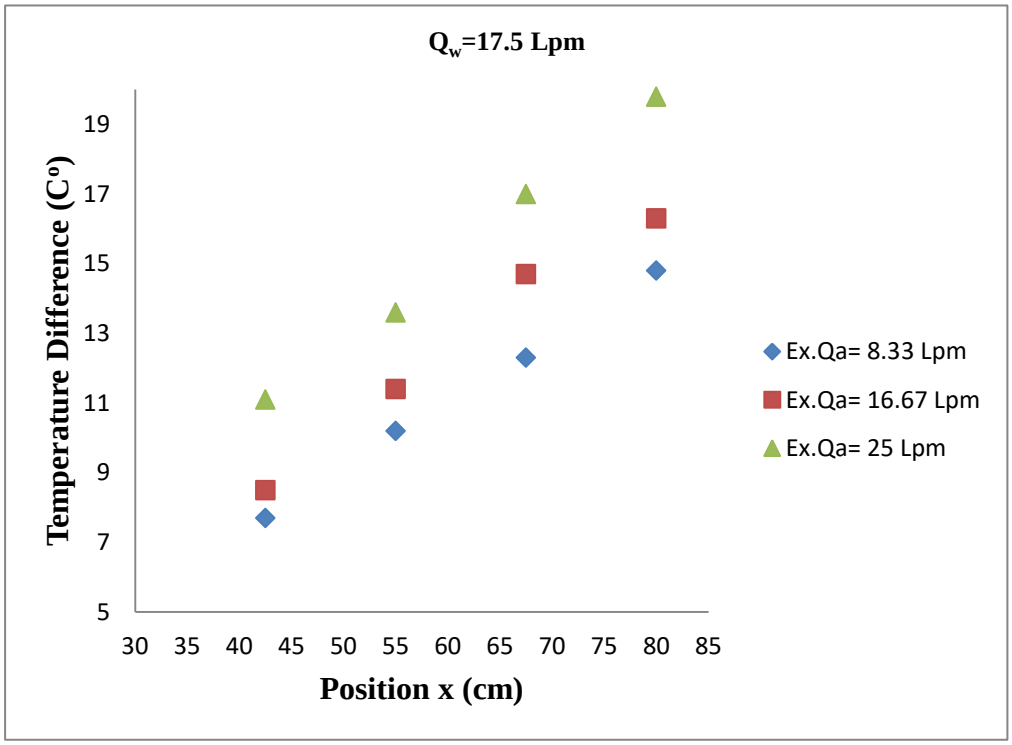

Figure (5-43) The temperature difference between two-phase flow (water and air) and oval tube surfaces at many positions in the duct (x = 42.5, 55, 67.5, and 80 cm) with delta winglets as vortex generators experimentally

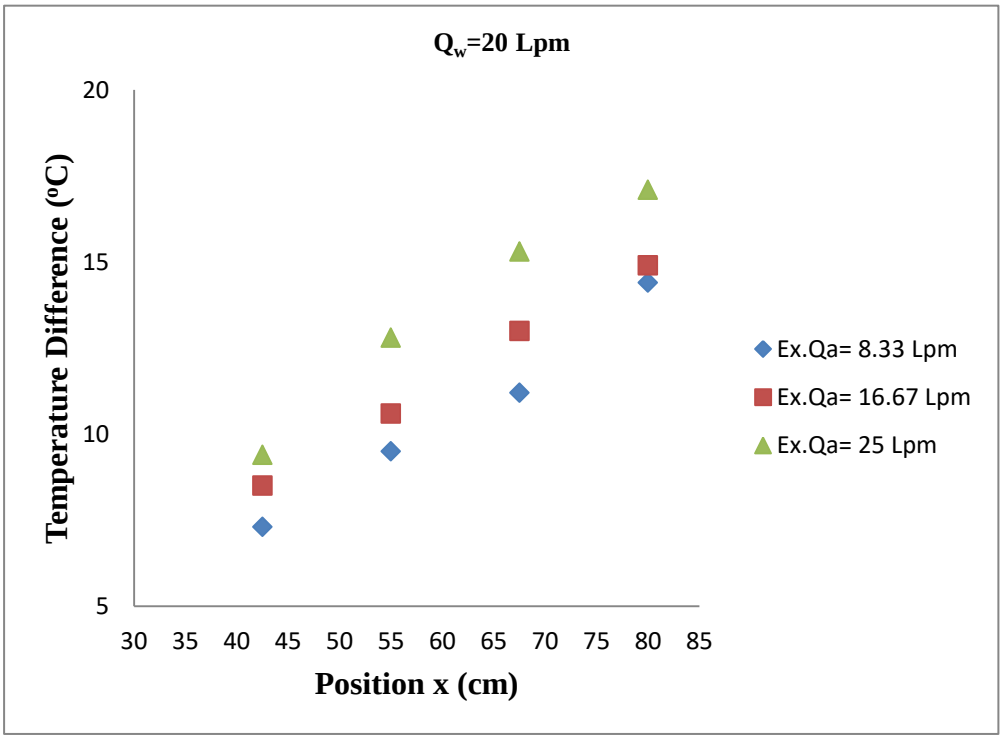

Figure (5-44) The temperature difference between two-phase flow (water and air) and oval tube surfaces at many positions in the duct (x = 42.5, 55, 67.5, and 80 cm) with delta winglets as vortex generators experimentally

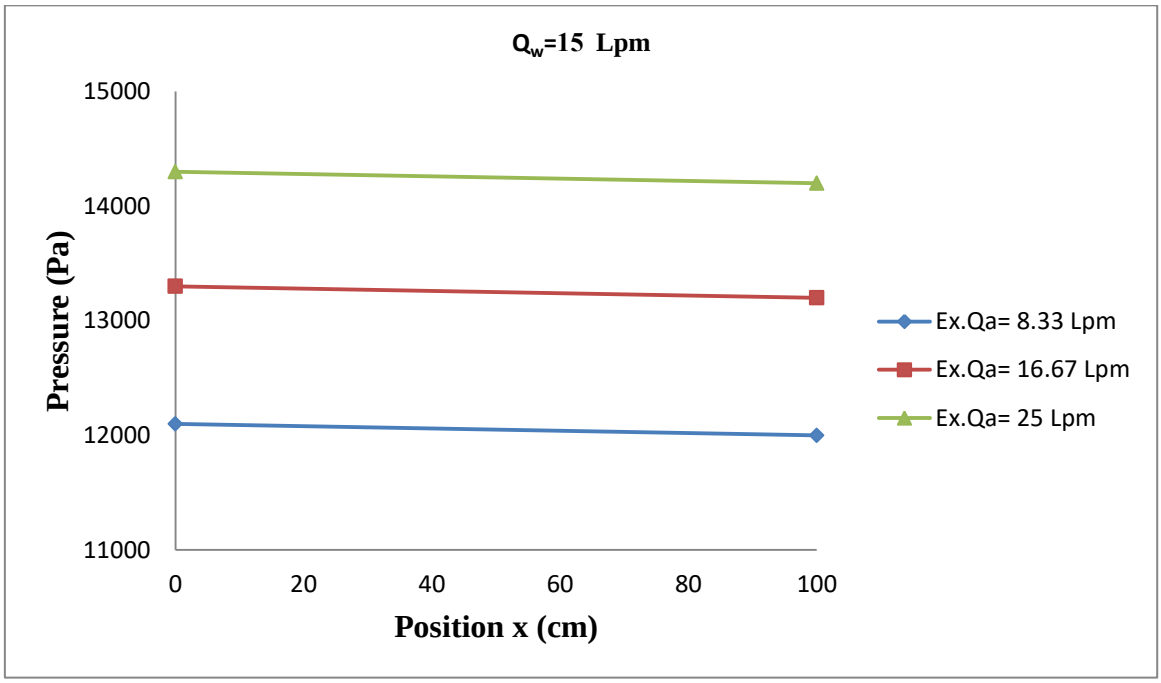

Figure (5-45) Inlet and outlet pressure in the duct with delta winglets as vortex generators

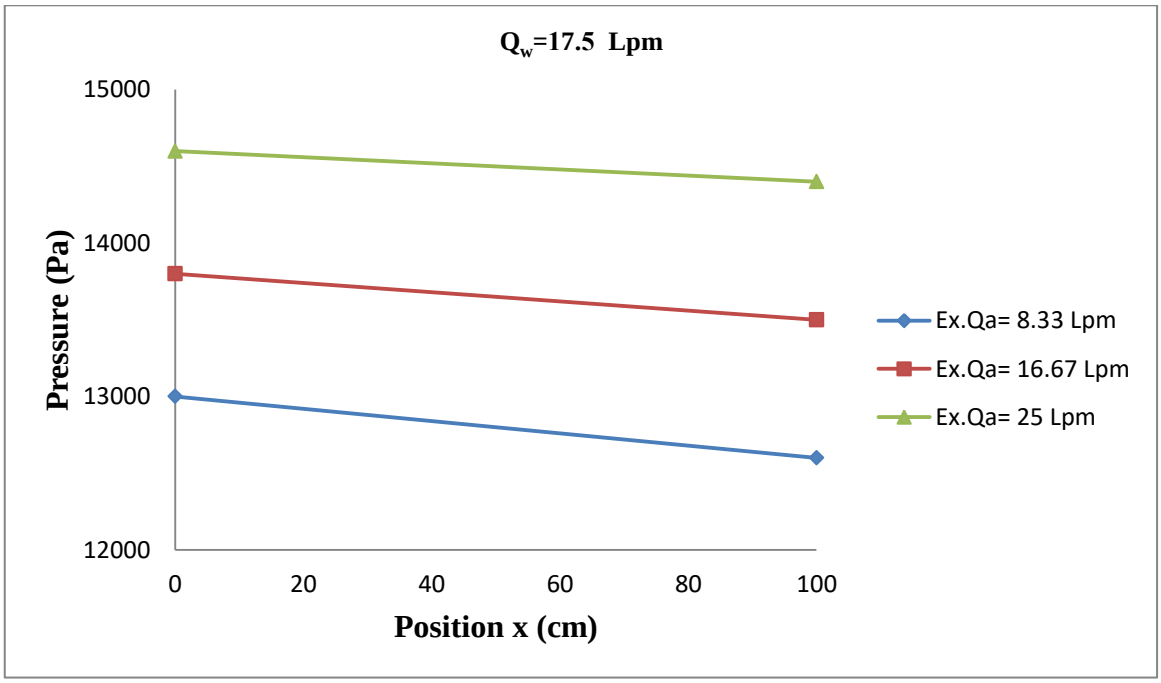

Figure (5-46) Inlet and outlet pressure in the duct with delta winglets as vortex generators

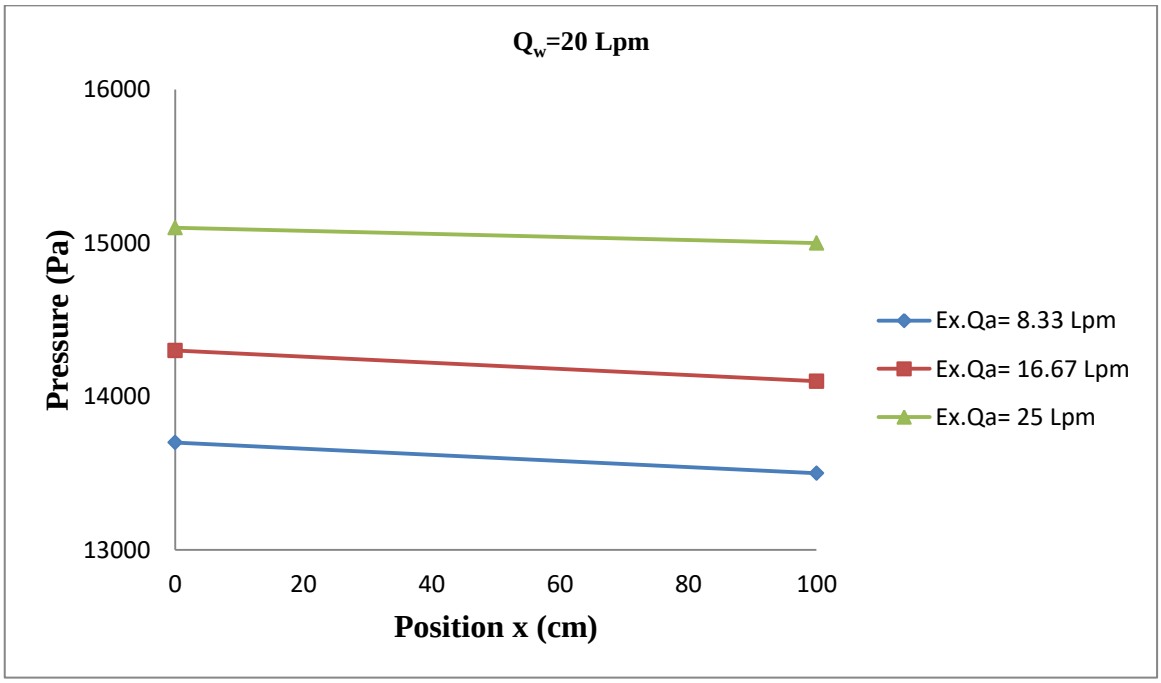

Figure (5-47) Inlet and outlet pressure in the duct with delta winglets as vortex generators

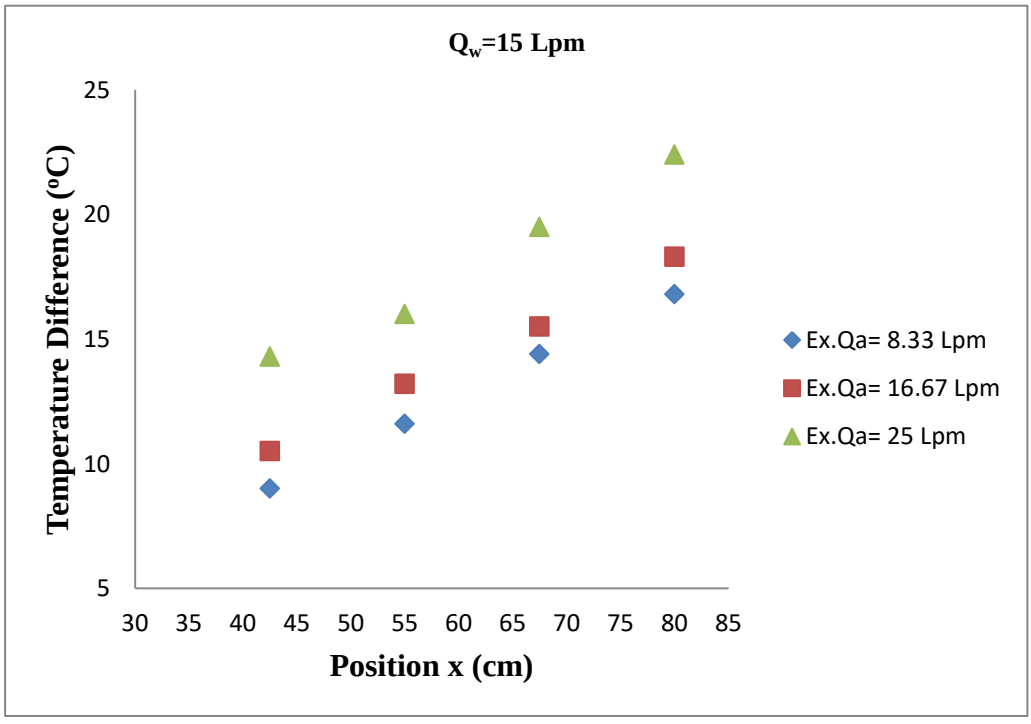

Figure (5-48) The temperature difference between two-phase flow (water and air) and oval tube surfaces at many positions in the duct (x = 42.5, 55, 67.5, and 80 cm) with rectangular winglets as vortex generators experimentally

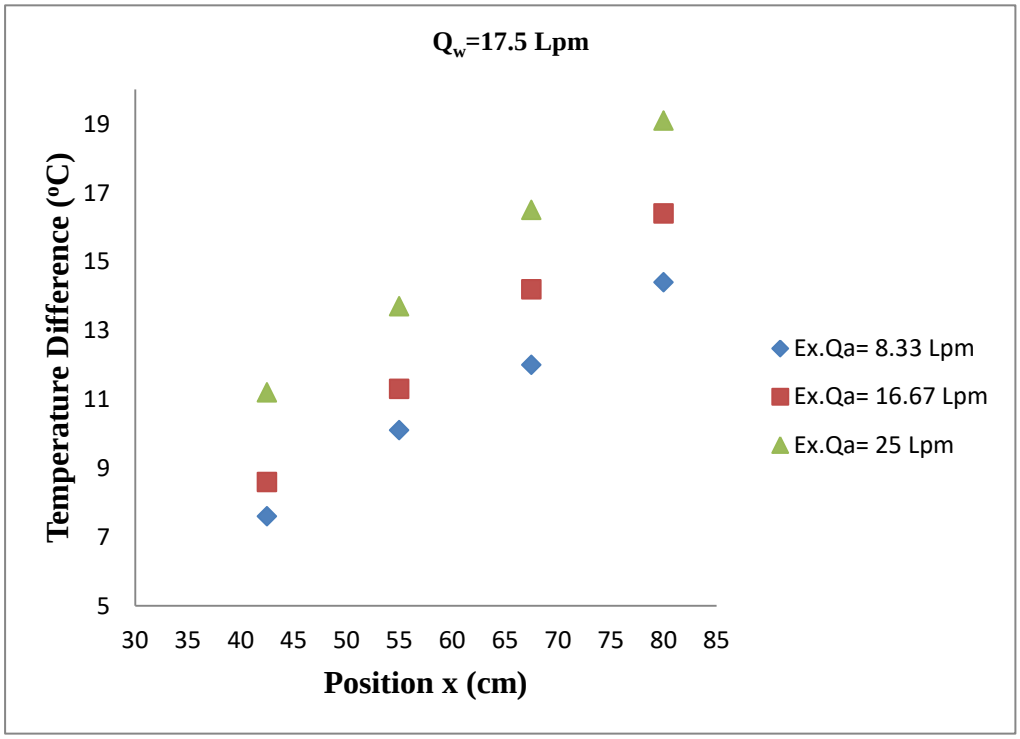

Figure (5-49) The temperature difference between two-phase flow (water and air) and oval tube surfaces at many positions in the duct (x = 42.5, 55, 67.5, and 80 cm) with rectangular winglets as vortex generators experimentally

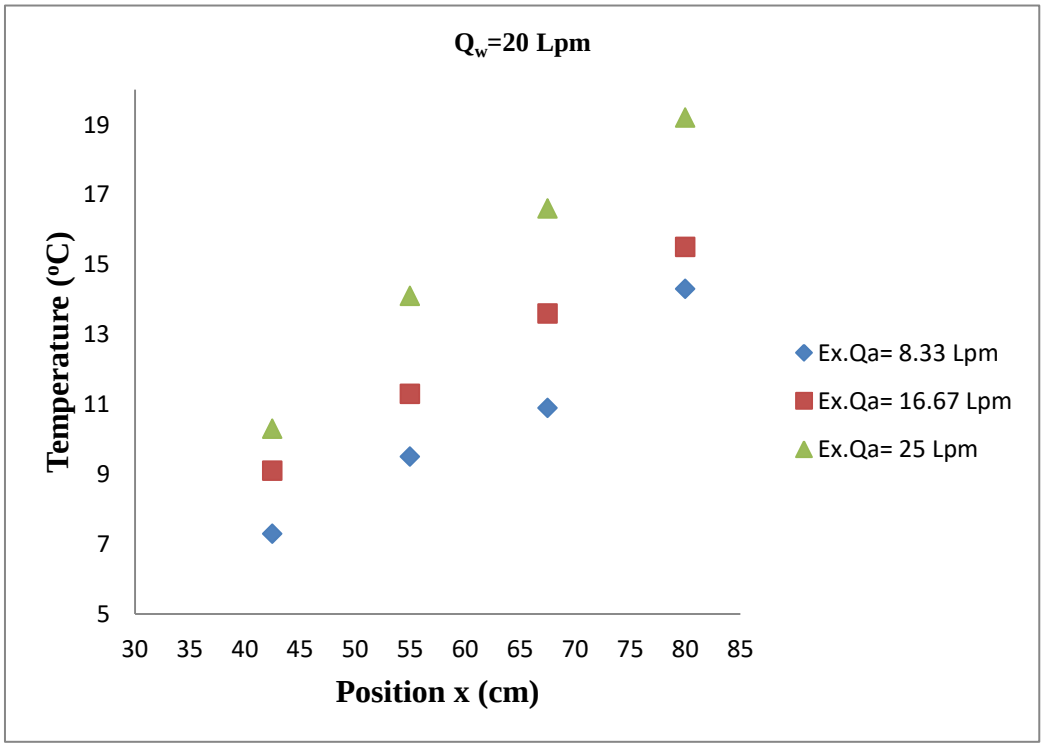

Figure (5-50) The temperature difference between two-phase flow (water and air) and oval tube surfaces at many positions in the duct (x = 42.5, 55, 67.5, and 80 cm) with rectangular winglets as vortex generators experimentally

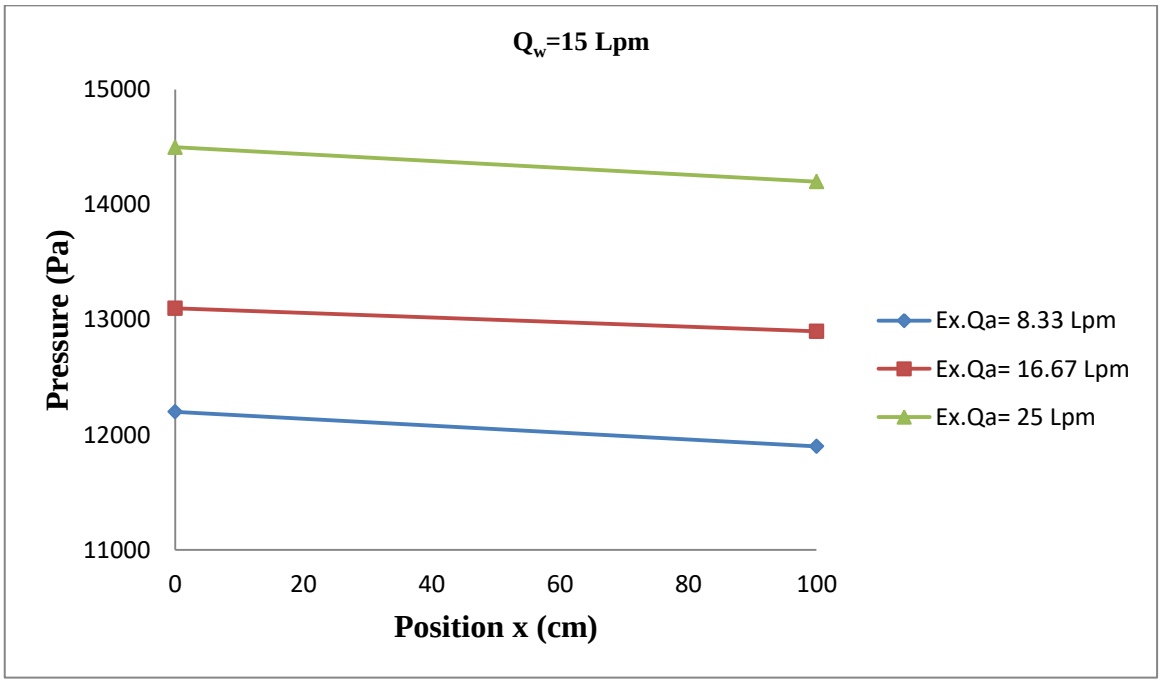

Figure (5-51) Inlet and outlet pressure in the duct with rectangular winglets as vortex generators

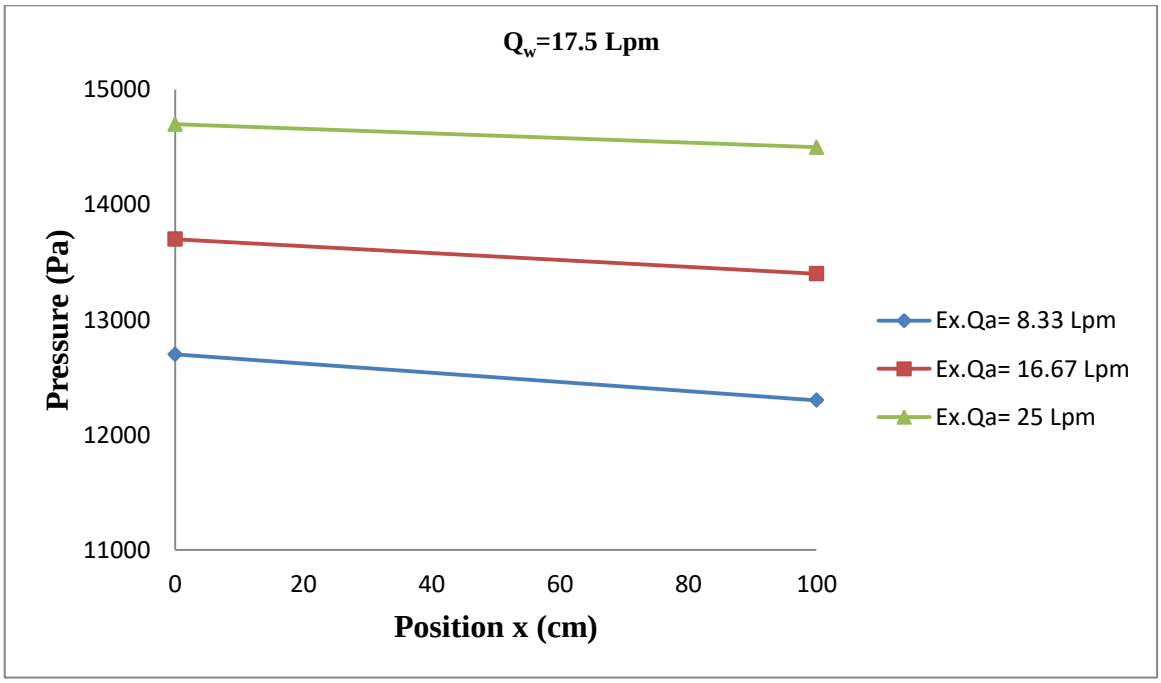

Figure (5-52) Inlet and outlet pressure in the duct with rectangular winglets as vortex generators

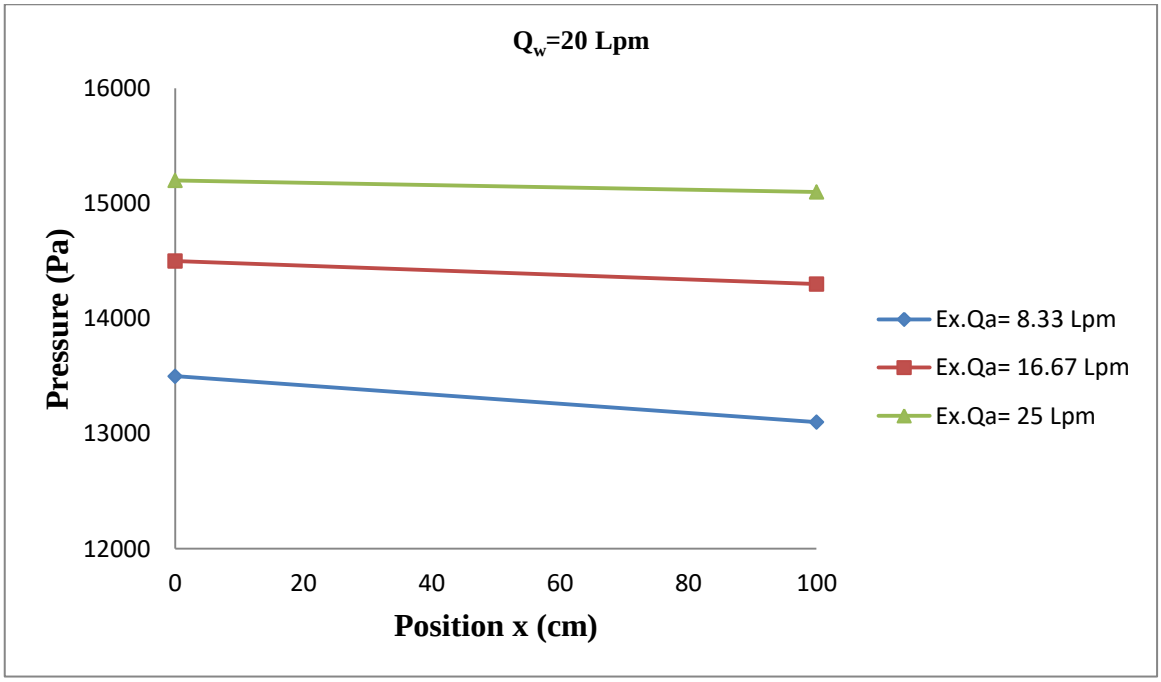

Figure (5-53) Inlet and outlet pressure in the duct with rectangular winglets as vortex generators

5.4.3 Regimes of flow in the duct

In this section, the digital camera shows the type of two-phase flow as digital images for experimental tests.

Figure (5-54) shows digital images of the twelve experimental tests without vortex generators for single and two-phase flow over the bank of oval tubes. The flow patterns in the duct at a flow rate of water and air (15) and (8.33) (Lpm), respectively, air bubbles appear inside the water in the two-phase flow. The bubbles prefer to flow as bubbly patterns flow in the upper portion of the duct. Furthermore, at a flow rate of water and air (15) and (16.67) (Lpm), respectively, at the base of the duct, the water layer separating the air bubble from the wall becomes thicker than at the top. The bubble's nose is asymmetrical, and the flow is plug patterns. Finally, at a flow rate of water and air (15) and (25) (Lpm), respectively, the flow is also as plug patterns flow.

The flow patterns in the duct at a flow rate of water and air (17.5) and (8.33) (Lpm), respectively, air bubbles appear inside the water in the two-phase flow. The bubbles prefer to flow as bubbly patterns flow in the upper portion of the duct. Furthermore, at the flow rate of water and air (17.5) and (16.67) (Lpm), respectively, at the base of the duct, the water layer separating the air bubble from the wall becomes thicker than at the top. The bubble's nose is asymmetrical, and the flow is plug patterns. Finally, at the flow rate of water and air (17.5) and (25) (Lpm), respectively, in this situation, the water layer has been completely separated from the air layer. The water flow at the bottom of the duct is combined with the airflow at the top. As well as, the flow is stratified.

The flow patterns in the duct at a flow rate of water and air (20) and (8.33) (Lpm), respectively, at the base of the duct, the water layer separating the air bubble from the wall becomes thicker than at the top. The bubble's nose is asymmetrical, the flow is plug patterns, and the flow is Plug patterns. Furthermore, at a flow rate of water and air (20) and (16.67) (Lpm), respectively, in this situation, the water layer has been completely separated from the air layer. The water flow at the bottom of the duct is combined with the airflow at the top. As well as, the flow is stratified. Finally, at a flow rate of water and air (20) and (25) (Lpm), respectively, as air velocity increases in stratified flow, huge surface waves form on the water layer, and the flow becomes wavy, as well as the flow is wavy patterns flow.

Figure (5-55) shows digital images of the twelve experimental tests with delta winglets as vortex generators in the duct for single-phase and two-phase flows over the bank of oval tubes. Air bubbles appear inside the water in the two-phase flow with high velocity and random movement.

The flow patterns in the duct at a flow rate of water and air (15) and (8.33) (Lpm), respectively, air bubbles appear inside the water in the two-phase flow. The bubbles prefer to flow as bubbly patterns flow in the upper portion of the duct. Furthermore, at a flow rate of water and air (15) and (16.67) (Lpm), respectively, at the base of the duct, the water layer separating the air bubble from the wall becomes thicker than at the top. The bubble's nose is asymmetrical, and the flow is plug patterns. Finally, at a flow rate of water and air (15) and (25) (Lpm), respectively, in this situation, the water layer has been completely separated from the air layer. The water flow at the bottom of the duct is combined with the airflow at the top. As well as, the flow is stratified.

The flow patterns in the duct at a flow rate of water and air (17.5) and (8.33) (Lpm), respectively, air bubbles appear inside the water in the two-phase flow. The bubbles prefer to flow as bubbly patterns flow in the upper portion of the duct. Furthermore, at a flow rate of water and air (17.5) and (16.67) (Lpm), respectively, at the base of the duct, the water layer separating the air bubble from the wall becomes thicker than at the top. The bubble's nose is asymmetrical, and the flow is plug patterns. Finally, at a flow rate of water and air (17.5) and (25) (Lpm), respectively, in this situation, the water layer has been completely separated from the air layer. The water flow at the base with the airflow at the top of the duct produces stratified flow patterns.

The flow patterns in the duct at a flow rate of water and air (20) and (8.33) (Lpm), respectively, in this case, the separation of the water layer and air layer is complete. The water flows at the bottom of the duct, and the air at the top and the flow is stratified patterns flow. Furthermore, at a flow rate of water and air (20) and (16.67) (Lpm), respectively, as air velocity increases in stratified flow, huge surface waves form on the water layer, and the flow becomes wavy, as well as the flow is wavy patterns flow. Finally, at a flow

rate of water and air (20) and (25) (Lpm), respectively, as the air velocity is further increased in the wavy flow patterns region, the waves eventually become big enough to reach the top of the duct. These are transmitted at a high velocity and wet the entire duct surface, forming a water film between the bridging waves, and the flow is slug flow.

Figure (5-56) shows digital images of the twelve experimental tests using Rectangular winglets as vortex generators in the duct for single-phase and two-phase flows over the bank of oval tubes. Air bubbles appear inside the water in the two-phase flow with high velocity and more random movement. The flow patterns in the duct at a flow rate of water and air (15) and (8.33) (Lpm), respectively, air bubbles appear inside the water in the two-phase flow. The bubbles prefer to flow as bubbly patterns flow in the upper portion of the duct. Furthermore, at a flow rate of water and air (15) and (16.67) (Lpm), respectively, at the base of the duct, the water layer separating the air bubble from the wall becomes thicker than at the top. The bubble's nose is asymmetrical, and the flow is plug patterns. Finally, at a flow rate of water and air (15) and (25) (Lpm), respectively, in this situation, the water layer has been completely separated from the air layer. The water flow at the bottom of the duct is combined with the airflow at the top. As well as the flow is stratified.

The flow patterns in the duct at a flow rate of water and air (17.5) and (8.33) (Lpm), respectively, air bubbles appear inside the water in the two-phase flow. The bubbles prefer to flow as bubbly patterns flow in the upper portion of the duct. Furthermore, at a flow rate of water and air (17.5) and (16.67) (Lpm), respectively, at the base of the duct, the water layer separating the air bubble from the wall becomes thicker than at the top. The bubble's nose is asymmetrical, and the flow is plug patterns. Finally, at a flow rate of water and air (17.5) and (25) (Lpm), respectively, in this situation, the water

layer has been completely separated from the air layer. The water flow at the bottom of the duct is combined with the airflow at the top. As well as, the flow is stratified.

The flow patterns in the duct at a flow rate of water and air (20) and (8.33) (Lpm), respectively, in this situation, the water layer has been completely separated from the air layer. The water flow at the bottom of the duct is combined with the airflow at the top. As well as, the flow is stratified. Furthermore, at a flow rate of water and air (20) and (16.67) (Lpm), respectively, as air velocity increases in stratified flow, huge surface waves form on the water layer, and the flow becomes wavy, as well as the flow is Wavy patterns flow. Finally, at a flow rate of water and air (20) and (25) (Lpm), respectively, as the air velocity is further increased in the wavy flow patterns region, the waves eventually become big enough to reach the top of the duct. These are transmitted at a high velocity and wet the entire duct surface, forming a water film between the bridging waves, and the flow is slug flow patterns.

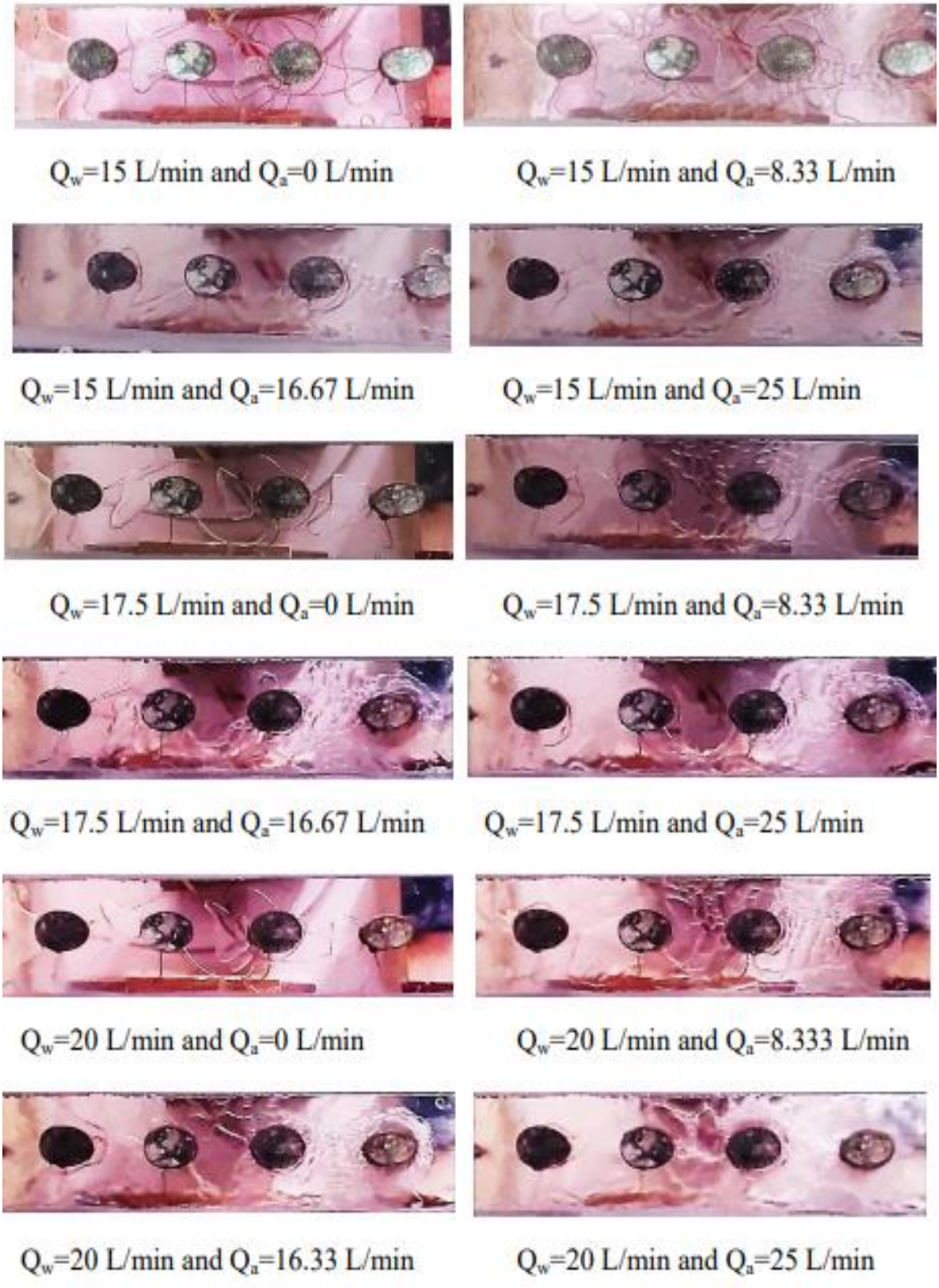

Figure (5-54) Digital images of the experimental tests without vortex generators

Figure (5-55) Digital images of the experimental tests with delta winglets

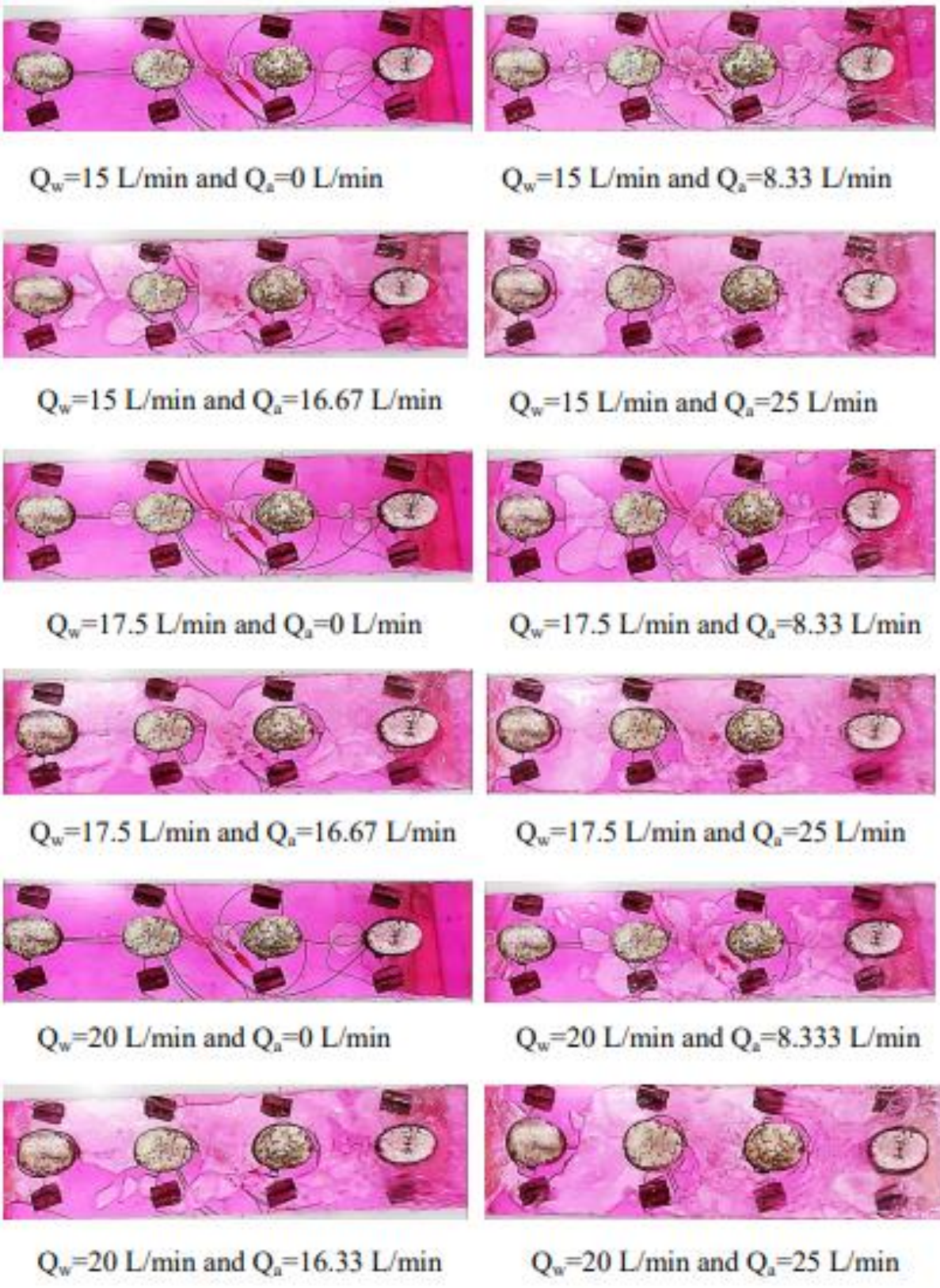

Figure (5-56) Digital images of the experimental tests with rectangular winglets

5.5. Numerical Results for the Experimental Work

Figures (5-57) to (5-67) show the numerical results for the experimental work of the increased water-air flow rates on the temperature gradient at various locations in the duct with a constant electrical power of (110 W) as a heat flux. The heat transfer coefficient decreases when the temperature gradient between single or two-phase flow and the surfaces of tube banks increases, and vice versa.

5.5.1. Single-phase flow

5.5.1.1 Effect of flow rate

Figure (5-57) illustrates the temperature gradient between water flow and oval tube surfaces at various locations in the duct without winglets, with delta winglets, and with rectangular winglets for three different water flow rates (15, 17.5 and 20 Lpm). The temperature gradient decreased as the flow rate of water increased, as observed in this figure.

Figure (5-57a) illustrates the temperature difference decreased by (7.76%) and (17.2%), respectively for without vortex generators. These results agree with [12 and 20] for reduced temperature gradient at the water flow velocity increased; therefore, the heat transfer coefficient increased.

Figure (5-58) illustrates the entrance and exit pressure for water flow at many points in the duct without winglets, with delta winglets, and with rectangular winglets for three different water flow rates (15, 17.5 and 20 Lpm).

Figure (5-58a) illustrates the pressure drop in the duct increased by (20.58%) and (58.27%), respectively for without vortex generators. The pressure drop in the duct increased as the water flow rate increased.

5.5.1.2 Effect of vortex generators

Figures (5-57b and c) illustrate the temperature difference decreased by (35.45%, 30.1%, and 38.9%), respectively with delta winglets, and finally (43.8%, 41.1%, and 37.2%), respectively with rectangular winglets.

Figures (5-58b and c) illustrate the pressure drop in the duct increased by (20.5%) and (16.8%) at a water flow rate of (15 Lpm) and (17.5 Lpm), respectively and increased by (3.9%) at a water flow rate of (20 Lpm) with delta winglets, and finally (21.45%, 24.75%, and 13.4%), respectively with rectangular winglets.

Figure (5-59a) illustrates the variation of a temperature gradient with Reynolds number in water flow over the bank of oval tubes without winglets generators. Due to a decrease in the temperature gradient between the water flow and surfaces of the oval tube, the heat transfer coefficient improved as the Reynolds number increased.

Figure (5-59b) represents the variation of the pressure reduction with Reynolds number in water flow over oval tube banks with an absence of winglets. As the Reynolds number grew, the duct pressure drop was increased.

Figure (5-59c) represents the Reynolds number performance parameter for water flow over oval tube banks without winglets. As the Reynolds number climbed, the performance parameter improved because the pressure in the duct and the temperature gradient between the water flow and the surfaces of the oval tube decreased. The delta winglets' performance is higher than that of the other two vortex generators. These results that examined the influence of different vortex generator forms on heat flow in the duct and showed that delta winglets provide the highest performance.

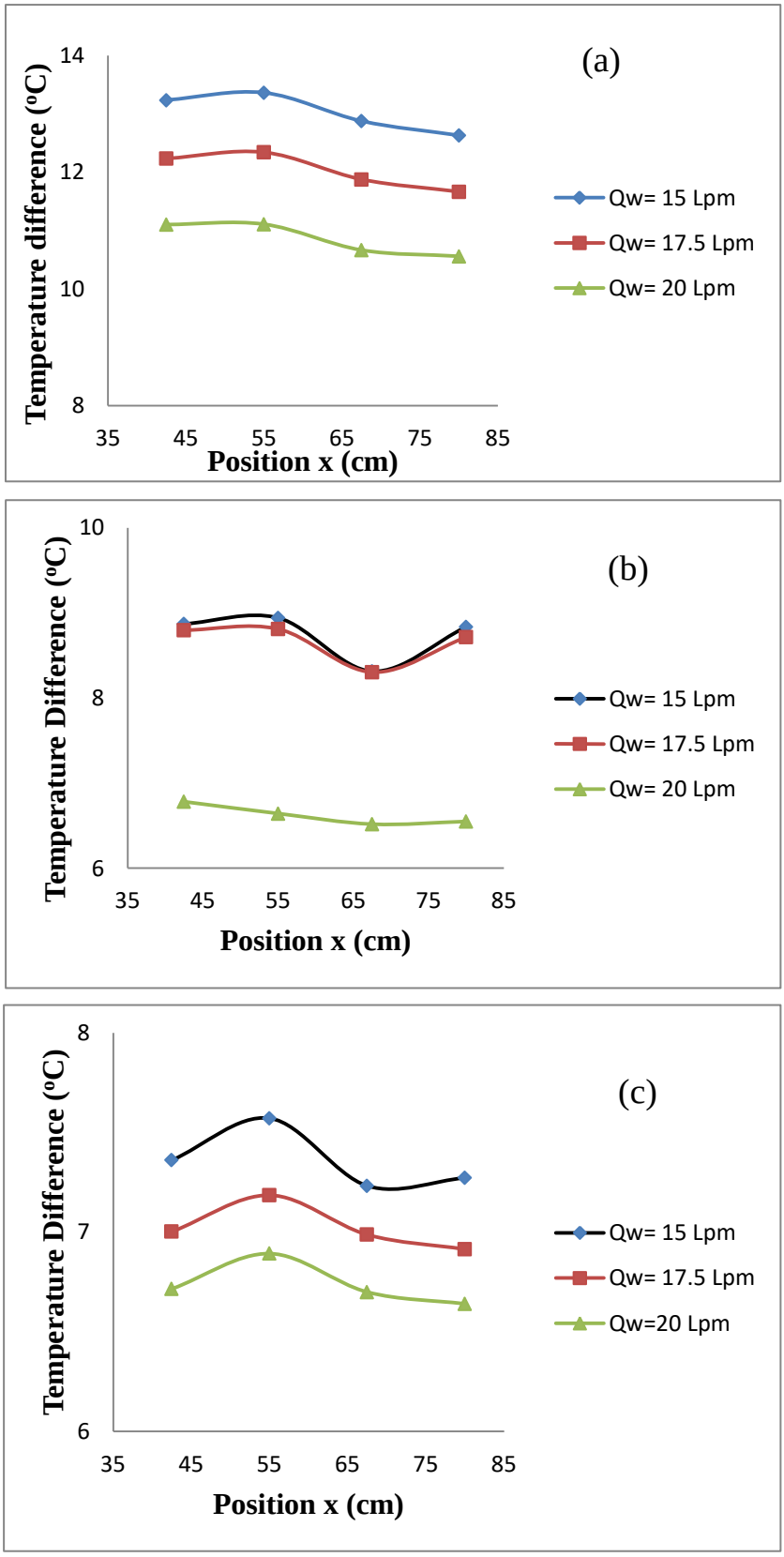

Figure (5-57) The temperature gradient between water flow and surfaces of an oval tube for various water flow rates (15, 17.5, and 20 Lpm) (a) without winglets (b) with delta winglets (c) with rectangular winglets

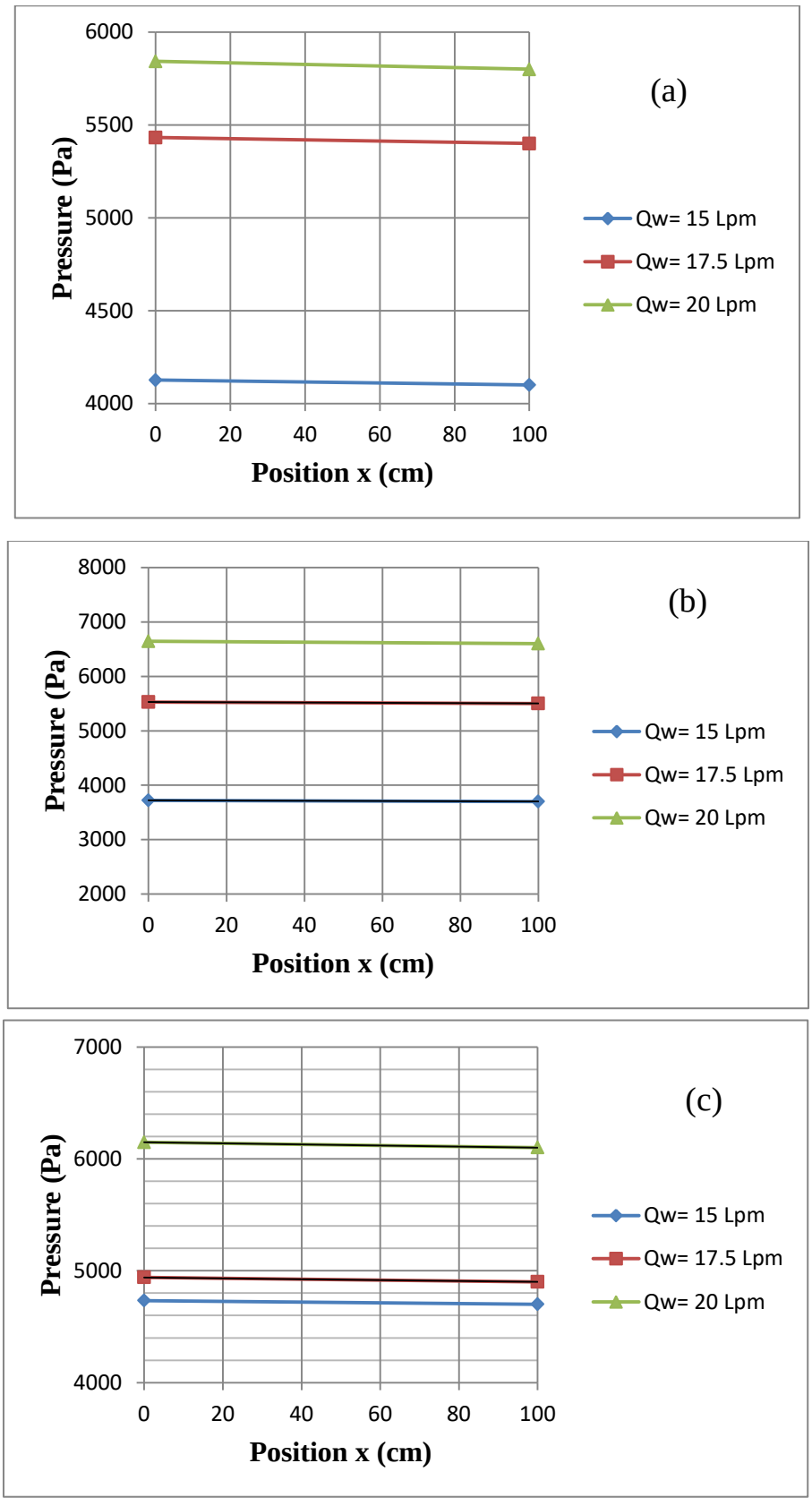

Figure (5-58) Inlet and outlet pressure in the duct for water flow (a) without winglets (b) with delta winglets (c) with Rectangular winglets

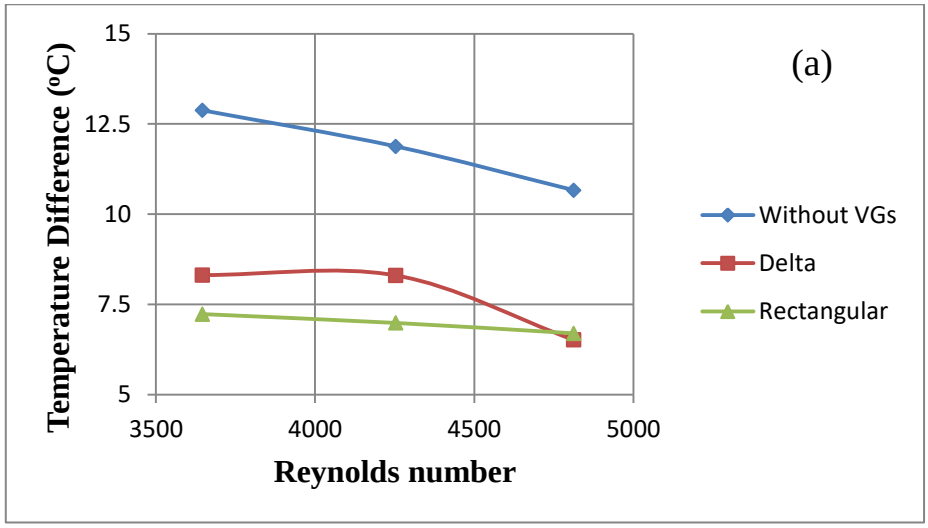

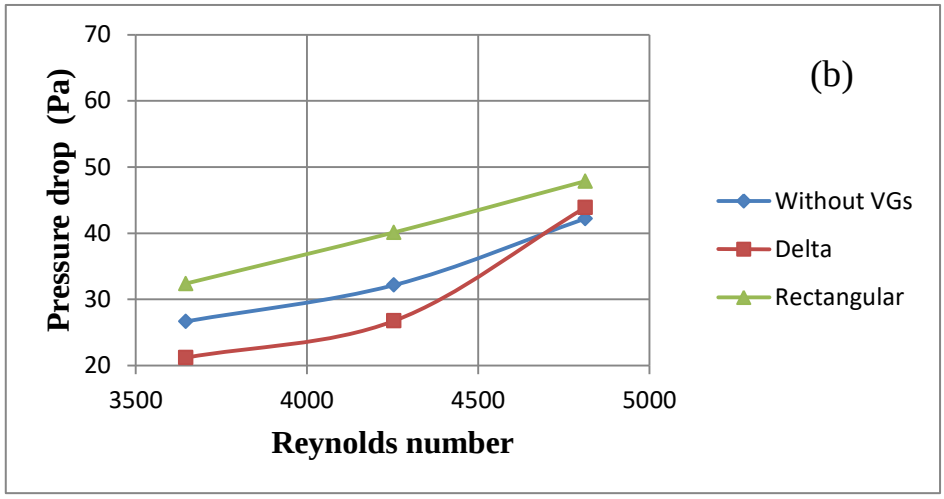

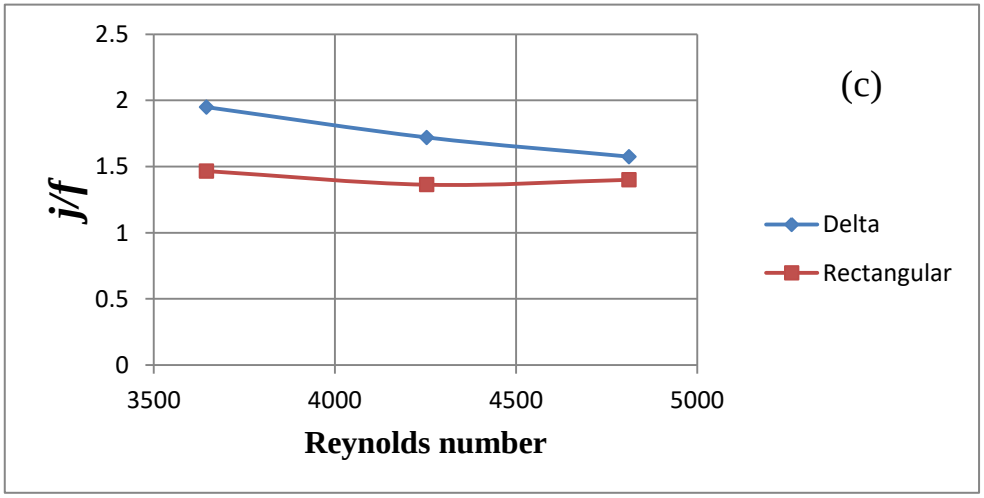

Figure (5-59) (a) The temperature gradient (b) Pressure drop (c) Performance parameter

5.5.2. Two-phase flow

5.5.2.1 Effect of flow rate

Figure (5-60) indicates that at a constant flow rate of water, the temperature gradient between water-air flow and surfaces of oval tubes increased. At these points, the airflow rate increases (8.33, 16.67, and 25 Lpm) with a constant water flow rate and heat flux. When the water and air flow rates increase without winglets, the rate of heat transfer decreases as the temperature gradient becomes less significant. The heat transfer coefficient improved as the temperature difference reduced because the winglets concentrated the working fluid on the tube surface with delta winglets and rectangular winglets used in the duct.

Figure (5-60a) illustrates the temperature difference decreased by (7.76%) and (17.2%), respectively without the vortex generator. The stagnation of the flow behind the tubes is clearly appearing in the case of tubes without vortex generators. This case illustrates the problem of low velocity of the fluid back the tubes that reduce the thermal performances of heat exchanger. As the increased frontal velocity causes the longitudinal vortices' velocity to rise, the fluid is transported from the wake zone of the tubes to the main flow regions, therefore promoting enhanced mixing of the fluid layers.

Figure (5-61) represents the inlet and outlet pressure in the duct for water-air flow at various points. At these points, the airflow rate increases (8.33, 16.67, and 25 Lpm) with constant heat flux and discharge of water. The pressure losses without winglets in the duct are reduced. Increased pressure drops compared to delta winglets and rectangular winglets are used in the duct that is not utilized.

Figure (5-61a) illustrates the pressure drop in the duct compared to the single-phase flow decreased by (52%, 104.5%, and 154%), respectively, at a constant discharge of water (15 Lpm), (43.73%, 88.66%, and 131.38%),

respectively, at a constant discharge of water (17.5 Lpm), and decreased by (43.54%, 84.97%, and 124.3%), respectively, at a constant discharge of water (20 Lpm) for without (VGs) case.

Due to the increased flow rate of water-air with delta winglets, pressure drops within the duct are minimized.

In addition, when the flow rate of water-air is raised in the absence of winglets in the duct, the pressure drop is reduced. Also, when rectangular winglets are used in the duct, the pressure losses are more significant than not. In addition, when the flow rate of water-air increases with rectangular winglets, the pressure losses in the duct are decreased.

5.5.2.2 Effect of vortex generators

Adding winglets to the duct can raise the surface velocity of water-air flow, hence enhancing the heat transfer coefficient by generating intense turbulence. The temperature gradient decreases as the flow velocity increases. When the flow is directed toward the surfaces of the oval tube, the temperature gradient is inversely related to the flow velocity. The airflow rate increased from (8.33, 16.67, and 25 Lpm) with a constant flow rate of water and heat power of (110 W).

Figure (5-60b) illustrates the temperature difference decreased by (44.67%, 44.9%, and 45%), respectively, at a constant discharge of water (15 Lpm), (41.88%, 42%, and 42.26%), respectively, at a constant discharge of water (17.5 Lpm), and decreased by (40.18%, 40.35%, and 40.474%), respectively, at a constant discharge of water (20 Lpm) with delta winglets.

Figure (5-60c) illustrates the temperature difference decreased by (43.33%, 43.53%, and 43.67%), respectively, at a constant discharge of water (15 Lpm), (25.9 %, 35.45%, and 35.8%), respectively, at a constant flow rate of water (17.5 Lpm), and decreased by (39.88%, 38.72%, and 34.676%),

respectively, at a constant discharge of water (20 Lpm) with Rrectangular winglets.

Figure (5-61b) illustrates the pressure drop in the duct compared to the single-phase flow decreased by (5.66%, 27.8%, and 40.6%), respectively, at a constant discharge of water (15 Lpm), (5.66%, 27.8%, and 40.6%), respectively, at a constant discharge of water (17.5 Lpm), and decreased by (5.66%, 27.8%, and 40.6%), respectively, at a constant discharge of water (20 Lpm) with delta winglets.

Figure (5-61c) illustrates the pressure drop in the duct compared to the single-phase flow decreased by (33.6%, 49.4%, and 58.3%), respectively, at a constant discharge of water (15 Lpm), (30.46%, 45.9%, and 54.9%), respectively, at a constant discharge of water (17.5 Lpm), and decreased by (28%, 43%, and 52%), respectively, at a constant discharge of water (20 Lpm) with rectangular winglets.

The effect of the Reynolds number for water-air flow over oval tube banks in a turbulent region on heat transfer rate and pressure reduction is essential for optimal design and location of vortex formation. Due to the decrease in pressure and temperature gradient between water-air flow and surfaces of the oval tube in the duct, the performance parameter was improved when the Reynolds number of water decreased and the Reynolds number of air grows at the flow rate of air increases (8.33, 16.67, and 25 Lpm) but the flow rate of water remains constant.

The variation of the temperature gradient with Reynolds number in water-air flow over oval tube banks without winglets, with delta winglets, and with rectangular winglets are represented in Figure (5-62). At a constant flow rate of water, the heat transfer coefficient increases as the temperature gradient between the water-air flow and surfaces of the oval tube decreases.

The variation of the drop in pressure with the Reynolds number in water-air flow over oval tube banks without winglets, with delta winglets, and with

rectangular winglets are visualized in Figure (5-63). When the Reynolds number of water and the Reynolds number of air increases, the pressure drop decreases in the duct with a constant flow rate of water.

The relationship between the Reynolds number and performance parameter in the water-air flow over oval tube banks with and without winglets is depicted in Figure (5-64). As water-air flow increased, the performance parameter improved. The vortex generators eliminate the zones of low-velocity behind the tubes. During the passing of the flow through the tube walls and vortex generators, the fluid flow separates into three primary zones; a very large zone located between (VGs) and the tube walls, where the flow is accelerated and swirl the stagnated fluid behind the tubes. The second zone located over (VGs) that presents the majority of the flow fields. The third region behind the (VGs) shows a zone of secondary recirculation of the flow. In other hand, adding the (VGs) near the surface of tubes, the fluid flows behind the tubes and significantly eliminates the hot points, which enhance the thermal performances of the fin and tubes heat exchangers.

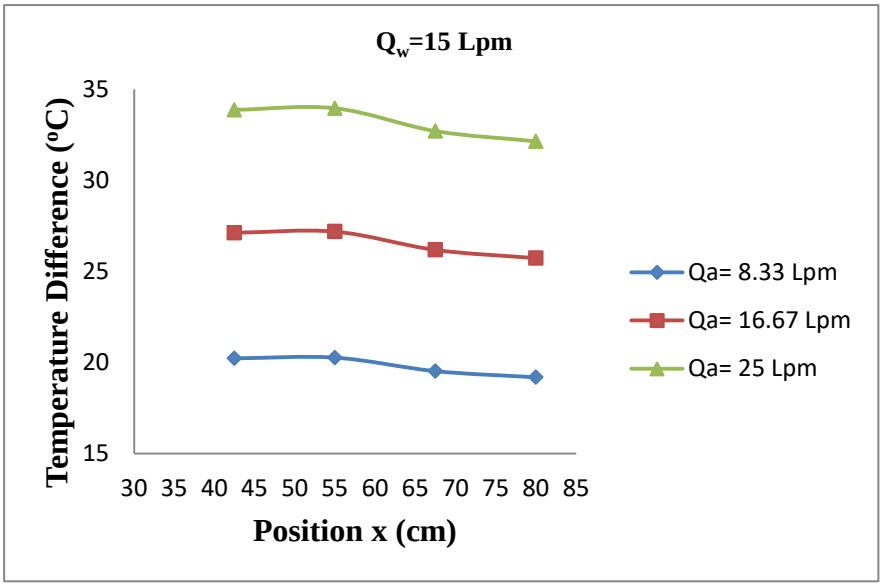
Q_w=15 Lpm
Temperature Difference (°C)
35
30
25
20
15
30 35 40 45 50 55 60 65 70 75 80 85
Position x (cm)
Qa= 8.33 Lpm
Qa= 16.67 Lpm
Qa= 25 Lpm

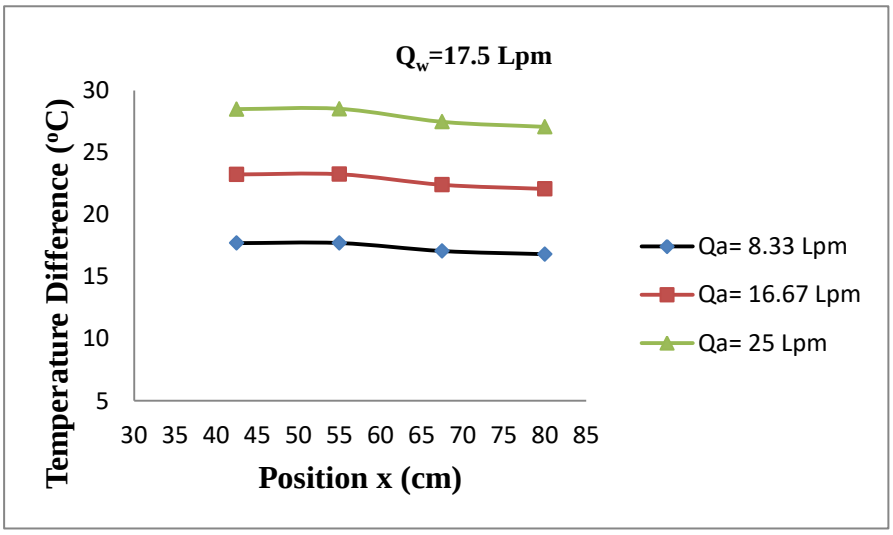
Q_w=17.5 Lpm
Temperature Difference (°C)
30
25
20
15
10
5
30 35 40 45 50 55 60 65 70 75 80 85
Position x (cm)
Qa= 8.33 Lpm
Qa= 16.67 Lpm
Qa= 25 Lpm

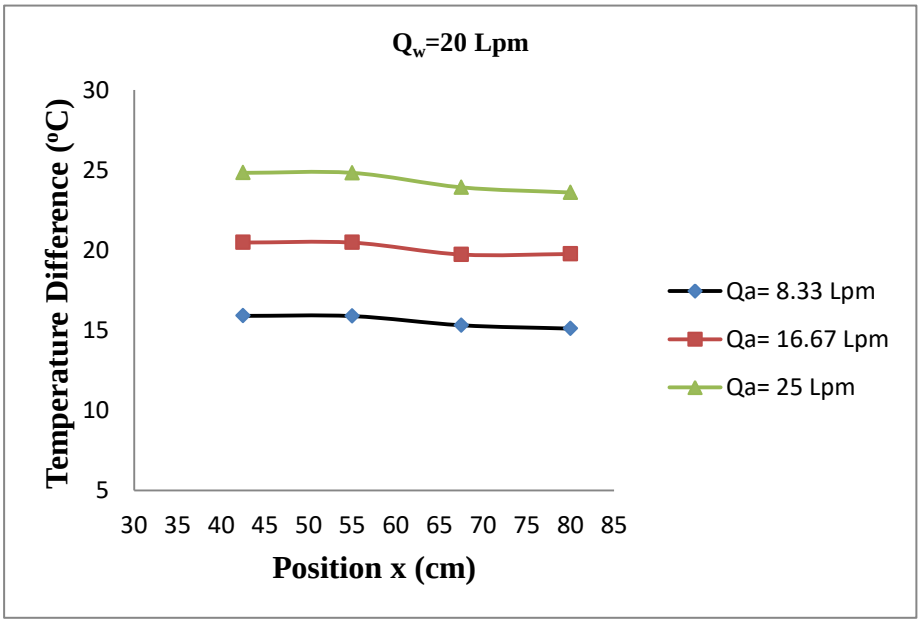
Q_w=20 Lpm
Temperature Difference (°C)
30
25
20
15
10
5
30 35 40 45 50 55 60 65 70 75 80 85
Position x (cm)
Qa= 8.33 Lpm
Qa= 16.67 Lpm
Qa= 25 Lpm

(a)

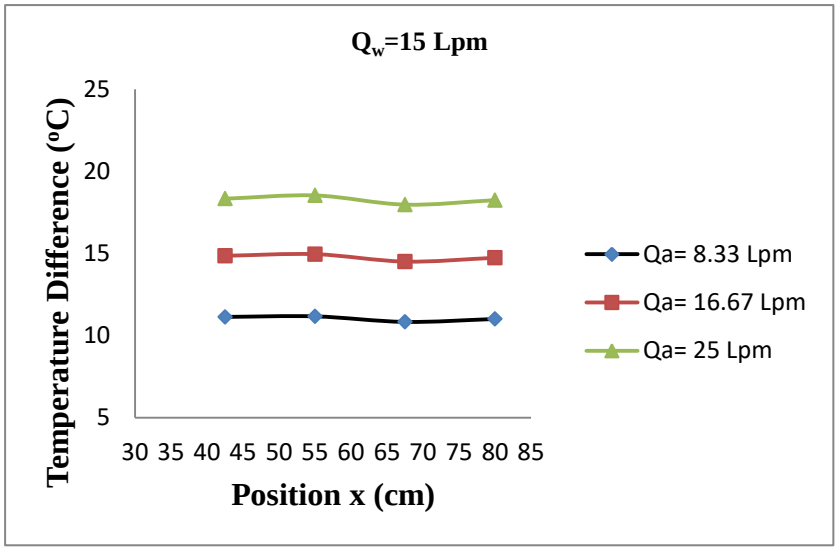
Q_w=15 Lpm
Temperature Difference (°C)
25
20
15
10
5
30 35 40 45 50 55 60 65 70 75 80 85
Position x (cm)
Qa= 8.33 Lpm
Qa= 16.67 Lpm
Qa= 25 Lpm

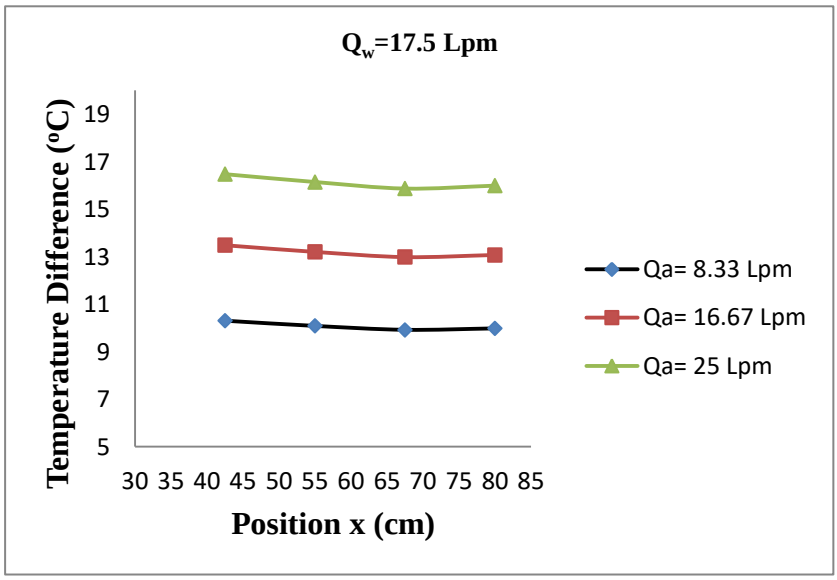
Q_w=17.5 Lpm
Temperature Difference (°C)
19
17
15
13
11
9
7
5
30 35 40 45 50 55 60 65 70 75 80 85
Position x (cm)
Qa= 8.33 Lpm
Qa= 16.67 Lpm
Qa= 25 Lpm

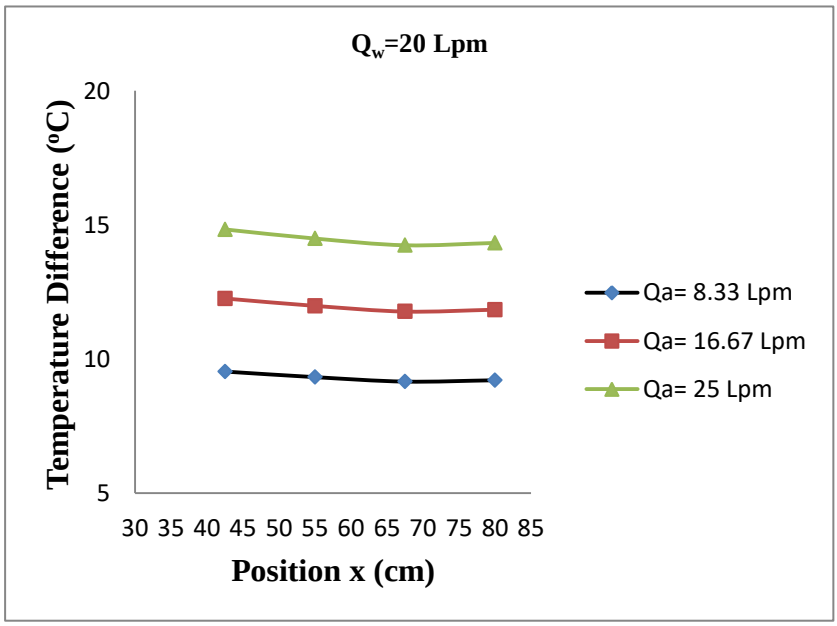
Q_w=20 Lpm
Temperature Difference (°C)
20
15
10
5
30 35 40 45 50 55 60 65 70 75 80 85
Position x (cm)
Qa= 8.33 Lpm
Qa= 16.67 Lpm
Qa= 25 Lpm

(b)

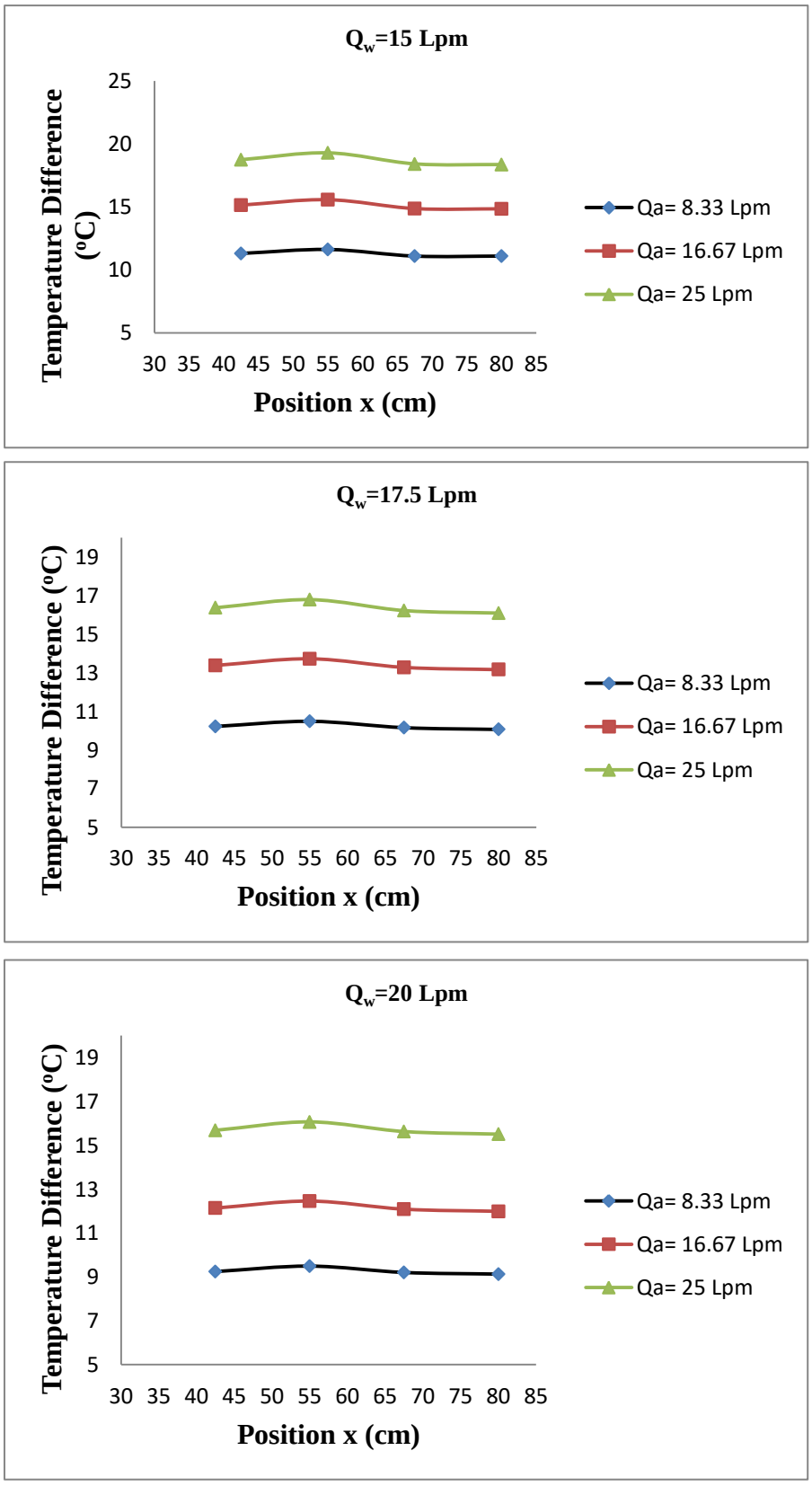

(c)

Figure (5-60) The temperature gradient between the flow of water and air with oval tube surfaces (a) without winglets (b) with delta winglets (c) with rectangular winglets

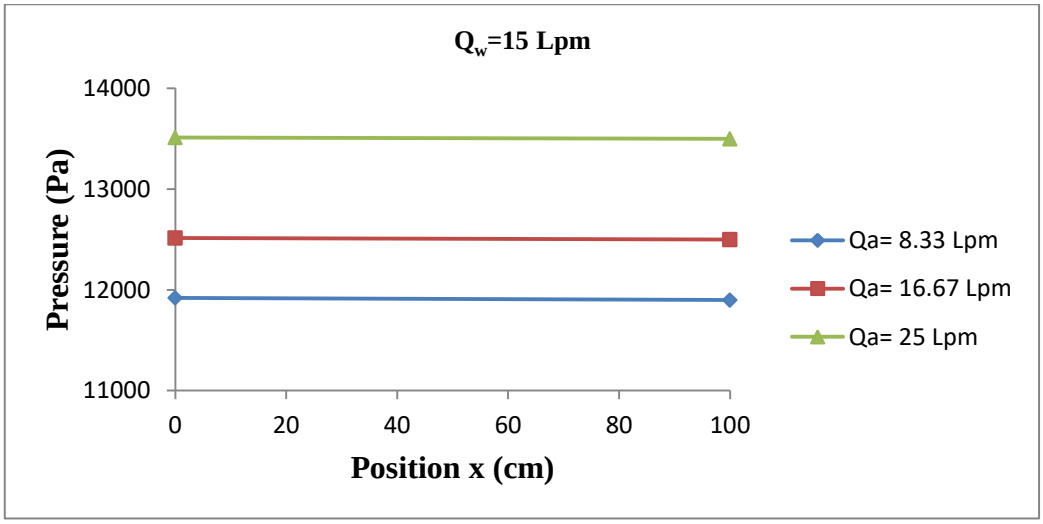
Q_w=15 Lpm
Pressure (Pa)
14000
13000
12000
11000
0
20
40
60
80
100
Position x (cm)
Qa= 8.33 Lpm
Qa= 16.67 Lpm
Qa= 25 Lpm

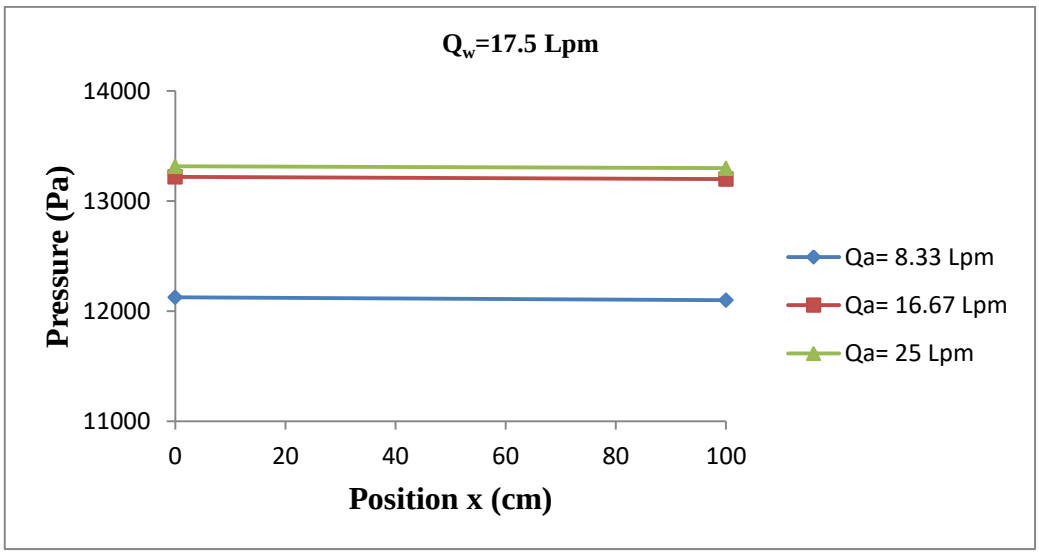
Q_w=17.5 Lpm
Pressure (Pa)
14000
13000
12000
11000
0
20
40
60
80
100
Position x (cm)
Qa= 8.33 Lpm
Qa= 16.67 Lpm
Qa= 25 Lpm

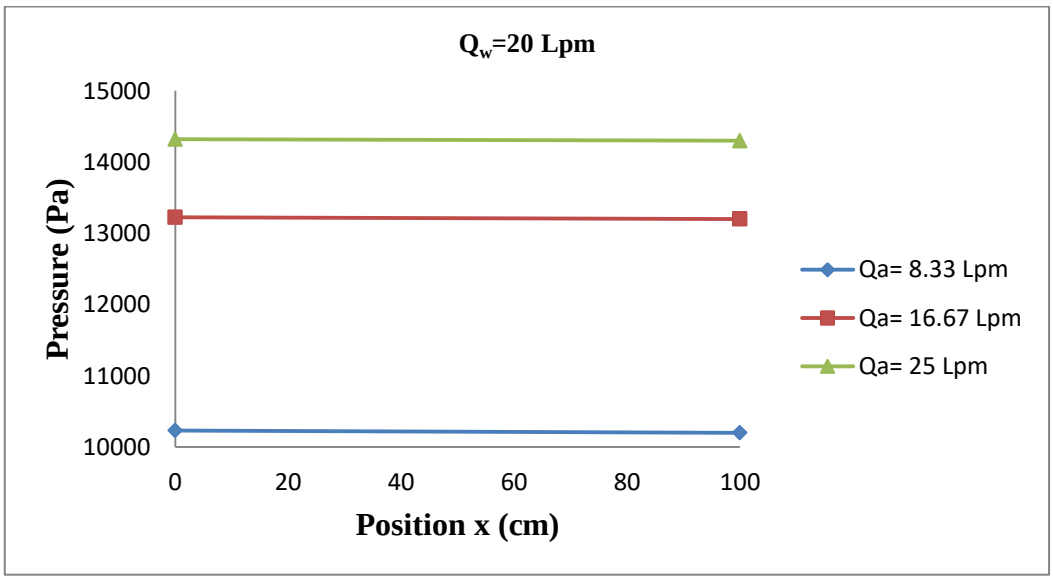
Q_w=20 Lpm
Pressure (Pa)
15000
14000
13000
12000
11000
10000
0
20
40
60
80
100
Position x (cm)
Qa= 8.33 Lpm
Qa= 16.67 Lpm
Qa= 25 Lpm

(a)

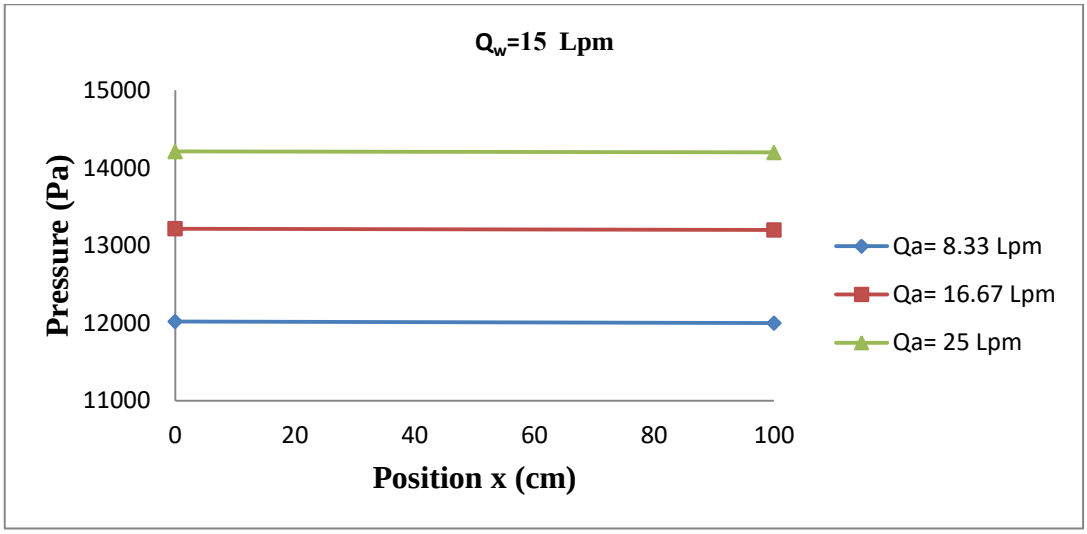
Q_w=15 Lpm
Pressure (Pa)
15000
14000
13000
12000
11000
0
20
40
60
80
100
Position x (cm)
Qa= 8.33 Lpm
Qa= 16.67 Lpm
Qa= 25 Lpm

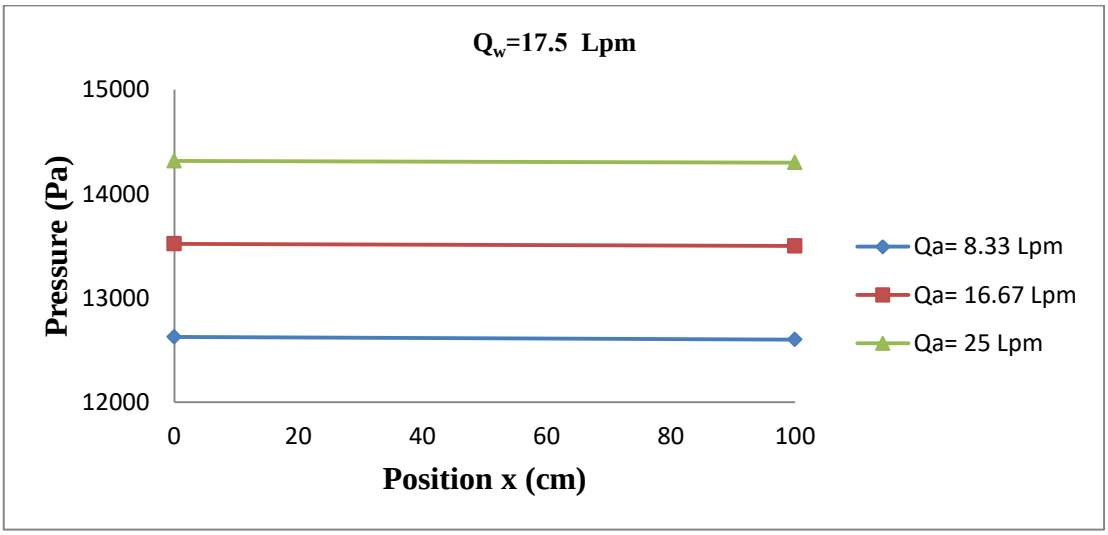
Q_w=17.5 Lpm
Pressure (Pa)
15000
14000
13000
12000
0
20
40
60
80
100
Position x (cm)
Qa= 8.33 Lpm
Qa= 16.67 Lpm
Qa= 25 Lpm

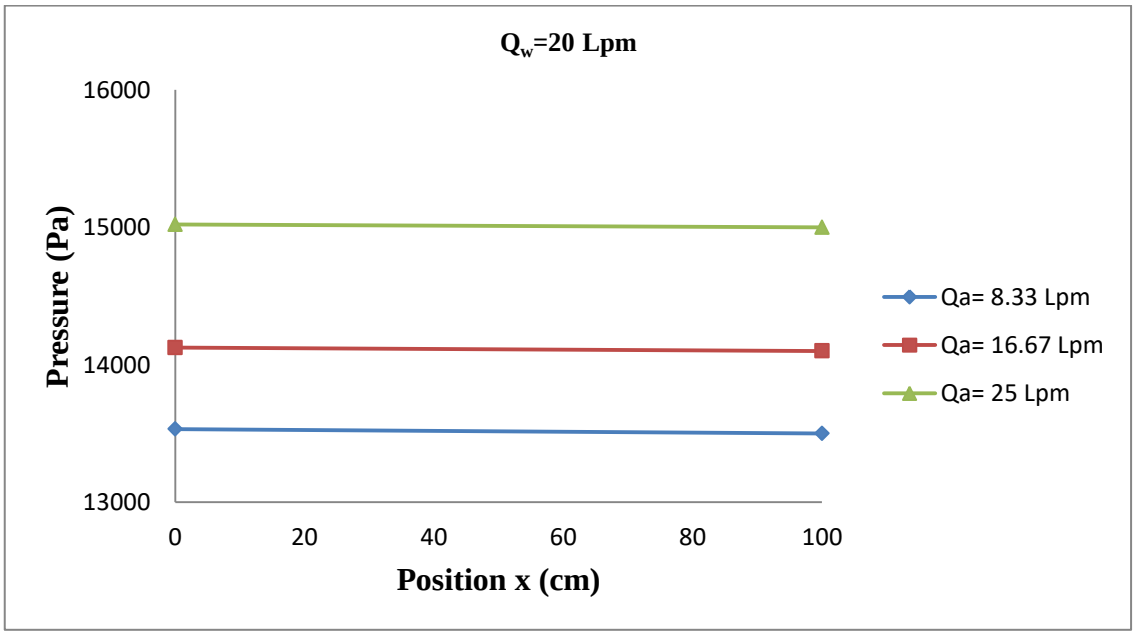
Q_w=20 Lpm
Pressure (Pa)
16000
15000
14000
13000
0
20
40
60
80
100
Position x (cm)
Qa= 8.33 Lpm
Qa= 16.67 Lpm
Qa= 25 Lpm

(b)

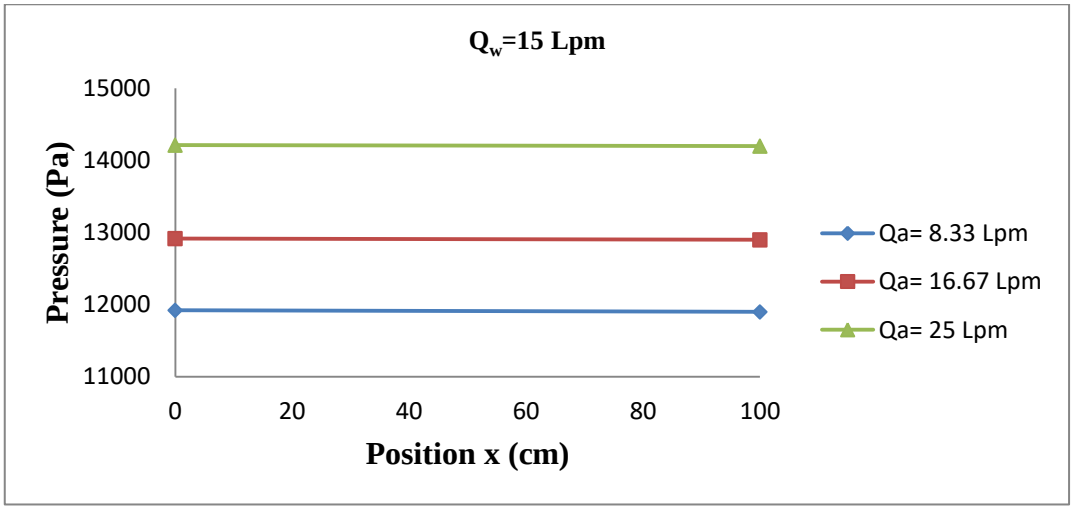

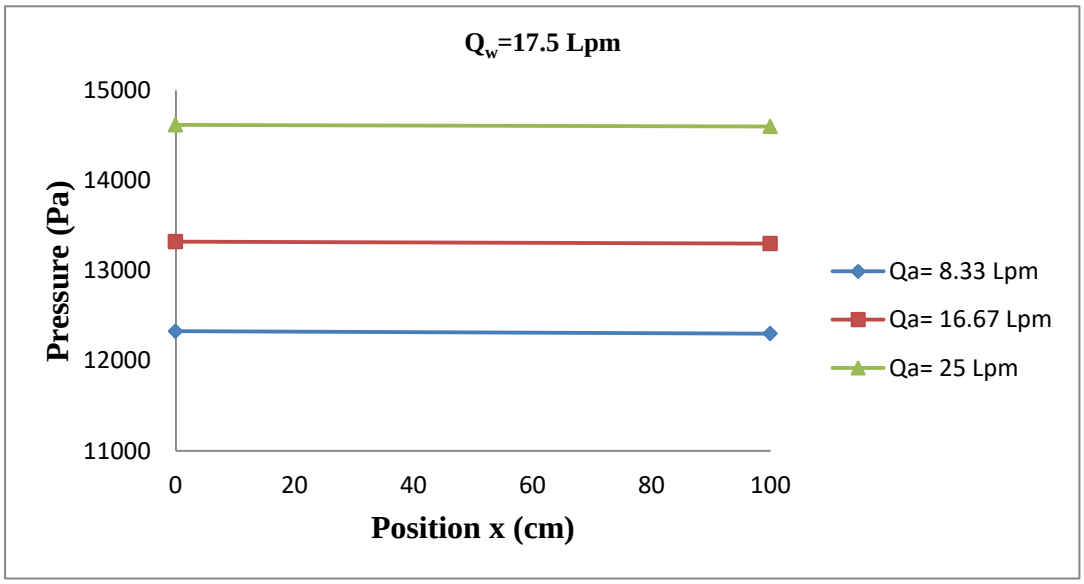

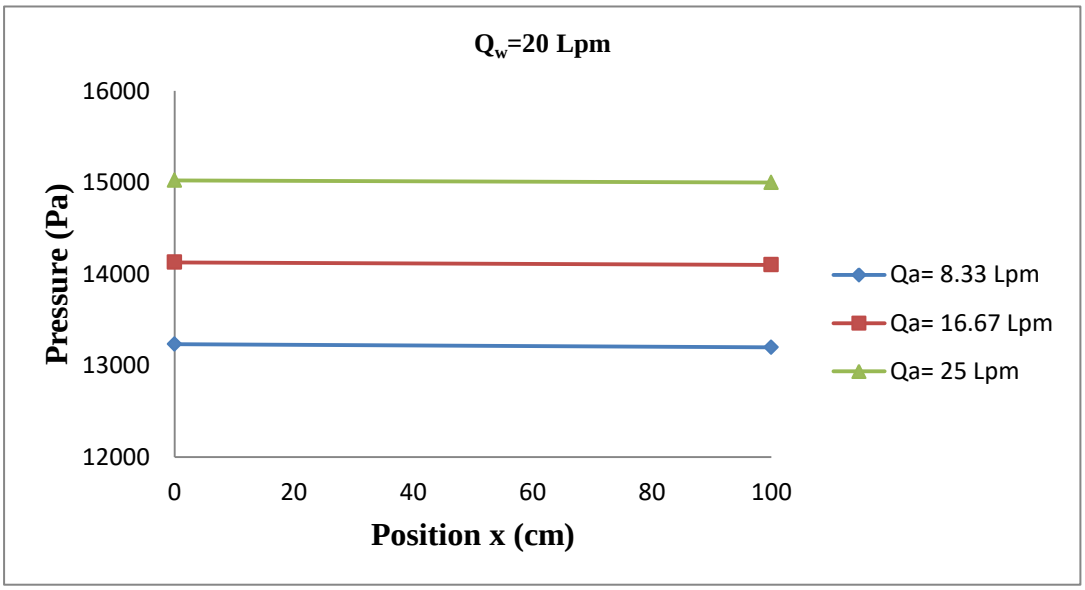

(c)

Figure (5-61) Inlet and outlet pressure in the duct (a) without winglets (b) with delta winglets (c) with rectangular winglets

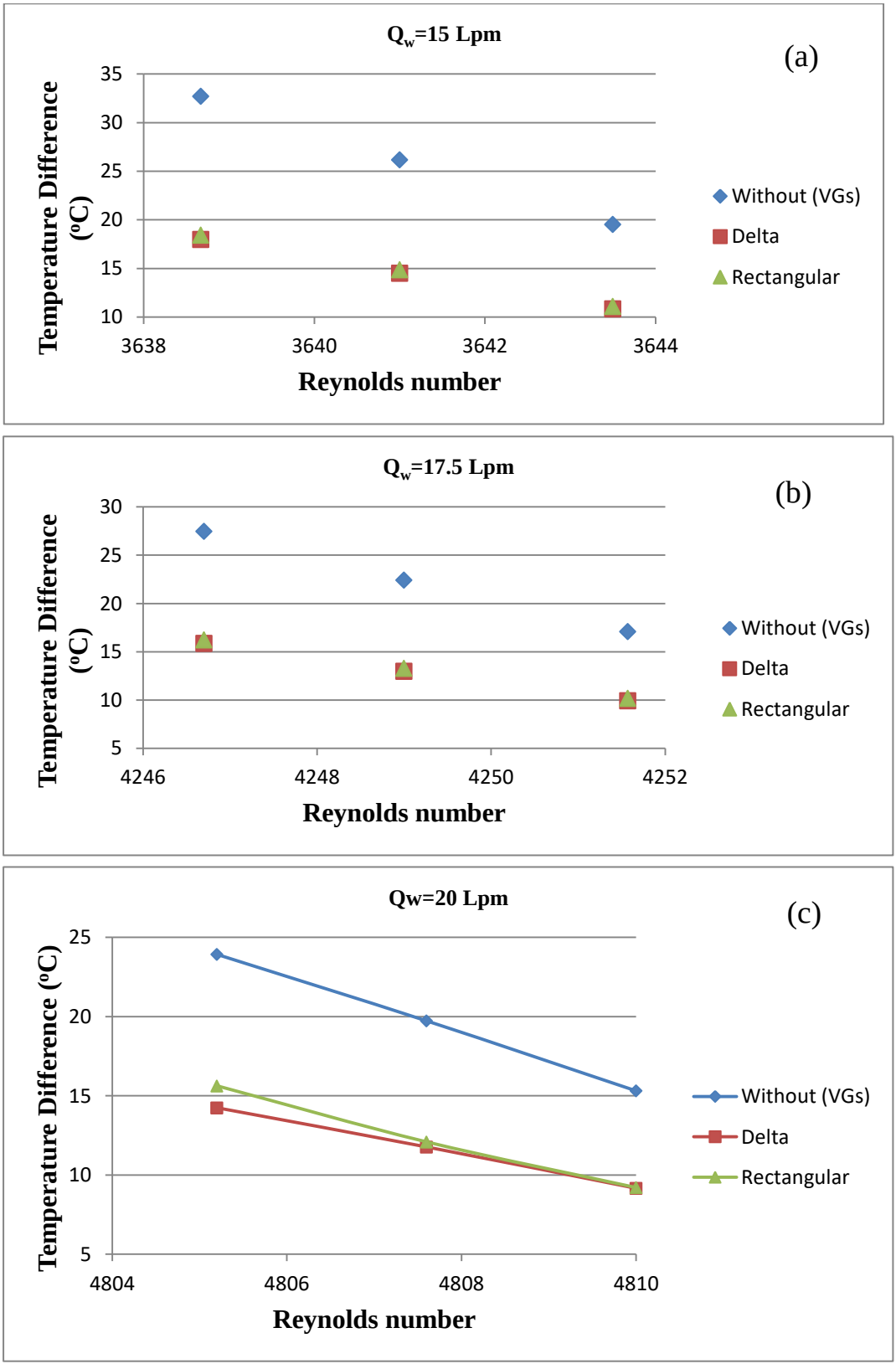

Figure (5-62) The temperature gradient at (a) Q_w= 15 Lpm (b) Q_w= 17.5 Lpm (c) Q_w= 20 Lpm

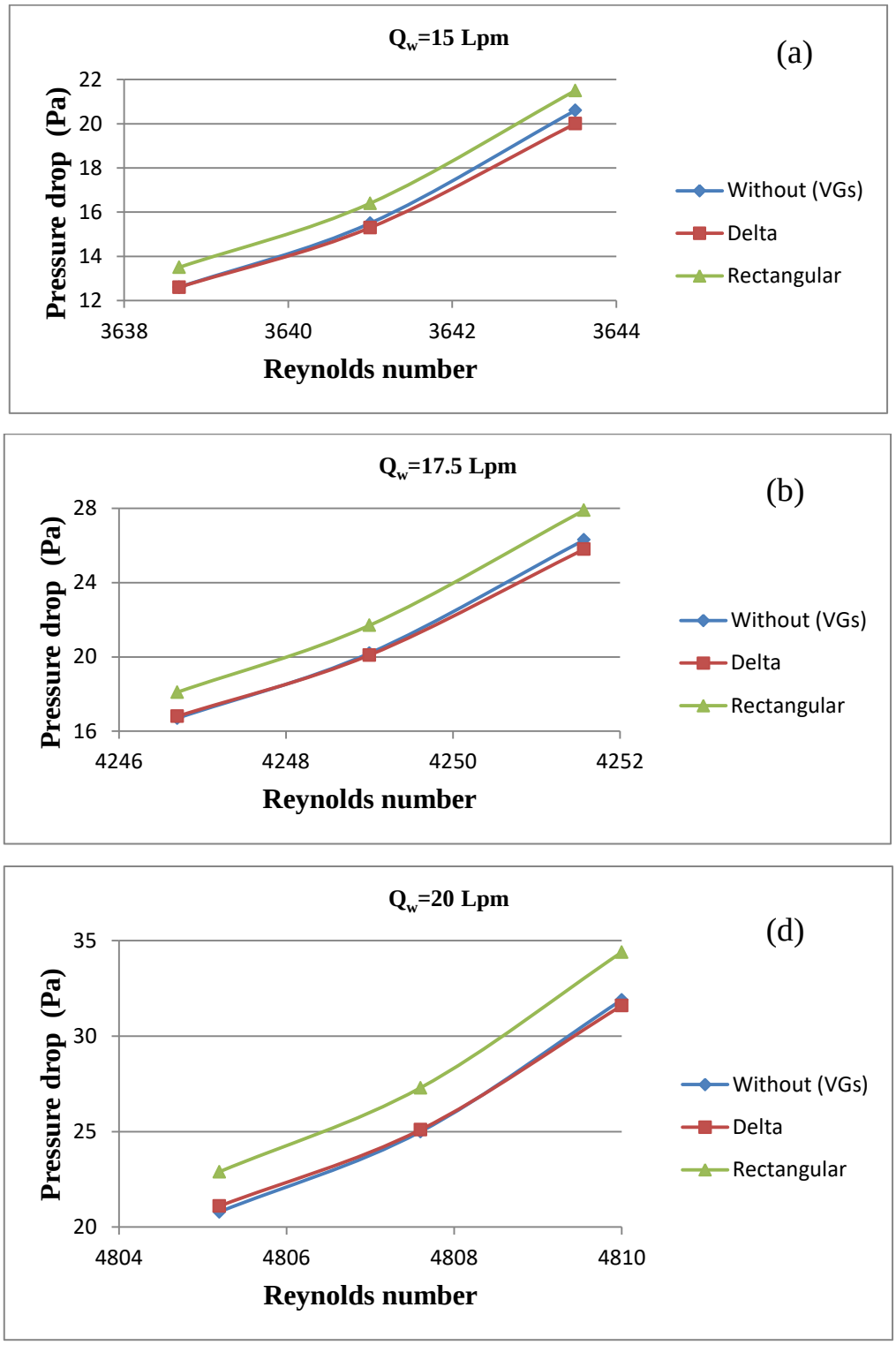

Figure (5-63) Pressure drop at (a) Q_w= 15 Lpm (b) Q_w= 17.5 Lpm (c) Q_w= 20 Lpm

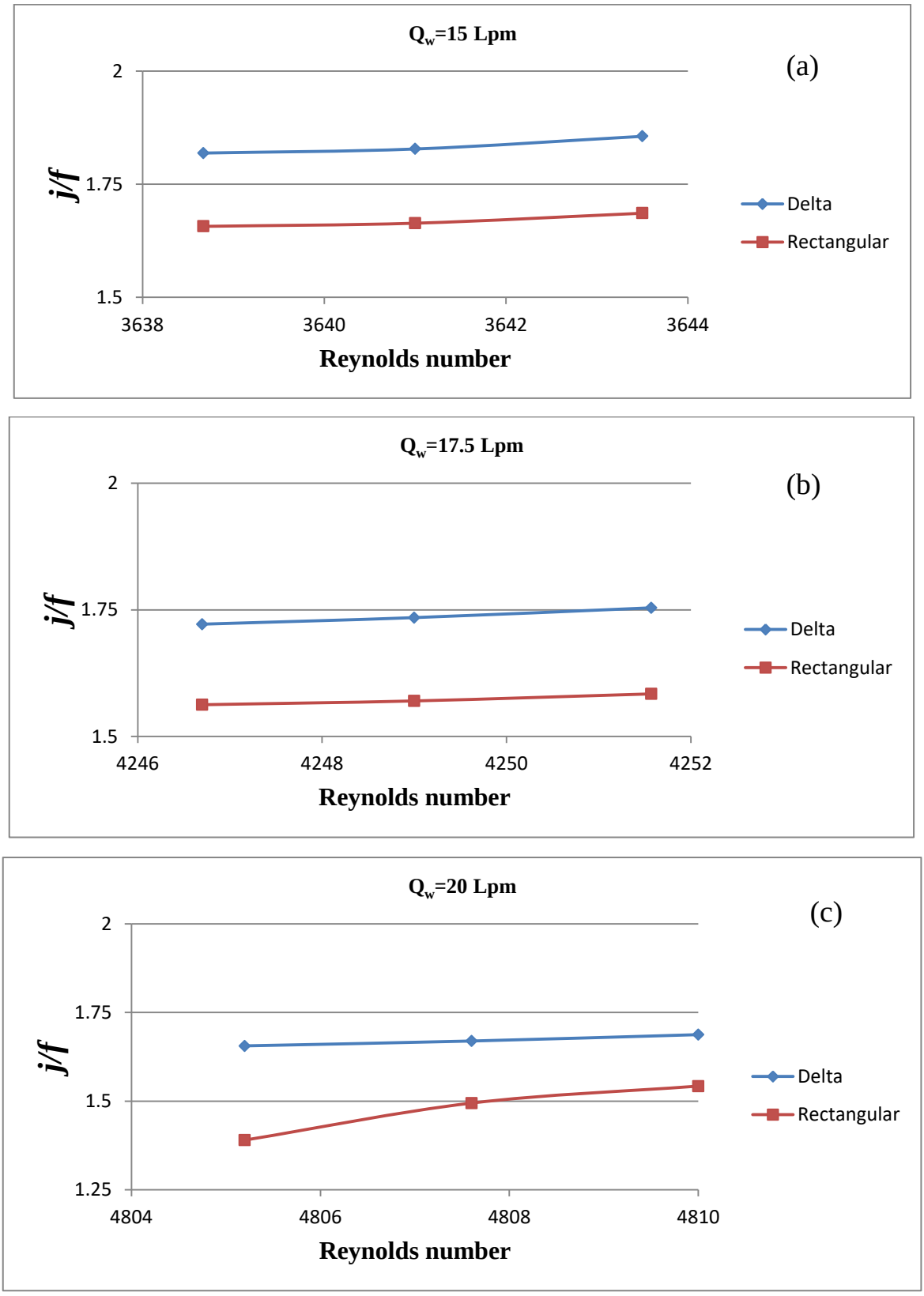

Figure (5-64) Performance parameter (a) Q_w= 15 Lpm (b) Q_w= 17.5 Lpm (c) Q_w= 20 Lpm

5.5.3 Velocity vector

Figures (5-65) to (5-67) illustrate that the velocity vector for water flow and mixture (water-air) flow with and without (VGs) from Workbench (ANSYS - FLUENT 19.0) when a flow rate of air increases (0, 8.33, 16.67, and 25) (Lpm) respectively, with constant a flow rate of water.

Figure (5-65) shows the velocity vector for single-phase and two-phase flow without vortex generators. As velocity increases, longitudinal vortices also increase. Longitudinal vortices move fluid from the wake zone of the tubes to the main flow regions, consequently enhancing the mixing of the bulk fluid.

Figure (5-66) shows the velocity vector for water flow and mixture (water-air) flow with delta winglets as (VGs). It can be observed that the flow velocity is increased, and the flow is directed toward the oval tube's surface by delta winglets.

Figure (5-67) shows the velocity vector for water flow and mixture (water-air) flow with rectangular winglets as (VGs). It can be observed that the flow velocity is increased, and the flow is directed toward the oval tube's surface by rectangular winglets.

The distributions of velocity at the entrance region are uniform. After the flow passes the first pair of winglet vortex generators, the flow velocity increases near the second row of oval tubes regimes, however it decreases after the winglet vortex generators. These characteristics are observed again between the second and third rows of oval tubes and winglet vortex generators.

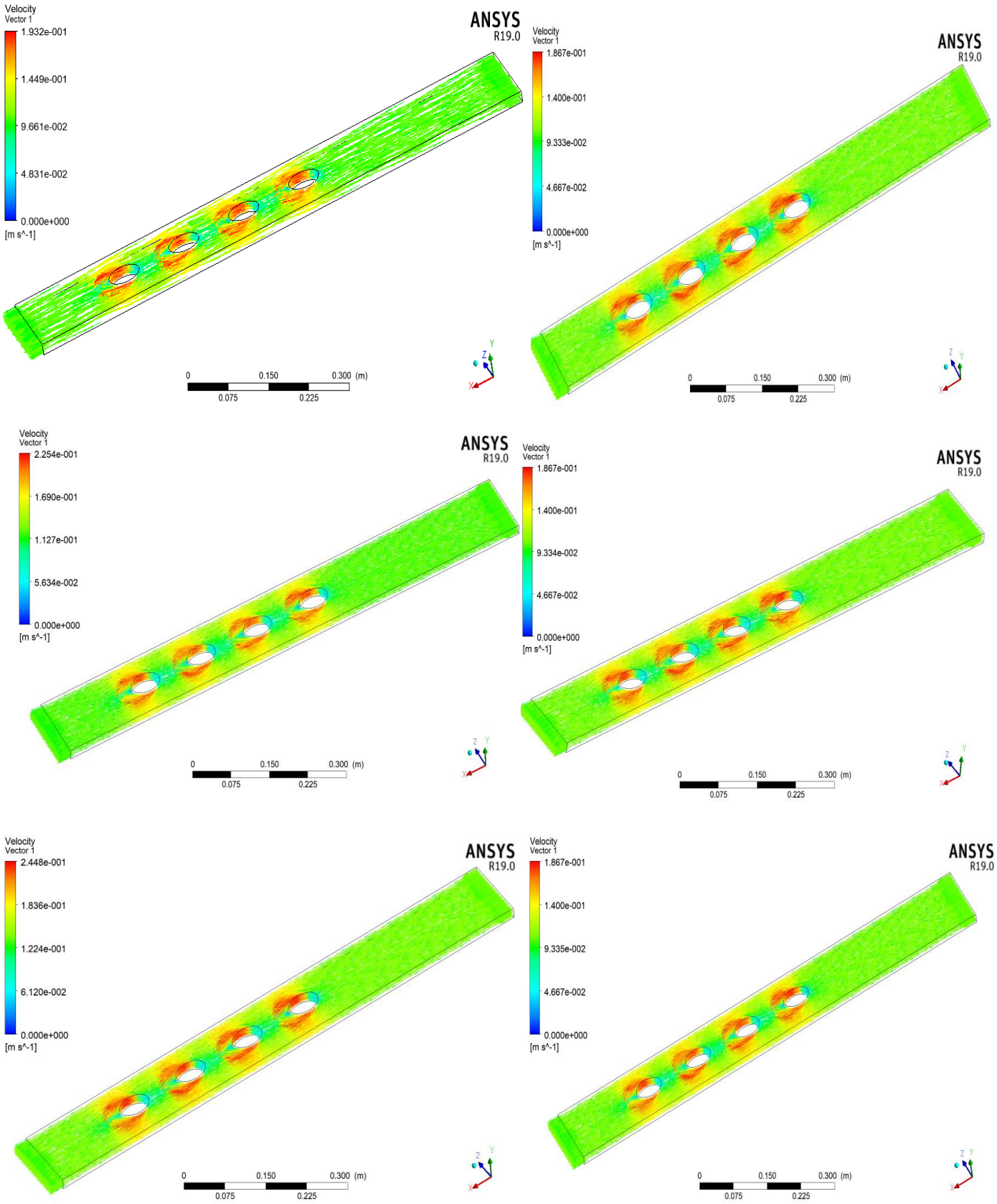
Velocity
Vector 1
1.932e-001
1.449e-001
9.661e-002
4.831e-002
0.000e+000
[m s^-1]
ANSYS
R19.0
0 0.150 0.300 (m)
0.075 0.225
Velocity
Vector 1
1.867e-001
1.400e-001
9.333e-002
4.667e-002
0.000e+000
[m s^-1]
ANSYS
R19.0
0 0.150 0.300 (m)
0.075 0.225
Velocity
Vector 1
2.254e-001
1.690e-001
1.127e-001
5.634e-002
0.000e+000
[m s^-1]
ANSYS
R19.0
0 0.150 0.300 (m)
0.075 0.225
Velocity
Vector 1
1.867e-001
1.400e-001
9.334e-002
4.667e-002
0.000e+000
[m s^-1]
ANSYS
R19.0
0 0.150 0.300 (m)
0.075 0.225
Velocity
Vector 1
2.448e-001
1.836e-001
1.224e-001
6.120e-002
0.000e+000
[m s^-1]
ANSYS
R19.0
0 0.150 0.300 (m)
0.075 0.225
Velocity
Vector 1
1.867e-001
1.400e-001
9.335e-002
4.667e-002
0.000e+000
[m s^-1]
ANSYS
R19.0
0 0.150 0.300 (m)
0.075 0.225

(a) (b)

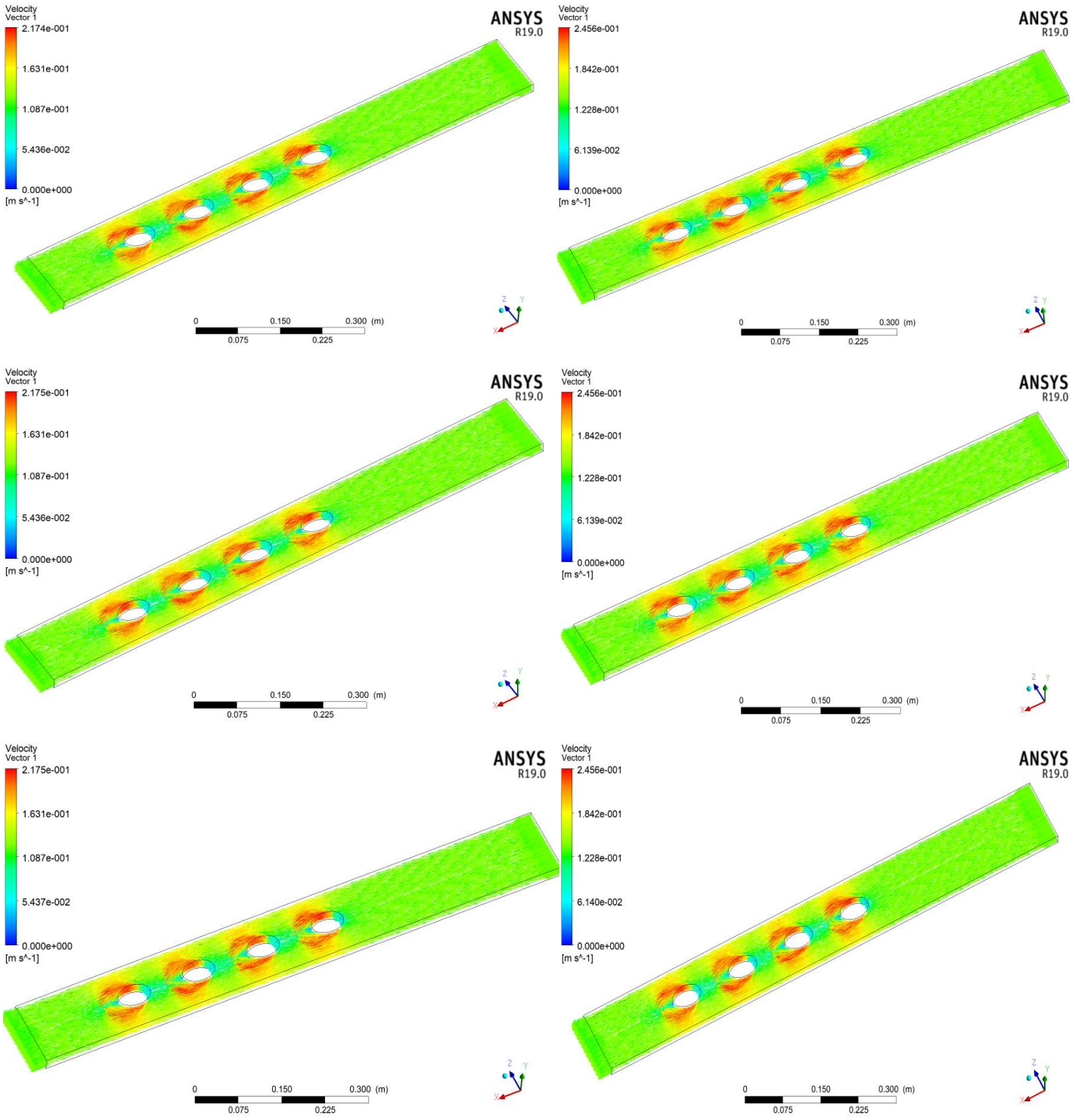

(c) (d)

Figure (5-65) The velocity vector without vortex generators (a) single-phase flow (b) two-phase flow at a flow rate of air 8.33, 16.67, and 25 Lpm respectively, with constant a flow rate of water 15 Lpm (c) 17.5 Lpm (d) 20 Lpm

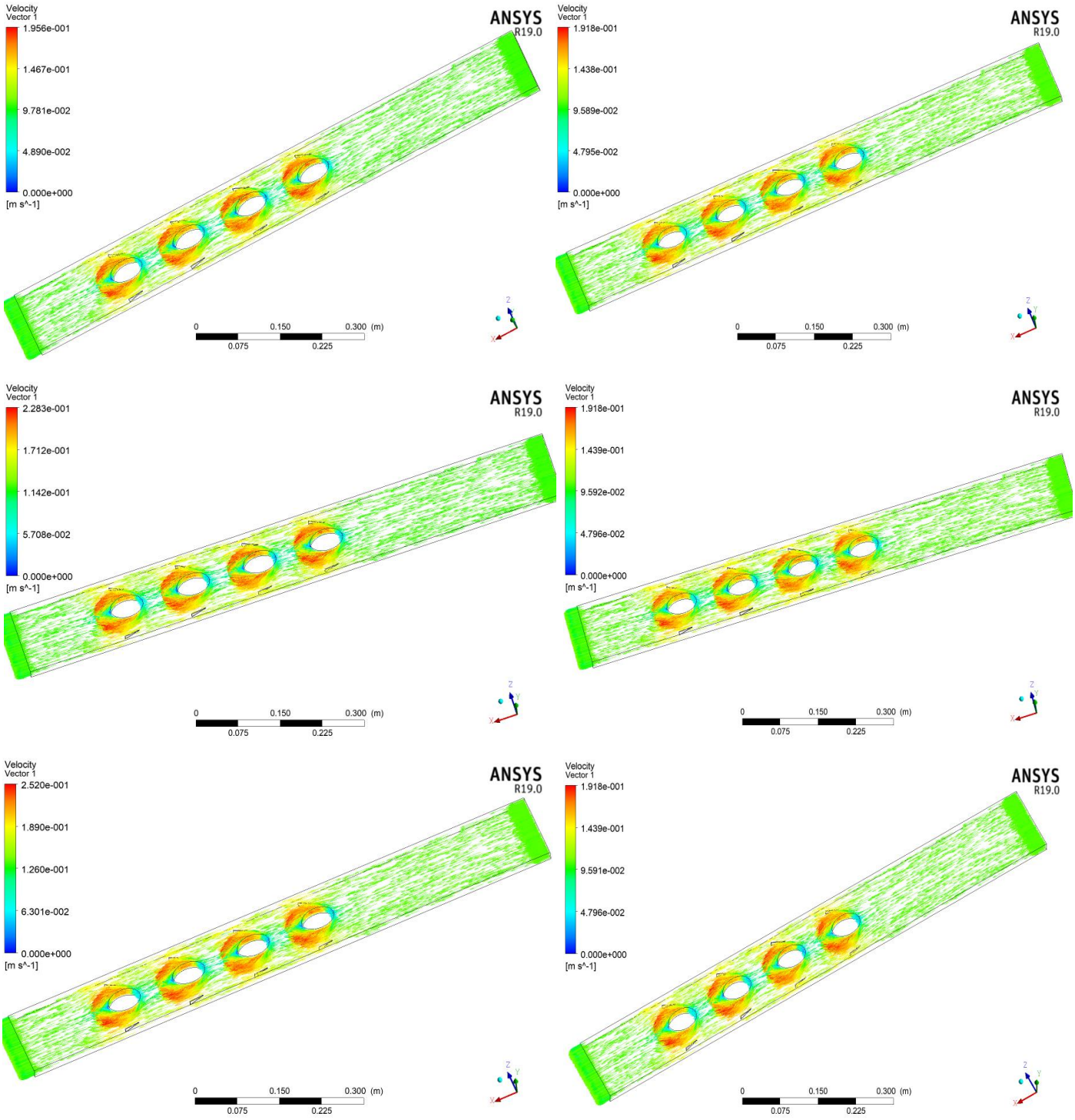
Velocity
Vector 1
1.956e-001
1.467e-001
9.781e-002
4.890e-002
0.000e+000
[m s^-1]
ANSYS
R19.0
0
0.150
0.300 (m)
0.075
0.225
Velocity
Vector 1
1.918e-001
1.438e-001
9.589e-002
4.795e-002
0.000e+000
[m s^-1]
ANSYS
R19.0
0
0.150
0.300 (m)
0.075
0.225
Velocity
Vector 1
2.283e-001
1.712e-001
1.142e-001
5.708e-002
0.000e+000
[m s^-1]
ANSYS
R19.0
0
0.150
0.300 (m)
0.075
0.225
Velocity
Vector 1
1.918e-001
1.439e-001
9.592e-002
4.796e-002
0.000e+000
[m s^-1]
ANSYS
R19.0
0
0.150
0.300 (m)
0.075
0.225
Velocity
Vector 1
2.520e-001
1.890e-001
1.260e-001
6.301e-002
0.000e+000
[m s^-1]
ANSYS
R19.0
0
0.150
0.300 (m)
0.075
0.225
Velocity
Vector 1
1.918e-001
1.439e-001
9.591e-002
4.796e-002
0.000e+000
[m s^-1]
ANSYS
R19.0
0
0.150
0.300 (m)
0.075
0.225

(a) (b)

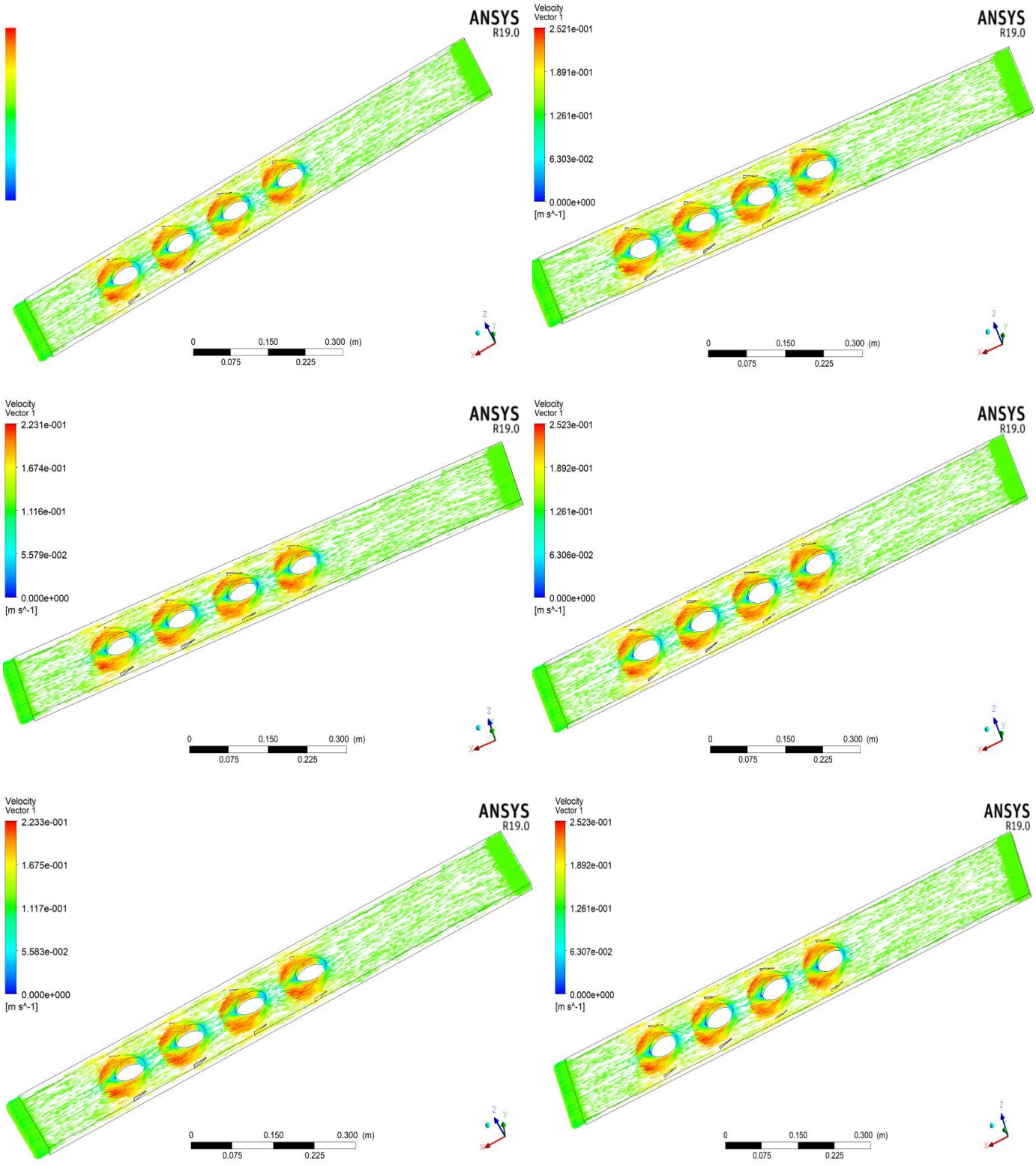

(c) (d)

Figure (5-66) The velocity vector with delta winglets as vortex generators (a) single-phase flow (b) two-phase flow at a flow rate of air 8.33, 16.67, and 25 Lpm respectively, with constant a flow rate of water 15 Lpm (c) 17.5 Lpm (d) 20 Lpm

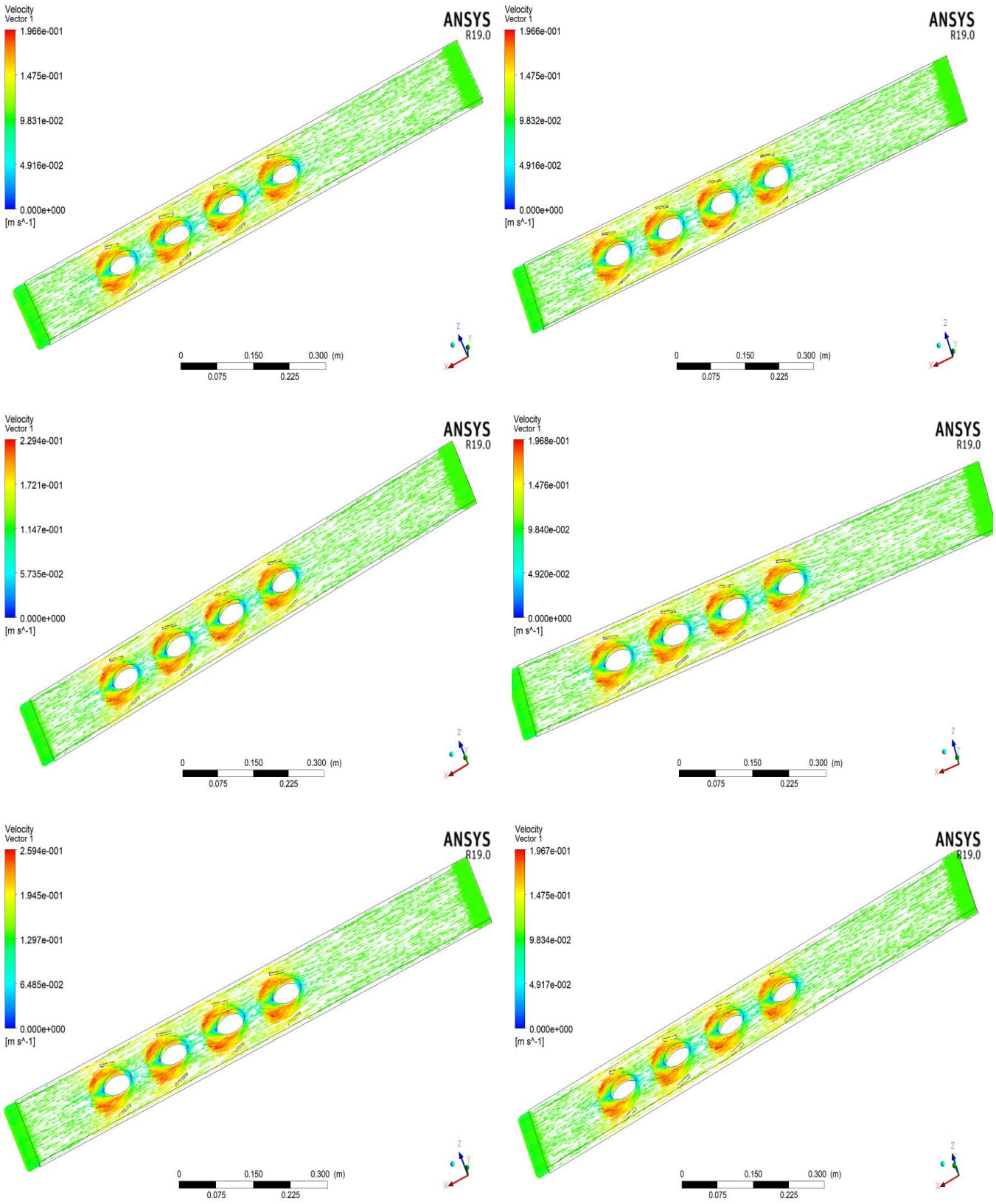
Velocity
Vector 1
1.966e-001
1.475e-001
9.831e-002
4.916e-002
0.000e+000
[m s^-1]
ANSYS
R19.0
0
0.150
0.300 (m)
0.075
0.225
Velocity
Vector 1
1.966e-001
1.475e-001
9.832e-002
4.916e-002
0.000e+000
[m s^-1]
ANSYS
R19.0
0
0.150
0.300 (m)
0.075
0.225
Velocity
Vector 1
2.294e-001
1.721e-001
1.147e-001
5.735e-002
0.000e+000
[m s^-1]
ANSYS
R19.0
0
0.150
0.300 (m)
0.075
0.225
Velocity
Vector 1
1.968e-001
1.476e-001
9.840e-002
4.920e-002
0.000e+000
[m s^-1]
ANSYS
R19.0
0
0.150
0.300 (m)
0.075
0.225
Velocity
Vector 1
2.594e-001
1.945e-001
1.297e-001
6.485e-002
0.000e+000
[m s^-1]
ANSYS
R19.0
0
0.150
0.300 (m)
0.075
0.225
Velocity
Vector 1
1.967e-001
1.475e-001
9.834e-002
4.917e-002
0.000e+000
[m s^-1]
ANSYS
R19.0
0
0.150
0.300 (m)
0.075
0.225

(a) (b)

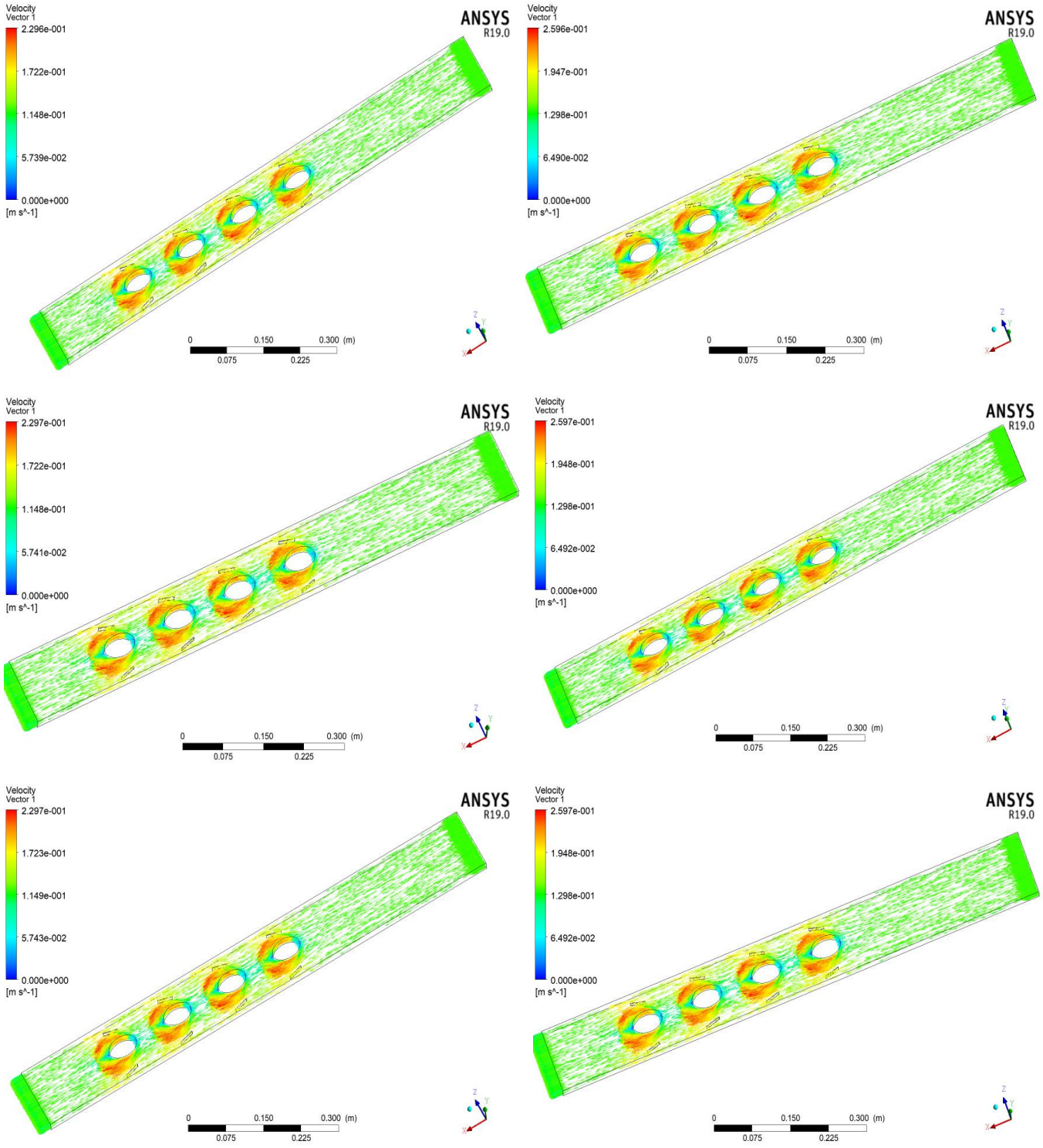

(c) (d)

Figure (5-67) The velocity vector with rectangular winglets as vortex generators (a) single-phase flow (b) two-phase flow at a flow rate of air 8.33, 16.67, and 25 Lpm respectively, with constant a flow rate of water 15 Lpm (c) 17.5 Lpm (d) 20 Lpm

5.6. Comparison between Numerical and Experimental Results

5.6.1 Single-phase flow

The effect of Reynolds number in single-phase flow over the bank of oval tubes under the Reynolds number range (3646-4813) on heat transfer rate and pressure drop is significant to reach optimum design and the best location for vortex generators.

Figure (5-68) shows the variation of (*Nu*) with Reynolds number in single-phase flow cross-bank of oval tubes with and without vortex generators experimentally and numerically. When the Reynolds number increased from (3646) to (4252) and (4813), the (*Nu*) increased by (8.3%) and (17%) numerically and by (8%) and (17.13%) experimentally, due to a reduction in the temperature difference between single-phase flow and oval tube surfaces. Increasing (Re) predictably results in a higher velocity of the more fluid is flushed from the hot wall side to the central cooled tube region, intensifying the mixing significantly. Hence, heat transfer is greatly enhanced. The fluid is at a lower temperature compared to the tube wall, as result, the fluid temperature increases at the tube wall; however, due to the symmetry boundary conditions (no thermal gradient) at the side walls or edges, the fluid temperature is same as that of the inlet temperature. Stagnant points are located on the tube surface while velocity increases towards the wall of the channel. However, variation in temperature at the tube surface with (Re) is evident.

Figure (5-69) represents compared without (VGs) at (Re = 3646) the (*Nu*) increased by (52.8%) numerically and by (53%) experimentally, at (Re = 4254) increased by (45.16%) numerically and by (45.67%) experimentally, and finally at (Re = 4812.5) increased by (46.4%) numerically and by (45.68%) experimentally with delta winglets. Also, represents compared without (VGs) at (Re = 3646) the (*Nu*) increased by (63.46%) numerically and by (62%) experimentally, at (Re = 4254) increased by (60.16%)

numerically and by (60.78%) experimentally, and finally at (Re = 4813) increased by (59.1%) numerically and by (58.56%) experimentally with rectangular winglets.

With (VGs) are used, the greater contact volume between mixing fluid results in a higher (*Nu*). The vortex flows, impinging flow and small vortices, created by the (VGs), are the cause for the heat transfer augmentation over the smooth case. It is found that the delta winglet vortex generators can help to enhance heat transfer rate due to the vortex flow induced from the vortex generators. The uses of the generators not only increase in heat transfer rate, but also increase in the pressure loss in the compact heat exchanger. Therefore, the thermal performance in the heat system should be considered on both the heat transfer augmentation and the increase in the friction factor.

Figure (5-70) shows a variation of the (*f*) with Reynolds number in single-phase flow cross-bank of oval tubes with and without vortex generators. Due to the narrow passages of fluid flow, (*f*) could have increased as the Reynolds number increased, resulting in a higher pressure drop in the duct according to the jet impingement effect.

Figure (5-71) shows the Reynolds number performance parameter in the single-phase flow cross-bank of oval tubes with and without vortex generators experimentally and numerically. The thermal performance, considered from the increase on the heat transfer and friction factor in the test section, when the Reynolds number increased, the performance parameter was reduced due to pressure drop increased in the duct. This results which studied the effect of different shapes from vortex generators in the duct on heat flow and found that delta winglets are given the best performance. The increase of the Nusselt number is due to the augmentation on the heat transfer coefficient when increasing the Reynolds number value. In range studies, the increase in the Nusselt number is found with increasing Reynolds number for all cases. The

friction factor tends to decrease with the rise of Reynolds number for all cases.

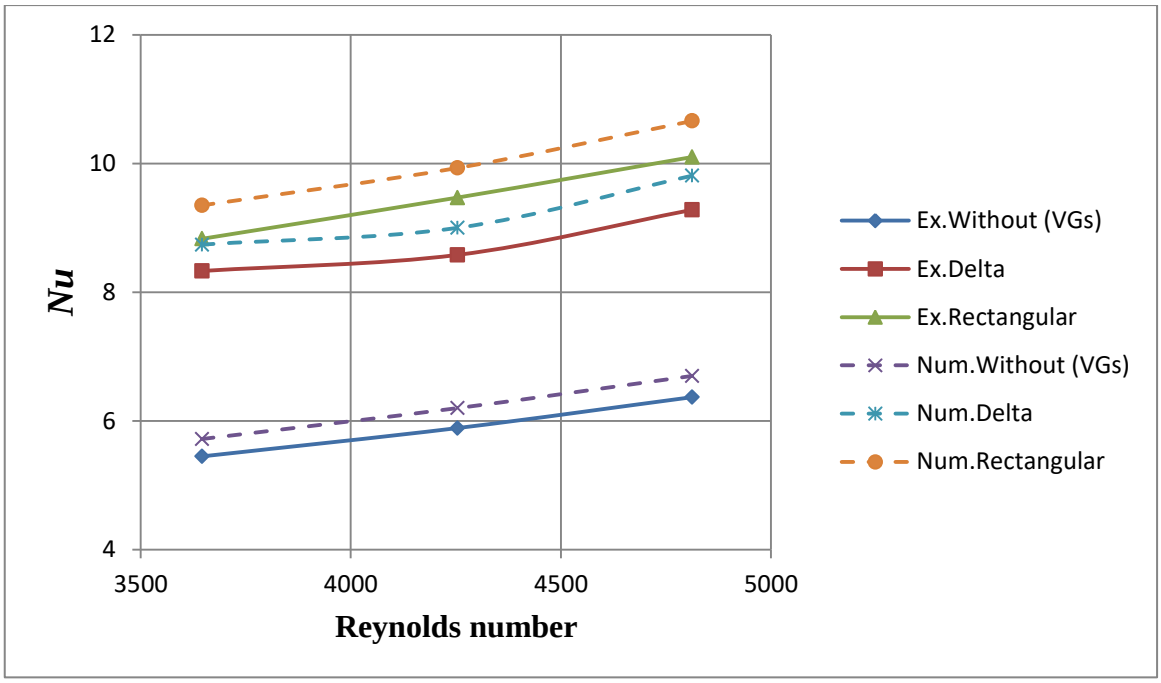

Figure (5-68) Variation of Nusselt number with Reynolds number in single-phase flow experimentally and numerically

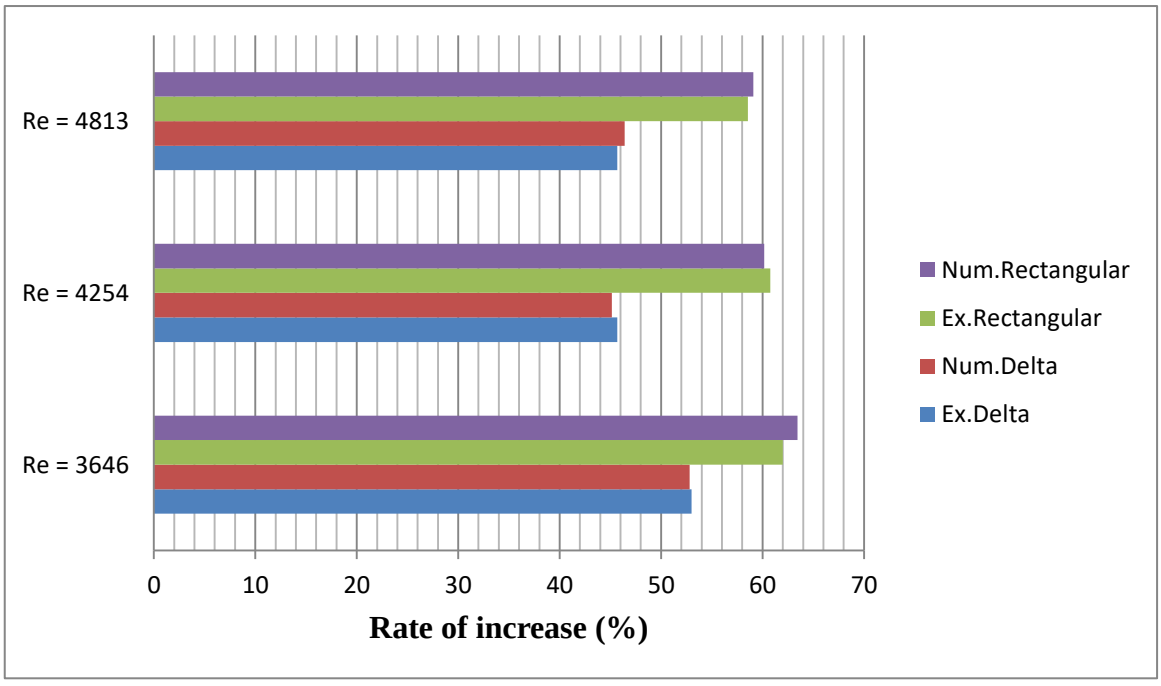

Figure (5-69) Rate of increase in (*Nu*) for single-phase flow

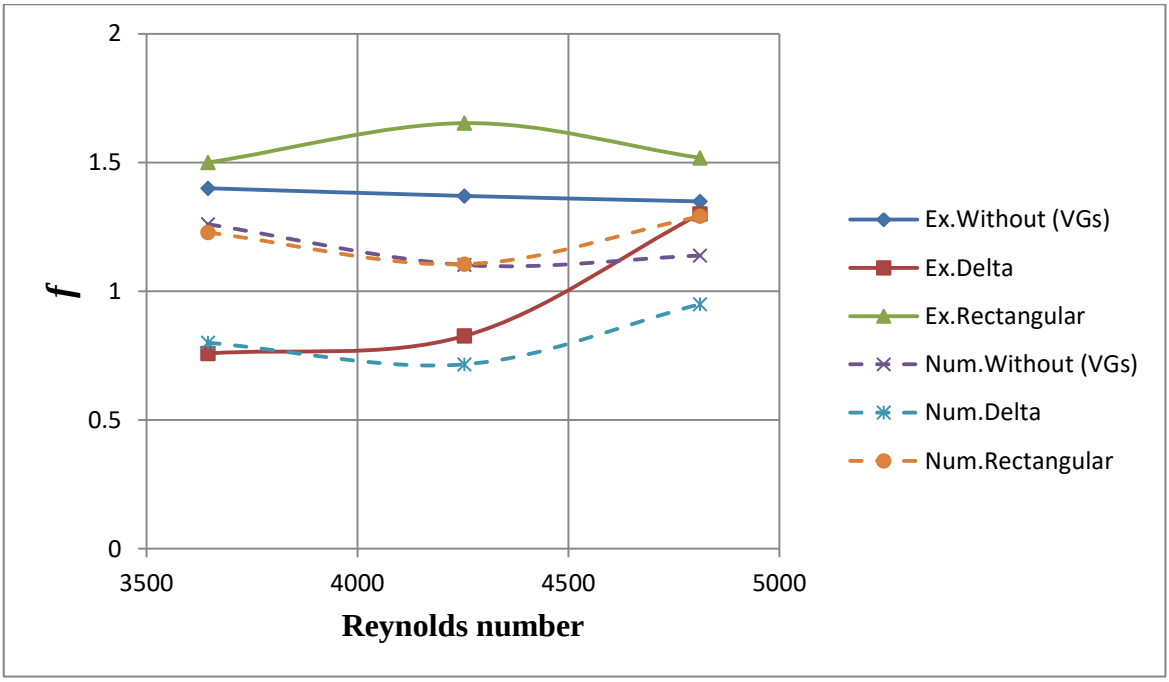

Figure (5-70) Variation of friction factor with Reynolds number in single-phase flow experimentally and numerically

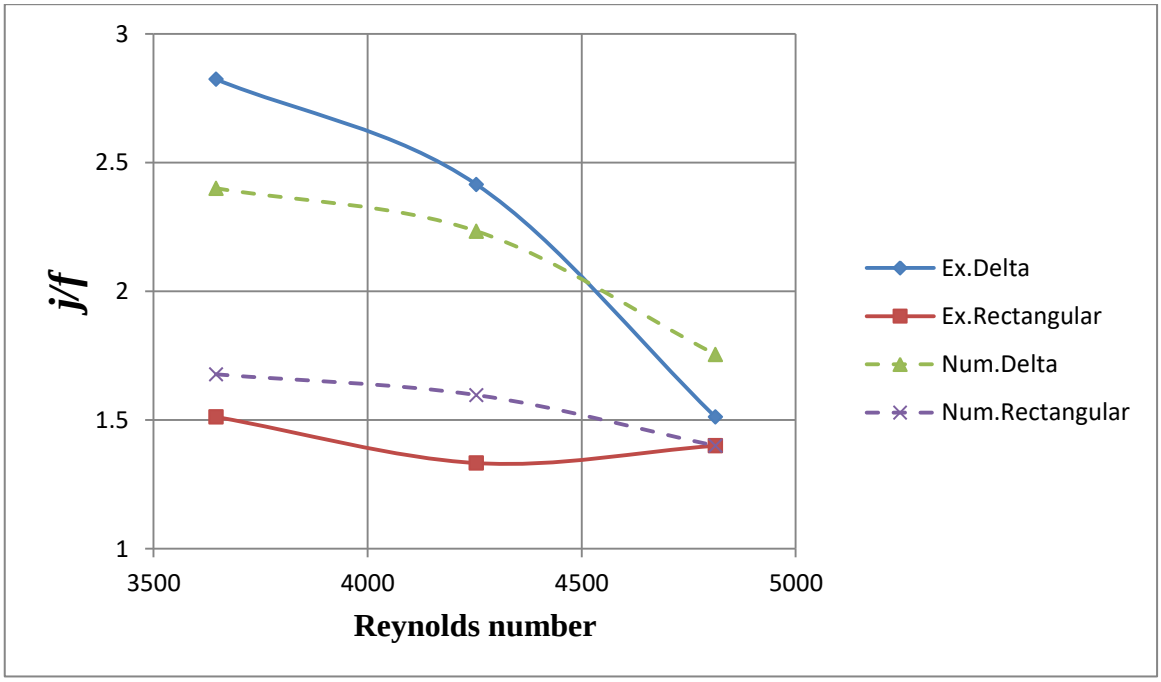

Figure (5-71) Performance parameter with Reynolds number in single-phase flow experimentally and numerically

5.6.2 Two-phase flow

The effect of the Reynolds number for two-phase flow over the bank of oval tubes under the turbulent area on heat transfer rate and reduction in pressure is significant to reach optimum design and the best location for vortex generation experimentally and numerically. The performance parameter was enhanced due to the reduction in pressure drop and the decreased temperature difference between the two-phase flow and oval tube surfaces in the duct. When the Reynolds number of water is decreased and the Reynolds number of air is increased, the airflow rate increases (8.33, 16.67, and 25 Lpm) with a constant water flow rate.

Figure (5-72) shows the variation of temperature difference with Reynolds number in a two-phase flow cross-bank of oval tubes with and without vortex generation. The heat transfer coefficient is increased due to a reduction in the temperature difference between two-phase flow and oval tube surfaces at a constant flow rate of water (15 Lpm).

Figure (5-73) shows the variation of the reduction in pressure with Reynolds number in a two-phase flow cross-bank of oval tubes with and without vortex generation. When the Reynolds number of water is decreased and the Reynolds number of air is increased, which causes pressure drop decreases in the duct at a constant flow rate of water (15 Lpm).

Figure (5-74) shows the relationship between the Reynolds number and performance parameter in the two-phase flow cross-bank of oval tubes with and without vortex generation. The performance parameter was enhanced because the flow rate of water and air increased experimentally and numerically except with Rectangular winglets. Delta winglets are given the best performance.

Figure (5-75) shows the variation of temperature difference with Reynolds number in a two-phase flow cross-bank of oval tubes with and without vortex generators. The heat transfer coefficient is decreased due to augmentation in

the temperature difference between two-phase flow and oval tube surfaces at a constant flow rate of water (17.5 Lpm).

Figure (15-76) shows the variation of the reduction in pressure with Reynolds number in a two-phase flow cross-bank of oval tubes with and without vortex generation. When the Reynolds number of water is decreased and the Reynolds number of air is increased, which causes pressure drop decreases in the duct at a constant flow rate of water (17.5 Lpm).

Figure (5-77) shows the relationship between the Reynolds number and performance parameter in the two-phase flow cross-bank of oval tubes with and without vortex generation. The performance parameter was enhanced numerically and decreased experimentally with increased flow rates of water and air. Delta winglets are given the best performance.

Figure (5-78) shows the variation of temperature difference with Reynolds number in a two-phase flow cross-bank of oval tubes with and without vortex generation. The heat transfer coefficient is decreased due to augmentation in the temperature difference between two-phase flow and oval tube surfaces at a constant flow rate of water (20 Lpm).

Figure (5-79) shows the variation of the reduction in pressure with Reynolds number in a two-phase flow cross-bank of oval tubes with and without vortex generation. When the Reynolds number of water decreases and the Reynolds number of air is increased, this causes pressure drop decreases in the duct at a constant flow rate of water (20 Lpm).

Figure (5-80) shows the relationship between the Reynolds number and performance parameter in the two-phase flow cross-bank of oval tubes with and without vortex generation. The performance parameter was enhanced because water and air flow rates increased experimentally and numerically except with rectangular winglets. Delta winglets are given the best performance.

Figure (5-81) represents compared without (VGs) at (Q_w =15 Lpm) and (Q_a =8.33, 16.67, and 25 Lpm). When (Re = 3644) the (*Nu*) increased by (80 %) numerically and by (81%) experimentally, at (Re = 3641) increased by (76.4%) numerically and by (60%) experimentally, and finally at (Re = 3639) increased by (81.6%) numerically and by (53%) experimentally with delta winglets. Also, represents compared without (VGs) at (Re = 3644) the (*Nu*) increased by (76.4%) numerically and by (71.7%) experimentally, at (Re = 3641) increased by (72.9%) numerically and by (58%) experimentally, and finally at (Re = 3639) increased by (75.3%) numerically and by (47%) experimentally with rectangular winglets. Also, represents compared without (VGs) at (Q_w =17.5 Lpm) and (Q_a =8.33, 16.67, and 25 Lpm). When (Re = 4252) the (*Nu*) increased by (63%) numerically and by (34%) experimentally, at (Re = 4249) increased by (68%) numerically and by (49%) experimentally, and finally at (Re = 4247) increased by (72%) numerically and by (51%) experimentally with delta winglets. Also, represents compared without (VGs) at (Re = 4252) the (*Nu*) increased by (64%) numerically and by (35.8%) experimentally, at (Re = 4249) increased by (67%) numerically and by (54%) experimentally, and finally at (Re = 4247) increased by (68%) numerically and by (55.6%) experimentally with rectangular winglets. Furthermore represents compared without (VGs) at (Q_w =20 Lpm) and (Q_a =8.33, 16.67, and 25 Lpm). When (Re = 4810) the (*Nu*) increased by (69%) numerically and by (70.4%) experimentally, at (Re = 4808) increased by (69%) numerically and by (72%) experimentally, and finally at (Re = 4806) increased by (64%) numerically and by (39%) experimentally with delta winglets. Also, represents compared without (VGs) at (Re = 4810) the (*Nu*) increased by (73.5%) numerically and by (74%) experimentally, at (Re = 4808) increased by (60.16%) numerically and by (60.78%) experimentally, and finally at (Re = 4806) increased by (49%) numerically and by (30%) experimentally with rectangular winglets.

Figure (5-82) illustrates a comparison of the optimal performance parameter for single-phase and two-phase flow over oval tube banks with delta winglets. Increasing (Re) predictably leads in a larger fluid velocity as more fluid is pumped from the hot wall side to the middle cooled tube area, hence increasing the mixing considerably. Hence, heat transfer is significantly improved. The fluid is at a lower temperature than the tube wall; hence, the fluid temperature increases near the tube wall. Nevertheless, owing to the symmetry boundary conditions (no thermal gradient) at the side walls or edges, the fluid temperature is the same as the entrance temperature. Points of stagnation are placed on the tube's surface, whereas velocity rises towards the channel wall. However, temperature variation at the tube surface with (Re) is apparent. When (VGs) are used, the increased contact volume between mixed fluids results in a greater (*Nu*). The vortex flows, impinging flow, and small vortices produced by the vortex generators (VGs) are responsible for the enhanced heat transfer compared to the smooth situation. Due to the vortex flow created by the vortex generators, it has been shown that delta winglet vortex generators can benefit in enhancing heat transfer rate. Use of the generators increases not only the heat transfer rate but also the pressure drop in the compact heat exchanger. And hence, the thermal performance of the heat system must take into account both the increase in heat transfer and the increase in friction factor.

The above observed that in all cases, any types of vortex generators were used in banks of the tubes that promoted thermo-hydraulic performance in the (HEs). There was usually a pressure drop which can illustrate as follows; for the case without used vortex generators, the resistance of the flow of air in the duct results only from the friction between water particles and duct walls with tube walls. The resistance of the airflow in the duct when vortex generators were used not only results from the friction between water particles and duct walls with tube walls but also from extra resistance, which causes an increase

in pressure loss through flow in the duct. The use of air as a second phase in the working fluid reduces pressure losses inside the duct because the friction of air particles with the duct wall and tube walls is lower than the friction of water particles in the duct; consequently, the addition of air is beneficial for reducing operating costs.

When the Reynolds number increased, (*f*) increased as a result of the narrow passages of the fluid flow, which could result in a jet impingement effect and consequently a higher pressure drops in the duct. Due to the increased in pressure drop inside the duct, the thermal performance decreased as a result of an increase in heat transfer and friction factor in the test section as the Reynolds number increased. This investigation looked into the effect of several vortex generator forms on heat flow and found that delta winglets provide the best performance. The increase in the Nusselt number is a result of the increase in the heat transfer coefficient as the Reynolds number increases. In all range investigations, an increase in the Nusselt number is linked to an increase in the Reynolds number. In all situations, the friction factor tends to decrease as Reynolds number increases.

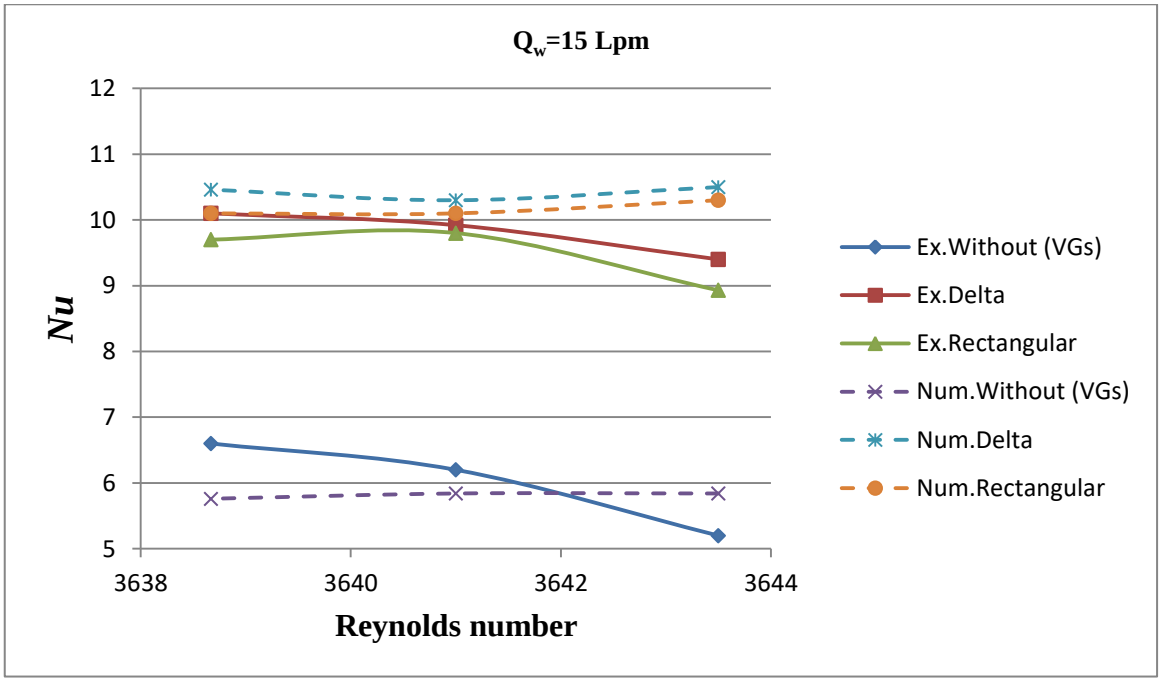

Figure (5-72) Variation of Nusselt number with Reynolds number at (Q_a= 8.33, 16.67 and 25 Lpm)

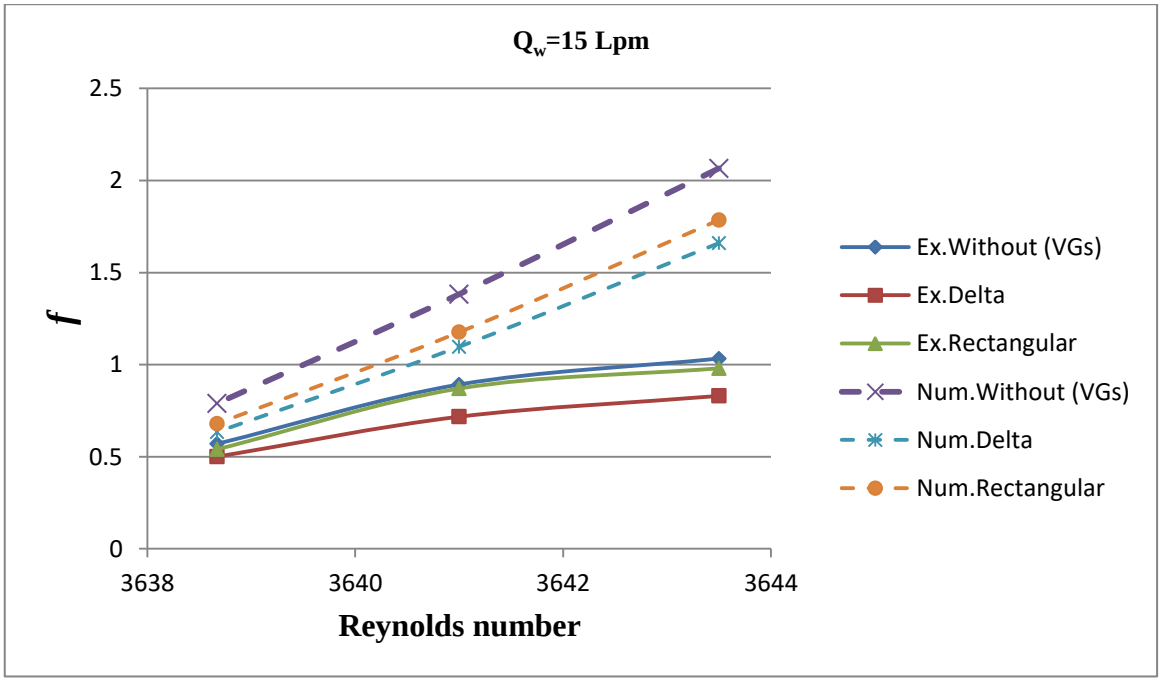

Figure (5-73) Variation of pressure drop with Reynolds number at (Q_a= 8.33, 16.67 and 25 Lpm)

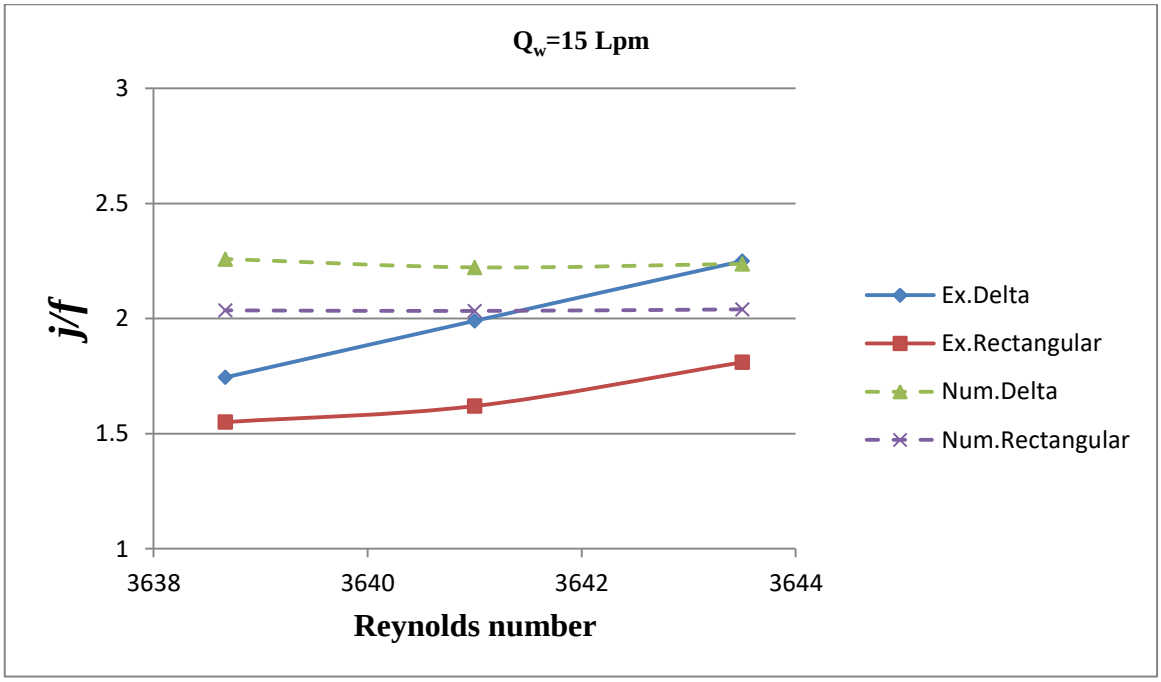

Figure (5-74) Performance parameter with Reynolds number at (Q_a= 8.33, 16.67 and 25 Lpm)

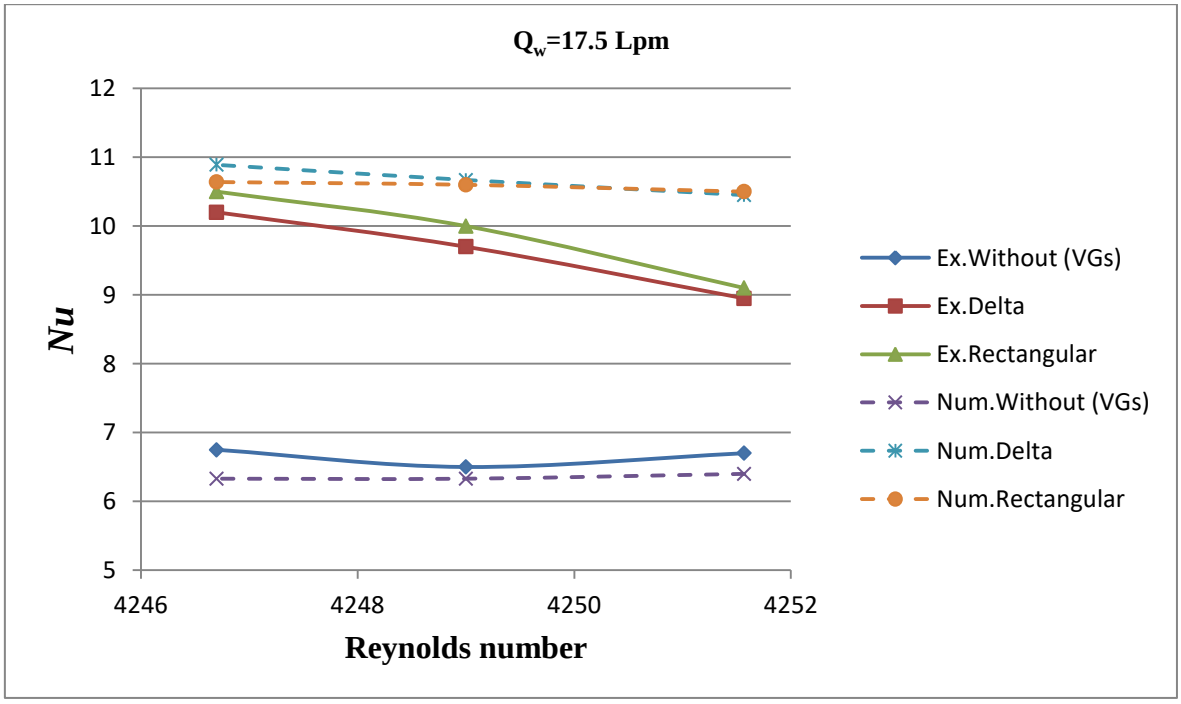

Figure (5-75) Variation of Nusselt number with Reynolds number at (Q_a= 8.33, 16.67 and 25 Lpm)

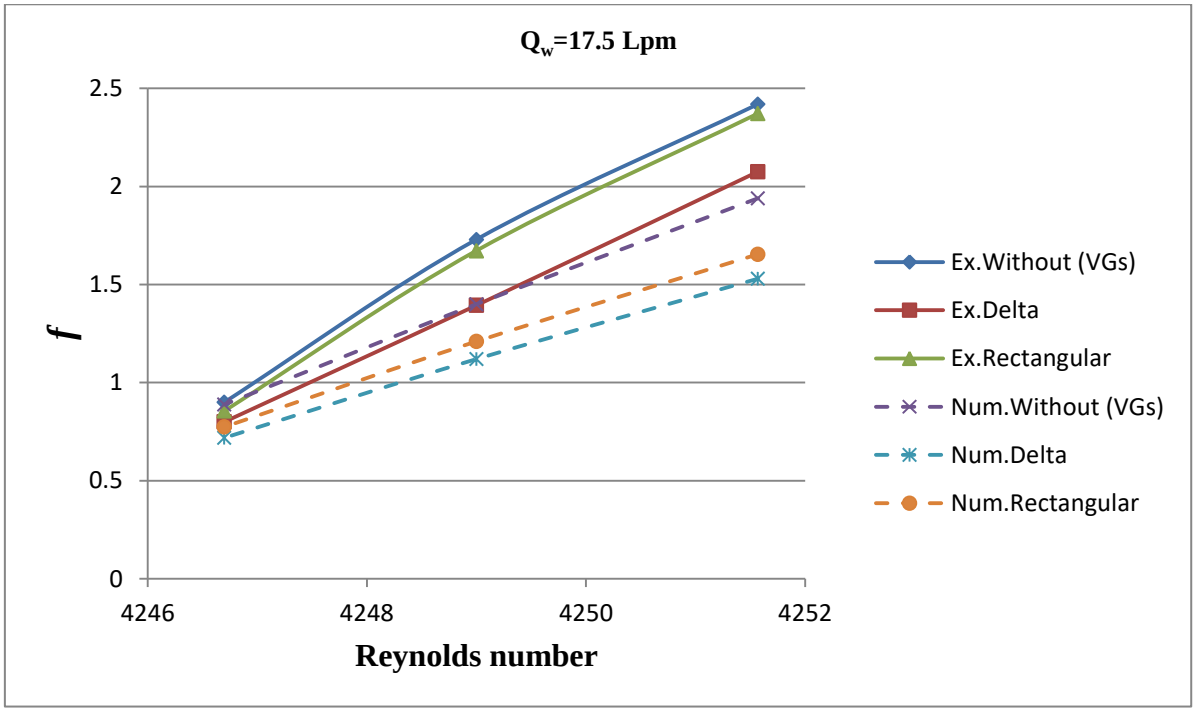

Figure (5-76) Variation of friction factor with Reynolds number at (Q_a= 8.33, 16.67 and 25 Lpm)

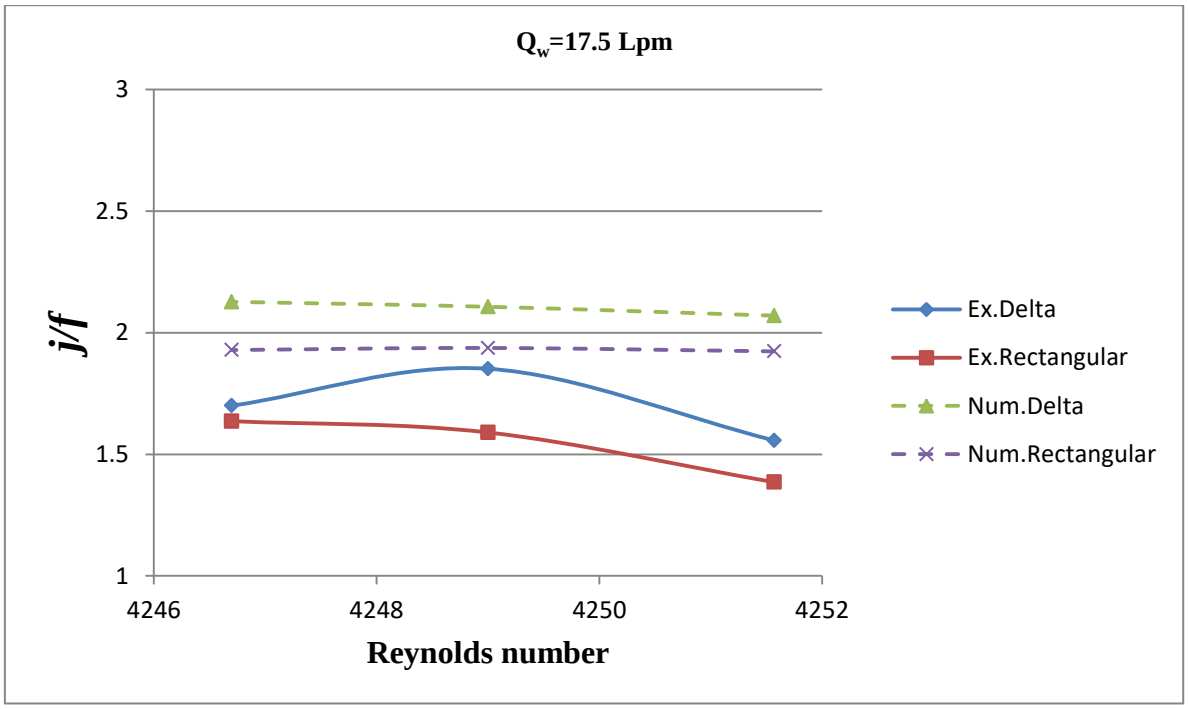

Figure (5-77) Performance parameter with Reynolds number at (Q_a= 8.33, 16.67 and 25 Lpm)

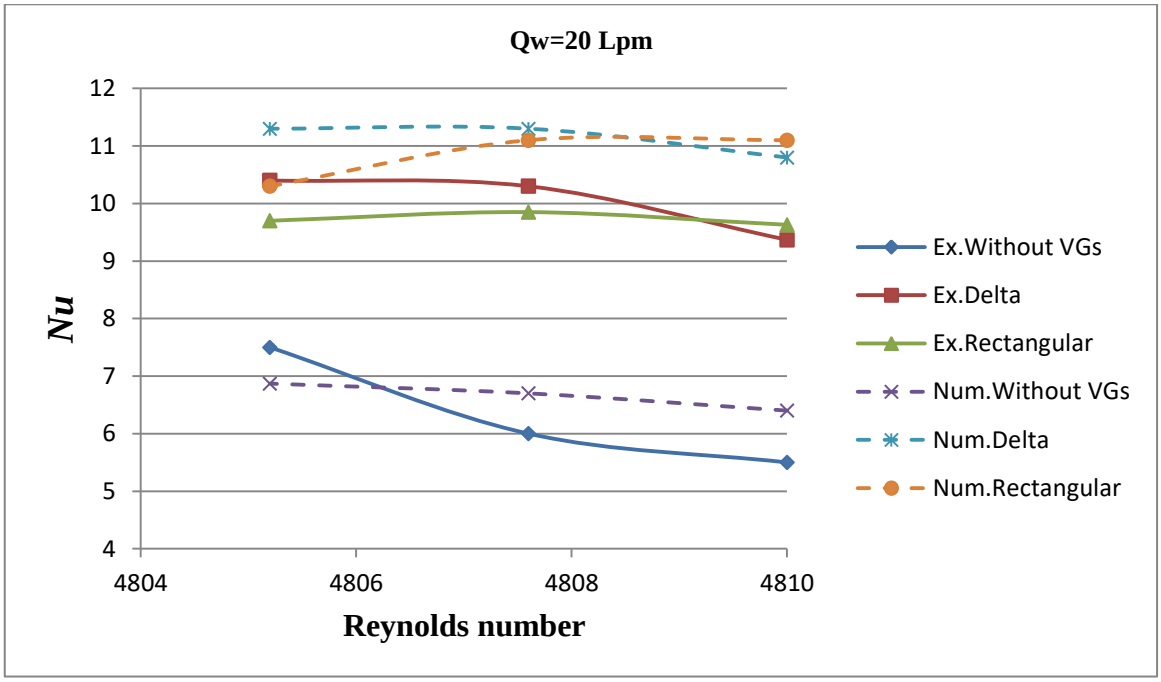

Figure (5-78) Variation of Nusselt number with Reynolds number at (Q_a= 8.33, 16.67 and 25 Lpm)

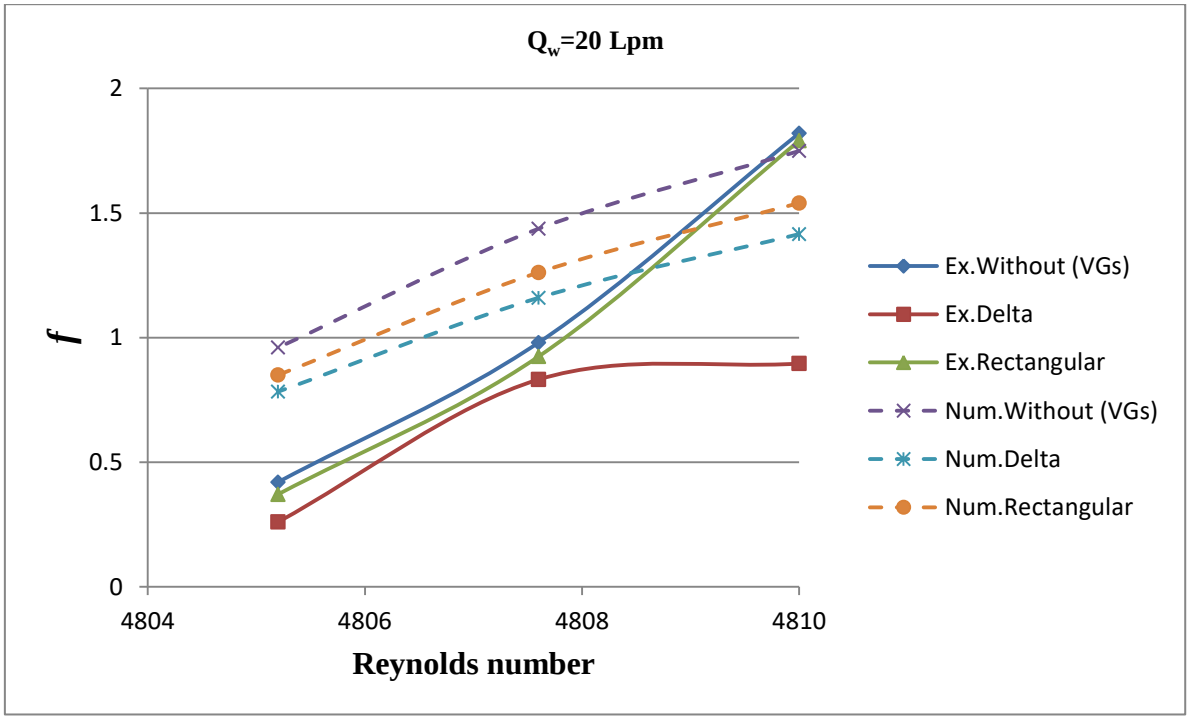

Figure (5-79) Variation of friction factor with Reynolds number at (Q_a= 8.33, 16.67 and 25 Lpm)

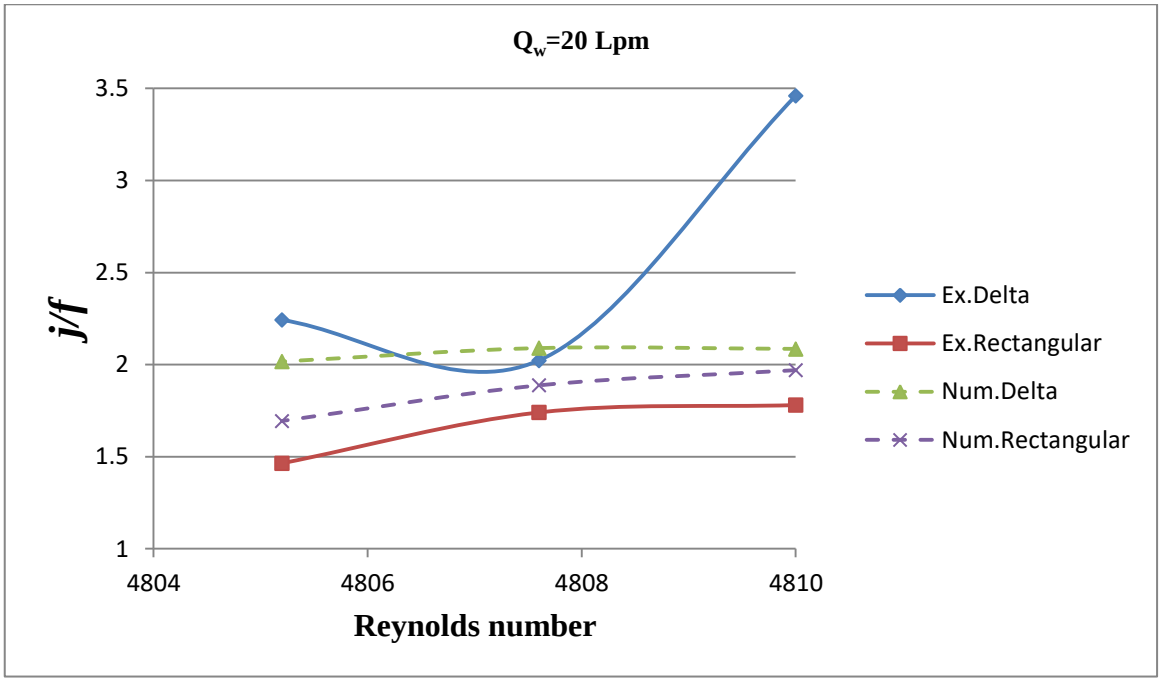

Figure (5-80) Performance parameter with Reynolds number at Q_a= 8.33, 16.67 and 25 Lpm

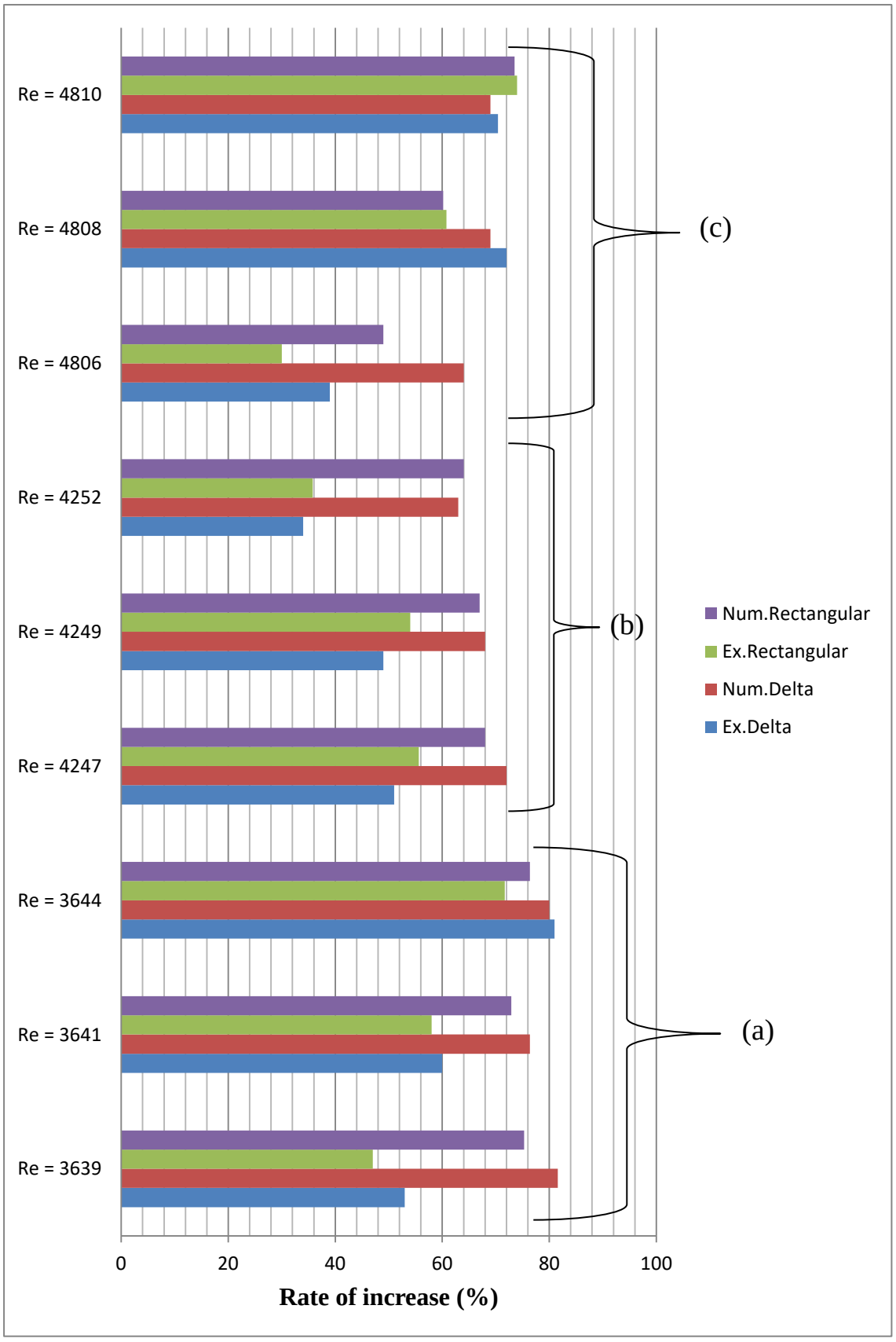

Figure (5-81) Rate of increase in (*Nu*) for two-phase flow at (Q_a= 8.33, 16.67 and 25 Lpm) (a) Q_w = 15 Lpm (b) Q_w = 17.5 Lpm (c) Q_w =20 Lpm

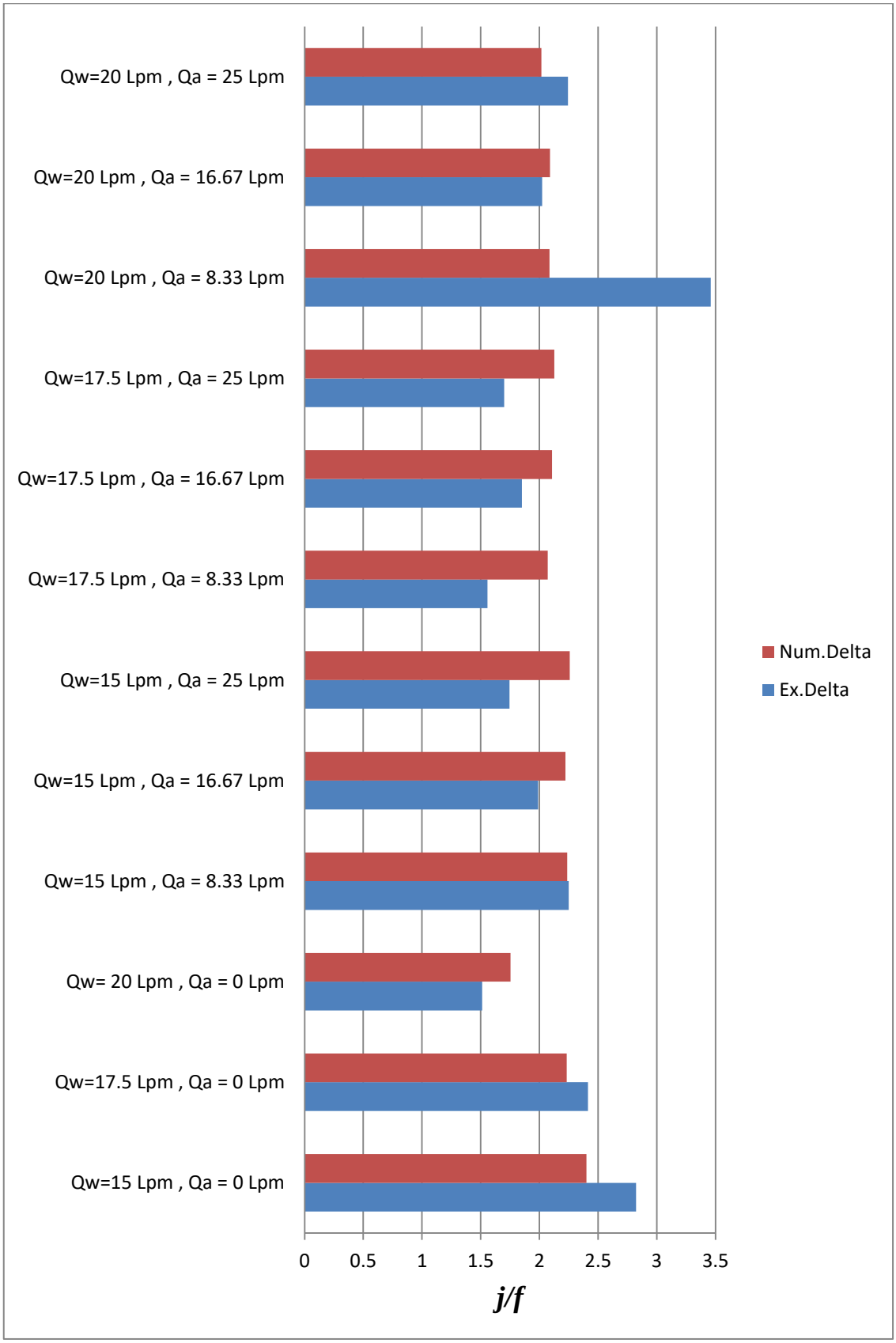

Figure (5-82) Comparison of the optimal performance parameter for single-phase and two-phase flow over oval tube banks with delta winglets

CHAPTER SIX
CONCLUSIONS AND SUGGESTIONS FOR FUTURE WORKS

6.1 Conclusions

In this work, thirty-six experiments were performed. In twenty-four situations of two-phase flow, the influence of various vortex generator types and water and air flow rates was tested. The experimental results have been contrasted with ANSYS FLUENT (19.0) simulation results. Also, Workbench 19.0 is used to compute the results of fifty-two cases for many configurations and analyzes to reach the optimum one. In this study, the performance of (VGs) is investigated based on the temperature gradient between the fluid flow and the surface of the tube bank, which corresponds to the pressure drops inside the duct. The best performance at the lowest temperature difference and the lowest pressure drops. The following observations can be written according to the results of the current work:

1. In a single-phase flow (water) when the Reynolds number increased from (3646) to (4252) and (4813), the (*Nu*) increased by (8.3%) and (17%) numerically and by (8%) and (17.13%) experimentally, without (VGs).
2. In a single-phase flow (water) when the Reynolds number increased from (3646) to (4252) and (4813), the (*f*) decreased by (12.5%) and (9.6%) numerically and by (2.1%) and (3.7%) experimentally, without (VGs).
3. In a single-phase flow (water), at (Re = 3646) the (*Nu*) increased by (52.8%) numerically and by (53%) experimentally, at (Re = 4254) increased by (45.16%) numerically and by (45.67%) experimentally, and finally at (Re = 4812.5) increased by (46.4%) numerically and by

(45.68%) experimentally with delta winglets compared to without (VGs).

4. In a single-phase flow (water), at (Re = 3646) the (*Nu*) increased by (63.46%) numerically and by (62%) experimentally, at (Re = 4254) increased by (60.16%) numerically and by (60.78%) experimentally, and finally at (Re = 4813) increased by (59.1%) numerically and by (58.56%) experimentally with rectangular winglets compared to without (VGs).
5. In a single-phase flow (water) the best performance parameter was found to be (2.4) numerically and (2.8) experimentally with delta winglets, (1.6) numerically and (1.5) experimentally with rectangular winglets.
6. In a two-phase flow (water-air), the (*Nu*) increased by (80%) numerically and by (81%) experimentally with delta winglets compared to without (VGs).
7. In a two-phase flow (water-air), the (*Nu*) increased by (76.4%) numerically and by (71.7%) experimentally with rectangular winglets compared to without (VGs).
8. In a two-phase flow (water-air), the (*f*) decreased by (19.65%) numerically and by (19.6%) experimentally with delta winglets compared to without (VGs).
9. In a two-phase flow (water-air), the (*f*) decreased by (13.5%) numerically and by (5%) experimentally with rectangular winglets compared to without (VGs).
10. In a two-phase flow (water-air), the best performance parameter was found to be (2.24) numerically and (2.25) experimentally with delta winglets, (2) numerically and (1.81) experimentally with rectangular winglets.

11. The best thermo-hydraulic performance is obtained by delta winglets at (15°) an angle of attack for the oval tube banks in the two-phase flow with (CFD) configuration and moderate turbulent flow rate.

6.2 Suggestions for Future Works

1. Other configurations, shapes, lengths, heights, and positions of vortex generators can be investigated numerically and experimentally.
2. Carrying out an experimental study on a wider Reynolds number than the one used in this study.
3. Studying (*Nu*), (*f*) and temperature distribution through noncircular tube banks heat exchangers with vortex generators.
4. Investigating the effect of phase-change of the working fluid in the heat exchanger with (VGs).

References

[1] Tiggelbeck S, Mitra N K, and Fiebig M, Comparison of wing-type vortex generators for heat transfer enhancement in channel flows, Heat Transfer, Volume 116, pp. 880–885, **1994**.

[2] K. Lunsford, Increasing Heat Exchanger Performance, Bryan Research & Engineering, Inc., **1998**.

[3] Jacobi A M and Shah R K, Heat transfer surface enhancement through the use of longitudinal vortices: a review of recent progress, Exp. Therm. Fluid Sci. Volume (11), pp. 295–309, **1995**.

[4] Ashish J. Modi and Manish K. Rathod, Comparative study of heat transfer enhancement and pressure drop for fin-and-circular tube compact heat exchangers with sinusoidal wavy and elliptical curved rectangular winglet vortex generator, International Journal of Heat and Mass Transfer, Volume (141), pp. 310–326, **2019**.

[5] G. Zhou and Q. Ye, Experimental investigations of thermal and flow characteristics of curved trapezoidal winglet type vortex generators, Applied Thermal Engineering, Volume (37), pp. 241-248, **2012**.

[6] Theodore L. Bergman, Adrienne S. Lavine, Frank P. Incropera and David P. Dewitt, Introduction to Heat Transfer, Sixth Edition, pp. 447-452, **2007**.

[7] S. Tiwari, D. Maurya, G. Biswas, and V. Eswaran, Heat transfer enhancement in cross-flow heat exchangers using oval tubes and multiple delta winglets, International Journal of Heat and Mass Transfer, Volume 46(15), pp. 2841–2856, **2003**.

[8] M.M. Awad, Two-Phase Flow, **2012**.

[9] Shih-I Pai, Introduction: Classification of Two-Phase Flows, https://link.springer.com/chapter/10.1007/978-3-322-86348-5_1, **1977**.

[10] Z. Fan, C. Ke, Z. Lufeng, A. Desmond, H. Bo, Y. Shouqi, Gas–Liquid Two-Phase Flow Investigation of Side Channel Pump: An Application of MUSIG Model, Mathematics. 8. 624. 10.3390/math8040624, **2020**.

[11] R. Every, R. Hughes, L. Koch, PAPER 10 – Pipeline Transportation of Coke in Petroleum Product, Advances in Solid–Liquid Flow in Pipes and its Application, pp. 165-174, ISBN 9780080157672,**1971**.

[12] S. Azbel and P. Cheremisinoff, Fluid Mechanics and Unit Operations, Ann Arbor Science Publishers, **1983**.

[13] P. Simeon, L. Sween, and C. Michael, plasma, Encyclopedia Britannica, https://www.britannica.com/science/plasma-state-of-matter, **2023**.

[14] G. F. Hewitt and N. S. Hall-Taylor, Annular Two-Phase Flow, Chemical Engineering Division, A.E.R.E., Harwell, England, **1970**.

[15] G. Biswas, N. K. Mitra, and M. Fiebig, Heat transfer enhancement in fin-tube heat exchangers by winglet type vortex generators, International Journal of Heat and Mass Transfer, Volume 37(2), pp. 283-291, **1994**.

[16] S. Hiravennavar, E. Tulapurkara, G. Biswas, A note on the flow and heat transfer enhancement in a channel with built-in winglet pair, Int. J. Heat Fluid Flow, Volume 28, pp. 299–305, **2007**.

[17] P. Chu, Y.L. He, Y.G. Lei, L.T. Tian and R. Li, Three-dimensional numerical study on fin-and-oval-tube heat exchanger with longitudinal vortex generators, Applied Thermal Engineering, Volume 29, 859‑876, **2009**.

[18] P. Chu Y. L. He, and W. Q. Tao, Three-Dimensional Numerical Study of Flow and Heat Transfer Enhancement Using Vortex Generators in Fin-and-Tube Heat Exchangers, Journal of Heat Transfer, Volume 131/091903-1, **2009**.

[19] Abdulmajeed A. Ramadhan, Numerical Study of Fluid Flow and Heat Transfer over a Bank of Oval-Tubes Heat Exchanger with Vortex Generators, Al-Anbar Journal for Engineering Science, Volume 5(1), pp.88-108, **2012**.

[20] Ya-Ling He, Pan Chu, Wen-Quan Tao, YuWen Zhang, Tao Xie, Analysis of heat transfer and pressure drop for fin-and-tube heat exchangers with rectangular winglet-type vortex generators, Applied Thermal Engineering, Volume 61, pp.770-783, **2013**.

[21] A.A. Gholami, Mazlan A.Wahid, and H.A. Mohammed, Heat transfer enhancement and pressure drop for fin-and-tube compact heat exchangers with wavy rectangular winglet-type vortex generators, International Communications in Heat and Mass Transfer, **2014**.

[22] Ahmed Khafeef Obaid Albdoor, Numerical Study of Fluid Flow and Heat Transfer over a Circular Tubes Bank of Heat Exchanger with Different Shapes of Vortex Generator, International Journal of Science and Research (IJSR), Volume 3 Issue 11, pp. 2032-2040, **2014**.

[23] Withada Jedsadaratanachai and Amnart Boonloi, Thermal performance assessment in a fin-and-oval-tube heat exchanger with delta winglet vortex generators, Journal of Mechanical Science and Technology, Volume 29 (4), pp. 1765-1779, **2015**.

[24] Gaofeng Lu, Guobing Zhou, Numerical simulation on performances of plane and curved winglet e Pair vortex generators in a rectangular channel

and field synergy analysis, International Journal of Thermal Sciences, Volume 109, pp. 323-333, **2016**.

[25] Wanling, Liangbi Wang, Yong Guan, and Wenju Hu, The effect of shape of winglet vortex generator on the thermal-hydrodynamic performance of a circular tube bank fin heat exchanger, Heat Mass Transfer DOI 10.1007/s00231-017-2042-3, **2017**.

[26] Hemant Naik and Shaligram Tiwari, Effect of winglet location on performance of fin-tube heat exchangers with inline tube arrangement, International Journal of Heat and Mass Transfer, Volume 125, pp.248–261, **2018**.

[27] Mohammad Rejaul Haque and Md. Ashiqur Rahman, Numerical investigation of convective heat transfer characteristics of circular and oval tube banks with vortex generators, Journal of Mechanical Science and Technology, Volume 34 (1), **2020**.

[28] Arvind Gupta, Aditya Roy, Sachin Gupta, and Munish Gupta, Numerical investigation towards implementation of punched winglet as vortex generator for performance improvement of a fin-and-tube heat exchanger, International Journal of Heat and Mass Transfer, Volume 149, 119171, **2020**.

[29] Hemant Naik, Shaligram Tiwari, Thermodynamic performance analysis of an inline fin-tube heat exchanger in presence of rectangular winglet pairs, International Journal of Mechanical Sciences, Volume 193, **2021**.

[30] H. Naik, S. Tiwari, Numerical investigations on fluid flow and heat transfer characteristics of different locations of winglets mounted in fin-tube heat exchangers, Thermal Science and Engineering Progress, Volume 22, 100795, **2021**.

[31] Yucheng Wang, Wensheng Zhao, Pengfei Wang, Jin Jiang and Xiangyu Luo, Thermal Performance of Elliptical Fin-and-Tube Heat Exchangers with Vortex Generator under Various Inclination Angles, Journal of Thermal Science, Volume 30, 257–270, **2021**.

[32] Weina Shi, Tengfei Liu, Kewei Song, Qiang Zhang, WanLing Hu, and LiangBi Wang, The optimal longitudinal location of curved winglets for better thermal performance of a finned-tube heat exchanger, International Journal of Thermal Sciences, Volume 167, 107035, **2021**.

[33] Jinlong Xie and Hsiao Mun Lee, Thermo-Hydraulic Performance of a Fin-and-Tube Heat Exchanger with Differently Configured Curved-Rectangular Vortex Generators, Heat Transfer Engineering, Volume 43, pp.63-82, **2022**.

[34] M. Fiebig, P. Kallweit, N. Mitra, S. Tiggelbeck, Heat transfer enhancement and drag by longitudinal vortex generators in channel flow, Experimental Thermal and Fluid Science, Volume 4 (1), pp. 103 – 114, **1991**.

[35] S.V. Garimella, P.A. Eibeck, Enhancement of single phase convective heat transfer from protruding elements using vortex generators, International Journal of Heat and Mass Transfer, Volume 34 (9), pp. 2431 – 2433, **1991**.

[36] St. Tiggelbeck, N.K. Mitra, M. Fiebig, Experimental investigations of heat transfer enhancement and flow losses in a channel with double rows of longitudinal vortex generators, International Journal of Heat and Mass Transfer, Volume 36 (9), pp. 2327 – 2337, **1993**.

[37] Fiebig M., Mitra N. K., and Valencia A., Local heat transfer and flow losses in fin-and-tube heat exchangers with vortex generators: A

comparison of round and flat tubes. Int. J. Experimental Thermal and Fluid Science, Volume 8, pp.35-45, **1994**.

[38] M.C. Gentry and A.M. Jacobi, Heat transfer enhancement by delta-wing vortex generators on a flat plate: vortex interactions with the boundary layer, Exp. Thermal Fluid Sci. Volume 14, pp. 231–242, **1997**.

[39] C.C. Wang, J. Lo, Y.T. Lin, C.S. Wei, Flow visualization of annular and delta winglet vortex generators in fin-and-tube heat exchanger application, International Journal of Heat and Mass Transfer, Volume 45 (18), pp.3803 – 3815, **2002**.

[40] K. Torii, K.M. Kwak and K. Nishino, Heat transfer enhancement accompanying pressure-loss reduction with winglet-type vortex generators for fin-tube heat exchangers, International Journal of Heat and Mass Transfer, Volume 45, pp. 3795-3801, **2002**.

[41] E. Kim, J.S. Yang, An experimental study of heat transfer characteristics of a pair of longitudinal vortices using color capturing technique, International Journal of Heat and Mass Transfer, Volume 45 (16), pp.3349 – 3356, **2002**.

[42] S.M. Pesteei, P.M.V. Subbarao, R.S. Agarwal, Experimental study of the effect of winglet location on heat transfer enhancement and pressure drop in fin-tube heat exchangers, Applied Thermal Engineering, Volume 25, pp.1684–1696, **2005**.

[43] K.M. Kwak, K. Torii, K. Nishino, Simultaneous heat transfer enhancement an pressure loss reduction for finned-tube bundles with the first or two transverse rows of built-in winglets, Experimental Thermal and Fluid Science, Volume 29 (5), pp.625 – 632, **2005**.

[44] C.B. Allison, B.B. Dally, Effect of a deltawinglet vortex pair on the performance of a tube–fin heat exchanger, International Journal of Heat and Mass Transfer, Volume 50, pp.5065–5072, **2007**.

[45] A. Joardar, A.M. Jacobi, Heat transfer enhancement by winglet-type vortex generator arrays in compact plain-fin-andtube heat exchangers, International Journal of Refrigeration, Volume 31 (1), pp.87 – 97, **2008**.

[46] M.J. Lawson, K.A. Thole, Heat transfer augmentation along the tube wall of a louvered fin heat exchanger using practical delta winglets, International Journal of Heat and Mass Transfer, Volume 51 (9 - 10), pp. 2346 – 2360, **2008**.

[47] Wisam Abed Kattea, An Experimental Study on the Effect of Shape and Location of Vortex Generators Ahead of a Heat Exchanger, Al-Khwarizmi Engineering Journal, Volume 8(2), pp.12- 29, **2012**.

[48] Guobing Zhou and Zhizheng Feng, Experimental investigations of heat transfer enhancement by plane and curved winglet type vortex generators with punched holes, International Journal of Thermal Sciences, Volume 78, pp.26-35, **2014**.

[49] P.S.B. Zdanski, D. Pauli, and F.A.L. Dauner, Effects of delta winglet vortex generators on flow of air over in-line tube bank: A new empirical correlation for heat transfer prediction, International Communications in Heat and Mass Transfer, Volume 67, pp.89–96, **2015**.

[50] Prasopsuk C., Experimental investigation of thermal performance enhancement in tubular heat exchanger fitted with rectangular-winglet-tape vortex generator, Engineering and Applied Science Research, Volume 43, pp. 279-282, **2016**.

[51] Syaiful, Nazaruddin Sinaga, Bambang Yunianto, and MSK. Tony Suryo Utomo, Comparison of Thermal-Hidraulic Performances of Vortex

Generators Mounted on Heated Plate: Experimental Study and Flow Visualization, IOP Conf. Series: Materials Science and Engineering 494, 012011, **2019**.

[52] Syaiful, Tri Wahyuni, Bambang Yunianto, and Nazaruddin Sinaga, Evaluation of Vortex Generators in the Heat Transfer Improvement of Airflow through an In-Line Heated Tube Arrangement, Fluids, Volume 6(10), pp.344, **2021**.

[53] Jin-Sheng Leu, Ying-Hao Wu, and Jiin-Yuh Jang, Heat transfer and fluid flow analysis in plate-fin and tube heat exchangers with a pair of block shape vortex generators, International Journal of Heat and Mass Transfer, Volume 47, pp.4327–4338, **2004**.

[54] A. Yousif, Enhancement of Heat Transfer from Heated Cylinder inside Duct by Using Vortex Generator, Ph.D thesis, university of technology, mechanical engineering department, **2006**.

[55] A. Awaad and K. Al-Khishali, Numerical And Experimental Investigations Of The Vortex Generators Effect In Duct Heaters, Thesis in Machines and Equipments Engineering Department, University of Technology, **2012.**

[56] Kutiaba JM Al-khishali and Munzer SY Ebaid, Numerical and experimental investigations of shape and location of vortex generators on fluid flow and heat transfer in a constant heat-fluxed rectangular duct, Advances in Mechanical Engineering, Volume 7(11), pp. 1–21, **2015**.

[57] M. Hosseini, D.D. Ganji, and M. Aghajani Delavar, Experimental and numerical evaluation of different vortex generators on heat transfer, Applied Thermal Engineering, Volume 108, pp.905-915, **2016**.

[58] Mohamed A. Abdelatief, Sayed Ahmed E., and Osama M. Mesalhy, Experimental and numerical study on thermal-hydraulic performance of

wing-shaped-tubes-bundle equipped with winglet vortex generators. Springer-Verlag GmbH Germany, **2017**.

[59] M.J. Li, H. Zhang, J. Zhang, Y.T. Mu, E. Tian, D. Dan, X.D. Zhang, and W.Q. Tao, Experimental and numerical Study and Comparison of Performance for Wavy Fin and a Plain Fin with Radiantly Arranged Winglets around Each Tube in Fin and tube Heat Exchangers, Applied Thermal Engineering, S1359-4311(17)35702-2, **2018**.

[60] Victor Udoewa and Vinod Kumar, Computational Fluid Dynamics, George Washington University, USAID Development Engineer, **2012**.

[61] Bakker A., "Applied Computational Fluid Dynamics, Mesh Generation", Computational fluid dynamics lectures, www.bakker.org, **2002-2006**.

[62] Ali A. Shbeeb and Ala'a A. Mahdi, "Experimental and Numerical Investgation of Displacement Ventilation System with Assessment of Four Turbulence Models", Thesis in University of Babylon, College of Engineering, Department of Mechanical Engineering, **2016**.

[63] ELIN STENMARK," On Multiphase Flow Models in ANSYS CFD Software", CHALMERS UNIVERSITY OF TECHNOLOGY, Master's Thesis in Applied Mechanics, Göteborg, Sweden **2013**.

[64] Fluent User's Guide, "Modeling Multiphase Flows", Fluent Inc., September 29, **2006**.

[65] Vejahati, F., Mahinpey, N. , Ellis N., and Nikoo M. B., "CFD Simulation of Gas–Solid Bubbling Fluidized Bed: A New Method for Adjusting Drag Law", Canadian Society for Chemical Engineering, Volume 87, pp. 19-30, **2009**.

[66] Abdulnaser Sayma," Computational fluid dynamics", handbook, **2009**.

[67] Jannot, Yves and Degiovanni, Alain, Physical Properties of Air and Water, **2018**.

[68] Sarah H. Oleiwi and Riyadh S. S. Al-Turaihi, Experimental Investigation of Multiphase Flow in Fluidized Bed Column, College of Engineering at the University of Babylon, **2015**.

[69] H. P. Lehmann, X. Fuentes-Arderiu, and L. F. Bertello, Glossary of Terms in Quantitles and UNITS IN Clinical Chemistry, International Union of Pure and Applied Chemistry, 2nd Edition, Volume 68 (4), pp.957-1000, **1996**.

[70] H. Pedram, H. Alireza, E. Hamid, and L. Navid, High Reynolds Gas-Liquid Two Phase Flow Around a Triangular Body, Biennial Conference on Engineering Systems Design and Analysis, ASME 12th, **2014**.

[71] K. Pooranachandran, V. Kumaresan, and V. Ramalingam, Fanning friction (f) and colburn (j) factors of a louvered fin and flat tube compact heat exchanger, Thermal Science, **2015**.

[72] Z. K. Kadhim and H. O. Mery, Free convection from optimum sinusoidal surface exposed to vertical vibrations, Int. J. Mech. Eng. Technol., Vol. 7, No. 1, pp. 214–224, **2016**.

[73] Theodore L. Bergman, Adrienne S. Lavine, Frank P. Incropera and David P. Dewitt, Introduction to Heat Transfer. Sixth Edition, pp. 491, **2007**.

[74] R. S. Figliola and D. E. Beasley, Theory and Design for Mechanical Measurements, Second Edition, Vol. 20, No. 3. John Wiley & Sons, **1995**.

[75] M. Fiebig, A. Valencia, and N. K. Mitra, Wing-type vortex generators for fin-and-tube heat exchangers, Exp. Therm. Fluid Sci., Volume 7 (4), pp. 287-295, **1993**.

[76] G.S. Mostafa, Two-Phase Flow, Boiling and Condensation (In Conventional and Miniature Systems), Pressure Drop in Two-Phase Flow, 10.1017/CBO9780511619410(8), pp. 207–227, **2007**.

[77] A. Muhammad and B. Arafat, Heat transfer enhancement using different types of vortex generators (VGs): A review on experimental and numerical activities, Thermal Science and Engineering Progress, Volume 5, pp. 524-545, **2018**.

1) Water flow meter calibration

Table (A-1) contains calibration data, and Figure (A-1) depicts the calibration curves for the water flow meter

Table (A-1) Calibration Data

Q_a (L/min)	V (L)	t (min)	Q_t (L/min)
15	40	2.68	14.925
20	40	2.014	19.86
25	40	1.611	24.83
30	40	1.342	29.8

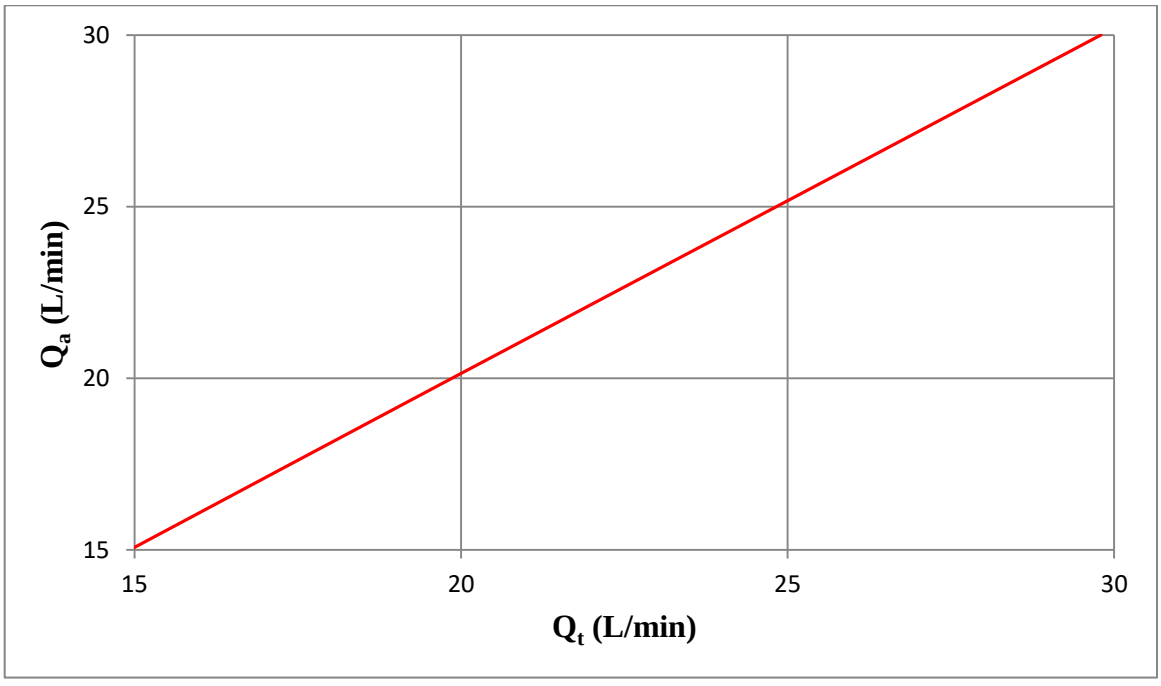

Figure (A-1) Flowmeter calibration curve

2) Calibration of the Thermocouple

Table (A-2) explains the result of calibrating the thermocouple. The calibration and the correlation between the reference value and the indicated values are shown in Figures (A-2) and (A-3).

Table (A-2) Thermocouple Calibration Data

Set value ℃	Reference value °C	Indicate value °C	Correlation value °C
10	11.35	10.80	0.55
50	50.51	49.00	1.51
70	71.07	69.20	1.87
100	101.73	100.60	1.13

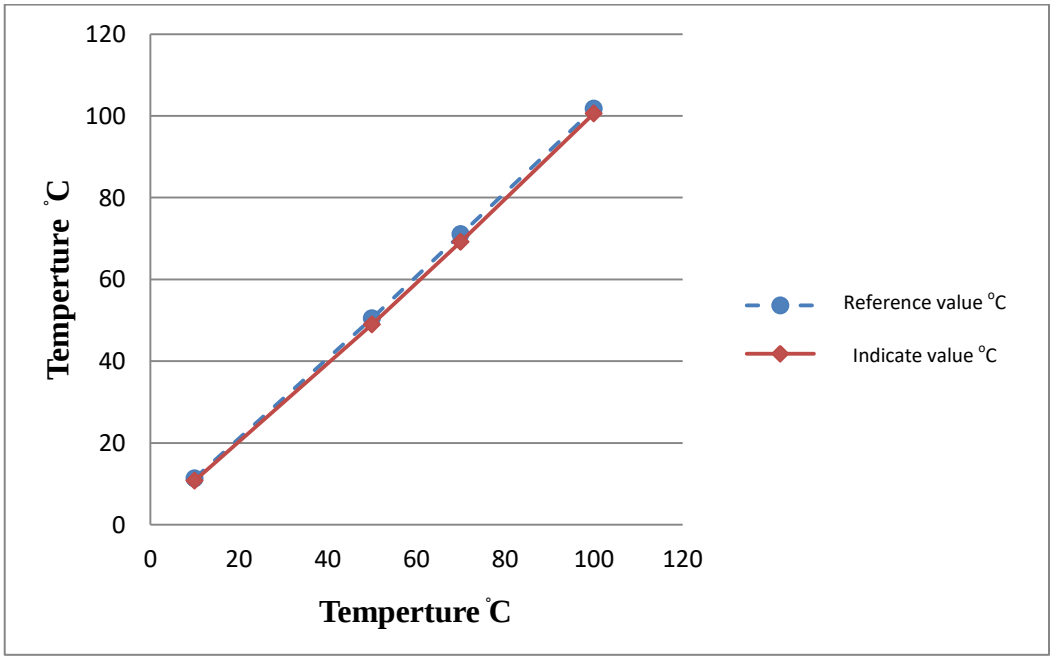

Figure (A-2) The relationship between the reference and the indicated values of the temperatures

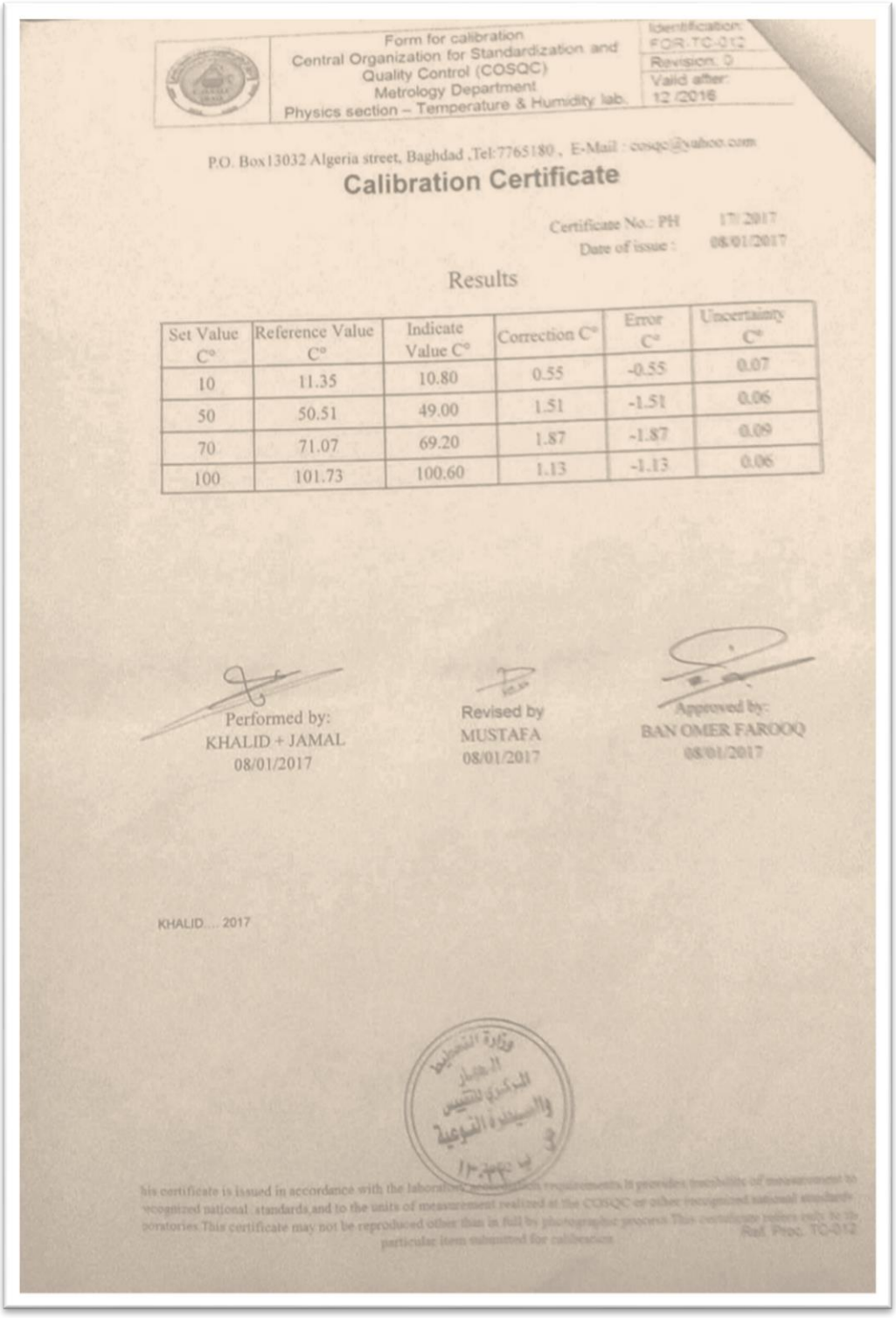

Form for calibration
Central Organization for Standardization and Quality Control (COSQC)
Metrology Department
Physics section – Temperature & Humidity lab.

Identification: FOR:TC-012
Revision: 0
Valid after: 12 /2016

P.O. Box13032 Algeria street, Baghdad ,Tel:7765180 , E-Mail : cosqc@yahoo.com

Calibration Certificate

Certificate No.: PH 17/ 2017
Date of issue : 08/01/2017

Results

Set Value C°	Reference Value C°	Indicate Value C°	Correction C°	Error C°	Uncertainty C°
10	11.35	10.80	0.55	-0.55	0.07
50	50.51	49.00	1.51	-1.51	0.06
70	71.07	69.20	1.87	-1.87	0.09
100	101.73	100.60	1.13	-1.13	0.06

Performed by:
KHALID + JAMAL
08/01/2017

Revised by
MUSTAFA
08/01/2017

Approved by:
BAN OMER FAROOQ
08/01/2017

KHALID.... 2017

his certificate is issued in accordance with the laboratory ... requirements. It provides traceability of measurement to recognized national standards, and to the units of measurement realized at the COSQC or other recognized national standards laboratories.This certificate may not be reproduced other than in full by photographic process.This certificate refers only to the particular item submitted for calibration. Ref. Proc. TC-012

Figure (A-3) Thermocouple Calibration

The Uncertainty: to calculate the uncertainty of the experimental results the following parameter is concerned:

1) The mean value of the variable x calculated as: $\bar{x}_{mean} = \frac{\sum_1^n x_i}{n}$

2) The standard deviation of x, given by: $\sigma = \sqrt{\frac{\sum_1^n (x_i - \bar{x})^2}{n-1}}$

3) The standard error is given by: $\sigma_m = \frac{\sigma}{\sqrt{n}}$

4) The uncertainty of variable x given by: $x = \bar{x} \pm \sigma_m$

The calculation of uncertainty for the performance parameter (*j/f*) is shown in the table below:

No	The variable	The tested values	$\bar{x}_{mean}$	σ	σ_m	x	Uncertainty
Performance parameter for flow with delta (VGs)							
1	x1	2.8					
2	x2	2.73	2.7525	0.036	0.018	2.7705	0.0065
3	x3	2.76				2.7345	-0.0066
4	x4	2.72					

Performance parameter for flow with rectangular (VGs)							
1	x1	1.512					
2	x2	1.52	1.5155	0.0127	0.00635	1.52185	0.0042
3	x3	1.5				1.50915	-0.004208
4	x4	1.53					

1) Circular Tube Banks ($\alpha = 15^{\circ}$)

- The temperature difference between two-phase flow (water and air) and circular tube surfaces at many positions in the duct (x = 42.5, 55, 67.5, and 80 cm) in (^{o}C)

X-Position (cm)	Without Vortex	CFU Delta	CFD Delta	CFU Rectangular	CFD Rectangular	CFU Zikzak	CFD Zikzak	CFU Sinusoidal	CFD Sinusoidal
42.5	16.9	11.301	10.794	10.354	10.494	10.555	9.78	10.059	10.128
55	17.373	10.193	10.603	10.318	10.772	10.34	9.967	9.488	10.127
67.5	14.974	10.832	10.82	10.516	10.065	9.939	10.063	9.891	10.309
80	16.803	10.648	10.548	10.861	10.783	10.866	10.357	9.599	9.997

- Inlet and outlet pressure in the duct in (Pa)

X-Position (cm)	Without Vortex	CFU Delta	CFD Delta	CFU Rectangular	CFD Rectangular	CFU Zikzak	CFD Zikzak	CFU Sinusoidal	CFD Sinusoidal
0	23.1361	20.94	21.29	23.1821	23.248	31.28	31.56	44.0536	33.7974
100	0.00889211	0.095	0.1192	0.101766	0.100015	0.1157	0.102	0.073435	0.126243

2) Oval Tube Banks ($\alpha = 15^{\circ}$)

- The temperature difference between two-phase flow (water and air) and circular tube surfaces at many positions in the duct (x = 42.5, 55, 67.5, and 80 cm) in (^{o}C)

X-Position (cm)	Without Vortex	CFU Delta	CFD Delta	CFU Rectangular	CFD Rectangular	CFU Zikzak	CFD Zikzak	CFU Sinusoidal	CFD Sinusoidal
42.5	18.977	11.448	11.308	11.719	11.298	10.817	10.861	10.819	10.629
55	17.107	11.331	10.985	11.587	11.398	11.128	10.892	10.398	10.638
67.5	19.171	11.023	11.083	10.951	10.954	10.877	10.882	10.96	10.966
80	17.063	11.201	10.867	11.412	10.929	11.147	10.755	10.596	10.491

- Inlet and outlet pressure in the duct in (Pa)

X-Position (cm)	Without Vortex	CFU Delta	CFD Delta	CFU Rectangular	CFD Rectangular	CFU Zikzak	CFD Zikzak	CFU Sinusoidal	CFD Sinusoidal
0	19.48	17.999	18.1718	19.6443	19.5879	25.5389	25.771	32.2946	27.2303
100	0.0159	0.0962	0.09339	0.092254	0.101866	0.07153	0.07520	0.10934	0.08165

3) Single-phase flow

- Nusselt number with Reynolds number in single-phase flow experimentally and numerically

Re	Ex.Without (VGs)	Ex.Delta	Ex.Rectangular	Num.Without (VGs)	Num.Delta	Num.Rectangular
3645.95	5.45	8.33	8.83	5.72	8.74	9.35
4254	5.89	8.58	9.47	6.2	9	9.93
4812.5	6.37	9.28	10.1	6.7	9.81	10.66

- Friction factor with Reynolds number in single-phase flow experimentally and numerically

Re	Ex.Without (VGs)	Ex.Delta	Ex.Rectangular	Num.Without (VGs)	Num.Delta	Num.Rectangular
3645.95	1.4	0.758	1.5	1.26	0.8	1.2278
4254	1.37	0.82639	1.65278	1.10196	0.7162	1.10516
4812.5	1.34876	1.3	1.518	1.1386	0.95	1.291

- Performance parameter with Reynolds number in single-phase flow experimentally and numerically

Re	Ex.Delta	Ex.Rectangular	Num.Delta	Num.Rectangular
3645.95	2.8229769	1.512	2.4	1.67748
4254	2.41494646	1.332724	2.233481	1.596975
4812.5	1.51147	1.4	1.754857	1.4

4) Two-phase flow

- Nusselt number with Reynolds number in two-phase flow experimentally and numerically at (Q_w = 15 Lpm) and (Q_a= 8.33, 16.67 and 25 Lpm)

Re	Ex.Without (VGs)	Ex.Delta	Ex.Rectangular	Num.Without (VGs)	Num.Delta	Num.Rectangular
3643.5	5.2	9.4	8.93	5.84	10.5	10.3
3641	6.2	9.92	9.8	5.84	10.3	10.1
3638.67	6.6	10.1	9.7	5.76	10.46	10.1

- Friction factor with Reynolds number in two-phase flow experimentally and numerically at (Q_w = 15 Lpm) and (Q_a= 8.33, 16.67 and 25 Lpm)

Re	Ex.Without (VGs)	Ex.Delta	Ex.Rectangular	Num.Without (VGs)	Num.Delta	Num.Rectangular
3643.5	1.03295	0.83	0.98	2.0659	1.66	1.78539
3641	0.8918485	0.716976	0.87	1.382365	1.096973	1.17584
3638.67	0.57	0.5	0.54	0.789177	0.634436	0.679753

- Performance parameter with Reynolds number in two-phase flow experimentally and numerically at (Q_w = 15 Lpm) and (Q_a= 8.33, 16.67 and 25 Lpm)

Re	Ex.Delta	Ex.Rectangular	Num.Delta	Num.Rectangular
3643.5	2.2497057	1.81	2.237575	2.04
3641	1.99	1.62	2.222548	2.0332
3638.67	1.7445	1.55	2.25889	2.035739

- Nusselt number with Reynolds number in two-phase flow experimentally and numerically at (Q_w = 17.5 Lpm) and (Q_a= 8.33, 16.67 and 25 Lpm)

Re	Ex.Without (VGs)	Ex.Delta	Ex.Rectangular	Num.Without (VGs)	Num.Delta	Num.Rectangular
4251.57	6.7	8.95	9.1	6.4	10.45	10.5
4249	6.5	9.7	10	6.33	10.67	10.6
4246.7	6.75	10.2	10.5	6.33	10.89	10.64

- Friction factor with Reynolds number in two-phase flow experimentally and numerically at (Q_w = 17.5 Lpm) and (Q_a= 8.33, 16.67 and 25 Lpm)

Re	Ex.Without (VGs)	Ex.Delta	Ex.Rectangular	Num.Without (VGs)	Num.Delta	Num.Rectangular
4251.57	2.42	2.075733	2.3722672	1.94	1.53	1.6546564
4249	1.73	1.394	1.67286	1.4	1.12	1.21
4246.7	0.9	0.8	0.855479	0.88855	0.7186	0.7742

- Performance parameter with Reynolds number in two-phase flow experimentally and numerically at (Q_w = 17.5 Lpm) and (Q_a= 8.33, 16.67 and 25 Lpm)

Re	Ex.Delta	Ex.Rectangular	Num.Delta	Num.Rectangular
4251.57	1.55737	1.385538	2.07036	1.923549
4249	1.852	1.59	2.107	1.937514
4246.7	1.7	1.6365	2.127251	1.929

- Nusselt number with Reynolds number in two-phase flow experimentally and numerically at (Q_w = 20 Lpm) and (Q_a= 8.33, 16.67 and 25 Lpm)

Re	Ex.Without (VGs)	Ex.Delta	Ex.Rectangular	Num.Without (VGs)	Num.Delta	Num.Rectangular
4810	5.5	9.37	9.63	6.4	10.8	11.1
4807.6	6	10.3	9.85	6.7	11.3	11.1
4805.2	7.5	10.4	9.7	6.87	11.3	10.3

- Friction factor with Reynolds number in two-phase flow experimentally and numerically at (Q_w = 20 Lpm) and (Q_a= 8.33, 16.67 and 25 Lpm)

Re	Ex.Without (VGs)	Ex.Delta	Ex.Rectangular	Num.Without (VGs)	Num.Delta	Num.Rectangular
4810	1.82	0.8958	1.79	1.749	1.415369	1.54
4807.6	0.98	0.83176	0.924177	1.43698	1.1598	1.2615
4805.2	0.42	0.2597	0.371	0.9599	0.782838	0.84962

- Performance parameter with Reynolds number in two-phase flow experimentally and numerically at (Q_w = 20 Lpm) and (Q_a= 8.33, 16.67 and 25 Lpm)

Re	Ex.Delta	Ex.Rectangular	Num.Delta	Num.Rectangular
4810	3.46	1.78	2.085278	1.96975
4807.6	2.0226187	1.74	2.089639	1.88717
4805.2	2.2425876	1.46415	2.01686	1.693877